2023 Astrophotonics Roadmap

pathways to realizing multi-functional integrated astrophotonic instruments

Jovanovic, Nemanja; Gatkine, Pradip; Anugu, Narsireddy; Amezcua-Correa, Rodrigo; Basu Thakur, Ritoban; Beichman, Charles; Bender, Chad F.; Endo, Akira; Soliman, Sherif; More Authors

DOI
10.1088/2515-7647/ace869

Publication date
2023

Document Version
Final published version

Published in
JPhys Photonics

ROADMAP • **OPEN ACCESS**

2023 Astrophotonics Roadmap: pathways to realizing multi-functional integrated astrophotonic instruments

Journal of Physics: Photonics

ROADMAP

2023 Astrophotonics Roadmap: pathways to realizing multi-functional integrated astrophotonic instruments

Nemanja Jovanovic[1,57,*], Pradip Gatkine[1,57,*], Narsireddy Anugu[2], Rodrigo Amezcua-Correa[3], Ritoban Basu Thakur[10,50], Charles Beichman[4], Chad F. Bender[5], Jean-Philippe Berger[6], Azzurra Bigioli[7], Joss Bland-Hawthorn[8], Guillaume Bourdarot[9], Charles M Bradford[10], Ronald Broeke[11], Julia Bryant[8], Kevin Bundy[12], Ross Cheriton[13], Nick Cvetojevic[14], Momen Diab[15], Scott A Diddams[16], Aline N Dinkelaker[17], Jeroen Duis[18], Stephen Eikenberry[3], Simon Ellis[19], Akira Endo[20], Donald F Figer[21], Michael P. Fitzgerald[22], Itandehui Gris-Sanchez[23], Simon Gross[24], Ludovic Grossard[25], Olivier Guyon[5,26,27,28], Sebastiaan Y Haffert[5], Samuel Halverson[10], Robert J Harris[29,30], Jinping He[31,32], Tobias Herr[33], Philipp Hottinger[34], Elsa Huby[35], Michael Ireland[36], Rebecca Jenson-Clem[12], Jeffrey Jewell[10], Laurent Jocou[37], Stefan Kraus[38], Lucas Labadie[39], Sylvestre Lacour[35], Romain Laugier[7], Katarzyna Ławniczuk[11], Jonathan Lin[22], Stephanie Leifer[40], Sergio Leon-Saval[56], Guillermo Martin[37], Frantz Martinache[14], Marc-Antoine Martinod[7], Benjamin A Mazin[41], Stefano Minardi[42], John D Monnier[43], Reinan Moreira[44], Denis Mourard[14], Abani Shankar Nayak[45], Barnaby Norris[8], Ewelina Obrzud[46], Karine Perraut[37], François Reynaud[25], Steph Sallum[47], David Schiminovich[48], Christian Schwab[49], Eugene Serbayn[10], Sherif Soliman[18], Andreas Stoll[17], Liang Tang[31,32], Peter Tuthill[8], Kerry Vahala[40], Gautam Vasisht[10], Sylvain Veilleux[51], Alexander B Walter[10], Edward J Wollack[52], Yinzi Xin[1], Zongyin Yang[53], Stephanos Yerolatsitis[3], Yang Zhang[54] and Chang-Ling Zou[55]

[1] Department of Astronomy, California Institute of Technology, Pasadena, CA, United States of America
[2] The CHARA Array of Georgia State University, Mount Wilson Observatory, Mount Wilson, Altadena, CA 91203, United States of America
[3] CREOL, The College of Optics and Photonics, University of Central Florida, Orlando, FL, United States of America
[4] IPAC/NASA Exoplanet Science Institute, Jet Propulsion Laboratory, California Institute of Technology, Pasadena, CA, United States of America
[5] Steward Observatory, University of Arizona, Tucson, AZ, United States of America
[6] Univ. Grenoble Alpes, CNRS, IPAG, 38000 Grenoble, France
[7] Institute of Astronomy, KU Leuven, Celestijnenlaan 200D, 3001 Leuven, Belgium
[8] Sydney Institute for Astronomy (SIfA), School of Physics, The University of Sydney, Sydney, Australia
[9] Max Planck Institute for Extraterrestrial Physics, Garching, Germany
[10] Jet Propulsion Laboratory, California Institute of Technology, Pasadena, CA, United States of America
[11] Bright Photonics BV, Eindhoven, The Netherlands
[12] Department of Astronomy and Astrophysics, University of California, Santa Cruz, CA, United States of America
[13] Advanced Electronics and Photonics Research Centre, National Research Council Canada, Ottawa, Canada
[14] Université Côte d'Azur, Observatoire de la Côte d'Azur, CNRS, Laboratoire Lagrange, Nice, France
[15] Dunlap Institute for Astronomy and Astrophysics, University of Toronto, Toronto, Canada
[16] Electrical, Computer and Energy Engineering and Department of Physics, University of Colorado, Boulder, CO, United States of America
[17] Leibniz Institute for Astrophysics Potsdam (AIP), Potsdam, Germany
[18] PHIX Photonics Assembly, Enschede, The Netherlands
[19] Australian Astronomical Optics, Astrophysics and Space Technologies Research Centre, Macquarie University, North Ryde, NSW, Australia
[20] Faculty of Electrical Engineering, Mathematics and Computer Science, Delft University of Technology, Delft, The Netherlands
[21] Center for Detectors, Rochester Institute of Technology, Rochester, NY, United States of America
[22] Department of Physics and Astronomy, University of California, Los Angeles, CA, United States of America
[23] ITEAM Research Institute, Universitat Politècnica de València, Valencia, Spain
[24] MQ Photonics Research Centre, School of Engineering, Macquarie University, North Ryde, NSW, Australia
[25] Limoges, CNRS, XLIM, UMR 7252, F-87000 Limoges, France
[26] Subaru Telescope, National Astronomical Observatory of Japan, National Institute of Natural Sciences, Hilo, HI, United States of America
[27] Astrobiology Center of NINS, Osawa, Mitaka, Tokyo, Japan
[28] College of Optical Sciences, University of Arizona, Tucson, AZ, United States of America
[29] Max-Planck-Institute for Astronomy, Heidelberg, Germany
[30] Department of Physics, Durham University, Durham, United Kingdom
[31] National Astronomical Observatories, Nanjing Institute of Astronomical Optics & Technology, Chinese Academy of Sciences, Nanjing, People's Republic of China

OPEN ACCESS

RECEIVED
24 October 2022

REVISED
28 April 2023

ACCEPTED FOR PUBLICATION
18 July 2023

PUBLISHED
30 October 2023

[32] Key Laboratory of Astronomical Optics & Technology, Nanjing Institute of Astronomical Optics & Technology, Chinese Academy of Sciences, Nanjing, People's Republic of China
[33] Deutsches Elektronen-Synchrotron DESY, Germany and Universität Hamburg, Hamburg, Germany
[34] Landessternwarte, Zentrum für Astronomie der Universität Heidelberg, Heidelberg, Germany
[35] LESIA, Observatoire de Paris, Université PSL, CNRS, Sorbonne Université, Université Paris Cité, Meudon, France
[36] The Australian National University, Canberra, Australia
[37] Université Grenoble Alpes, CNRS, IPAG, 38000 Grenoble, France
[38] Department of Physics and Astronomy, University of Exeter, Exeter, United Kingdom
[39] I. Physikalisches Institut, Universität zu Köln, Zülpicher Str. 77, 50937 Cologne, Germany
[40] Department of Applied Physics, California Institute of Technology, Pasadena, CA, United States of America
[41] Department of Physics, University of California, Santa Barbara, CA, United States of America
[42] Ams-OSRAM, Jena, Germany
[43] Department of Astronomy, University of Michigan, Ann Arbor, MI, United States of America
[44] Ultra-Low Loss Technologies, Santa Barbara, CA, United States of America
[45] Institut für Angewandte Physik, Friedrich-Schiller-Universität Jena, Jena, Germany
[46] Centre Suisse d'Electronique et de Microtechnique, Neuchâtel, Switzerland
[47] Department of Physics and Astronomy, University of California, Irvine, CA, United States of America
[48] Department of Astronomy and Columbia Astrophysics Laboratory, Columbia University, New York, NY, United States of America
[49] School of Mathematical and Physical Sciences, Macquarie University, Sydney, NSW, Australia
[50] Department of Physics, California Institute of Technology, Pasadena, CA, United States of America
[51] Department of Astronomy and Joint Space-Science Institute, University of Maryland, College Park, MD, United States of America
[52] NASA Goddard Space Flight Center, Greenbelt, MD, United States of America
[53] College of Information Science and Electronic Engineering, State Key Laboratory of Modern Optical Instrumentation, Zhejiang University, Hangzhou, People's Republic of China
[54] Electrical and Computer Engineering Department, University of Maryland, College Park, MD, United States of America
[55] CAS Key Laboratory of Quantum Information, University of Science and Technology of China, Hefei, Anhui, People's Republic of China
[56] Sydney Astrophotonics Instrumentation Laboratory (SAIL), School of Physics, The University of Sydney, Sydney, Australia
[57] Guest editors of the Roadmap.
* Authors to whom any correspondence should be addressed.

E-mail: nem@caltech.edu and pgatkine@astro.ucla.edu

Keywords: astrophotonics, spectrograph, lanterns, detectors, PICs, hybridization, integration

Abstract

Photonic technologies offer numerous functionalities that can be used to realize astrophotonic instruments. The most spectacular example to date is the ESO Gravity instrument at the Very Large Telescope in Chile that combines the light-gathering power of four 8 m telescopes through a complex photonic interferometer. Fully integrated astrophotonic devices stand to offer critical advantages for instrument development, including extreme miniaturization when operating at the diffraction-limit, as well as integration, superior thermal and mechanical stabilization owing to the small footprint, and high replicability offering significant cost savings. Numerous astrophotonic technologies have been developed to address shortcomings of conventional instruments to date, including for example the development of photonic lanterns to convert from multimode inputs to single mode outputs, complex aperiodic fiber Bragg gratings to filter OH emission from the atmosphere, complex beam combiners to enable long baseline interferometry with for example, ESO Gravity, and laser frequency combs for high precision spectral calibration of spectrometers. Despite these successes, the facility implementation of photonic solutions in astronomical instrumentation is currently limited because of (1) low throughputs from coupling to fibers, coupling fibers to chips, propagation and bend losses, device losses, etc, (2) difficulties with scaling to large channel count devices needed for large bandwidths and high resolutions, and (3) efficient integration of photonics with detectors, to name a few. In this roadmap, we identify 24 key areas that need further development. We outline the challenges and advances needed across those areas covering design tools, simulation capabilities, fabrication processes, the need for entirely new components, integration and hybridization and the characterization of devices. To realize these advances the astrophotonics community will have to work cooperatively with industrial partners who have more advanced manufacturing capabilities. With the advances described herein, multi-functional integrated instruments will be realized leading to novel observing capabilities for both ground and space based platforms, enabling new scientific studies and discoveries.

Contents

1. Introduction

Nemanja Jovanovic and Pradip Gatkine
Department of Astronomy, California Institute of Technology, Pasadena, CA, United States of America

Status

Astrophotonics is simply defined as the application of photonic technologies to astronomy. Like many fields of technology-driven science, astrophotonics directly benefits from the multi-decade and multi-billion dollar investments in photonics by industry, especially by telecommunications. Photonic technologies are appealing because they can provide many avenues for controlling and manipulating light, including spectral dispersion, spectral, spatial, and polarization filtering, phase and amplitude modulation, light generation, frequency shifting, and light detection to name a few. In addition, operating at the diffraction limit of the input telescope means that the instrument can have the smallest possible footprint for a given set of specifications, reducing volume, mass and cost [1, 2]. Guiding the light in fibers or waveguides in a photonic integrated circuit (PIC) allows further reductions in instrument size by enabling flexible integration of many functions optimized for a specific science case and the elimination of bulk optics in most cases leading to extreme miniaturization, which can more readily be thermally and mechanically stabilized. Unlike bulk optics, photonic technologies can be highly replicable, offering dramatic cost savings once produced in volume. A highly replicable diffraction-limited instrument can be readily deployed to numerous observatories and achieve the same performance, potentially providing cost-savings by eliminating the prototypical nature of current astronomical instruments.

With such favorable properties, photonic technologies stand to impact many areas of astronomy. Leveraging the replicability for example, means that low cost massively multiplexed spectroscopic surveys could be enabled in the future. These would allow the measurement of large samples of spectroscopic redshifts, constrain galaxy evolution through tracers of star formation, outflows, etc, and enable detailed compositional study of stellar populations to name a few. On the other hand, the diffraction-limited nature of photonics makes them directly applicable to point-source-like targets that typically rely on adaptive optics (AO) observations. These include the study of exoplanets and disks, young stellar objects, evolved stars, active galactic nuclei, and nuclear star cluster kinematics for example.

Despite its origin in the late 1970s, and pioneering overviews about the prospects of photonics in the 90's [3], the field of astrophotonics was first recognized as a sub-field of astronomical instrumentation in 2009, when the editors of Optics Express [4] solicited a special issue on the topic for the first time. Although then already a thriving field, it has grown over the last 14 years as shown in figure 1, which highlights some of the various technical developments resulting in two further special issues being developed in 2017 and 2021 respectively [5, 6].

Numerous technologies have been advanced over the past decade. Here we briefly highlight a few success stories. The photonic lantern (PL) was invented to exploit the coupling advantages of multimode (MM) fibers and the stability of single-mode fibers (SMFs) for use in astronomy [7]. This mode converting device has since undergone extensive technical development [13–21] and now a device that converts a MM input into 19 SM outputs can routinely do this with a throughput >95% at 1550 nm. The lantern device was leveraged to realize a complex spectral filter that could suppress the telluric OH emission [9, 22]. This was achieved by inscribing complex fiber Bragg gratings (FBGs) and attaching them to each of the SM outputs of a lantern, before recombining the filtered signal into a MM fiber and feeding a downstream spectrograph [23–25]. This spectral filtering capability enabled accurate sky-subtraction in the near-infrared (NIR), key to advancing faint observations in that region. Regarding calibration, laser frequency combs (LFCs) provide an ultra-stable set of highly dense comb lines across large bandwidths [26, 27], making them the perfect tool for calibrating a spectrograph [28, 29]. These tools have been optimized for astronomy for the past decade [30, 31] and are now becoming commonplace for use with precision radial velocity (RV) spectrographs [32]. Finally, in the field of interferometry, the GRAVITY instrument is a long-baseline interferometer that can combine the four 8 m telescopes at the VLT in the NIR K-band centered at 2.2 μm. It does this using a photonic beam combiner chip [33] and provides milli arcsec spatial resolution, microarcsecond astrometric precision, and high throughput thanks to the large telescopes and AO systems, which have enabled many transformative discoveries [34–37].

With these successes and a long list of possible technologies and functions to explore, astrophotonics has a huge potential to impact astronomy. This potential was recently outlined in several whitepapers [38, 39] solicited by the National Academy of Sciences for the US Decadal survey and later explicitly called out in the survey itself [40]. Specifically the survey stated 'The possibility of obtaining extremely high-precision radial velocities, of the order of a 10 cm s^{-1} or better, as well as direct imaging of exoplanets may largely rely on the maturity of SMFs and on-chip nulling interferometers'.

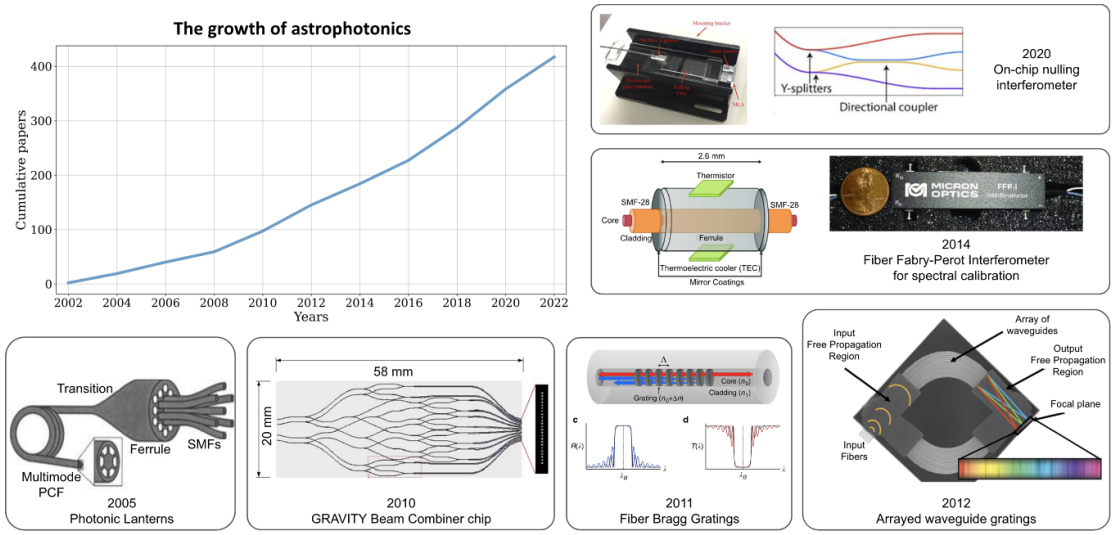

Figure 1. Top left: a plot showing the growing trajectory of research in the field of astrophotonics, compiled using NASA ADS search engine. The surrounding insets show examples of various technologies representing the sub-fields in astrophotonics, as they matured for on-sky demonstration. These examples include: photonic lanterns. Reproduced with permission from [7] © The Optical Society. Photonic beam combiners for interferometry with GRAVITY. Reproduced with permission from [8]. Fiber Bragg gratings for atmospheric OH emission suppression. Reproduced with permission from [9]. Arrayed waveguide gratings for spectroscopy. Reproduced with permission from [10] © The Optical Society. Fiber-based Fabry–Perot interferometer for spectral calibration. Reproduced from [11]. © IOP Publishing Ltd. All rights reserved. And an on-chip nulling interferometer. Reproduced with permission from [12]. This is just a small subset of a large family of astrophotonic technologies that have been developed and demonstrated over the last two decades.

Importantly, astronomy driven technology developments have broader applicability which could improve funding for such developments. For example, the all-photonic flattener on a chip [41, 42] may find application beyond astronomy for gain flattening [43, 44], temporal pulse shaping [45, 46] as well as for targeted excitation of particular molecular species [47]. In addition, PLs are being considered for spatial division multiplexing in telecommunications [48] as well for high efficiency free-space optical communications [49]: the latter is critical to ensuring high data rates for future astronomy and planetary science missions and may also find application in microscopy. These are just a few examples of the potential of astrophotonics to impact society more generally.

Despite these successes, astrophotonic technologies require further developments in nearly all cases to advance them to facility-class instrument science readiness and/or expand capabilities. With this roadmap, we aim to outline some key areas development should be focused on to advance the field and allow for truly integrated, multi-functional instruments to be realized that advance scientific investigation. The choice of development areas outlined in this work was driven by (1) relevant technologies demonstrated by the community with the potential for further growth and (2) promising opportunities given recent technological advances to address outstanding goals. The areas of development covered in this article are non-exhaustive and other areas should also be considered.

Roadmap organization and goals

The roadmap explores the status of currently used technologies and outlines other promising choices that should be investigated. The aim is to highlight the potential astronomical applications of a range of technologies and provide guidance on the specific developmental path to realize that promise including, developing more advanced design tools, prototyping, fabricating, characterizing, packaging, integrating, field testing, and science demonstration. The roadmap is broken up into five key thematic areas which span all of astrophotonics as follows:

Light injection, wavefront control, and light transport

The efficient coupling of light into photonic technologies is the first step in being able to utilize them for astronomical instruments. Given photonic devices generally operate at or near the diffraction limit, the ability to couple light from a telescope into such a device relies on either an AO system to correct for the wavefront in the optical/infrared [50] (common to most large 5 m+ telescopes) or a mode-matching solution, be it a with a PL [18, 20], an integral field unit (IFU), or a series of small telescopes more closely matched to the Fried parameter, r_0 [51]. In addition, with advances in AO systems that can now generate reasonable correction across large fields (MCAO; ∼25% Strehl over ∼2 arcminute fields-of-view [52]) and

references therein, when combined with low-mode-count PLs, efficient multi-object (MO) photonic instruments can be realized.

Photonic technologies can also be used to produce signals critical to driving the AO system, and offer numerous advantages including eliminating non-common path and chromatic errors. Next-generation instrument architectures will merge photonic wavefront sensing and science instruments and result in integrated instruments with superior performance.

Once light is coupled to a photonic system, light transport is the next critical aspect to ensure the light can be efficiently routed to the science instrument. Optical fibers are ideally suited to this and here we explore a range of new silica fiber architectures that enable photonic applications to currently un-explored wavelength ranges with advantageous properties (dispersion, polarization, bandwidth, few-mode vs SM, etc.).

Spectroscopy and spectral filtering

Spectroscopy is a key analytical tool in an astronomers toolbox. It can be used in several ways: to disperse the light for scientific measurement as well as for spectral filtering applications. Photonic dispersing elements in the form of arrayed waveguide gratings (AWGs) have been tested for their suitability for astronomy, but need further developments to optimize throughput, bandwidth, polarization response as well as to scale to higher resolution before wide astronomical application. Apart from AWGs, other photonic technologies provide a plethora of novel approaches to the dispersion problem including dispersed Fourier transform interferometers consisting of Mach–Zehnder interferometers (MZIs) and AWGs, ring-resonator enhanced spectrometers and integrated serpentine grating spectrometers to name a few. These technologies need to be explored to ascertain their scientific potential and demonstrate the technical advantages and to assess challenges to implementation.

Critical to exploiting photonic spectroscopy is being able to realize the devices in wavebands other than the NIR, where telecommunications has already invested heavily. Photonics is evolving in the visible, so we outline photonic efforts to develop platforms, both photonic integrated circuits (PICs) and fiber based, that are promising at more extreme wavelengths like the UV ($<$400 nm) and in the MIR ($>$2.5 μm). AWGs for example have already been built and demonstrated efficiently at sub-mm wavelengths, and in the roadmap we look at further advances needed to optimize these devices, as well as a pathway to large field-of-view instruments.

Spectral filtering is a critical capability. Technologies like FBGs are very mature, but require further development to be applicable to wavebands other than the NIR. Micro-ring resonators, which form tiny resonant cavities and waveguide Bragg gratings, are less mature and need more significant advancements, including utilizing smaller feature sizes, enabling complex filters and reducing cladding mode coupling, but offer the potential to integrate them with other components on PICs.

The applications of filtering devices are growing as well. Optical cross-correlation for example looks at introducing a paradigm shift in how instruments are built, eliminating the need for extremely costly high pixel count arrays, if efficient and flexible filters can be realized to process the light optically. This would be transformative for instruments designed for extremely large telescopes.

Spectral calibration

Key to extracting physical quantities via spectroscopy is the ability to calibrate the spectrograph. Photonics offers the ultimate wavelength calibration tool: the LFC. An LFC can be stabilized to extreme levels over decades [26, 27], meeting even the most demanding science needs in astronomy (e.g. extreme precision radial velocity (EPRV)). Although LFCs are becoming common at many observatories, they are still complex and costly, and lack reliable spectral coverage in the blue, as needed for the most precise RV measurements of Sun-like stars. In addition, LFCs offer the potential for non-spectroscopic calibration applications, including extreme time keeping for very long baseline interferometers as well as metrology.

To maximize the benefit to spectroscopy, the spectral profile of the comb lines in an LFC spectrum must be flattened, or be made more uniform to fit within the spectrometer's dynamic range. On-chip flattener technology has only recently been explored for astronomy and requires further development. In particular, investigation is needed into the optimal device design given the LFCs optical properties, the number of channels that can be realized on a single chip, how to build devices that span several astronomical bands, and the prospects for devices in the visible region.

An alternative calibration technology that offers a compact, portable, cost effective solution to wavelength calibration is the Fabry–Perot etalons. In recent years, these devices have been commissioned at several observatories with precision RV instruments (e.g. ESPRESSO, HARPS, NEID, HPF, SPIROU, Maroon-X). Their spectrum can be readily engineered to provide very broad wavelength coverage including the UV range, and linewidth and spacing precisely matched to the spectrograph. While etalons have demonstrated very reliable operation, and excellent short term stability, they exhibit long term drifts that are

wavelength dependent, likely due to aging effects in the mirror coatings, necessitating the use of other, absolute calibrations sources to periodically recalibrate the etalon spectrum and track the long term drift. The mechanism responsible for the chromatic drifts needs to be identified and the coating effects mitigated before Etalons can become stand-alone calibrators at extreme precisions.

Interferometry

Interferometry is a powerful approach to reach angular resolutions beyond that of single telescopes so one can study the environment in the immediate vicinity of the host target. While GRAVITY has led to groundbreaking results in the NIR with its classical ABCD beam combiner approach, several technical advancements can be undertaken to extend the scientific reach including improving the throughput in several spectral ranges, increasing the Fourier coverage by combining more telescopes, and integrating active fringe tracking capabilities onto the beam combining chips. As an alternative, discrete beam combiner (DBC) technologies are a promising approach that may simplify beam combination circuits when >4 telescopes need to be combined due to their implementation of straight SM waveguides in a lattice. But, the technology also requires their operational bandwidths to be extended and at the same time, realize a smart algorithm for finding the best input configurations and the geometry of the lattice when the number of input telescopes increases. Given their substantial differences, we discuss classical ABCD based beam combiners and DBCs in separate chapters.

In parallel to advancing beam combiner technologies, developing the components to allow kilometric baselines by using optical fibers is also critical. This requires the development of low loss fibers across the NIR and MIR regions (1–17 μm), a careful understanding of the dispersion properties of fibers and how to compensate for delays with fibers as well as FBGs, and to determine if photonic fringe tracking, via piezo stretched fibers or thermal or electro-optic (EO) phase shifters on-a-chip will be sufficient to replace bulk optic delay lines. Birefringence and diattenuation will also need to be closely studied.

For high-contrast applications, nulling interferometry is the desired approach and the roadmap outlines the components (tri-couplers, achromatic phase shifters, etc) needed to realize high performance circuits in future at both NIR and MIR wavelengths. To eliminate any stellar leakage the circuit architecture also needs further development, with approaches like kernel nulling showing promise, but careful evaluation is needed. Fiber and PL nulling rely on a fiber or a mode-selective photonic lantern (MSPL) to be positioned directly in the telescope focal plane. Although they are simple to implement, the contrast will be limited without further investigations into (1) the ability of the cladding to suppress the rejected stellar light and (2) the limitations of cross-coupling in MSPLs. A PIC-based beam combiner is a promising solution to calibrate the leaked light of a PL nuller to enhance the null, but needs to be studied in detail to determine the optimum architecture of the circuit.

Finally we can consider other techniques used in radio astronomy, including heterodyning and frequency conversion. The latter allows the thermal IR photons to be converted to the visible or the near infrared where detectors are abundant and thermal background is no longer the limiting factor. Moreover the combination of the heterodyne or frequency conversion and the use of photonic technologies borrowed from the telecommunication world offers the possibility of linking the telescopes of an array to the central interferometric correlator without the need for costly and hard-to-maintain infrastructure. Interestingly, the combination of a heterodyne approach and single-photon quantum technologies may allow highly efficient interferometric schemes. However, to realize functioning instruments in the MIR one needs broader bandwidths using faster mid-infrared (MIR) detectors, phase-stable mid-IR LFCs and broadband nonlinear conversion crystals.

Realizing efficient, multi-functional instruments

The ultimate goal is to route and process the light collected from the telescope completely in photonics to the detectors (see figure 2 for an example of an integrated photonic instrument concept). Photonics offers many useful functions to achieve this, each optimized across a broad range of disparate materials and platforms. To advance towards realizing instruments on-a-chip, efficient hybridization will be necessary. Mastering repeatable high-efficiency packaging to deliver ultra-low loss coupling from fiber arrays to PICs, and between disparate PIC platforms optimized for various functions (silica-on-silicon (SOS), ion-exchange waveguides in glass, silicon nitride, silicon on insulator, etc) will be necessary. In addition, fan-out devices, needed to go from the output of multi-core fibers (MCFs) to PICs will need to be further developed to reduce losses. Active circuits will also require electrical integration and possibly laser sources for calibration and/or metrology.

Repeatable and robust packaging—integration of various technologies to make a single functioning device will be critical. Fabrication and packaging of most photonic devices is still a niche industry or done on an individual basis, we need to better utilize the expertise of the broader integrated photonics industry and for their capabilities to evolve and mature (e.g.: multi-project wafer (MPW) runs, detector integration, fiber

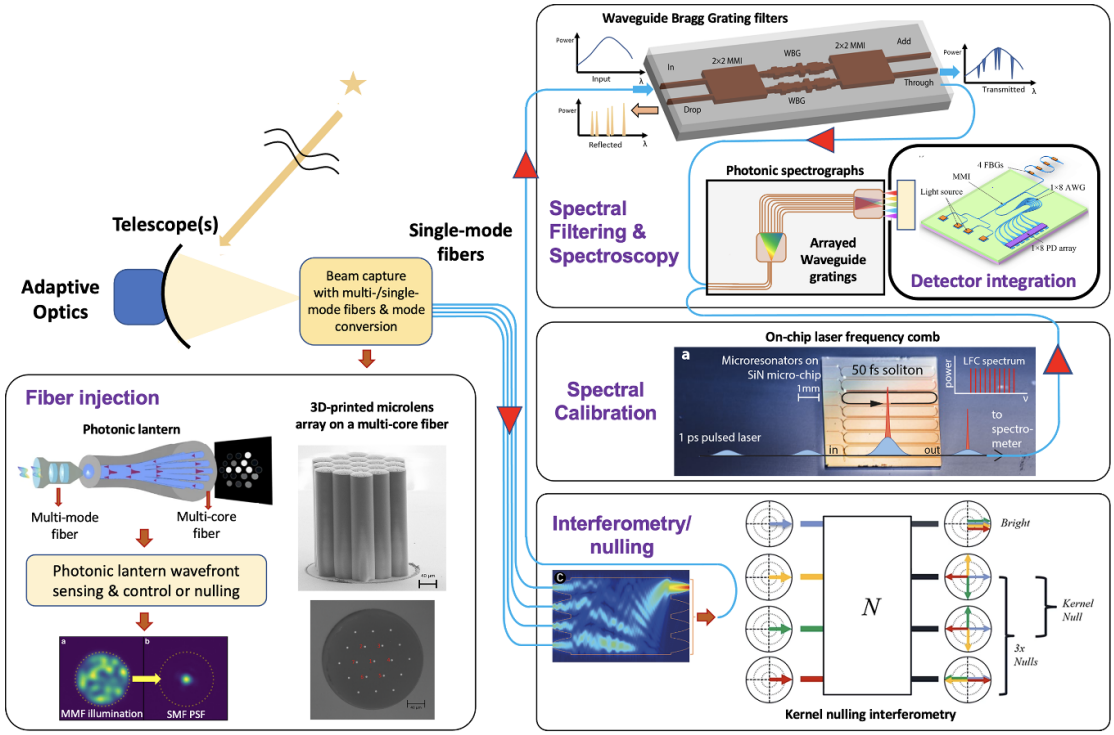

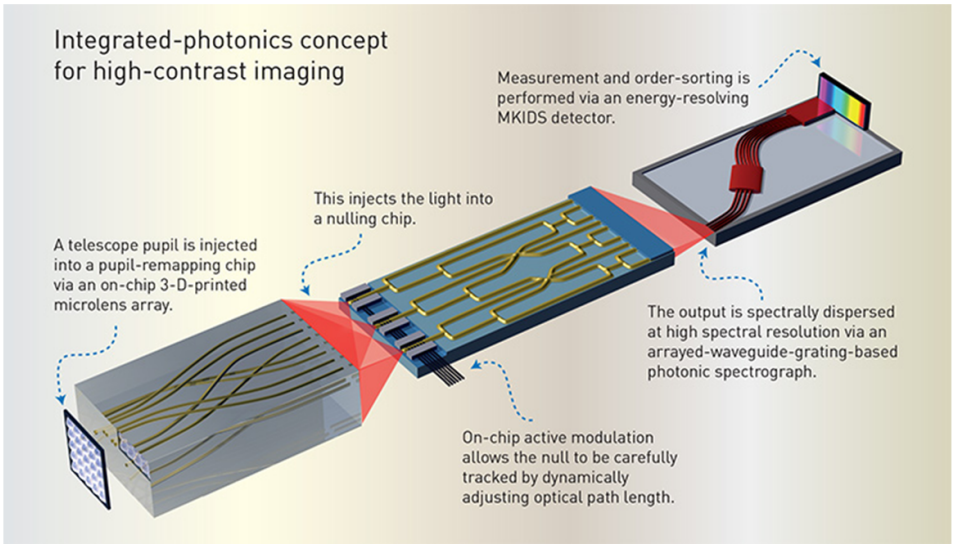

Figure 2. (Top) The five main subcategories of the roadmap are shown with example technologies that can be used in each, as well as an example potential implementation. Some of the technologies shown here include: fiber injection (with photonic lanterns [20], lantern-based wavefront sensing (Reproduced from [53]. CC BY 4.0.) and 3D-printed microlens arrays on multi-core fibers (Reproduced with permission from [54])), spectral filtering and spectroscopy (using complex waveguide Bragg gratings (Reproduced with permission from [55] © The Optical Society) and arrayed waveguide gratings [56]), spectral calibration (with on-chip laser frequency combs (Reproduced with permission from [57])), interferometry (using Kernel-phase nulling [58]), and detection integration. Reproduced from [59]. CC BY 4.0. (Bottom) A future vision for an integrated photonic high-contrast imaging instrument. Micro-lenses segment the pupil plane, a pupil remapper routes the light to a nulling beam combiner chip which has active control for fringe tracking, before light is injected into an arrayed waveguide grating (AWG) to disperse the light and then onto a detector (image taken from [60]).

to chip to free space/detector packaging). Standardization within the photonic industry will dramatically reduce costs for future devices.

Detector integration with PIC or fiber devices will be key to realizing an integrated instrument. Semiconductor detectors operating at temperatures closer to where photonics are typically operated could be integrated via single pixel photo-diodes on the chip, on an active chip which is flip chipped onto the passive device, via linear arrays which are edge coupled to the PIC or 2D arrays that image the beams ejected out of the top surface of the PICs, via grating or vertical couplers. These options need to be studied in more detail to understand the relative pros and cons and for example at which pixel count to transition from single pixel

photodiodes to arrays. Losses of the various outcoupling options (edge, vertical, grating couplers) need to be minimized over broadbands as well. The role of micro-optics needs to be better understood.

To push the sensitivity of detection, photonics could be integrated with superconducting detectors as well. Both microwave kinetic inductance detectors (MKIDs) and superconducting nanowire single photon detectors (SNSPDs) run at much lower temperatures (<4 K), but provide extreme sensitivity photon counting capabilities, free from dark current and read noise. The mismatch in materials between those used for PICs and detectors means further studies are needed to determine the optimum route to integrate them. In addition, superconducting detectors and circuit structures should be optimized for IFUs in the THz as well.

Community development

In addition to the technical developments outlined above, the community needs development as well. Firstly, there is a lack of astrophotonics experts primarily because universities nurture astronomers or photonics technologists. Although specialists are needed, the field also requires interdisciplinary experts that can understand the astrophysics science cases, formulate requirements and then design and realize photonic instruments. New bridges between workforce training centers and new pipelines to bring people into the field are needed. In addition, multidisciplinary centers such as innoFSPEC (Germany) fuel innovation in astrophotonics by bringing together expertise from different fields.

Secondly, the community is not representative of society at large as is the case of the parent field—astronomical instrumentation. As a first step towards addressing the latter point, the community should leverage the initiatives developed by professional societies like SPIE, Optica and AAS, who frequently have discussions, training and workshops on various topics about diversity, equity and inclusivity at conferences, to name a few. At the local level, revising admissions and hiring, retention and advancement practices to eliminate biases and increase diversity and equity are critical.

Realizing the potential of astrophotonics is contingent upon developing a talented, robust and diverse workforce. This work force will not be developed without significant and directed attention and effort by the community.

Concluding remarks

The series of papers that follow elaborate on these five technical themes, each outlining the status, current and future challenges, and advances in the science and technology to meet the challenges for 24 key areas of the astrophotonics field. The technical developments specified in the roadmap will require development of the workforce, adding new interdisciplinary specialists and creating a more diverse and a robust community. Through close collaboration between academia, which is better positioned to advance concepts, designs and qualify devices, and industry partners who are better positioned to provide fabrication and packaging, the technical developments outlined can most efficiently be realized. While astrophotonics has great science potential, currently the field is not funded at a level that can sustain large infrastructure upgrades for PIC, fiber, and packaging advancements. Instead, the field will benefit from continued investments by industries such as telecommunications, AR/VR headsets, photonics for satellites, and LIDAR for autonomous vehicles. Conversely, those fields will also benefit from astrophotonic driven developments. Despite this, the astronomical community must stay engaged with industry partners to provide them with guidance on the needs of the community as well as to be inspired by advances in vendor capability.

Acknowledgments

This work was supported by the National Science Foundation under Grant No. 2109232 and support for P Gatkine was provided by NASA through the NASA Hubble Fellowship Grant HST-HF2-51478.001-A awarded by the Space Telescope Science Institute, which is operated by the Association of Universities for Research in Astronomy, Incorporated, under NASA Contract NAS5-26555.

2. Symbiosis between adaptive optics and photonics: the path to fully integrated instruments

Philipp Hottinger[1], *Olivier Guyon*[2,3,4,5] *and Rebecca Jenson-Clem*[6]
[1] Landessternwarte, Zentrum für Astronomie der Universität Heidelberg, Heidelberg, Germany
[2] Subaru Telescope, National Astronomical Observatory of Japan, National Institute of Natural Sciences, Hilo, HI, United States of America
[3] Astrobiology Center of NINS, Osawa, Mitaka, Tokyo, Japan
[4] Steward Observatory, University of Arizona, Tucson, AZ, United States of America
[5] College of Optical Sciences, University of Arizona, Tucson, AZ, United States of America
[6] Department of Astronomy and Astrophysics, University of California, Santa Cruz, CA, United States of America

Status

Most 8–10 meter class telescopes are equipped with AO to compensate for atmospheric turbulence. All AO systems rely on wavefront sensor(s) (WFS) to measure optical aberrations, deformable mirror(s) (DMs) for optical correction, and computational methods for linking WFS measurements to DM commands. Yet their design details vary considerably depending on the telescope environment and the intended science application.

Laser guide stars (LGS) assisted wavefront sensing enables AO-corrected observations of fields with no bright star, such as the galactic center [61, 62]. The AO-corrected field of view (FoV) can be extended by using multiple DMs and WFSs [52] to support, for example, crowded-field astrometry or MO spectroscopy (e.g. Gemini's GEMS and GNAO, VLT's MAVIS [63] and Subaru's ULTIMATE [64]).

Extreme-AO systems (ExAO), on the other hand, are optimized for performance over a small field-of-view around bright natural guide stars, integrating high actuator count DMs with advanced wavefront control methods. Several such systems have been deployed for imaging exoplanets, including Gemini/GPI [65], VLT/SPHERE [66], Subaru/SCExAO [67], and Magellan/MagAO-X [68]. Focal plane WFSs can address remaining wavefront distortions such as non-common path aberrations (NCPA) and thermally-induced phase discontinuities [69], using a wide range of algorithms and approaches [70–72].

Thanks to excellent AO correction in the (near-)IR over a small FoV of $\sim\leqslant 50''$ on large telescopes, starlight can now efficiently be coupled into SMF for high angular and spectral resolution spectroscopy, with an efficiency closely linked to Strehl ratio (SR). Jovanovic *et al* [50] achieved coupling efficiencies of over 50% with SRs of 60% in H-Band at Subaru/SCExAO, Crass *et al* [73] >35% in Y- and J-Band with LBTI/iLocater, and Delorme *et al* [74] coupling efficiences of 60% aim to reach coupling efficiencies of 60% in K- and L-Band with Keck2/KPIC. Photonic SM components extend SMF use to multiple telescopes [75], and compact integral-field spectroscopy with approaches including hexabundles [76], SCAR [77, 78], and 3D-M3 [54].

With the intermediate SRs of 10%–20% delivered in near-IR by wide FoV ($\sim\geqslant 100''$) AO systems, coupling into a single SMF becomes less efficient. Modal conversion with photonic lanterns (PLs) [7] can couple light to multiple SMFs to feed downstream SMF-base instrumentation such as a fiber-bragg gratings (FBG) for airglow suppression of OH emission lines in the H-Band [23]. Alternatively, few-mode fibers can make use of this partial AO correction like NIRPS [79] but these are prone to the negative impact of modal noise.

AO subsystems could individually be replaced by maturing photonic technologies, offering identical or enhanced functionalities in a miniaturized and integrated footprint. The manufacturing processes often allow *in-situ* alignment [80] that reduces operational complexity and increases optical stability. One of the most promising applications is the use of PLs as focal plane WFS with the potential to supplement well-established pupil plane WFSs as compact additions to sense residual aberrations (see section 3 for more details). Large systems would benefit from the reduced complexity and smaller footprint of these sensors, enabling better scalability for Multi-Object-AO and Multi-Conjugate-AO systems requiring multiple WFSs and thus making it easier to achieve better AO performance over a wide FOV. Goodwin *et al* [81] introduced the concept of a miniaturized Shack-Hartmann WFS with similar benefits.

To optimally exploit photonic technologies, they should not simply replace individual conventional components but rather aim to be integrated as part of the science instrument and the AO system. This type of hybridization will make telescope optics more resource efficient as it reduces optical and mechanical footprint and complexity. One partially integrated approach has been proposed by Dietrich *et al* [82] for reconstructing tip-tilt with a multi-core SMF equipped with an 3D-printed lenslet array and tested on-sky with a refined design utilizing a micro-lens ring tip-tilt sensor (MLR-TT sensor) by Hottinger *et al* [83].

There, wavefront sensing is integrated into a vital part of the science instrument, in this case with simultaneous SMF coupling. While tip-tilt sensing is only a limited functionality, it shows the advantages such an integrated approach can have as it reduces complexity by replacing multiple bulk optic components while almost completely eliminating NCPA.

This interplay between AO and instrument has led to demand and existence of test environments that allow transition of the development from laboratory to on-sky performance in order to mature existing concepts. These are core objectives of the SCExAO testbench at Subaru [67] and Canary at WHT [84].

Current and future challenges

Efficient injection of astronomical light into photonic devices requires exquisite wavefront quality and stability, beyond what is achieved with AO on large telescopes. Reliable, efficient and stable coupling will require further improvements in AO performance, with particular attention to vibration control and atmospheric dispersion correction. Proper optical matching of the telescope beam to the fundamental mode of the SMF is also important [85]; phased induced amplitude apodization has already been shown to have the potential to significantly increase single mode (SM) fiber coupling [50, 86].

Modern AO systems' demanding wavefront quality requirements on large telescopes drive them to employ fast, sensitive and accurate WFS s driving high-count DMs, with higher optical complexity and use of advanced wavefront control algorithms. Precise calibration of system components (WFS, DM) and control of residual NCPA is becoming increasingly critical. This is especially essential in HCI applications requiring starlight suppression by nulling or coronagraphy to support the direct imaging and spectroscopic characterization of exoplanets. Photonic technologies can provide the high performance interferometric wavefront sensing solutions to meet this challenge, combining high sensitivity with large dynamical range, and providing wavelength diversity. This interferometric approach to wavefront sensing is well-suited for a second-stage high-precision WFS/C following a more conventional AO correction so that starlight is efficiently coupled to the photonic device(s). These benefits have recently been demonstrated on-sky with the PL [87] and the GLINT instrument [88, 89]. To fully realize this potential, the interferometric WFS output signals will need to be used for real-time active wavefront control, either by DM actuation or in-chip phase modulation. Wavefront information is then extracted by direct measurement of interferometic phases, as is done in multi-telescope inteferometers.

Manufacturing capabilities of photonic components are often still insufficient for astronomy applications, with most new developments driven by the much more broadly funded telecommunication industry which usually has less demanding requirements on optical throughput, pathlength control, and broadband performance. The astronomical community has the chance to contribute in these new areas, expanding the range of applications of photonic devices. When astrophotonics aims to integrate or replace full-scale AO systems, scaling of these devices also becomes an issue as the number of coherent elements scales with $\sim \left(r_0 / D^2\right)$ and so will the required number of individual sensor readout and pathlength control units. In the near future, photonics-based AO systems could be deployed as small units downstream of AO systems using bulk optics, while full-scale photonics AO systems on large telescopes will require more development.

Practical challenges of astrophotonic technologies need to be considered as these are often a new class of manufactured devices that need special attention. For small scale refraction components, 3D-printed microlenses fabricated using two-photon lithography allow high flexibility in free-form shapes and enable the possibility for *in-situ* printing providing integrated alignment [80]. But this also means that care needs to be taken for handling these devices during transportation and employment as their structural integrity and the bond joint between components is vital to their performance. SMFs feature a mode-field diameter (MFD) that varies slightly between manufacturing batches. For maximum coupling between separate fibers, the MFD needs to be matched. Ultra-fast laser inscription [90, 91] can be used for precise waveguide design and is continuing to mature but many manufacturing challenges such as reliable waveguide printing, limited refractive index contrast, and high attenuation still remain. In particular, these considerations will also be essential when astrophotonic devices are to be employed at space based observatories as the environmental impact regarding vibrations, temperature, pressures and background radiation pose an additional challenge.

Advances in science and technology to meet challenges

There are two main roads towards an increased symbiosis between astrophotonic instruments and AO. Firstly, individual photonic components can be employed to augment conventional systems, for example by providing a second stage WFS, or by performing a science measurement well suited for photonic approaches downstream of high performance AO correction. In the long term, photonic devices can potentially also replace parts of conventional AO systems, for example as the main WFS. Secondly, photonic components will be tightly integrated together as a system performing a wide range of functions, leading to more compact,

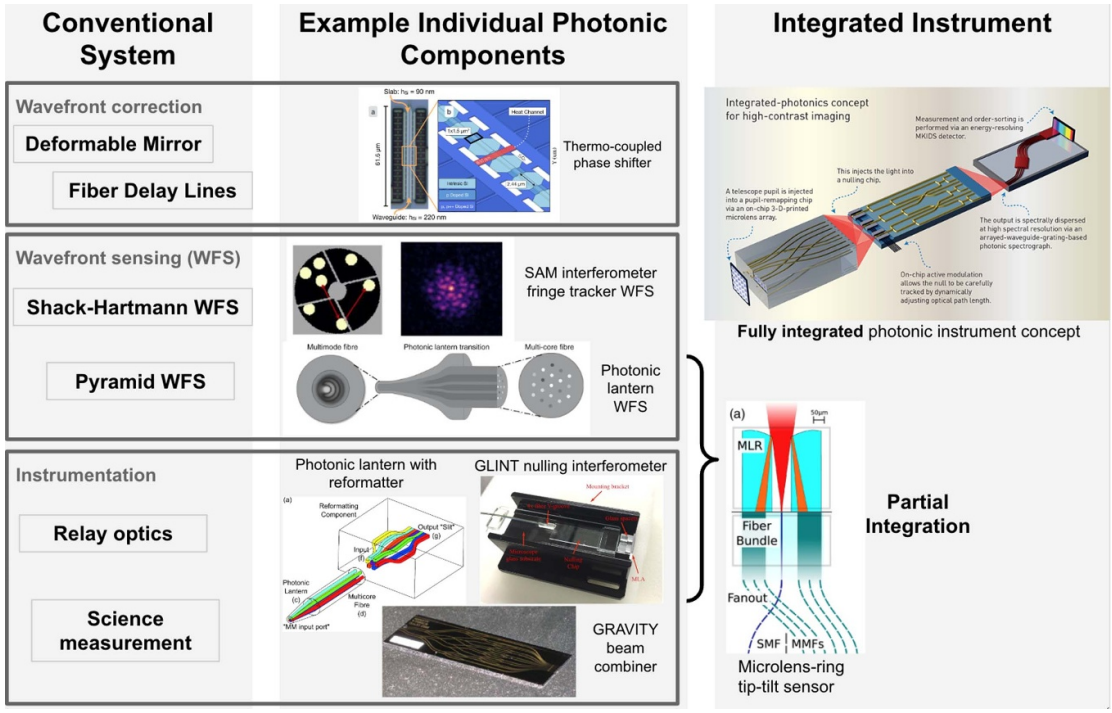

Figure 3. Overview of conventional adaptive optic (AO) systems, potential photonic counterparts and additions, as well as integrated instrumental concepts. Individual concepts: Thermo-coupled phase shifter. Reprinted with permission from [92] © The Optical Society. Sparse aperture masking (SAM) interferometry fringe tracker WFS. Reprinted with permission from [93] © SPIE. Photonic lantern WFS. Reproduced from [53]. CC BY 4.0. Photonic lantern with reformatter. Reproduced from [94]. CC BY 4.0. GLINT nulling interferometer. Reproduced from [12]. CC BY 4.0. Gravity beam combiner. Reproduced with permission from [75]. Microlens-ring tip-tilt (MLR-TT) sensor. Reproduced with permission from [83] © The Optical Society. Integrated photonic instrument illustration by Phil Saunders. Reproduced with permission from [60] © The Optical Society.

less complex instrument systems that enable high automation both in manufacturing as well as in operation. Some concepts enable new optical approaches potentially surpassing the performance and capability of conventional systems. Figure 3 brings together these points, showing the existing individual photonic components that correspond to or can supplement conventional systems (center column) as well as integrated concepts where photonic components are part of a larger instrument (right column).

A general challenge in the development of astrophotonic components is the adaptation of photonic components to the requirements of astronomical observations. Three requirements that are significantly less stringent in telecommunication application play a central role in astrophotonics. Firstly, the wavelength performance needs to be enlarged to broader bands as both instrument sensitivity and science goals require throughput and optical performance over a larger wavelength range. Secondly, throughput of astrophotonic devices has only a very small loss budget as most scientific observations are performed in the photon starved regime. Thirdly, environmental stability cannot always be guaranteed in observatories, imposing higher tolerances on temperature, humidity, and mechanical constraints.

The deployment of the photonic beam combiner at GRAVITY [75] has indeed shown that photonics can already individually replace conventional components and uniquely enable high precision astrophysical measurements. In general, evolution for these components is slow as these concepts need to prove their optical performance and optical efficiency before consideration for large scale investments. Adoption of astrophotonic solutions in major astronomical instrumentation projects relies on successful proof-of-concept demonstrations, preferably performed on-sky. To boost development, access to and support from state-of-the-art AO instrumentation on large telescopes should be prioritized.

As outlined in the previous sections, astrophotonic technologies are already bringing advances in wavefront sensing, although they currently support a moderate number of wavefront modes. Two main approaches are on the horizon. Firstly, interferometric wavefront sensing between multiple telescopes for facilities like VLTI/GRAVITY and CHARA or within the same large telescope aperture as demonstrated in FIRST [95] and GLINT [12], offering nanometer-level phase precision simultaneously with spectral resolution thanks to wavelength-dispersed fringes. Secondly, PLs and MCFs can reduce optical elements and thus provide a simple high-throughput alternative to bulk optics slit formatting, light transport, etc. Additionally, in these applications, the photonic device can perform low-order wavefront sensing of a few

modes and operates as a final-stage WFS downstream of the high-order AO system. In the near future, these few-mode devices could be integrated with the kHz-speed AO correction by feeding back into the upstream AO system.

For WFS control, communication between different subsystems must be established. The use of machine learning (ML) algorithms is explored in a number of projects and shows potential to solve some of the challenges associated with analysis of complex sensor data as was demonstrated in PL-WFS demonstration by [53]. The use of these algorithms is already widespread in many real time applications outside astronomy, and will need to be accommodated in observatories as well. The astronomical context will require operation in the kHz regime with a wide variety of input data from both optical and environmental sensors such as accelerometers, temperature sensors, and seeing measurements. The computational infrastructure must be expanded to fulfill this need, including the corresponding telemetry data filter and storage which is needed for both analysis and future algorithm training as well as specialized ML inference hardware. Linear and higher order reconstruction methods have also been explored by [96].

Photonic devices can integrate wavefront correction as on-chip phase shifters, a highly miniaturized equivalent to optical delay lines used in interferometers. While current interferometer systems use mechanically driven fiber delay lines, photonics provides several solutions that can potentially offer control authority into the kHz regime, including thermoacoustic devices [97], thermo-coupled [92], EO phase shifters [98] and piezo-actuated phase shifters [99]. Additionally to classical wavefront correction, fast photonic-based pathlength modulation can reveal incoherent exoplanet light within the coherent starlight residual when performing high-contrast imaging (HCI).

Photonic components can both transport and modify the transported light. This enables combinations of these functions where a fraction of the guided photons is used for sensing. Such integration of AO and science acquisition in a single compact photonic device will allow for new self-calibrating and self-tuning capabilities to be a core feature of the instrument design. This architecture is particularly attractive for HCI, where a photonic nulling chip could iteratively reconfigure its internal phase delays [100] or drive external DM(s) to maintain optimal broadband null depths. By integrating science measurement and WFS functions within the same photonic chips, the stable relationship between WFS and science outputs can be measured and leveraged for self-calibration of science measurements down to the photon noise residual [88].

Concluding remarks

Given the rapid pace of development of photonics applications to AO and astronomical instrumentation over the last decade, and the growing number of successful on-sky demonstrations, photonic technologies and devices are poised to play an increasing role in astronomy. Progress in this area is driven by advances in underlying core technologies, maturation of instrument designs incorporating emerging photonics solutions, and access to increasingly powerful AO systems providing the suitable wavefront quality on large astronomical telescopes.

Integration of AO and astronomical measurement functions in a single photonics-based system will be particularly enabling, providing in a compact format a rich set of functionalities with high stability and accurate calibration of science measurements. In order to realize this potential, further developments will need to include both lab prototyping activities and on-sky prototyping demonstrations. In this paper we have summarized the vast variety of different components involved, hinting at the challenges that lie ahead when all these systems are aimed to be combined. Sustained collaborative efforts between phononics experts and on-sky AO-equipped development platforms and photonics-capable instruments have been, and will continue to be particularly instrumental in maturing photonics systems for astronomy.

Acknowledgments

We thank R J Harris for the fruitful discussions on the topic. P H is supported by the Deutsche Forschungsgemeinschaft (DFG) through Project 326946494, ‘Novel Astronomical Instrumentation through Photonic Reformatting’. O G acknowledges support from NASA Grant 80NSSC19K0336 and JSPS Grant 21H04998 supporting development of advanced WFS techniques including photonic devices. O G and R J-C acknowledge support from the Heising-Simons foundation.

3. Photonic lantern wavefront sensing and control

Barnaby Norris[1], *Jonathan Lin*[2], *Robert J Harris*[3,4], *Aline N Dinkelaker*[5] *and Momen Diab*[6]
[1] Sydney Institute for Astronomy (SIfA), School of Physics, The University of Sydney, Sydney, Australia
[2] Department of Physics and Astronomy, University of California, Los Angeles, CA, United States of America
[3] Max-Planck-Institute for Astronomy, Heidelberg, Germany
[4] Department of Physics, Durham University, Durham, United Kingdom
[5] Leibniz Institute for Astrophysics Potsdam (AIP), Potsdam, Germany
[6] Dunlap Institute for Astronomy and Astrophysics, University of Toronto, Toronto, Canada

Status

Astronomy has been revolutionized by the adoption of AO [101], where the wavefront of light, corrupted by Earth's turbulent atmosphere, is sensed, analyzed and corrected. This allows diffraction-limited, HCI of targets such as exoplanets, and is key to enabling the full potential of the upcoming Extremely Large Telescopes. Existing AO systems generally measure the wavefront error at the pupil plane, using WFSs such as a Shack–Hartmann or pyramid sensor [102]. These sensors are blind to highly problematic modes such as petaling (phase shear at the pupil plane around the telescope spiders [103]), and suffer from NCPA with respect to the science focal plane. In a standard imaging system, the focal plane image alone cannot be used to sense the wavefront since it contains only intensity (not phase) information about the PSF.

Placing a PL at the focal plane, allows the *complex* amplitude of the PSF, and hence the wavefront, to be directly measured (see figure 4 for examples). A PL is a passive device that consists of sets of waveguides with different numbers of modes, between which light is transferred [7, 20], see also section 4. Of particular interest is when the MM waveguide at the input tapers into several SM waveguides at the output, the number of which matches or exceeds the number of spatial modes at the input. The excitation of modes in the MM end of the PL is a direct function of the spatially-dependent complex amplitude of the injected PSF. If the transfer function of the PL is known, the wavefront can be reconstructed from the PL's SM outputs. But this transfer function is only known by measurement post-fabrication, since the fabrication process is not deterministic.

The PL-WFS offers several advantages: it is sensitive to any mode which affects the PSF, including modes to which pupil-plane WFSs are blind, it makes optimal use of detector pixels (one pixel per mode) minimizing detector noise, and the entire device fits within a standard fiber connector making it ideal for MO systems. The output can also be spectrally dispersed via a prism or grating (see sections 6 and 7), to achieve wavelength-resolved wavefront sensing, useful in breaking phase-wrapping degeneracy (such as seen in petaling) and to measure atmospheric scintillation. It can also be used for PSF reconstruction. Perhaps most significantly, a fully photonic device has high stability and is ideal for optimally injecting light into a SM fiber (for subsequent spectroscopy [104], interferometry [12], etc) wherein it offers a truly zero NCPA WFS (see *hybrid MSPL* below).

The relationship between low-order wavefront modes (such as Zernike aberrations) and PL outputs has been shown [105] as well as laboratory and on-sky demonstrations of wavefront reconstruction. These include a 19-mode PL-WFS and a neural network reconstructor using a multi-core-fiber based PL [53] and a pupil plane low-order WFS [106].

Research is underway to evaluate the efficacy of different PL types and algorithms for WFSing. Both optical-fiber-based [7] and ultrafast laser inscribed (ULI) lanterns [107] are being investigated, as well as MSPLs [108, 109]. While in a standard PL each SM output is a complex linear combination of the complex input mode amplitudes, in a MSPL a one-to-one mapping between the modes excited at the MM port and the SMFs can be engineered [19]. This can ideally match the modes coupled to those in the PSF [110]. However, the number of modes that MSPLs can multiplex is limited by device length and core diameter, with the length of the required taper proportional to the square of the number of modes [111], and therefore MSPLs are not expected to be effective in WFSing applications [96].

A so-called *hybrid* MSPL can circumvent this limitation; here, all light propagating in the fundamental (LP_{01}) mode is routed to a single output, and higher order modes are used for WFSing. In this case, the higher order outputs drive the AO system to maximize coupling in the LP_{01} mode, which is then routed to the SM science instrument. Alternative modes could be made selective instead if desired. Importantly, this selectivity is maintained over a broad bandwidth [112], such as the 1.5 μm–1.8 μm range demonstrated in this reference.

With ongoing developments and diverse configurations, PLs have the potential to provide solutions for a broad range of WFS applications (see figure 5 for an example of PL WFS integration).

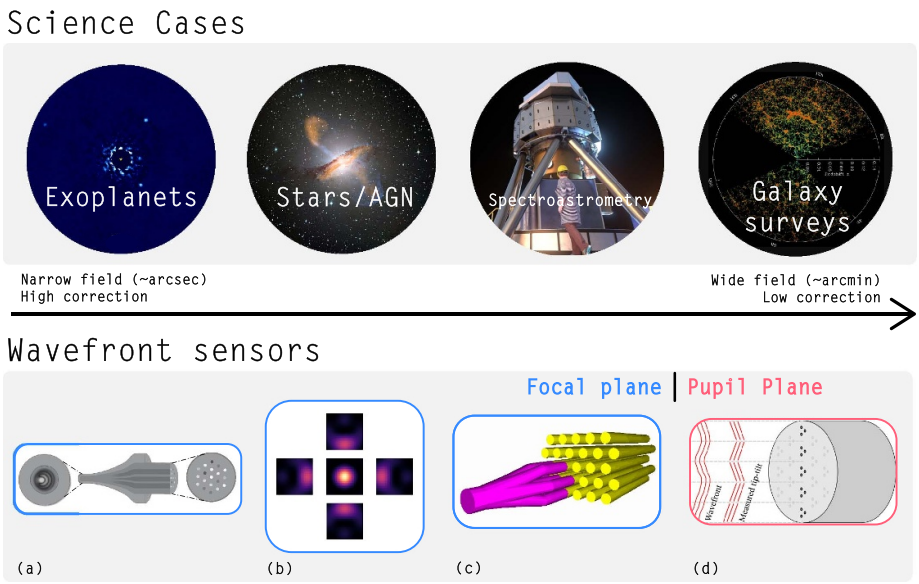

Figure 4. Different photonic lantern wavefront sensor designs (bottom) and their potential applications (top): the highest level of correction/narrow field-of-view on the left, and lower level of correction/wide field-of-view on the right. Blue indicates focal plane and red indicates pupil plane WFS. Image credits for the insets (top row, 'Science Cases'): 'Exoplanets': Jason Wang (Northwestern)/William Thompson (UVic)/Christian Marois (NRC Herzberg)/Quinn Konopacky (UCSD), 'Stars/AGN': ESO/WFI (Optical); MPIfR/ESO/APEX/A.Weiss et al (Submillimetre); NASA/CXC/CfA/R.Kraft et al (x-ray), 'Spectroastrometry': ESO, 'Galaxy surveys': M. Blanton and SDSS. Insets for the wavefront sensors (bottom row): (a) Reproduced from [53], CC BY 4.0. (b) Reproduced with permission from [105]. (c) Reprinted with permission from [113] © The Optical Society. (d) Reproduced from [106], CC BY 4.0. The source images for the 'Science Cases' insets and references [53, 106] are licensed under a Creative Commons Attribution 4.0 International License (https://creativecommons.org/licenses/by/4.0/).

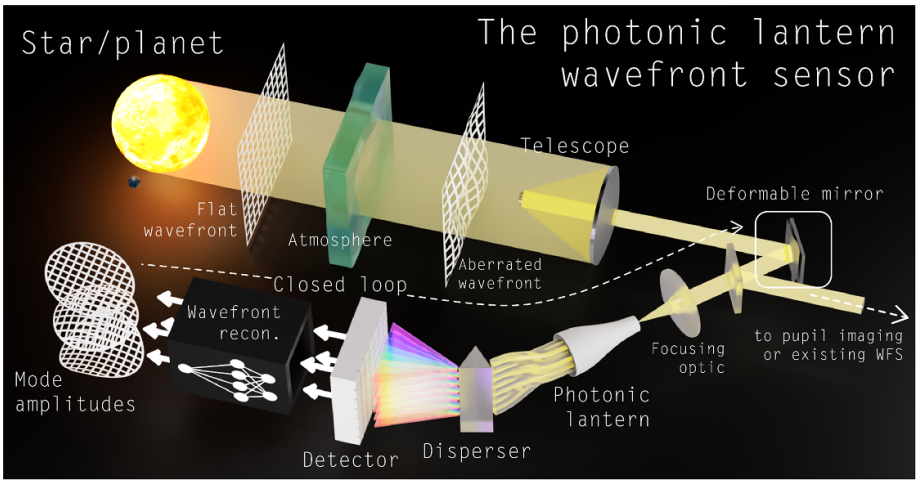

Figure 5. Overview of a PL-WFS system. Light arrives at the telescope distorted from the atmosphere. After the telescope mirrors, the light is guided to a photonic lantern, where it is distributed between different channels and exits at multiple outputs. Here, it can be spectrally dispersed and is then detected. The data can be used directly for scientific analysis as well as wavefront reconstruction (e.g. using a neural network), with the results feeding back to a deformable mirror earlier in the optics chain for wavefront correction.

Current and future challenges

One difference to overcome between the PL-WFS and traditional WFSs is that PL-WFSs are non-linear. Since the measured quantity is the SM output intensity (the square of the complex amplitude), the transfer function mapping wavefront phase to output flux is non-linear (and non-monotonic for large phase errors [53], since the coupling is cycling in a sinusoid-like fashion between constructive and destructive interference as phase-difference increases). Therefore, for wavefront reconstruction (e.g. for closed-loop AO) the standard linear reconstruction algorithms only work over small wavefront error ranges, where the transfer function is locally linear. One option is to use a higher order (e.g. quadratic) reconstruction algorithm [96] or to use a fully non-linear inference model (e.g. neural network [53]). An alternative approach is to instead

optimize for PL linearity, either altering the PL itself or through additional optics such as phase masks and beam recombiners.

While measurements of on-sky wavefronts have been demonstrated [87], the next step is to deploy a PL-WFS in a closed loop configuration on-sky. The current challenge is deploying a suitable (e.g. non-linear) wavefront reconstruction algorithm that can operate with sub-millisecond latencies and integrating it into existing AO software, while running in parallel with existing high-order WFSs. Additionally, while the compact size of a PL-WFS makes it ideal for MO WFSing, algorithms and instruments to exploit this are yet to be developed.

To date, only low-order (<20 modes) PL-WFSs have been demonstrated. For high-order AO applications such as speckle suppression many more modes would be advantageous. PLs with many 100s of modes have been produced (e.g. using a cascaded design [21]), but not yet routinely. The difficulty in implementing algorithms for 100 or even 1000 mode PL WFsing is yet to be determined. An alternative could be to use microlens arrays to reduce the number of modes in each lantern, such as the WFS proposed by [106].

A high mode-count PL becomes especially important for imaging, wherein each mode corresponds to one spatial element of the image. This is an important goal, as obtaining a full complex image of the science target would allow speckles and the science object to be optimally disambiguated—currently one of the greatest challenges in HCI [114]. A suitable architecture (and algorithm) to measure this, along with the coherence properties of the source, is an active area of research. One possibility is to interferometrically recombine the outputs of the PL to measure their complex amplitudes [113, 115]. Alternatively, the interferometry could take place within the PL itself, with the number of PL outputs being made greater than the number of input modes, thus oversampling, and encoding phase, amplitude and spatial coherence directly into the output intensities.

While the design parameters of fiber-based PLs can be broadly specified, the tapering-based fabrication process means that the exact transfer function cannot be specified, and tapering parameters are set empirically [116]. A precise, deterministic fabrication method would enable more specialized and optimized designs. Deterministic fabrication would address the mismatch between the 'ideal' PLs assumed in simulations, and real PLs, which feature slightly mispositioned cores, non-circular claddings, and other defects. The simulation process also faces other challenges, such as the high computational cost and approximations of standard beam propagation algorithms (such as the beam propagation method (BPM)), reducing the accuracy of future high mode-count models.

One promising application is the use of the PL-WFS (possibly with hybrid MSPL fiber injection) on arrays of small telescopes. Their small apertures offer high SRs with only low-order correction such as that provided by a MSPL. Light from multiple telescopes could then be efficiently injected into SMFs and (in)coherently combined for diffraction-limited spectroscopy, or interferometry. A general challenge, however, is the overall lower flux collected by these smaller telescopes, requiring the PL-WFS system to match the brightness limit of any other WFS in the system.

Advances in science and technology to meet challenges

More accurate, deterministic control of PL parameters during fabrication would enable devices to be manufactured whose properties match those in the simulated design. Most mature photonic fabrication techniques such as photolithography are limited to two-dimensional structures, making them unsuitable for PLs. Current fiber-based PLs are produced via tapering on fusion splicing glass processing machines, making reliable and repeatable fabrication difficult. Increased demand for PLs in industry (e.g. telecommunications) may lead to PL-oriented glass processing machines. ULI is a promising technology, allowing the use of more arbitrary structures to construct the PL. This technology is still developing, and generally has lower refractive index contrast and worse control than fiber-tapering methods, but the field is evolving rapidly [90, 91].

For any fabrication technique, accurate simulations require a better understanding of how errors in the manufacturing process propagate to actual WFS behavior. For end-to-end simulations, the source of wavefront error represented should be refined to incorporate errors from a wider range of on-sky and instrumental sources. Advances in numerical simulation algorithms are also needed, both for increases in accuracy (e.g. adopting a fully vectorial BPM technique or finite-difference time-domain method) and speed. Fully differential numerical models would also be extremely useful to enhance the optimization processes. Together these will allow production of devices with precisely optimized imaging/wavefront sampling.

Advancements in AO algorithms are required, including optimization of non-linear algorithms (e.g. neural networks) at low-latency kilohertz rates for closed-loop operation. The performance of these algorithms under a range of conditions must be carefully characterized to achieve the reliable, routine operation demonstrated by standard AO algorithms. Beyond WFSing, performing full coherent imaging—simultaneously measuring the image and wavefront, and its spatial coherence properties—will require innovation in analysis and image reconstruction. New detector technologies, especially

photon-counting, wavelength-resolved detectors such as MKIDS (see section 25), would also offer a huge advantage as they have effectively zero read-noise and would allow high spectral resolution (acting as cross-dispersion for an Echelle spectrograph), but are currently limited to low photon-count rates.

Due to their stability, compact form factor and high sensitivity due to optimal detector usage, PL WFSing may become invaluable for space-based telescopes. Since they operate in the low wavefront error regime, a high mode-count PL could be the only WFS (both for speckle control and mirror phasing), relaxing the need for separate pupil-plane WFS and optics. As highlighted by the Roman space telescope coronagraph technology demonstration [117] the success of future high resolution space telescopes will be contingent on WFSing and control. WFSing and control is also critical for optical communications between space and ground. Before PLs can be deployed in these contexts, these components will have to be space qualified by means of environmental testing and technology demonstrator missions using small satellites.

Concluding remarks

The use of PLs for wavefront sensing is a novel application and has already seen a surge of interest. Advantages include the ability to perform direct measurements of both phase and amplitude at the focal or pupil plane, inherent compactness and stability, optimal use of detector pixels, and the ability to perform optimal injection of starlight into one SMF (acting as a zero non-common-path WFS). While the concept has been demonstrated in laboratory and in open loop on-sky experiments, further development is required to enable widespread adoption. This includes implementing low-latency non-linear control algorithms and developing deterministic, accurate fabrication methods coupled with precise simulations. Full coherent imaging (wavefront and image measurement) is also on the horizon. There is a strong research effort by multiple groups worldwide to investigate these aspects, and programs to test PLs on major telescopes are already underway.

Acknowledgments

B R M N acknowledges support from the Australian Research Council, Discovery Early Career Researcher Award (DE210100953).

R J H would like to thank the Deutsche Forschungsgemeinschaft (DFG) for their support through Project 326946494, 'Novel Astronomical Instrumentation through photonic Reformatting'.

A N D acknowledges support by the Bundesministerium für Bildung und Forschung (BMBF) through the Project 03Z22AN11.

This material is based upon work supported by the National Science Foundation Graduate Research Fellowship Program under Grant No. DGE-2034835. Any opinions, findings, and conclusions or recommendations expressed in this material are those of the author(s) and do not necessarily reflect the views of the National Science Foundation. This work was also supported by the National Science Foundation under Grant No. 2109232.

4. Spectroscopic applications enabled by photonic lanterns

Sergio-Leon Saval[1], *Steph Sallum*[2], *Stephen Eikenberry*[3] *and Kevin Bundy*[4]
[1] Sydney Astrophotonics Instrumentation Laboratory (SAIL), School of Physics, The University of Sydney, Sydney, Australia
[2] Department of Physics and Astronomy, University of California, Irvine, CA, United States of America
[3] CREOL, The College of Optics and Photonics, University of Central Florida, Orlando, FL, United States of America
[4] Department of Astronomy and Astrophysics, University of California, Santa Cruz, CA, United States of America

Status

Conventional astronomical fiber-fed spectrographs use MM optical fibers to feed telescope light to a disperser. These fibers can be sized to match the width of the point-spread function (PSF), providing more efficient light capture compared to their telecom counterpart, SMFs [118]. However, these spectrographs are larger and limited in spectral resolution compared to diffraction-limited platforms fed with SM fibers. These have recently been demonstrated for precision RV measurements [119–121] for example, but require high performance AO systems to prevent significant fiber coupling losses [50, 122]. PLs offer a powerful solution for efficient diffraction-limited spectroscopy by converting MM inputs to SM outputs (figure 6(A) and (C)). This reduces AO performance requirements, enabling near-diffraction-limited spectroscopy at the outputs [123–125]. As a result, PLs have recently emerged as a viable technology for the following applications: spectro-astrometric imaging; efficient combination of light from small telescope arrays; and massively-multiplexed spectroscopy for wide fields of view.

Spectroastrometry (SA [126];) involves using spectral centroid shifts to infer the presence of wavelength-dependent morphology within the diffraction limit (as depicted in figure 7(C)). Traditionally carried out with slit spectrographs both with and without AO (e.g. [127]), conventional SA's astrometric precision is set by the PSF width and signal-to-noise ratio, with precision <1 mas for the best AO experiments [128]. Even AO-corrected SA can suffer from PSF variability (e.g. [129]), and PLs have recently been demonstrated in simulation as an avenue for recovering SA signals in the presence of variable correction [130] (figure 7(C)). For example, hydrogen line signals from accreting planets can be recovered for achievable tip-tilt jitters of 0.1 λ/D. Furthermore, since SM output intensities encode pupil plane phase variations, PL spectro-astrometry does not suffer from position angle degeneracies present in conventional approaches, making it a promising technique for complex scenes such as resolved circumstellar disks and outflows.

A second PL application involves combining light from arrays of incoherently-linked smaller telescopes. Such arrays have recently emerged as a reduced-cost (by $\sim$10$\times$ per unit area) method of increasing telescope collecting area for spectroscopy of faint sources [131–134]. In the PolyOculus implementation (figure 7(A)), packs of semi-autonomous, small (25–40 cm), off-the-shelf telescopes comprise the array [132]. PLs that incoherently combine several multi-/few-mode fibers into a single MM fiber offer particular advantages for combining the light, because they preserve etendue without oversized downstream pupils [132]. PolyOculus has demonstrated '7-pack' PL light combiners with $>$90% efficiency across the visible [135], producing a collecting area equivalent to a $\sim$0.9 m telescope (figure 7(B)). Furthermore, using multiple seven-pack arrays, the PL outputs can be spliced to optical fibers which then feed into another PL combiner. This approach can be extended, providing a hierarchical scaling to build collecting areas equivalent to the 30–40 m diameter mirrors of upcoming Extremely Large Telescopes.

Finally the ability of astronomical spectrometers to measure multiple target spectra simultaneously (i.e. the multiplex; e.g. SDSS, DESI, SAMI; [136–138]), has enabled major progress in cosmology, galaxy formation, and stellar astrophysics. The state-of-the-art is the DESI facility, which collects 5000 simultaneous fiber spectra across an eight square degree field on a 4 m telescope. Future instruments with 4–10 times greater multiplex on larger telescopes are already under consideration. With a conventional design, such an instrument would be impractical, exceeding the cost of the telescope itself. Mass-produced photonic spectrometers, however, offer a path toward greatly reducing the 'cost per spectrum' (e.g. a 'spectrometer-on-a-chip'; sections 6 and 7). Because these devices typically demand single- or few-mode input, PLs will play an important role by extracting the modal components of potentially thousands of on-sky sources.

Current and future challenges

Currently, PLs have achieved high performance with transmission efficiency of $>$90%. However, lanterns have been constrained in terms of the number of inputs and outputs. PLs with up to 19 output SMs are fairly standard, but larger port number devices would be desirable. They would enable more efficient combiners

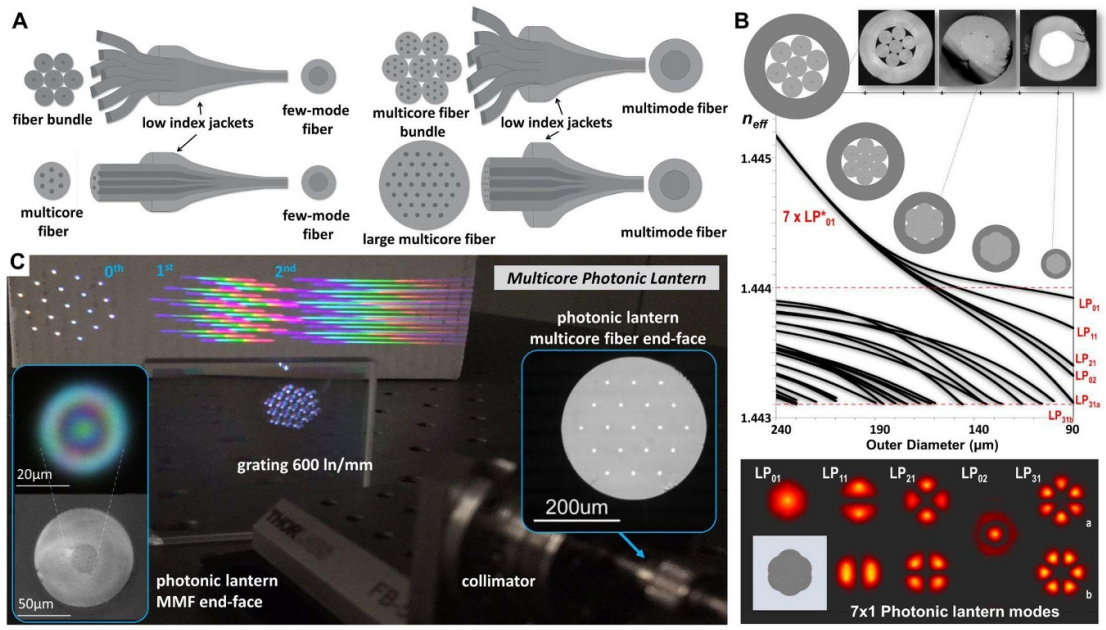

Figure 6. (A) Schematics of all-fiber photonic lanterns, including: few-moded photonic lanterns conventionally fabricated using single-mode fibers or a single multicore (left), and highly-multimode photonic lanterns fabricated from one or several multicore fibers (right). (B) Simulation of the modal evolution as a function of the waveguide tapering factor, including cross-sectional images of a 7 × 1 photonic lantern along the transition and the supported simulated modes. (C) Actual images of a multicore photonic lantern device 'converting' multimode light in the visible (450–750 nm) to an array of single-mode outputs wavelength-dispersed by a volume holographic grating in the lab.

for telescope arrays, more versatile reformatting for integral field and multiplexed spectroscopy, and more detailed recovery of asymmetries via spectro-astrometry.

Increasing the number of PL modes relies on increasing the number of fibers or cores in a multicore (figure 6(A)). Scaling to a large number of fibers is challenging due to manufacturing limitations related to handling hundreds of individual fibers and limitations on the maximum diameter handled by glass processing equipment (e.g. splicing, tapering). However, MCFs reduce some manufacturing limitations and could offer hundreds to thousands of cores. To date, the devices with the highest port counts constructed from individual SMFs are 1 × 61 [14], and 1 × 88 with reduced SMF cladding diameters [20]. The largest single multi-core PL with SM cores have 121 cores [139]. A 600 μm-diameter, 511-core multi-core lantern was reported in Birks 2015. However, this PL, intended for fiber scrambling, contained a mix of SM and few-mode cores.

The need for high-performance, wide-field AO presents an additional challenge for high-multiplex instruments with large fields-of-view (e.g. >1° diameter; [136–138]). Diffraction-limited performance on large ground-based telescopes across several arcminutes is currently infeasible, although modest corrections are possible with ground-layer adaptive optics (0.3″ FWHM over 8 arcminute fields; [140]) and multi-conjugate adaptive optics (MCAO; ∼25% Strehl over ∼2 arcminute fields-of-view [52]; and references therein). For instruments with fields-of-view comparable to MCAO correction, the architectural goal would be to optimize coupling efficiency, number of modes, and field-of-view, to achieve acceptable coupling efficiency without prohibitively high requirements on the number of lanterns, outputs, and instruments. While the AO system can reduce the number of modes, high-performance low-mode-count (<19) lanterns will be needed to take full advantage. Although such devices have been demonstrated, reliable reproduction and connectorization of such lanterns remains a challenge. For wider fields—i.e. where Strehl remains low—the challenge lies in identifying and filtering the most valuable SMs from the low-Strehl, multi-mode light. For example, a PL 'speckle spectrograph' (where individual speckles are spatially directed to a spectrograph; [141]) may reduce sky noise and boost signal-to-noise, compensating for ignoring many fainter, more spatially-distributed modes.

Advances in science and technology to meet challenges

One solution to increase the desired number of modes (i.e. inputs/outputs) in PLs systems may be to implement 'hierarchical' PLs [21]. In this concept, a large field-of-view PL efficiently separates the light into a large (but manufacturable and manageable) number of MM output fibers. Each multi-mode output feeds into another PL that further subdivides the light. This cascade can be repeated until each output reaches the

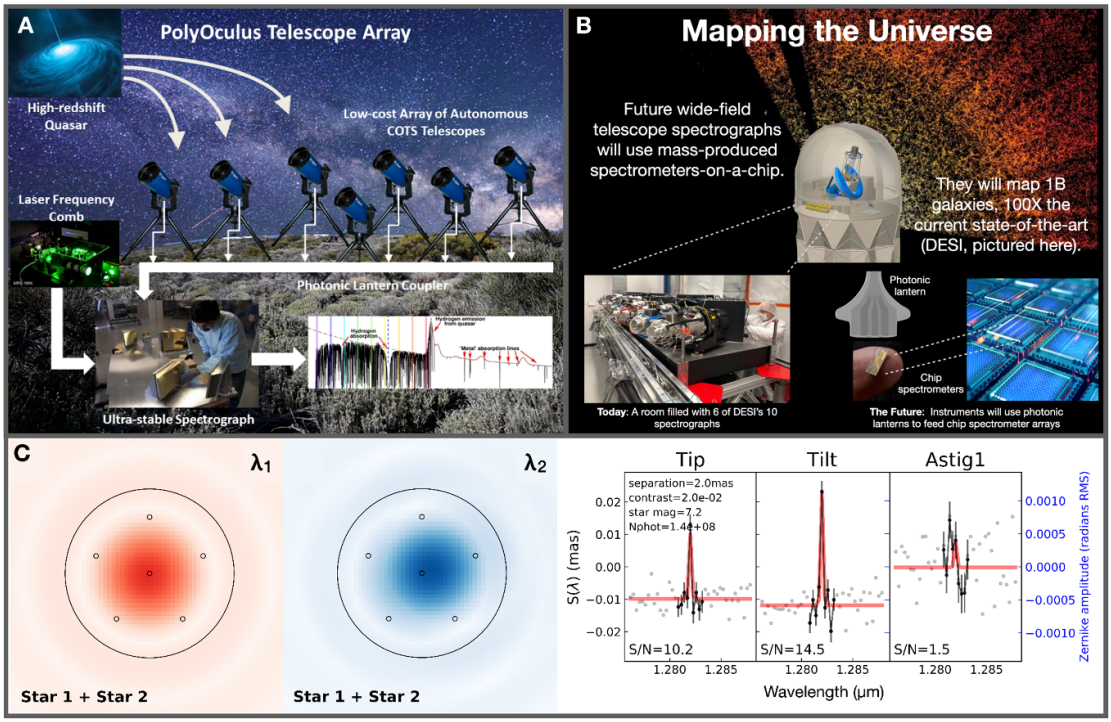

Figure 7. Spectroscopic photonic lantern applications. (A) Schematic layout of the PolyOculus telescope array concept. An array of small autonomous telescopes point to the same target on the sky, with fiber optic feeds coupled via high-efficiency photonic lanterns into a single fiber, which feeds into a scientific detector. (B) Illustration of the state of the art in massively-multiplexed spectrographs, future instruments enabled by photonic lanterns and chip spectrometer arrays, and their anticipated science outcomes. (C) Simulation of photonic lantern spectroastrometry. Companions with excess flux relative to the primary star at specific wavelengths (left) can be detected within the classical diffraction limit by measuring spectral centroid shifts. These signals can be modeled as Zernike modes, illustrated in the right panels showing an injected and recovered protoplanet with Pa-β excess emission (adapted from [130]). Reprinted with permission from [Xanadu X8 quantum photonic processor: Xanadu]. Reproduced from [130].

desired modal content—be it single-, few-, or (smaller) multi-mode. With this approach, lanterns with relatively modest output numbers (∼19) could approach ten-thousand-mode outputs with only three hierarchical levels.

Generally, fabricating complex lanterns as described above is possible, with limitations imposed by the system's scientific and/or technical applications. For example, limitations to realizing practical, high-order lanterns are imposed by the need to potentially share light between a science instrument and a WFS, in which case some cores would physically be split off from others. These requirements will impact both the manufacturability and functionality of the lantern. Additionally, manufacturing and engineering challenges will need to be overcome to achieve integration and connectorization of these systems for rugged use in observatory environments.

Hybrid PL devices may soon allow for increasing the number of modes while improving AO performance [87]. Hybrid PLs are made with dissimilar fibers, and can divide light from an MM fiber into separate science and wavefront sensing fiber arrays. These could potentially bring the best of both worlds: single- or few-mode fiber coupling to a science instrument, and simultaneous wavefront sensing without non-common path errors (as discussed in section 3). This would, for example, improve spectroastrometric precision by providing a better, more stable point spread function, and by allowing for selection of science fibers that optimally recover asymmetries in the target. Furthermore, deploying many of these devices could improve AO correction for large fields-of-view, highly-multiplexed instruments, enabling more efficient spectroscopy of faint, distant objects.

Concluding remarks

PLs present an opportunity for efficient, diffraction-limited spectroscopy using both single-object and wide-field, highly-multiplexed instruments. While these devices have been demonstrated to provide high coupling efficiency for a small number of inputs/outputs, their versatility for astronomical observations would be improved by: (1) manufacturing devices with larger numbers of inputs/outputs, increasing the number of PL modes, (2) developing techniques to extract the most valuable modes from low-Strehl light, and (3) manufacturing devices where outputs can be physically separated for simultaneous applications

(i.e. science and wavefront sensing, which would improve AO performance for both narrow and wide fields-of-view). Future applications of these enhanced PLs will lead to new observational constraints for a wide range of sub-fields, from cosmology, to galactic astrophysics, to stellar and planetary formation and evolution.

Acknowledgments

This work was also supported by the National Science Foundation under Grant No. 2109232.

5. New optical fibers for astrophotonics

Stephanos Yerolatsitis[1], *Rodrigo Amezcua-Correa*[1], *Itandehui Gris-Sanchez*[2] *and Julia Bryant*[3]
[1] CREOL, The College of Optics and Photonics, University of Central Florida, Orlando, FL, United States of America
[2] Institute of Telecommunications and Multimedia, Universitat Politècnica de València, Valencia, Spain
[3] Sydney Institute for Astronomy (SIfA), School of Physics, The University of Sydney, Sydney, Australia

Status

Fiber optics have been used in several diverse areas of astronomy since the early 1980s [142–145] and are nowadays commonly deployed at a large number of telescopes. They have been routinely used to transport light from the telescope's focal plane to a spectrograph and to optically multiplex telescopes, linking remote instruments to enable interferometric observations [143, 146, 147]. In this regard, fiber optics has become a powerful tool used to simultaneously observe thousands of astronomical objects, allowing the realization of massive spectroscopic surveys for the first time (2dFGRS: [148], SDSS: [149]) and integral field spectroscopic surveys (SAMI: [136], MANGA: [137]) Most of these developments in astronomical instrumentation have so far relied almost exclusively on using optical fibers as efficient light pipes. However, processing light in an optical fiber system can provide unprecedented opportunities in many areas of astronomical instrumentation where current approaches are still in need of a solution. In practice, fibers are already providing some degree of signal processing in telescope settings, for example, they are used as spatial [150, 151] and spectral [24] filters, efficient mode scramblers [17], to feed light into PICs [152, 153] and in the development of PLs to mention a few [20, 154]. The difficulty of implementing new fiber technologies and PICs in general for astronomical instruments arises from the MM nature of the light being collected at the telescope's focal plane. This demands fibers and fiber devices supporting 1000s of spatial modes with low loss, broadband operation, and for some applications without significant mode mixing. High performance adaptive optic systems can help reduce the number of modes that need to be supported, but are limited to narrow fields of view (1–2 arcminutes) [52].

In the last decade, the demand to increase capacity in optical communication systems ensued a flurry of activities on space division multiplexing that utilizes spatial modes in MM and multicore fibers in addition to conventional multiplexing techniques. These research activities not only led to new classes of MM and multicore optical fibers but also new components to tailor and control MM light [48, 155–157]. These optical fiber-technology advances greatly overlap with and can drive the development of specialty tools for astronomical instrumentation.

This paper focuses on silica fibers, but we note that fibers for mid-IR wavelengths based on other glass materials have evolved tremendously and are also important for astrophotonics instrumentation. Here, we outline opportunities with new fiber designs and describe their challenges and necessary advances for their successful employment in current and future astronomical instruments.

Current and future challenges

Few Mode, MM, and Multicore Fibers are any fiber supporting more than one spatial mode, including graded-index, flat-top, and fibers with unique refractive index profiles.

Graded index fibers exhibit less mode coupling compared to step-index fibers, due to their refractive index profiles. Therefore, graded-index fibers or fibers with specially tailored refractive index profiles can be used to reduce focal ratio degradation (FRD). On the other hand, flat-top fibers are specially designed to scramble the mode content propagating in their core, by tailoring the mode power distribution. They can thus achieve a complete mixing between the modes of the fiber, enabling strong mode-scrambling of the output pattern of the fiber. These fibers can be used to mitigate modal noise which can cause inaccuracies in the measured spectra for RV observations [158]. Multicore fibers with graded index cores or flat-top cores can also be realized. Different types of multicore fibers have been extensively investigated in telecommunication applications as a way to increase transmission capacity. We show some examples in figure 8. It is important to highlight complementary technologies such as fan-ins [157] and 3D-printed microlenses [82, 159, 160] to couple light to each core/channel and to increase coupling efficiency and decrease the gaps in the IFU have seen tremendous advances. Nevertheless, developing broadband low-loss complementary technologies with a large-number of spatial channels remains a challenge and an active area of research.

Fibers with unique index profile: By tailoring the refractive index profile of solid core fibers, fibers with unique performance capabilities can be realized. Here, we discuss two such examples. The first is an Airy fiber: a fiber featuring a complex refractive index profile (shown in figure 9) that allows the efficient coupling of an Airy pattern mode, increasing the coupling efficiency from the telescope to the fiber up to 93.7%. A

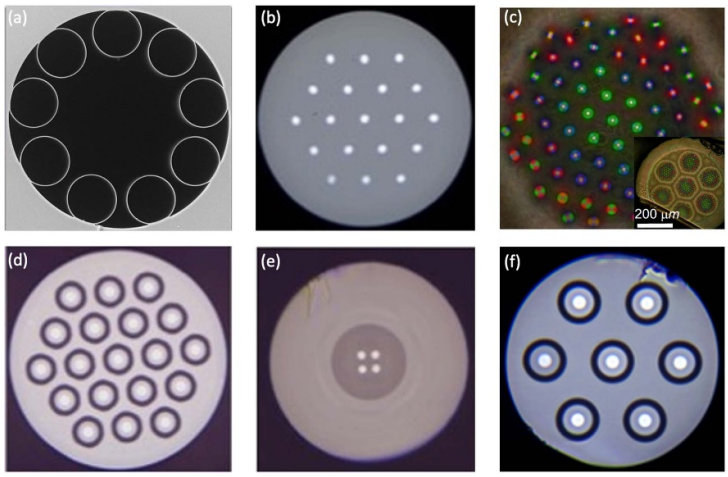

Figure 8. (a) Scanning electron image of an AR-HCF. The hollow-core is surrounded by an antiresonant cladding structure which consists of nine thin silica tubes. (b)–(f) Micrographs of multicore fibers featuring different index profiles and wavelength operation range.

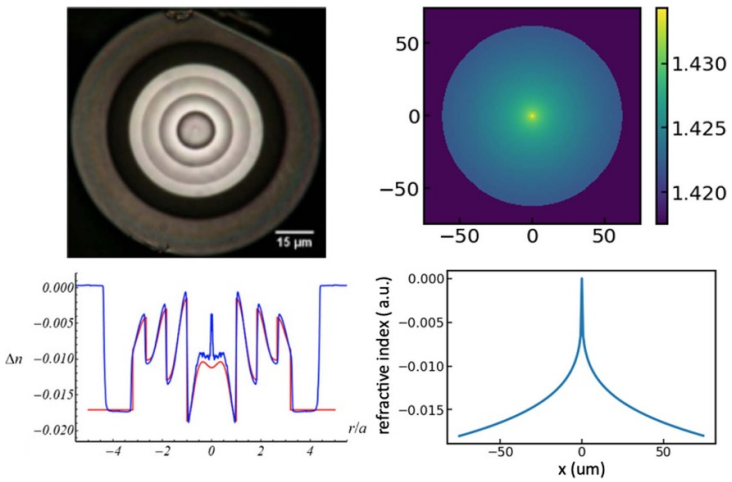

Figure 9. (top left) Optical micrograph of the Airy fiber (bottom left) physical refractive index profiles of the designed Airy (red), and of that of the PCVD preform (blue). Reproduced from I. Gris-Sánchez *et al* [161], (CC-BY 4.0). (top right) 2D theoretical refractive index profile of a fiber with logarithmic profile.(bottom right) 1D refractive index profile of the same fiber (relative to undoped silica). Reproduced from [161]. CC BY 4.0.

significant improvement over the theoretical limit (80%) of coupling a beam from a circular aperture to the fundamental mode (Gaussian-like) of an ordinary step-index SMF. This was achieved by inversely designing the fiber to support an approximate Airy pattern [161]. Nevertheless, due to the complex refractive index profile, the fiber guides more than one mode, while the airy mode is not the lowest order mode of the structure.

The second example is a fiber featuring a logarithmic index profile [162]. In many applications including astronomical instrumentation, it is desirable to effectively combine light from different sources. This is usually done by fusing and tapering gradually many fibers together. In this process, the main limiting factor on the number of fibers that can be combined is the fulfillment of the adiabatic criterion which in turn dictates the requirement of a minimum transition length. In contrast, an optical fiber with a logarithmic refractive index profile can be adiabatically tapered over any length, however short, enabling the development of a new class of fiber components, including couplers and PLs. The fiber's mode field distribution is independent of the fiber's size and therefore does not change as the fiber is tapered down (i.e. it remains the same along the transition). Nevertheless, developing low-loss PLs using such fibers that support a large number of modes (>1000) still remains a significant challenge that needs to be addressed. The required transition length for adiabatic propagation increases with increasing number of supported modes and can become the limiting factor for realistic implementations.

Hollow core fibers (HCFs): Recent advances in the design of HCFs led to the development of a new class of antiresonant HCFs with remarkably low losses [163, 164]. In their simplest form, these fibers consist of a hollow core with a ring of anti-resonant cladding tubes surrounding the core as shown in figure 8. A unique feature of HCFs is that most of the light (>99.99%) can be guided in the central air-core with only a tiny fraction of light overlapping with the surrounding glass structure, hence increasing the optical damage threshold, and reducing material absorption significantly. In addition, these fibers are simpler to manufacture, omitting the complicated structure of previous HCFs. By precisely designing the structure of this fiber to match specific conditions (such as the core-to-cladding tubes ratio), SM behavior can be achieved. Due to their remarkable transmission properties, recent interest led to the first experimental realization of AR-HCFs with extremely low loss (0.174 dB km^{-1} at 1550 nm which is on the same scale as SMF) and improved guidance [163]. This recent spark of interest opens up possibilities in developing novel HCFs for guidance in wavelengths that silica fibers cannot operate such as UV (even extreme-UV) and mid-IR. In turn, these wavelengths can result in spectroscopic measurements that are currently prohibited due to the use of conventional fibers. For example, the UV spectrum can be utilized to interrogate the planetary atmospheres for specific molecular species. In addition, UV LGS are interesting alternatives to Rayleigh guide star AO applications [165, 166]. HCFs offer the prospect of being able to mount the laser in a stable environment off-telescope and transport the light to the launch telescope via fibers, improving safety at the observatory as compared to mirror relays as well as providing improved stability for the launched laser. In the mid-IR (>2.0 μm), there is currently only one fiber fed spectrograph in operation [74] and it utilizes ZBLAN fibers. These fibers are significantly more lossy than HCFs and therefore HCFs could enable a wave of fiber-fed spectrographs operating at the diffraction-limit in the mid-IR [121]. Such spectrographs could be utilized for RV measurements, the direct characterization of exoplanets and brown dwarfs [167] and for studying highly redshifted light of distant galaxies, newly forming stars, and faintly visible comets. Finally, HCF fibers could also be used to realize very long baseline (km scale) MIR interferometers, which are not possible with current technologies (see section 18 for details). Processes leading to the routine connectorization and termination of AR-HCFs need also to be investigated. This in turn will enable the successful incorporation of AR-HCFs to existing photonic technologies.

AR-HCFs are inherently MM although they suffer from mode-dependent loss; higher-order modes tend to attenuate quicker compared to the fundamental mode. Nevertheless, AR-HCFs can be designed such that the higher-order modes have comparable losses to the fundamental mode. In order to achieve this and maintain low-loss guidance, additional cladding elements are utilized [168–170]. Similar to standard solid-core fiber, we can increase the number of guided modes by increasing the HCF's core size. MM AR-HCFs can significantly increase the collection efficiency of any system at wavelengths (such as visible/UV and mid-IR) where the performance of silica is hindered due to photodarkening/solarization and where other multicomponent glass fibers have not reached the required performance levels. Current fabrication processes prohibit the realization of continuous long lengths of AR-HCFs, especially for mid-IR applications where the core size and the surrounding structure of the HCF need to be significantly larger to achieve the desired low-loss guidance compared to near-IR/visible wavelengths. It is important to mention technologies such as mode adapters/reformatters, fiber combiners and splitters also need to be developed to effectively incorporate these fibers with current technologies [171].

Fiber materials other than silica: Alternative materials such as ZBLAN and chalcogenide are also used to construct optical fibers and have been used in astronomy [74], and silicon core fibers with low-loss optical windows upto 3.3 μm [172] However, the former technologies are extremely brittle. This not only makes handling them difficult, but also limits the maximum length of a single piece to the order of 70–100 m. Although there are efforts being made to improve losses, these fibers still have a long way to go to reach the maturity and applicability of silica fibers.

Advances in science and technology to meet challenges

In addition to the fiber technologies outlined above, complementary technologies like fiber components need to advance for these fibers to be applicable to astronomy. For future applications, we envision the development of a range of in-line fiber technologies based on these novel fibers. These can include broadband fiber splitters, polarization beam splitters, large-channel fan outs, etc. New functionalities can be incorporated to the fibers, for example, separating the cores from a MCF to perform different measurements. These devices will require new fabrication techniques and may need other materials.

HCFs with polarization-maintaining properties and HCF devices such as beam-splitters could have a major impact on future astronomical instruments. Nevertheless, as mentioned above, to achieve HCFs with improved performance and low-loss guidance in the mid-IR and UV region new fabrication techniques need to be exploited. At these wavelengths, any non-uniformities at the final structure of the fiber will have

significant implications in their optical performance. Precise control of the drawing process of these fibers needs to be exploited.

A significant challenge that needs to be addressed is the scalability of the technology for the next-generation of fibers that scramble or prevent scrambling of the modes; i.e. to achieve the desired performance with an increased number of modes. To accomplish this, designs with complex refractive index profiles need to be exploited as increasing the number of modes (by increasing the core size) of the current fiber designs will result in degraded performance. Artificial intelligence (AI) techniques can be utilized for this purpose, enabling for the first time the realization of fibers with unique refractive index profiles designed specifically for astronomical applications.

Current MCF technologies have enabled significant advances in various areas of astronomy. Nevertheless, there is a constant desire to increase the number of cores as well as the packing efficiency (>90%) of these MCFs. Minimizing the gaps between cores enables more efficient collection of astronomical light and eliminates the need of lens arrays at the input to these fibers. Nevertheless, the core-to-core coupling increases significantly with decreasing separation. A significant challenge that needs to be overcome is minimizing the core-to-core coupling and therefore maintaining the uncoupled nature of the fiber. One way to increase the packing efficiency while minimizing the coupling between cores is by using cores with different refractive-index profiles including complex profiles. This is again an area where AI can be of significant value. In addition, it is important to mention that developing fan-outs for MCFs with many cores is not straightforward. Nevertheless, complementary technologies such as ultra-fast laser inscription can be utilized for this to develop high-precision fan-out systems [173].

Concluding remarks

In recent years, fiber optic technology has seen tremendous advances which resulted in the development of unique fiber designs. These advances can feed the development of a new class of astronomical instruments. Fibers with unique profiles can be used either to effectively scramble the light or to minimize FRD. Novel fiber designs such as the log fiber and Airy fiber can be utilized in the fabrication of fiber devices for feeding light to the next generation of spectrographs. Furthermore, hollow-core fibers hold great promise in advancing the field of astronomical instrumentation. Low-loss hollow-core fibers for visible/UV and mid-IR guidance can be employed for new astronomical surveys, collecting light at wavelengths where previously we could not imagine that it would have been possible.

6. Getting on-chip arrayed waveguide grating spectrographs ready for astronomy

Pradip Gatkine[1], *Andreas Stoll*[2] *and Yang Zhang*[3]
[1] Department of Astronomy, California Institute of Technology, Pasadena, CA, United States of America
[2] Leibniz Institute for Astrophysics Potsdam (AIP), Potsdam, Germany
[3] Electrical and Computer Engineering Department, University of Maryland, College Park, MD, United States of America

Status

The volume, mass, cost, and complexity of seeing-limited spectrographs grow as the square of the telescope diameter. Building on-chip astrophotonic spectrographs is a promising approach for both ground- and space-based telescopes in order to achieve compactness (given the SMF feed), flexibility (with the ability to manipulate the amplitude, phase, and polarization in waveguides), thermo-mechanical stability (given the small size and no moving parts), and cost-effective replicability. They are ideally suited for capturing the adaptive-optics-corrected light and realizing various science cases, such as characterizing exoplanet atmospheres, precision RV measurements, stellar chemistry/kinematics, planetary missions, and remote sensing. Multi-object spectroscopy can also be achieved by leveraging the stackability and replicability of the chips. The benefits of astrophotonic spectrographs go well beyond astronomy including biomedical sensors, industrial chemical detection, etc [174].

AWGs and photonic echelle gratings (PEGs) are well-known and mature technologies used in photonic wavelength-division-multiplexing [175]. However, astronomical spectroscopy poses unique and stringent specifications including high efficiency, broadband (eg: J and H bands), high resolving powers ($\lambda/\Delta\lambda > 10\,000$), and polarization independence [56, 176]. While PEGs can deliver high resolving powers, achieving smooth on-chip reflecting surfaces is challenging due to fabrication limitations [177]. AWGs, on the other hand, require simpler fabrication schemes and can deliver high efficiency (>75%), which makes them more suitable for astrophotonic spectroscopy [10]. Hence, we focus on improvements needed in the AWG architecture to make it science-ready. Cascaded dispersive architectures (two or more on-chip dispersers) are also widely discussed offering various benefits, such as on-chip order separation, adaptable component design, and potential tunability (eg: micro-ring resonator + AWG [178, 179] or cascaded AWG [180, 181]). Since AWGs require long path delays with bends, low-loss material platforms are desirable, with the most promising being Silica and silicon nitride.

Silica

Silica-based passive integrated photonic device technology is an attractive choice for astrophotonics due to the high coupling efficiency to fibers and excellent transmission characteristics from the visible to the NIR (J, H, and K-bands). Astrophotonic AWGs on a 2% refractive index contrast silica platform with R $\sim$ 10 000–36 000 and efficiencies of up to 72% in the H-band have been recently demonstrated experimentally, using three-stigmatic-point geometry for focal field flattening [182].

SiN and high-contrast AWGs

AWGs need curved waveguides to introduce the path differences. Smaller radii of curvatures can help achieve smaller device footprints, and hence lower susceptibility to material/process variation (and thus, the effective index variation) across the chip. The higher contrast ratio offered by the silicon nitride (Si_3N_4) material platform allows low-loss radii of curvature as small as 100 μm, depending on the thickness of Si_3N_4 [183]. Further, ultra-low propagation loss has been demonstrated in Si_3N_4 over a broad band (400–2400 nm) [184], making it suitable for astronomy [185]. This has encouraged several implementations of Si_3N_4 AWGs [186–188].

Current and future challenges

For astrophotonic spectrographs, the primary losses occur at the interfaces between the telescope focal plane and optical fibers, between fibers and photonic chips due to imperfect mode matching, and within the PICs due to propagation losses and scattering at discontinuities of the effective refractive index. Efficient coupling of starlight to SMFs becomes increasingly challenging with growing telescope diameter and focal spot size. However, coupling to SMFs with AO on large telescopes (>4 m) is becoming more common now [189] and is discussed in section 2. The current challenges in making the photonic spectrographs science-ready are discussed below.

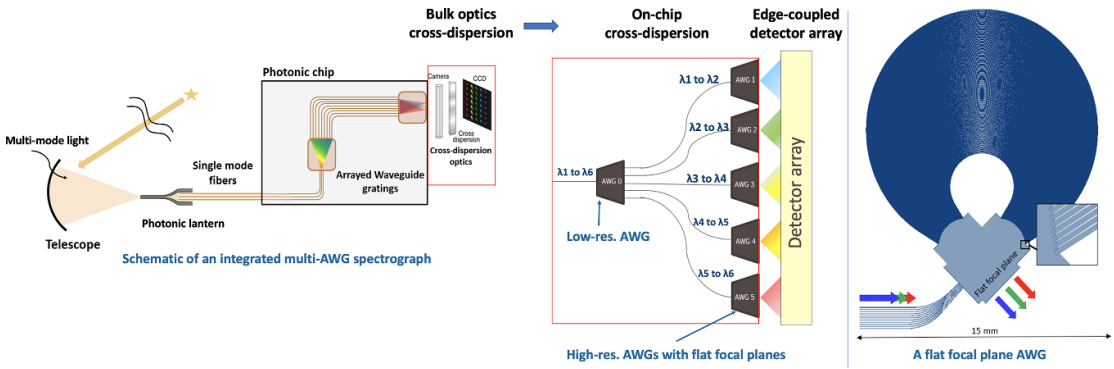

Figure 10. *Left:* the schematic of a conventional AWG spectrograph from telescope to detector (with bulk optics cross-dispersion), and that of a cascaded AWG architecture with on-chip order separation and an edge-coupled detector array. *Right:* three-stigmatic-point AWG architecture in a folded configuration.

AWG loss

The biggest source of insertion loss in an AWG is the waveguide-slab interface [187]. Interface losses occur mostly during the two transitions between the waveguide array and the free propagation slabs. Hence, achieving the highest efficiency across these transitions is crucial. Further, coupling of light into and out of the chip is a key contributor to the loss due to mode mismatch and Fresnel reflection, particularly for high-contrast integrated platforms such as Si_3N_4. Recent developments in low-loss on-chip spot-size converters/tapers [190] and off-chip interposers have demonstrated high fiber-chip coupling efficiency [191].

Phase errors

High-resolution AWGs ($R > 20\,000$) require a larger number and longer length of arrayed waveguides, leading to a significant increase in the footprint of the device. Phase errors arise due to material/process variations across the chip, causing systematic and random variations in the effective refractive indices of individual waveguides. They become more significant as AWG size increases [192, 193]. Phase errors degrade the AWG performance by decreasing power in the main lobe and increasing the cross-talk. For instance, an AWG at $R \gtrsim 24\,000$ requires precise control of the optical path lengths of the order of ∼10 ppm to ensure sharp constructive-interference peaks with minimal crosstalk [194, 195]. Fabrication of such high-R AWGs becomes increasingly difficult with a larger ($N > 300$) number of arrayed waveguides due to path length accumulation of several centimeters. Correcting the phase errors using EO, thermo-optic effect or piezoelectric modulation is possible [196]. However, incorporating a phase shifter (∼1 mm × 1 mm size) for every waveguide ($N \sim$ hundreds) can prohibitively increase the chip size and cost (see section 23 for more details).

Cross-dispersion

The free spectral range (FSR) of high-resolution AWG devices varies between 10 and 20 nm which necessitates spectral order separation by cross-dispersion to cover a range of several hundred nanometers or an astronomical band. Semi-integrated spectrographs achieve order separation using bulk-optics cross-dispersion, which limits the potential for miniaturization [152, 197]. Truly integrated spectrographs require full integration of imaging optics and detectors on the chip [198, 199]. Alternatively, on-chip order separation using tandem/cascaded AWG architectures [181] will help achieve direct edge-coupling with off-chip detector arrays (figure 10). Implementation of ultra-low-loss single-stage AWGs and minimizing the inter-channel spectral dropout in the coarse AWG stage are essential to enable low-loss tandem AWGs.

AWG focal plane

The AWG focal plane is curved (Rowland circle). In conventional AWGs, the output spectrum is discretely sampled by the waveguides in discrete spectral channels, leading to inter-channel gaps. However, in astronomy, a continuous, gapless spectrum is desired. To achieve that, the curved focal plane of the AWG needs to be imaged, which poses challenges in cleaving along the curved surface and imaging a curved plane on a flat detector [200]. The three-stigmatic-point technique can help achieve a flat focal plane (figure 10(b)), thus alleviating these challenges [182, 201–203]. The flat focal plane minimizes the defocusing aberration of off-centered channels and allows a direct bonding of the detector to the focal plane of the chip. Accurately etching/cleaving/polishing the chip-edge to expose the exact focal plane is important to minimize defocusing.

Polarization dependence

Most photonic waveguides are birefringent (i.e. different effective indices for TE and TM modes) due to imperfect symmetry of the waveguide cross-section shape. At high resolving powers ($R > 20\,000$), waveguide birefringence causes significant relative separation in the TE- and TM-mode spectral channels, resulting in broadening of the composite channels and reduced spectral resolution in the unpolarized regime. High-resolution AWGs are therefore restricted to fully polarized light unless waveguide birefringence can be adequately compensated for. One solution is to split the polarization using low-loss free-space or fiber-based or on-chip polarization splitters (e.g. [204]), and then rotate the TM-polarized output (e.g. [205, 206]) to feed two copies of the TE-optimized AWG. Alternatively, birefringence-compensating designs such as waveguide cross-section engineering [207], varying waveguide width within the array [208], or slanted FPR-waveguide array interface [209] can be used.

Advances in science and technology to meet challenges

To achieve the vision of compact, fully integrated, high-resolution/broadband, and massively replicable astrophotonic spectrographs/IFUs for ground- and space-based telescopes, the following advances are critical, addressing the challenges of throughput, phase errors, and imaging of the dispersed spectrum.

1. **Innovative AWG component designs for low on-chip loss:** Tapers have proven effective in minimizing FPR-waveguide interface loss. Specific taper geometries can achieve an adiabatic transition. Sub-wavelength structures [210, 211], multi-mode interferometers (MMIs), and inverse-design tapers [212] can also be used to eliminate interface losses. UV-lithography limits the closest separation between the tapers (due to minimum feature size ∼200 nm), thus creating gaps, which lead to losses. E-beam lithography is well-suited to fill these gaps (minimum feature size ∼5 nm), however, it is not scalable. Hence, novel designs (eg: with thinner waveguide cores) are needed that can offer ultra-low loss with the scalable stepper-lithography process [213, 214].
2. **Phase-error correction:** Current state-of-the-art AWGs use EO, piezoelectric [215], or thermo-optic phase shifters integrated on the arrayed waveguides for post-fabrication phase-error correction [196, 216]. However, the elimination of phase errors at the source using tighter fabrication process control and minimal-phase-error designs [217] is the ideal solution for achieving high-throughput, high-resolution AWGs. Phase error control techniques for silica AWG devices require post-fabrication phase error measurements and treatment by UV trimming [218], which is not feasible for mass production unless automated post-processing facilities are implemented. An alternative novel method of phase control can be implemented via programmable photonics [219], allowing *in-situ* phase adjustments on individual optical paths, which opens the possibility of mass-produced self-correcting AWGs.

   A novel architecture called reusable-delay line AWG utilizes an optimized array of directional couplers to distribute the input signal from the delay line into the free propagation region (figure 11.(4)). It is a potential solution to reduce the impact of fabrication imperfections and non-uniformity for ultra-high resolution ($R > 50\,000$) AWGs [220]. This architecture can be ∼100 times more compact than the traditional AWGs.
3. **On-chip order separation:** Tandem AWGs can be designed to separate the spectral orders to cover broad bands uniformly (figure 10). For the micro-ring resonators + AWG concept (figure 11), the quality factor of the resonators is the source of the high spectral resolving power. It is challenging to choose the radius of the rings such that the set of peaks is shifted very slightly to achieve uniform coverage. However, the peaks can be tuned after fabrication using thermo-optic modulators.
4. **Efficient coupling of light into and out of the chip:** The light can be efficiently injected from SMFs to waveguides using lensed fibers and/or adiabatic inverted tapers (∼95%) [190]. For certain material platforms, inverse designs [221, 222] or low-loss interposers are more appropriate [223]. Getting the light out of the chips efficiently is challenging for high-index-contrast materials (Si_3N_4, SOI). Currently, high-NA microscope objectives are used to image the AWG focal plane onto a detector. However, they have a small FoV (∼1 mm). With the goal of moving away from bulk optics, one could consider solutions such as NA-matched microlens arrays with 100% fill factor [224–226] or 3D-printed lenses on chip [80, 227] need to be explored for better integration.
5. **Detector integration:** Several approaches are being tried to achieve true integration of photonic spectrographs + detectors, with no moving parts. Integration of energy-resolving MKIDs as cross-dispersing detectors is a promising approach (see section 25). Alternatively, tandem AWGs perform on-chip cross-dispersion and allow direct integration of detectors via heterogeneous material platforms (eg: Si + Ge or Si + InP) [228,229,234]. Small-pitch linear detector arrays need to be developed for directly butt-coupling with the output FPR of cascaded AWGs (figure 10(a)). Other approaches include sending the light upwards from the chip using efficient grating couplers/metamaterial optimized for

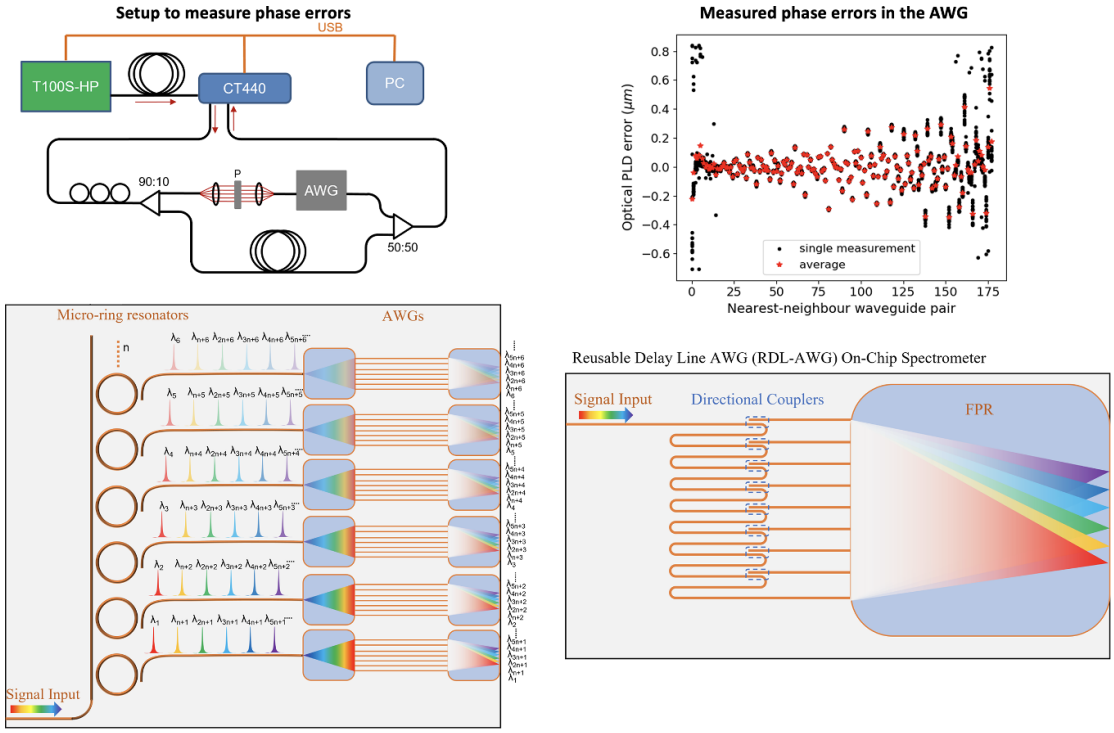

Figure 11. Top-left: fiber-based frequency domain interferometer setup to measure AWG path-length errors; Top-right: measured optical path length error between adjacent waveguides in a silica AWG . Reproduced from [233]. CC BY 4.0. © [2022] IEEE. Bottom-left: an integrated photonic chip with a cascaded array of ring resonators (thermally tunable) and AWGs. Bottom-right: a schematic of the arrayed waveguide grating with reusable delay lines (RDL-AWG). Reprinted, with permission, from [220].

different wavelengths [230] (for discrete AWGs) or an inclined reflective edge or micro-mirror arrays [231] (for both discrete and continuous AWGs) (sections 24 and 25). It is much simpler to image the discrete waveguide outputs as opposed to a continuous AWG focal plane onto a detector. New design efforts are needed in FPR-waveguide tapers (at output) to achieve a discrete-output AWG that can still sample the complete spectrum gaplessly.

6. **Beyond near-IR:** The scientific scope of photonic spectrographs can be dramatically increased by extending to wavelengths ranging from near-ultraviolet to MIR. Further developments are needed in new materials such as AlN-on-Sapphire for UV [232] and chalcogenide glass or Si/Ge for developing low-loss AWGs in the mid-IR. The specific challenges and advances are discussed in sections 8 and 9.
7. **Space readiness:** A stable, durable, and crack-free fiber-chip bond is of particular importance for applications that require operation at cryogenic temperatures, as well as space applications in hard vacuum. Refractive index matching gap fillers/gels/oils are not suitable for these conditions due to solidification at low temperatures and potential outgassing. The impacts of radiation-induced degradation and temperature-induced core-cladding stresses need to be assessed on the overall throughput.
8. **AWG spectrograph throughput outlook:** The main throughputs in a photonic spectrograph are SMF-to-chip, on-chip, and chip-to-detector throughputs. We present the current state-of-the-art and optimized throughputs in the future to give a near-term throughput outlook.

AWG spectrographs: Current overall throughput and near-term outlook.

Component	Current throughput	Optimized throughput
SMF-to-chip efficiency	95%	95%
AWG throughput	70% (Silica AWG)	85% (optimized tapers)
AWG to free-space	80%	95% (with AR coating + output facet optimization)
Relay optics + cross dispersion	50% (prism + lenses)	70% (optimized cascaded AWG)
Total throughput	**∼26%**	**∼53%**

Concluding remarks

Astrophotonic spectrographs offer significant advantages for both ground- and space-based telescopes, particularly at high spectral resolution. Multi-pronged developmental work is currently being pursued with several novel photonic technologies to achieve the vision of compact, high-throughput, fully integrated (with fibers and detectors), and highly replicable photonic spectrographs to augment both ground- and space-based astronomy.

Acknowledgments

Support for P Gatkine was provided by NASA through the NASA Hubble Fellowship Grant HST-HF2-51478.001-A awarded by the Space Telescope Science Institute, which is operated by the Association of Universities for Research in Astronomy, Incorporated, under NASA Contract NAS5-26555. P Gatkine would further like to acknowledge support from the Wilf Family Discovery Fund in Space and Planetary Science, funded by the Wilf Family Foundation, as well as the support from Keck Institute for Space Studies at Caltech. Some of this research was carried out at Caltech and the Jet Propulsion Laboratory and funded through the President's and Director's Research & Development Fund program. Y Zhang is supported by National Science Foundation (NSF) under Grant 1711377 and the National Aeronautics and Space Administration (NASA) under Grant 16-APRA 16-0064.

7. New directions in photonic spectrograph architectures

Pradip Gatkine[1], *Chang-Ling Zou*[2], *Zongyin Yang*[3], *Jinping He*[4,5] *and Ross Cheriton*[6]
[1] Department of Astronomy, California Institute of Technology, Pasadena, CA, United States of America
[2] CAS Key Laboratory of Quantum Information, University of Science and Technology of China, Hefei, Anhui, People's Republic of China
[3] College of Information Science and Electronic Engineering, State Key Laboratory of Modern Optical Instrumentation, Zhejiang University, Hangzhou, People's Republic of China
[4] National Astronomical Observatories, Nanjing Institute of Astronomical Optics & Technology, Chinese Academy of Sciences, Nanjing, People's Republic of China
[5] Key Laboratory of Astronomical Optics & Technology, Nanjing Institute of Astronomical Optics & Technology, Chinese Academy of Sciences, Nanjing, People's Republic of China
[6] Advanced Electronics and Photonics Research Centre, National Research Council Canada, Ottawa, Canada

Status

Bulk-optic, seeing-limited astronomical spectrographs have limitations like high complexity, large size, mass, and high cost, which scale quadratically with the telescope diameter. Integrated photonic spectrographs can address these concerns by enabling high-stability, high-precision dispersion spectral processing for many science cases. Astronomical spectrographs require high efficiency, large spectral bandwidth (e.g. J-H bands: 1200–1700 nm), low or high resolving powers ($R = \lambda/\Delta\lambda \sim$ 1000–100 000), and in most cases, polarization insensitivity, which each present a different set of challenges. Some of the potential use cases include: **(a)** high-precision radial velocity (RV) measurements of stars to constrain exoplanet masses ($R >$ 80 000, RV precision $\sim$10 cm s^{-1}), **(b)** high-resolution spectroscopy to characterize exoplanet atmospheres composition, measuring stellar composition and kinematics ($R \sim$ 30 000), **(c)** diffraction-limited MO spectroscopy of crowded fields to measure stellar properties in extreme environments ($R >$ 10 000), **(d)** low-cost spectrographs for rapid spectroscopy of a large number of transients on small telescopes ($R \sim$ 3000), and **(e)** ultra-compact spectrographs for space-based telescopes and planetary missions.

Currently, AWGs are the most prominent candidate architecture for astrophotonic spectroscopy [2, 10, 182]. Conventional high-resolution AWG spectrographs require bulk-optic cross-dispersion to achieve broadband coverage. However, we envision fully integrated on-chip spectrographs that would lead to ultra-stable monolithic instruments. Challenges with the AWGs and potential solutions are discussed in section 6. While astrophotonic AWG spectrographs have been demonstrated over the last decade, the phase errors in the AWG chips pose a significant barrier for $R >$ 10 000 [195, 233]. This paper therefore focuses on emerging photonic architectures to expand to higher resolving powers ($R >$ 10 000).

Several novel photonic spectrograph architectures [56, 176] are on the horizon with the potential to overcome the limitations of AWGs and enable improved integration with detectors. In this paper, we present a non-exhaustive list of promising new spectrograph architectures, their unique advantages, and the developments needed to make them science-ready.

Current and future challenges

Here, we discuss the specific architectures, the advantages they offer, and the challenges that need to be addressed in the future to make them suitable for astronomy.

Ring resonator-enhanced spectrographs

Achieving a truly integrated broadband photonic spectrograph requires an on-chip separation of the overlapping spectral orders of the AWG. One solution is to use an AWG with high-resolution and low FSR (Eg: R $\sim$ 30 000, FSR $\sim$ 10 nm) followed by an array of microring resonators (MRRs) as filters to separate the spectral orders [235, figure 12(a)]. MRRs can also be placed after a coarse AWG to achieve high spectral resolution within each AWG output channel. Cascaded AWG-MRR spectrographs have also been produced with detectors on a single chip [178, 236], creating a fully integrated spectrograph.

The resonance wavelengths of MRRs are highly sensitive to fabrication errors and temperature fluctuations without active thermal tuning. In addition, to achieve a broadband, high-resolution AWG + MRR spectrograph (figure 12(a)), we need:

$$\text{Total } \# \text{ of MRRs} = (\# \text{ of AWG channels}) \times (\# \text{ of AWG spectral orders}).$$

This implementation can quickly result in thousands of MRRs and tuning elements, presenting a serious integration challenge. Advanced routing and packaging strategies, such as the use of flip chip bonding with vias, may be necessary to integrate these components.

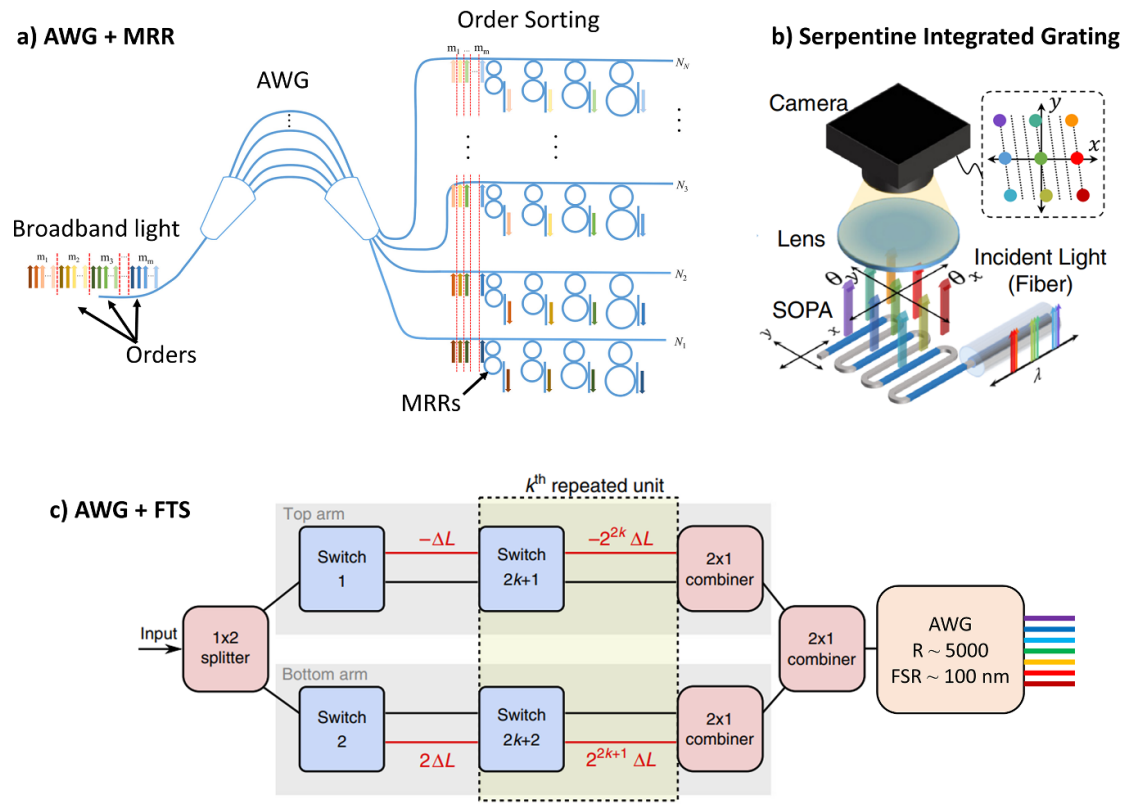

Figure 12. (a) A schematic showing the concept of high-resolution AWG with MRRs at the output channels to separate the overlapping spectral orders. (b) The concept of a serpentine integrated grating using a serpentine optical phased array (SOPA), providing high-resolution dispersion along the *y*-axis (with long cumulative phases), and low-resolution separation along the *x*-axis. Reprinted with permission from [244] © The Optical Society. (c) A schematic showing the concept of switchable path delays in an FTS and the AWG dispersing the FTS fringes to effectively create a dispersed FTS architecture. Reproduced from [242]. CC BY 4.0.

Fourier-transform spectrographs

Fourier-transform spectrographs (FTSs) are an architecture that can offer ultra-high-resolution spectroscopy for bright sources [237] by deducing the optical spectrum from an interference pattern generated as a function of the optical path length difference. This method enables the use of a single-channel detector that can be directly integrated into a photonic FTS chip. However, broadband photonic FTSs are limited by photon noise and waveguide dispersion, which degrades the fringe quality, and the throughput limit [238]. Stationary wave integrated FTS (SWIFTS), which reconstructs the spectrum by sampling the standing wave created by forward and reflected waves within a waveguide-mirror configuration, faces a similar narrow-band challenge due to the undersampling of the standing waves [239, 240]. However, a dispersed FTS architecture (e.g. FTS + AWG) could resolve these issues [241].

An FTS + AWG concept (figure 12(c)) effectively multiplies the resolving power of low-resolution, broadband AWGs (e.g. FSR = 100 nm, $R = 5000$) using an upstream FTS with switch-selectable path delays. Kita *et al* [242] experimentally demonstrated the switchable FTS concept with a 64-channel FTS (figure 12(c)) and a single photodiode. This concept can be adapted to multiply the resolving power of the AWG by a factor of $2^k - 1$, where k is the number of phase-shift units incorporated in the circuit. The switchable FTS modulates the spectrum as we switch through the path delays. This allows us to reconstruct the spectrum at a much finer wavelength step within each AWG channel, effectively multiplying the AWG resolving power, while maintaining a high FSR.

Various challenges need to be addressed to make FTS-AWG architectures suitable for astronomy. It requires high-precision measurement of the output power and detailed high-resolution calibration to reliably retrieve the spectrum at high resolving power. Hence, a stable, low-noise detector array is highly desirable. Implementation of integrated photodetectors (PDs) will enable a highly compact, and stable high-resolution photonic spectrograph. Furthermore, this architecture requires broadband 50–50 splitters and thermally-controlled photonic switches (to switch between path delays) that offer ultra-low loss and minimal crosstalk to enable easier spectral reconstruction. Achieving ultra-low propagation losses (<0.1 dB cm^{-1}) is critical to minimize the impact of the long path delays.

Serpentine integrated grating spectrograph

Current high-resolution AWGs require cross-dispersion to separate the spectral orders and prevent spectral overlap in each channel. While cascaded AWGs can help resolve this issue, they can be too large for fabrication on a single chip and would require very long (>1000 pixels) linear detector arrays to sample the spectral elements. The serpentine integrated grating (SIG, figure 12(b)) can help alleviate this problem by naturally allowing a 2D sampling of the spectrum. This architecture uses a long folded delay line with grating couplers to create a large optical delay path along two dimensions (high-dispersion along the column and 'order separation' along the serpentine row) in a compact integrated device footprint [243]. The grating couplers send the light upward, thus achieving two goals—high spectral resolution and easy imaging of the 2D spectrum from above the chip. This method requires high index-contrast waveguides, such silicon-on-insulator (SOI) and silicon-nitride (SiN) platforms, which allow sharp low-loss bends (with radii as small as ∼10 μm), to enable several centimeters of path delay in a small footprint (∼few mm^2). An SIG spectrograph with R ∼ 100 000 and ∼6750 spectral bins over the 1540–1650 nm range has recently been demonstrated on the SOI platform [244].

High losses of the device in the SIG demonstration (−36 dB) need to be addressed to make it viable for astronomical spectroscopy. The main contributors to the loss were: straight-to-bend waveguide tapers (8.4 dB = 0.07 dB per taper × 120 tapers), input fiber-waveguide edge couplers (7 dB due to mode-mismatch), and the on-chip grating couplers (16 dB). Optimized transition tapers can offer ultra-low-loss U-bends ([245], 0.0022 dB per taper). Similarly, high-efficiency broadband edge-couplers need to be engineered (e.g. [246, 247]: >90% efficiency). High-efficiency grating couplers are challenging to realize. However, apodized designs [248] and dimension reduction techniques can reduce the design parameter-space and device optimization time [249]. Alternatively, low-loss 3D circuit fabrication will allow easier integration of the device [250].

Microcomb-based spectrometer

The ultimate resolution of an on-chip disperser is limited by the total optical path difference (OPD) in the dispersive elements. Further spectral resolution increases could be obtained by converting the optical frequency to electronic RF frequency by measuring the heterodyne beating signal between the signal light and a local oscillator (LO). The microcomb source, which is generated by dissipative Kerr solitons in a laser-driven integrated microresonator [251], provides an excellent LO for an integrated spectrometer (for bright objects), as it delivers a series of comb lines with a precise and fixed FSR. Innovations such as battery-operated integrated comb generators [252], octave-spanning microcombs [57, 253], and frequency stabilization [215, 254] have recently been demonstrated experimentally.

By mixing the input signal with the microcomb, the optical signal frequency can be converted to an RF signal due to the beating between the input light and a nearby comb line. Using an integrated silica microresonator to generate a microcomb with a 22 GHz repetition rate (i.e. frequency spacing between comb lines), a spectrometer has been demonstrated with a frequency uncertainty of around 4 MHz [255].

This spectrometer architecture faces various challenges: (i) the resolution of the frequency measurement is limited by the frequency instability (∼MHz) of the comb lines of an unlocked microcomb. The frequency instability mainly comes from two sources, the instability of the drive laser, and the thermal stability of the MRR. (ii) There is ambiguity in determining the frequency and power of the heterodyne signal due to ambiguity in determining the closest comb line. This ambiguity could be resolved by simultaneously beating the signal with two independent comb sources with different repetition rates, and the optical signal frequency could be determined by comparing the two beating frequencies (dual-comb spectroscopy). Alternatively, the two comb sources could be provided by a single microresonator by either employing different mode families [255] or switching the repetition rate in real time [256].

Computational spectroscopy

A significant departure from the traditional dispersive approaches is the use of computational techniques to decode spectral information from precalibrated encoded information to produce an enhanced spectrum beyond the limitations of gratings/filters. So far, complex spectral-to-spatial [257, 258] and multiplexed spectral response [259, 260] strategies have been proposed for encoding spectral information (figure 13(a)). In the complex spectral-to-spatial encoding process, incident light is dispersed by random media, such as disordered materials or MM fibers to form an overlay of encoding patterns created by individual wavelengths. The multiplexed spectral response encoding is an alternative to spatially dispersed wavebands. This encoding can be achieved in the filters or detectors themselves. A unique precalibrated wavelength-responsivity library is then used for decoding the incident spectrum.

Both encoding strategies can offer high throughput compared to dispersive spectrometers. Moreover, a higher spectral resolution can be achieved in the same device area compared to traditional photonic

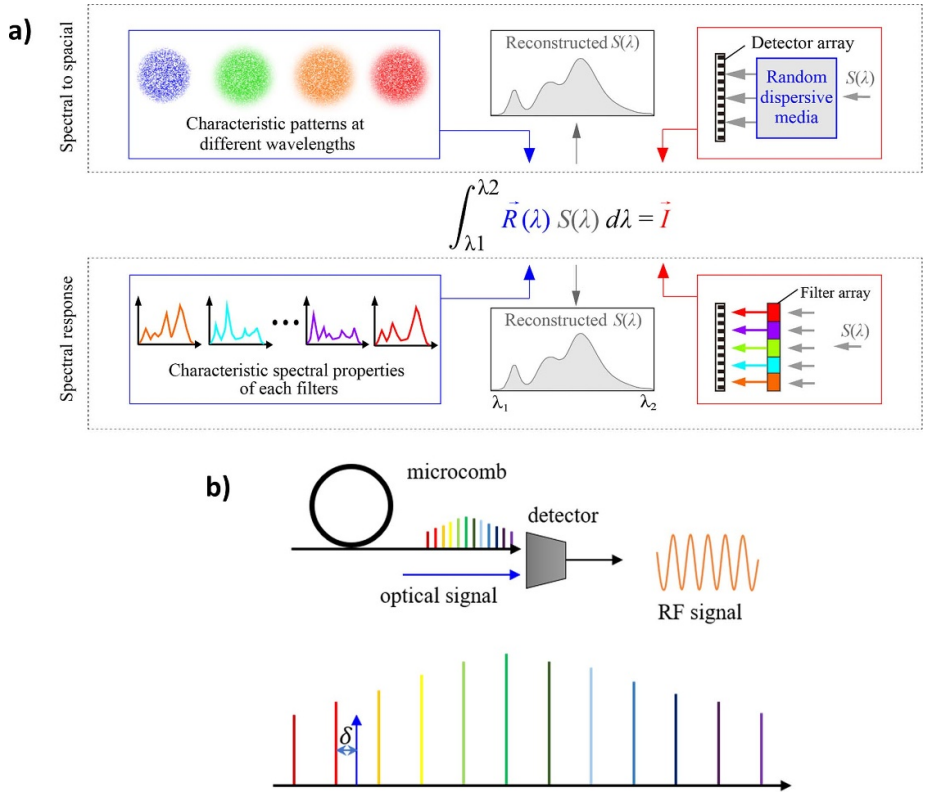

Figure 13. (a) Two encoding schemes of computational spectrographs are shown here. The top part shows the pattern-to-spectrum reconstruction for random dispersive media, and the bottom part shows the reconstruction from a calibrated spectral response library. Both require advanced reconstruction algorithms for robust reconstruction. (b) The concept of an optical signal mixed with a microcomb to create an RF beat signal for high-resolution spectral reconstruction.

spectrographs, since the scattering pattern is not restricted by the effective index or path lengths as in traditional architectures. Emerging strategies use inverse design to specify the desired output spectrum, and iterative steps to generate non-intuitive, disordered geometries for computational spectroscopy that can meet the requirements of the output spectrum [257]. The compactness of the geometry means shorter propagation lengths and smaller chips, leading to lower phase noise and higher thermal stability.

Another computational architecture photonic cross-correlation [261] uses tunable spectral filters to process the entire spectrum for a set of specific spectral lines, enabling higher throughputs and the use of a single detector channel (detailed discussion in section 12).

However, computational spectrometers face certain challenges in reconstructing robust results. The results are accurate with sparse spectra, but if the input is a broadband spectrum, the result is vulnerable to distortion. Furthermore, significant computational resources are required for both the spectrograph design generation and spectrum-interpretation algorithms to achieve high performance. Another challenge is their limited spectral bandwidths. This can be mitigated by appending compact computational/inverse-designed spectrographs to AWG output channels to perform broadband, high-resolution spectroscopy.

Advances in science and technology to meet challenges

Significant efforts are needed in several directions including computational reconstruction, heterogeneous material platforms and fabrication, inverse design, precision calibration, light routing schemes, and integration of photonics, electronics, and detectors, to achieve fully integrated high-resolution, broadband photonic spectrographs for ground- and space-based telescopes. These advances are summarized in table 1. We can classify key advances in three categories:

a. **Design and fabrication of low-loss components:** Fully integrated cascaded spectrograph concepts are viable only with low-loss, broadband individual stages. Major losses occur at interfaces with mismatched refractive indices. Highly efficient taper designs are required for waveguide to SMF, waveguide to free space, SM to MM, and straight-to-bend waveguide transitions. Similarly, ultra-low loss and broadband splitters are essential for all interferometric architectures (Eg: FTS + AWG). For SIGs, a significant effort

Table 1. Spectrograph architectures, challenges, and future advances.

	New architectures (with main advantages)	Challenges	Advancements required
1	Ring resonator-enhanced (high resolution and bandwidth)	• Thermal cross-talk • Complex electrical integration	• High-throughput AWG designs • Thermal stability when driving MRRs • Scalable thermo-optic control of large arrays of MRRs
2	FTS + AWG hybrid (multiplies the resolving power of the AWG)	• High-precision output power measurement • Loss in the delay lines • Broadband splitters	• Integrated detector arrays • Ultra-low propagation loss • Ultra-broadband splitters/switches (sub-wavelength inverse-design can help)
3	Serpentine integrated spectrograph (easy integration with detectors and $R \sim 100\,000$)	• Throughput • Straight-to-bend taper losses • Fiber-waveguide losses • Grating coupler losses	• Cross-section optimization • Inverse design • Broadband grating couplers optimized for the specific waveband of the spectrograph
4	Microcomb-based (ultra-high $R > 100\,000$)	• Comb line stability • Ambiguity in determining the relevant comb frequency	• Self-referenced comb • Advanced on-chip resonator stabilization • Fast/accurate repetition rate switching
5	Disorder modes (no FSR overlap, compactness)	• Spectral bandwidth • Fabrication quality to enable higher resolution and throughput	• Large device areas to enable greater performance • Greater computing resources for larger 3D structure simulations • Novel metasurface realizations
6	Computational Spectrometers (mitigates architecture-dependent performance limitations)	• Low stability • Noise sensitivity • Reliability over larger bandwidths	• Accurate and fine coding strategies • Powerful reconstruction algorithms • Computational techniques to complement traditional dispersive spectrometers such as AWGs

is required in developing high-efficiency vertical grating couplers for launching the dispersed light perpendicularly for simpler 2D detector integration [262].

b. **Computational advances:** Computational spectroscopy and dispersed FTS implementations will greatly benefit from high-precision spectral calibration, and state-of-the-art spectral reconstruction techniques (eg: ML-based elastic-D1 regularization [242]). Further, novel algorithms are needed for forward modeling and inverse-design optimizations (bandwidth, throughput) on large photonic components in various spectrograph architectures [263, 264]. Fast approximate solvers for scattered fields are critical to optimizing large surfaces that can be thousands of wavelengths in diameter [265].

c. **Integration with detectors and electronics:** Future implementations should aim to integrate the detection array monolithically into the photonic chip itself or couple the light onto a nearby external detector with minimal optics for low cost, compactness, and improved throughput. Efforts are needed to develop reliable fabrication recipes in heterogeneous material platforms (eg: InGaAs-SiN [266], NbN/WSi/MoSi-SiN [267]) allowing a large number (thousands) of on-chip pixels. Ongoing efforts in kilopixel SNSPD arrays [268] are promising with improvements expected in efficiency and dark current. Industrial foundries are well-placed to offer these to the broader photonics community (see sections 24 and 25).

Conclusion

The new directions in astrophotonic spectrographs have the potential to overcome many of the limitations with the prevalent AWG architectures. Further developments in photonic fabrication, computation, complexity and complete integration need to be leveraged for building compact, efficient, and broadband astrophotonic spectrographs.

Acknowledgments

Support for P Gatkine was provided by NASA through the NASA Hubble Fellowship Grant HST-HF2-51478.001-A awarded by the Space Telescope Science Institute, which is operated by the Association of Universities for Research in Astronomy, Incorporated, under NASA Contract NAS5-26555. Some of this research was carried out at the California Institute of Technology and the Jet Propulsion Laboratory and funded through the President's and Director's Research & Development Fund and the Center for Innovation Fund programs.

8. The emergence of UV astrophotonics

David Schiminovich[1], *Simon Gross*[2], *Lucas Labadie*[3], *Reinan Moreira*[4] *and Pradip Gatkine*[5]
[1] Department of Astronomy and Columbia Astrophysics Laboratory, Columbia University, New York, NY, United States of America
[2] MQ Photonics Research Centre, School of Engineering, Macquarie University, North Ryde, NSW, Australia
[3] I. Physikalisches Institut, Universität zu Köln, Zülpicher Str. 77, 50937 Cologne, Germany
[4] Ultra-Low Loss Technologies, Santa Barbara, CA, United States of America
[5] California Institute of Technology, Pasadena, CA, United States of America

Status

Although early ultraviolet (UV) photonic devices were developed nearly 50 years ago (e.g. [269]), progress towards widespread application has been slow. A limited number of materials can be used to fabricate UV (<400 nm) optoelectronic devices, particularly those with high index, and scattering, losses and damage susceptibility can severely reduce performance. Below ∼200 nm, O_2 in the atmosphere is highly absorbing, necessitating operation in vacuum. When viewing the night sky from the ground, the ozone layer (O_3) absorbs incoming photons shortward of 320 nm; astrophysical telescopes and instruments operating in the near-UV and shortward must be situated in—and qualified for—space.

The astrophysical benefits of a space-based UV observatory have long been recognized [270] efficient and solar-blind sensor technologies for astronomy]. The Hubble Space Telescope (HST) has been transformative, particularly for its moderate-to-high UV spectroscopic capabilities that probe numerous atomic and molecular lines. HST has obtained spectra of hot young and evolved stars and white dwarfs, active galactic nuclei, star-forming galaxies, galactic nebulae, supernova remnants, and protoplanetary disks, and absorption (and emission) from the multiphase interstellar, circumgalactic and the intergalactic media. The next leap forward, in the form of the Habitable Worlds Observatory (HWO; based in part on LUVOIR and HabEx Concepts), could target the same UV O_2 and O_3 absorption signatures that confound UV observations on Earth, but that might serve as candidate biosignatures on distant exoplanets (see figure 14). Such flagship mission concepts are currently developed around relatively mature UV technologies although UV photonics could indeed play a role on the HWO and pathfinder missions.

UV astrophotonics has yet to demonstrate the 'on-sky' maturity achieved by the NIR counterparts discussed extensively in this roadmap. But substantial progress in UV photonics exists elsewhere. Early developments in UV nonlinear optics, harmonic generation, low-loss optical fibers, damage mitigation, and materials selection have led to recent successes. Novel material platforms have been developed that enable photonic operation at blue/UV wavelengths. These are mainly driven by life-science and quantum optics applications, sensing, spectroscopy and optical clocks (see [271] for a comprehensive review). In light of these developments, the nascent field of UV astrophotonics may finally be emerging.

Current and future challenges

Photonic technologies for the UV domain

Early developments in UV nonlinear optics, harmonic generation, low-loss optical fibers, damage mitigation, and materials selection have enabled recent efforts to demonstrate the potential and feasibility for a broad suite of photonic technologies in the UV.

With photon energies exceeding the Si bandgap, UV/visible photonics pose distinct materials, design and fabrication challenges as compared with the NIR. Issues include limited material, dispersion and photon source selection; increased absorption and scattering losses; decreased performance due to material impurities and defects. High energy photons and high intensities can induce defects that increase losses, an effect known as photodarkening [272], which leads to a degradation of performance over time. UV PICs require smaller structures compared to their established NIR counterparts. This puts the required feature sizes closer to the resolution limit of wafer-scale lithography which in turn reduces yield. Nevertheless, some of these challenges and issues may ultimately be exploited for the design of sensitive probes and sensors, and engineered quantum emitters.

Overcoming the challenges in the UV may enable astrophotonic solutions for optimal telescope-instrument coupling, foreground suppression (e.g. geocoronal Lyman alpha), interferometry and very high resolution spectroscopy, and light sources. Space-based UV instruments also stand to substantially benefit from new technologies that reduce volume, mass and power, and number of reflective and transmissive surfaces.

Material choices and fabrication platforms

The bandgap of an optical material ultimately provides a lower wavelength-bound for its suitability as a waveguide substrate (see figures 14(b) and 15(b)). Deposited thin films that serve as guiding layers often

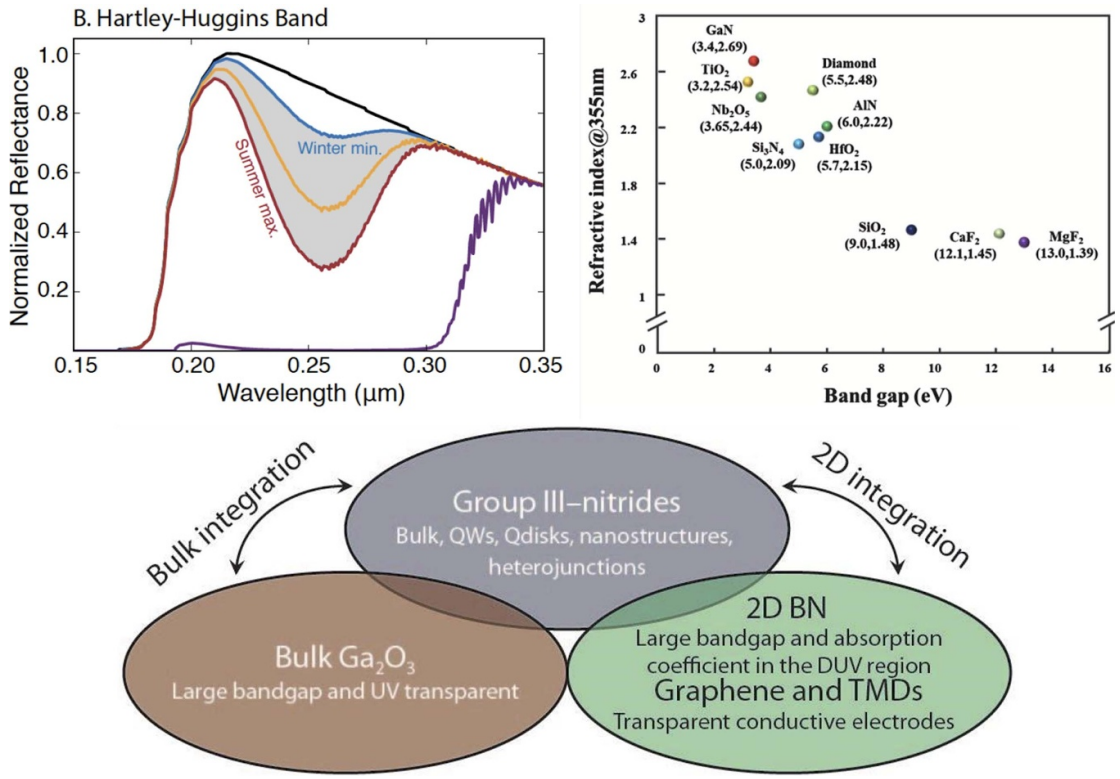

Figure 14. Top left: habitable planet temporally varying UV biosignature—ozone oscillations in response to biogenic O2 seasonality. Reproduced from [273]. © IOP Publishing Ltd CC BY 3.0. Top right: UV Material Properties. Reproduced from [274]. CC BY 4.0. Bottom row: Broad upcoming directions in UV photonics and their interplay, including hybridization of Group III-nitrides, III-oxides, and two-dimensional materials. Reproduced from [275]. © IOP Publishing Ltd. All rights reserved.

cannot achieve the same optical quality as their bulk counterparts. Impurities in the deposited films lead to energy levels within the bandgap that reduces their UV wavelength cut-off. At short wavelengths, Rayleigh scattering becomes a dominant loss mechanism where light scatters at grain boundaries of polycrystalline materials as well as scattering from the residual sidewall roughness of the patterning process used to define the waveguides [276]. Such losses can be mitigated by using single-crystalline materials and improved photolithography.

At UV and visible wavelengths [271], identifies materials for PIC and wafer-scale blue and UV photonic applications, highlighting silicon nitride Si_3N_4 (>400 nm), tantalum pentoxide Ta_2O_3 (>300 nm), amorphous aluminum oxide Al_2O_3 (>250 nm) and aluminum nitride AlN (>200 nm) as leading material platforms. Alternatively to wafer-scale lithography, UV and blue wavelength waveguides have been demonstrated in polymers [277], with losses <1 dB cm^{-1} at 266 nm, as well as in glass substrates [278, 279] using ultrafast laser inscription (ULI) [91, 280]. Looking to the future, these will be supplemented by other 3D and 2D wide and ultra-wide bandgap materials (e.g. III-N, AlGaN, Ga_2O_3, hexagonal boron nitride, silicon carbide, diamond), metamaterials. Many of these materials have already seen application in the development of UV-efficient and solar-blind sensor technologies for astronomy [281, 301]. A novel advance is a 2nd-harmonic-generating and focusing metalens using ZnO resonators for the vacuum UV [282] and a first XUV metalens [283]. See figures 14(b), (c) and 15(b) for an overview of potential UV astrophotonics materials.

Although UV advances have yet to achieve theoretical performance limits, recent successes include a crystalline, wurzite AlN-on-Sapphire ([232]; cf roadmap section 6) PIC integrated platform/waveguide with high-Q into the UV, targeting control and connectivity for quantum computing (see also [284]). Other examples include SiN on Al_2O_3 down to 372 nm [302] as well as low-loss UV waveguides made using atomic layer deposition of Al_2O_3 (see figures 15(a) and (b)). Potential issues with sapphire and other materials are the lattice mismatch (see e.g. [275, 303]). Another promising platform is an AlGaN waveguide on SiC substrate which, as an example, has been used to achieve the shortest wavelength LED (210 nm) to date [285]. Deep UV AlGaN LEDs (~250 nm) have been life-tested for the Laser Interferometer Space Antenna (LISA) mission, allowing low-power contactless discharge of test masses [286, 287].

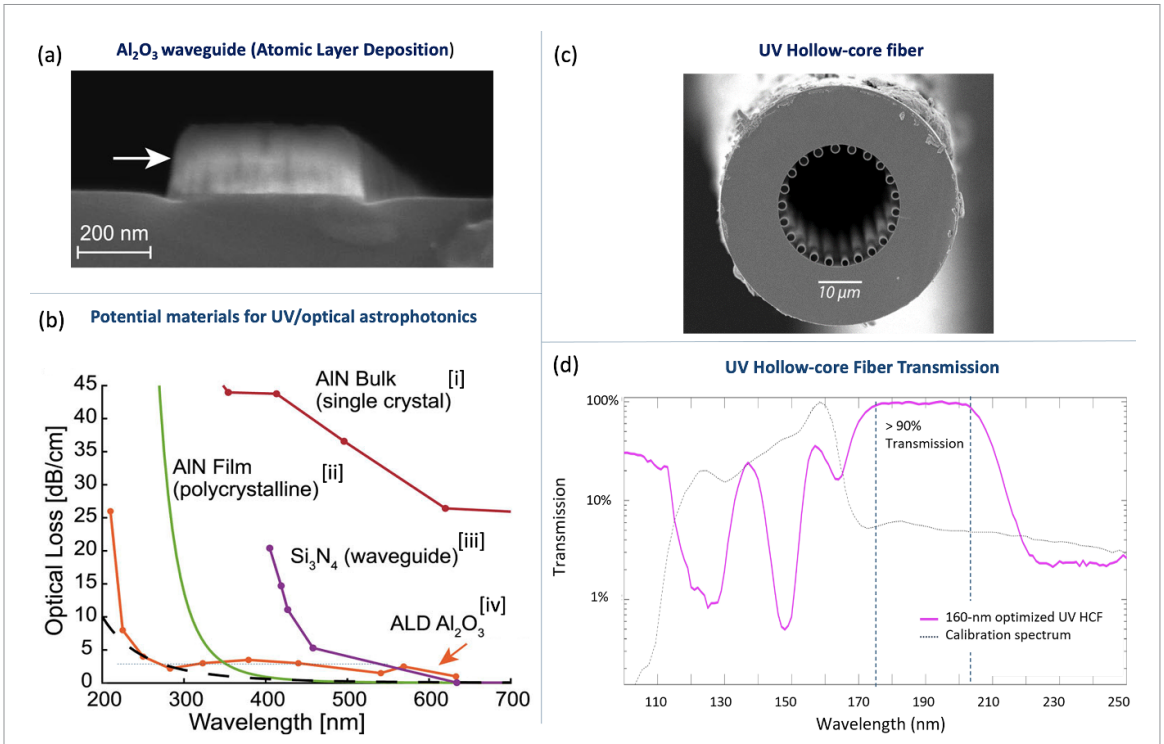

Figure 15. (a) Scanning Electron Microscope image of Al_2O_3 waveguide cross-section fabricated using atomic layer deposition (ALD). Reprinted from [300], with the permission of AIP Publishing. (b) A plot showing optical losses in various materials being explored for UV and optical astrophotonics [i] [ii] [iii] [iv]. ALD Al_2O_3 is a potential low-loss material for UV waveguides and photonic devices. (c) The cross-section of a UV hollow-core fiber. Reproduced with permission from [297]. (d) The transmission profile of the UV hollow-core fiber shows high-throughput transmission across a broad band, thus getting closer to the stringent requirements in astronomy.

Future progress in materials and platforms requires mitigating sidewall roughness, mode and interface engineering and improved crystal growth. A future challenge for UV astrophotonics is to clearly highlight the dominant materials and an optimal platform (or platforms); this will facilitate incorporation into novel instrument design solutions.

Fiber Optics -Losses, Coupling and Interfacing

Although UV-transmitting fiber optics have been available for decades, future gains can be made by extending to shorter wavelengths (<200 nm), reducing transmission losses and increasing solarization resistance. Current technologies seeing continued development include transmissive step-index fiber (UV grade silica [288, 289], fluoride and flurophosphate [290]) and solarization-free anti-resonant hollow core fiber technologies [291–293]. Photonic crystal and hollow-core fibers have also been used for the development of UV-visible photonic sources (e.g. harmonic generation, frequency comb [294], and supercontinuum source [295]). The FIREBall stratospheric balloon experiment [296] flew 200 nm-transmitting high-OH fused silica fibers. New instrument concepts are also incorporating hollow core fibers for the deep UV ([297] also see figure 15).

UV PICs suffer from the same mode-mismatch challenges between PIC waveguide and optical fiber as their NIR counterparts. In the NIR, low-loss coupling between fibers and PIC uses mode-matching tapers that utilize a lower refractive index contrast material than the PIC itself to expand the MFD and match to commercial fibers. At UV wavelengths, no such tapers have been demonstrated yet. Liu *et al* [284] reviewed several methods of fiber-to-chip interfacing for AlN platforms in the UV, including laser cleaving and ion beam milling (see their table 2). In the UV, smaller waveguide dimensions and thus MFDs make this task more difficult. Single-mode optical fibers for the UV are preferably designed for a large MFD to reduce the intensity in the core and avoid solarization [298]. Solarisation can be avoided entirely by moving to a hollow-core fiber design [299]. Yet hollow-core fibers feature an even larger core and hence mode-field mismatch to the PIC.

The most common method to attach fibers to PICs is using UV-curing adhesive (Ref to section 23). These adhesives should feature a high transparency to avoid absorption losses, yet UV curing requires sensitization to UV light which induces absorption bands, in particular at 365 nm. This contradicts the requirement for high UV transparency. When using photonic crystal fibers [298] or hollow core fibers [299],

the adhesive can infiltrate the fiber via capillary forces which influence the guiding properties of the fiber and induce additional losses if the fiber ends are not collapsed.

A challenge remains to determine the optimum way to mode match in the UV and identify the ideal solution to connecting fibers to PICs for maximum efficiency.

Advances in science and technology to meet challenges

UV PIC development is likely to include further progress towards robust, low loss, higher-Q devices. With Rayleigh scattering increasing into the blue/UV, improvements such as those seen in CMOS foundry-based devices with low-roughness waveguides patterned on Si_3N_4 [304] are needed. Recent developments include the fabrication of UV ring resonators [305], UV AWGs [235] with high bandgap photonic materials coupled with UV/VIS transmitting substrates.

Finally, radiation hardening will become an increasingly important challenge in the mid-term future for space applications of astrophotonics, regardless of the frequency range. This is also relevant for other fields such as satellite-based quantum technologies where efforts in this direction have already been made [306] (targeting predominantly the VIS/NIR domain.)

An interesting direction to guide future UV astrophotonic development is consideration of the design requirements of the HWO. Despite its large aperture (e.g. 6–10 m), it is unlikely to be diffraction-limited in the far and near-UV. UV astrophotonic technologies may provide new avenues for reaching the highest possible resolution and sensitivity limits, with more compact instruments. And we may soon see pathfinding UV astrophotonic instruments more routinely deployed on suborbital and smallsat missions. These advances will enable the study of exoplanet atmospheres and biosignatures, and high resolution absorption line studies of massive, faint baryonic structures observed throughout cosmic history.

Concluding remarks

The field of UV photonics has shown limited growth until the past decade. Recent advances driven by non-astronomical applications have demonstrated the promise of new materials, device platforms and interfacing technologies. As efficiency increases, and losses decrease, astronomical UV instruments stand to benefit from serious consideration of photonic design solutions. A key challenge will be converging on a suite of materials and a core toolkit of UV astrophotonic technologies that should then be qualified for the space environment. An important 5–10 year goal will be the realization of pathfinding UV photonic devices in a suborbital or orbital telescope.

Acknowledgments

L L acknowledges support from the German Ministry of Education and Research (BMBF, ALSI Project 05A14PK2) and the DFG (NAIR Project, Grant 326946494) in the field of mid-infrared astrophotonics. S G acknowledges funding by the Australian Research Council (FT200100590). Support for P Gatkine was provided by NASA through the NASA Hubble Fellowship Grant HST-HF2-51478.001-A awarded by the Space Telescope Science Institute, which is operated by the Association of Universities for Research in Astronomy, Incorporated, under NASA Contract NAS5-26555.

9. Advances in mid-IR astrophotonics

Lucas Labadie[1], *Simon Gross*[2], *Reinan Moreira*[3] *and David Schiminovich*[4]
[1] I. Physikalisches Institut, Universität zu Köln, Zülpicher Str. 77, 50937 Cologne, Germany
[2] MQ Photonics Research Centre, School of Engineering, Macquarie University, North Ryde, NSW, Australia
[3] Ultra-Low Loss Technologies, Santa Barbara, CA, United States of America
[4] Department of Astronomy and Columbia Astrophysics Laboratory, Columbia University, New York, NY, United States of America

Status

The development of PICs is driven by optical communication applications at wavelengths of 1.3 and 1.5 μm, utilizing silicon and its oxide form, SiO_2, such as SOS and Si/SiN-on-insulator (SOI) technologies [307–309]. These optical communication wavelengths overlap with the astronomical NIR wavelength band of 1–3 μm. In the context of astronomy, the GRAVITY instrument [75], operating at wavelengths of 2.0–2.4 μm and utilizing mature SOS technology, is an excellent example of the astrophysical yield of photonics in the NIR (cf section 15). Other mature NIR phototonic platforms include lithium niobate for instance, which is employed for signal modulation in data transmission and integrated quantum photonics [310, 311]. More recently, three-dimensional material structuring by the means of ULI has emerged as an alternative to lithographic fabrication to offer new opportunities for manufacturing photonic devices in the NIR and beyond [280, 312].

From an astrophysical perspective that needs panchromatic information, there is great interest in extending integrated photonics towards the MIR range beyond ∼3 μm [313]. At MIR wavelengths, the fields of young stellar objects, the spectral characterization of nearby exoplanets, or the study of the circumnuclear regions of active galaxies fully justify the extension of PICs into the 3–20 μm MIR wavelength range (figure 16).

To date, MIR photonics have yet to demonstrate the 'on-sky' maturity achieved by their NIR counterparts. In the MIR, the TISIS experiment at IOTA using a fiber X-coupler in the astronomical L-band (∼3.8 μm) for interferometric beam combination is the only 'on-sky' astrophotonic experiment undertaken thus far [314]. Most MIR integrated photonics and fiber demonstrations are laboratory-based and focused on the characterization of new devices and platforms. Originally motivated by the DARWIN/TPF mission to build a space interferometer, the effort has moved from simple waveguides and fibers [315–318] to more elaborate optical functions [319–323] such as couplers, splitters and beam combination circuits for ground-based astronomy. In the near future, the NOTT instrument at the VLTI [324] will eventually reach a new stage in on-sky use of MIR astrophotonics by employing a beam combiner for the 3.5–4.0 μm wavelength band.

Current and future challenges

Identifying priorities in the spectral bands of operation of MIR astrophotonics: Most astronomers interested in photonics tend to broadly define the MIR as the 3–20 μm range, which is difficult to cover with a single photonic technology/platform. Furthermore, PICs usually require SM behavior, in particular for interferometric applications. Extending the usable wavelength bandwidth of SM waveguides beyond one octave requires careful design to avoid higher order modes at short wavelengths and excessive bend losses at long wavelengths. One could isolate sub-bands of operation, such as matching the typical atmospheric transmission windows. In recent years, the 3–5 μm spectral range has seen the largest progress (figure 16, left), for instance, with significant advances in beam combination capabilities for interferometry using ULI [325]. In the 8–12 μm spectral range, a proof-of-concept of astronomical functions has been achieved [320, 326]. Recently, a silicon-germanium integrated Fourier transform spectrometer [327] was demonstrated at 7.7 μm using thermo-optic modulation (figure 16, center). To date, the only attempt to cover the ultrabroad MIR range 6–20 μm with a single technology and waveguide geometry used telluride (Te)-rich chalcogenide SM waveguides (figure 16, right), albeit at the cost of high propagation losses [328].

A future challenge resides in dividing the astrophotonic MIR range into several narrower spectral regions over which the overall performance can be maximized.

Material choices and fabrication platforms: Highly transparent materials in the MIR (chalcogenides, heavy metal oxides, fluorides, III–V materials, Ge/Si, …) are often more difficult to handle and process than the well-established $Si/SiN/SiO_2$ systems. MIR materials are generally less compatible with established fabrication techniques. For lithography, highly pure and defect-free thin-films are required and etch processes with minimal sidewall roughness. Suitable cladding materials are required to protect the

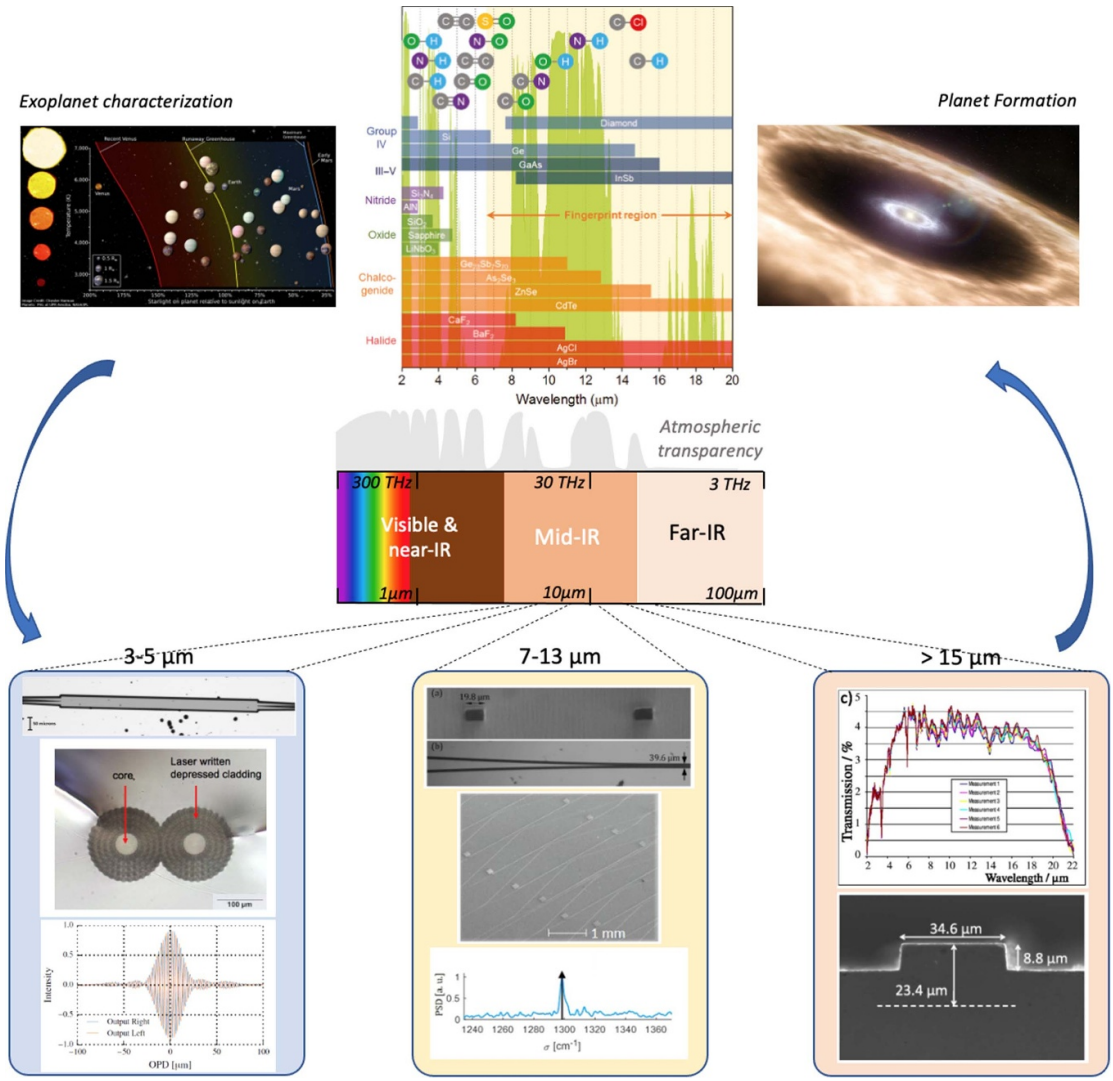

Figure 16. Global schematic view illustrating the links between some astrophysical objectives and the photonic technologies that require to be developed in the wavelength range addressed by this paper, namely the mid-infrared range beyond ∼3 μm. The top panels show two science cases that can particularly benefit from observations in the mid-IR: the spectroscopic characterization of exoplanet atmospheres in the fingerprint region where C/N/O based molecules can be detected and the mapping of planet-forming disks to understand the formation and evolution of young extrasolar systems [courtesy Chester Harman and ESO]. The chemical fingerprint region is linked to possible material platforms relevant for photonics in the top-central figure]. Reproduced from [wikipedia commons/chester harman]. CC BY-SA 4.0. Reproduced with permission from [332]. The middle panel shows that, next to the visible and near-IR range, the mid-IR range shows specific atmospheric transparency windows that can be technologically exploited for ground-based astronomy. The three bottom panels illustrate with examples the current yield of astrophotonics in three different accessible bands; Panel 3–5 μm range: *Top:* micrograph of a chalcogenide-GLS multimode interferometer fabricated by lithographic techniques. Reproduced from [eso0827a]. CC BY 4.0. Reprinted with permission from [330] © The Optical Society. *Center*: image of a ZBLAN coupler's end face. Reprinted with permission from [312] © The Optical Society. *Bottom*: MIR interferogram obtained with a ULI coupler in GLS glass delivering high interferometric contrast. Reproduced with permission from [322] © ESO. Panel 7–13 μm: *Top*: view of the front-face and coupling region of a ULI coupler in GeAsSe chalcogenide glass. Reproduced from [337]. CC BY 4.0. Reprinted with permission from (Vigreux 2011) © The Optical Society. *Center*: SEM picture of an MZI array using the Si:Ge platform for integrated Fourier transform spectroscopy at 8 μm. Bottom: reconstructed spectrum with a resolution $R \sim 100$ at 1300 cm^{-1}. Reproduced from [327]. CC BY 4.0. Panel >15 μm: SEM picture (bottom) of a chalcogenide rib waveguide showing continuous transparency from 4 to 20 μm [338]. The blue arrows illustrate the cycle that links the mid-infrared technologies to possible astrophysical science cases.

waveguides and a careful choice of carrier materials is also needed to avoid delamination due to thermal expansion coefficient differences. In contrast, ULI can directly modify highly pure bulk material, but generally cannot reach the high index contrasts of lithographic platforms, resulting in less compact waveguide circuits that are several centimeters in size rather than just a few millimeters, as commonly achieved with lithographic platforms. Hence the waveguide propagation losses are of great importance in ULI to maintain an overall high throughput. With several platforms/materials now tested (e.g. SiN/Si, SOI, Ti:LiNbO3, Si/Al_2O_3, GLS, Ge/Si.), the current status suggests that ULI in chalcogenide glasses (e.g. GLS, As_2Se_3, $Ge_{33}As_{12}Se_{55}$) is a promising combination for the spectral extension beyond 3.5 μm of interferometric beam combiners, owing to the relative simplicity and versatility of the manufacturing process

[326, 329]. Unlike lithography, ULI does not require any photomask and is a single-step fabrication process and thus enables rapid design iteration. Its ability to create 3D waveguides avoids waveguide crossings and thus the associated crosstalk that can be detrimental for high contrast interferometry. Lithographic fabrication of PICs, owing to its origins from the electronics industry, can provide a much higher fabrication throughput, yet to date astronomical applications typically only require a handful of devices. The photolithography and etching of chalcogenide films, already proposed for channel waveguides [316], is being studied to develop MM interference couplers [330]. Silicon- and silicon/germanium-based integrated photonics [331–333] as well as III–V semiconductors [334] are attractive for the field, but no dedicated astrophotonics device has been demonstrated yet.

A future challenge for MIR astrophotonics is therefore to clearly highlight a dominant and optimal platform (or platforms) in terms of device quality and broadband performance for identified sub-ranges. Furthermore, the availability of materials and substrates with excellent purity and batch-to-batch repeatability is a key aspect for manufacturing MIR PICs using different platforms.

Transparency/Losses (including Fresnel losses): Low loss PICs are a major requirement due to the intrinsic weakness of the distant astronomical sources being observed. The propagation losses for MIR SM waveguides are in the 0.1 dB cm^{-1}–3 dB cm^{-1} range (or 98% to 50% throughput over 1 cm) [332, 335, 336] within the wavelength sub-band of 3–5 μm, an order of magnitude larger than for NIR silica waveguides ($\sim$0.01–0.05 dB cm^{-1}, or down to 99% throughput per cm).

MIR materials with indices of $\sim$2.5 exhibit $\sim$15% Fresnel reflection losses per facet, and silicon or germanium even $>$30% per facet. Removing these losses requires broadband anti-reflection coatings on the small-sized input/output facets. Alternatively, materials with n $\sim$ 1.5 and thus lower Fresnel losses of only 4% have also been investigated, such as ZBLAN glass [312] for instance, albeit their transparency is limited to $<\sim$4 μm.

Reliably and reproducibly processing high purity and defect-free MIR materials for creating waveguides, waveguide bends and devices with $<$1 dB cm^{-1} losses are important future challenges for the progress of MIR astrophotonics. Furthermore, the ability to deposit broadband AR coatings on the chip/waveguide facets are of equal importance to maximize the throughput.

Coupling and Interfacing with fibers: Pigtailing PICs components for astronomical applications is an important aspect at all wavelengths, including in the MIR. Typically, MFD of MIR SM devices range from a few microns in high index contrast platforms to a few tens of microns for low field-confinement waveguides. The low-loss interfacing of MIR integrated photonics to commercial MIR fibers (e.g. fluoride, chalcogenide, silver halide or hollow core fibers) requires close matching in MFDs, as well as a good level of index matching or anti-reflection coatings to avoid reflection losses. In the NIR, well-developed and low-loss mode-matching taper designs are readily available to interface common PIC platforms to optical fibers. At MIR wavelengths, the diversity in optical, mechanical and thermal properties of the used materials as well as the high likelihood of the PIC and fiber being of dissimilar materials e.g. low-index fluoride fibers and high-index chalcogenide PIC, results in additional challenges. This is in contrast to NIR wavelengths where both interfaced ends are often made of silica glass. Moreover, the diversity in the fiber design (solid-core, hollow core, microstructured fibers; see section 5) driven by the requirement for increased wavelength transparency does add challenges as well as general handling, stripping and cleaving of MIR fibers. Also, polarization becomes important in high index contrast PIC systems, which exhibit a strong waveguide birefringence and polarization dependence in mode-field profile.

For the development of pigtailed MIR PICs, a critical challenge is to optimize the mode-matching between fibers and the integrated optic waveguides, at least for specific spectral sub-bands. An additional challenge is to identify a suitable, robust and stable method to attach MIR fibers to MIR PICs. This requires for instance a suitable IR-transparent glue with well characterized thermal behavior, or a thermal fusion process, in order to permanently attach optical fibers to the chips.

Advances in science and technology to meet challenges

MIR integrated photonics have focused on wavelengths around or below 10 μm. The 10–20 μm range, of interest for space missions such as the proposed LIFE interferometer [339], remains largely unexplored. The propagation losses are expected to be larger than a few dB cm^{-1}, at least in the SM regime [328]. While SM Hollow Core Waveguides were proposed to circumvent the limitation of dielectric materials, they were found

to strongly underperform [340] as has the alternative InGaAs/InP technology [341]. It has been estimated that a Germanium-Tin-Silicon platform could cover the 3–19 μm range with $\sim$2 dB cm^{-1} losses [342]. However, this remains to be proven experimentally.

The optimization of a 10–20 μm platform for astronomy could be expensive and would need to be supported by a long-term technology program justified by a major astrophysical initiative.

A critical aspect for MIR astrophotonics is the testing of operation at low or cryogenic temperatures, required to minimize thermal background. The GRAVITY experience has proven the operation of 2.0–2.4 μm pigtailed germanium-doped silica beam combiners at -80 °C [33], but MIR photonics may have to operate at lower temperature as, for instance, for the NOTT instrument.

Finally, radiation hardening will become an increasingly important challenge in the mid-term future for space applications of astrophotonics, regardless of the frequency range. This is also relevant for other fields such as satellite-based quantum technologies where efforts in this direction have already been made [306], targeting predominantly the VIS/NIR domain. In the future, since radiation hardness strongly depends on the material, specific tests for MIR integrated photonics will have to be implemented.

Concluding remarks

We have discussed the opportunities to extend the operation range of astrophotonics beyond the traditional VIS/NIR range into the MIR. The choice of material and compatible waveguide fabrication technologies is limited. Generally, MIR waveguides compared to their NIR counterparts exhibit larger losses and have to operate at extreme temperatures, which adds to the challenges. However, MIR photonics (waveguide and advanced devices such as on-chip spectrometers) have progressed significantly over the past 10 years, driven by other applications such as sensing, which the astrophotonics community can benefit from.

Acknowledgments

L L acknowledges support from the German Ministry of Education and Research (BMBF, ALSI Project 05A14PK2) and the DFG (NAIR project, Grant 326946494) in the field of mid-infrared astrophotonics. S G acknowledges funding by the Australian Research Council (FT200100590).

10. Integral field units for THz astrophysics

Akira Endo[1], *Charles M Bradford*[2], *Ritoban Basu Thakur*[2,3] *and Edward J Wollack*[4]
[1] Faculty of Electrical Engineering, Mathematics and Computer Science, Delft University of Technology, Delft, The Netherlands
[2] Jet Propulsion Laboratory, California Institute of Technology, Pasadena, CA, United States of America
[3] Department of Physics, California Institute of Technology, Pasadena, CA, United States of America
[4] NASA Goddard Space Flight Center, Greenbelt, MD, United States of America

Status

Superconducting astrophotonics will revolutionize submillimeter/millimeter astronomy ($f \sim 0.1$–1 THz, $\lambda \sim 0.3$–3 mm) by enabling massive IFUs, that can simultaneously measure the wideband spectrum of all points in a 2D image. A wide-field and wideband spectrometer in the far-infrared offers a sensitive and unique 3D approach to topics which bridge cosmology and astrophysics, in particular the earliest galaxies as they are born in the reionization epoch [343, 344]. Mm/submm wave-IFUs have yet to be realized because they are out of reach of existing technology such as heterodyne receivers, direct-detection cameras, and quasioptical spectrometers [345]. The physical wavelength scale makes it impractical to design quasioptical IFUs with many spatial pixels (spaxels) and spectral channels (voxels). The photonic architecture addresses this challenge by shrinking the optical path into equivalent guided waves along SM superconducting transmission lines and metamaterial structures [346]. For example, analogues of a high-order optical grating spectrometer and an FTS have been integrated on a chip, as shown in figures 17(e) and (f), respectively. The advantages of superconducting astrophotonic instruments (compared to their quasioptical equivalents [345]) are mechanism-free, compact, lightweight, and ultimately scalable designs. The utility of the superconducting photonic devices goes hand-in-hand with the rapid advances in far-IR/submm/mm detector array format and sensitivity, particularly for kinetic inductance detectors (KIDs) [347]. A full discussion of KIDs is beyond the scope here, but we refer the interested reader to articles by [348, 349], and references therein. KID-based instruments with total pixel counts of 10^5 or more are now conceivable, and photonic techniques are required to make optimal use of these large formats. For related developments at optical wavelength see section 24 (Mazin, Walter and Zou).

The development of superconducting astrophotonics to date has been largely focused on ultra-wideband filterbank spectrometers (figure 17(a)) or pseudo-grating spectrometers (figure 17(b)), which sort the light from a single sky mode into an array of spectral channels for detection. Examples of these implementations can be found in [350, 351], respectively. These dispersive approaches offer high sensitivity to individual sources, and are being used for detecting [CII] and CO lines in dusty star-forming galaxies at high redshift [352]. These spectrometers typically use a guiding structure created with patterned superconducting films (often niobium or NbTiN) and a thin dielectric (typically silicon nitride or silicon). For example, the on-chip FTS presented in figure 17(f) employs NbTiN/SiN/NbTiN microstrip lines. This architecture allows operation up to the Nb (or NbTiN) gap frequency of 690 GHz (1100 GHz), with spectral resolution generally limited by the loss in the dielectric (currently $R = f/\Delta f \sim 300$–500). Examples of on-chip filterbank spectrometers are Deep Spectroscopic High-redshift Mapper (DESHIMA) [350] that has seen astronomical first light on the Atacama Submillimeter Telescope Experiment 10 m, and SuperSpec [353, 354] which will soon be deployed on the 50 m Large Millimeter Telescope. Both use microstrip lines, with half-wave filters to define channel bandpasses. The Micro-Spec device employs a phased-array approach in which interference creates spectral channels via a lithographically patterned 2D multi-mode region [351, 355].

Another complementary approach which is emerging is an on-chip Fourier-transform spectrometer (FTS), called superconducting on-chip Fourier transform spectrometers (SOFTS), which employs an electrically tunable wave speed to modulate the phase delay [356]. See figure 17(c) for a schematic representation and operational principle. Each spatial mode of the spectrum is encoded in time and detected by a pair of detectors, enabling improved spectral recovery [357]. This allows spatial multiplexing at the expense of sensitivity in each spectral channel (due to the full band photon load on the detector). Another virtue of the SOFTS is that, like a classical FTS, the working resolving power is selectable in operation by simply adjusting the amount of phase delay used. SOFTS prototypes have been demonstrated at 10 GHz, with expectations for adaptation to higher frequencies.

Current and future challenges

The first generation of on-chip spectrometers (DESHIMA, SuperSpec) are offering photon-noise-limited performance, and others are coming soon (e.g. EXperiment for Cryogenic Large-Aperture Intensity Mapping [355], South Pole Telescope Summertime Line Intensity Mapper [354], SOFTS [357], Cambridge Emission

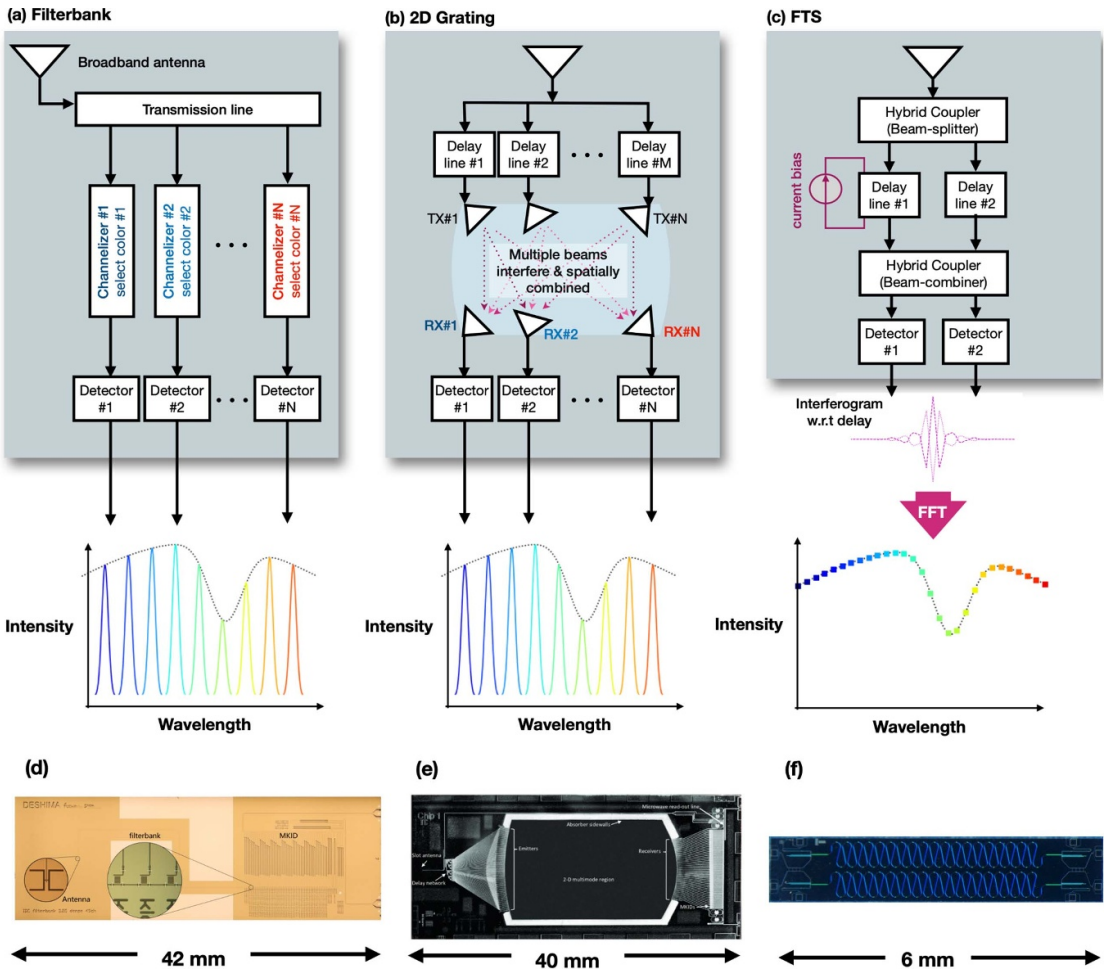

Figure 17. The top row shows the working principles of the superconducting photonics circuits of the (a) filterbank, (b) quasi-grating, and (c) FTS spectrometers. The bottom row shows photographs of examples of corresponding on-chip implementations: (d) [350], (e) [351], (f) [357].

Line Surveyor [358]. These demonstrations pave the way for larger, more powerful instruments. In considering approaches to the next generation instruments for wide-field science, a first-order figure of merit is simply the number of detectors that can be fielded (see figure 18). Whether they are multiplexed primarily spectrally as in the dispersive filter banks and pseudo-gratings, or spatially as in the SOFTS, the net spatial-spectral survey speed scales as the number of detectors, provided the detectors are photon-noise limited at their respective backgrounds [345]. While the legacy submm telescopes have modest field-of-view (e.g. Caltech Submillimeter Observatory/Leighton Chajnantor Telescope [359] with 15 arcmin giving 170 feeds at 220 GHz), new wide-field telescopes under development offer ample etendu (e.g. Fred Young Submillimeter Telescope which could feed some 10 000 devices at 220 GHz). As a result, in the near term the SOFTS and dispersive approaches could offer comparable survey speed. Assuming continued development in KID format to 10^5 pixels, the dispersive approach offers the ability to field more total detectors, and has the potential to become the preferred solution.

In any case, scaling to larger and dual-polarization array formats presents packaging challenges. For full spatial packing, ultimately the spectrometers must be either miniaturized greatly (so that each spectrometer unit cell is only a few wavelengths on a side and they can be positioned between the antennas in focal plane), or they need to be arrayed on chips which extend behind the telescope focal plane. The latter approach will require new antenna/coupling approaches.

Advances in science and technology to meet challenges

We observe that there are compelling scientific opportunities to be realized by pushing astrophotonic spectrometers to higher resolving power ($R > 10^3$), higher frequency (>1 THz) and total sensitivity. See figure 18 for a graphical summary of the achieved total spatial pixels (spaxels) and spectral channels (voxels) number. Expanding upon these implementations will require careful attention to dielectric material loss, potentially higher-gap superconductor materials, and either improving lithographic precision (down to tens

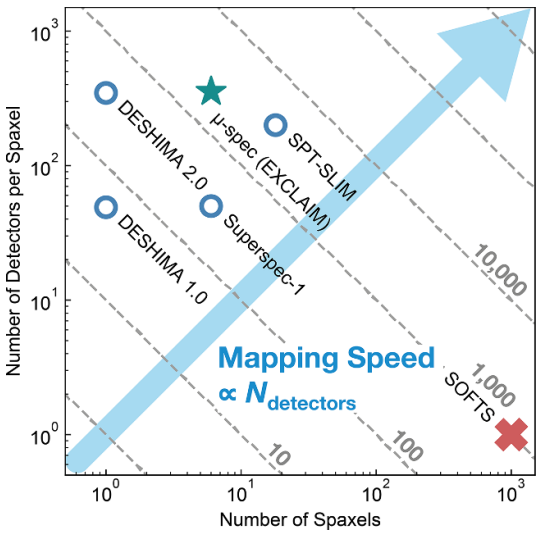

Figure 18. Current astrophotonic (imaging) spectrometers. The dashed lines represent constant total number of detectors $N_{\text{detectors}}$, which is the product of the number of spaxels (horizontal axis) and the number of detectors per spaxel (vertical axis). The mapping speed is proportional to $N_{\text{detectors}}$, regardless of whether the photonic device is a filterbank (○), an FTS (×), or a 2D grating (★).

of nanometers: [360]) or development of new designs. The challenges in the photonic elements (filters, delay lines, etc) reside in the direction of higher frequencies and higher spectral resolution, combined with a high optical efficiency on a system level. Because the resolving power scales with pathlength in the medium, higher frequency resolution requires low-loss transmission lines in the mm/submm frequency range. Another frontier is wider (>one octave) bandwidth. This could be particularly useful for study of individual point sources for which full-band spectra desired. For mapping however, arraying ultra-wide bandwidth SM photonic devices will ultimately be limited in either in beam aperture efficiency or focal plane filling factor, relative to ∼octave-band devices, which can be arrayed with good efficiency.

To improve the frequency resolution and optical efficiency of the photonic elements, dielectric materials with low losses are being investigated. Because coplanar waveguides suffer from large radiation losses, microstrip lines are a preferred option at mm/submm wavelengths. One possibility is to take a crystalline Si membrane from a SOI wafer and process on both sides [346]. Another approach is to deposit a dielectric film, which is more convenient for processing but has the disadvantage that amorphous dielectrics (e.g. SiNx with $Q_{\text{loss}} \sim 1 \times 10^3$ at 235 GHz [361], Si with $Q_{\text{loss}} \sim 3 \times 10^4$ at 350 GHz [362], and SiCx with $Q_{\text{loss}} \sim 1 \times 10^4$ at 270 GHz [363], at cryogenic temperatures) exhibit larger losses than crystals. It is notable that the physical loss mechanisms of amorphous and poly-crystalline dielectrics in the mm/submm are not well understood at cryogenic temperatures [364] (because experiments sensitive enough to measure losses at these low values are only recently being developed and applied, either optically [365] or on-chip [362, 363] and present an opportunity for potential improved performance.

To push beyond the gap frequency of NbTiN (1.1 THz), higher gap superconductors (e.g. MgB_2) must be used. Dielectric losses also increase with frequency (i.e. due to the presence of IR absorption bands wings) and may represent the next limiting factor [365]. In scaling to larger superconducting integrated photonic device formats control over transmission line losses, inter-element crosstalk [366] and unintended modal coupling [367] will become more pressing design considerations. These challenges are seen as manageable, however, will ultimately influence the device topology, layout, and packaging strategies.

An exciting platform for superconducting astrophotonics is space observatories. Here it is encouraging that KIDs have recently shown excellent noise equivalent power down to 3×10^{-20} W Hz$^{-0.5}$ [368]. The next challenge is to integrate this type of KID in an astrophotonic spectrometer. For space applications, mitigation of cosmic rays is also important [369]. Recent advances in wideband planar lens-antennas can be leveraged to meet the need for wideband optical coupling. Using these large-format IFUs strategies to achieve wide-band and field-of-view optical systems represents an additional challenge.

Concluding remarks

Similar to astrophotonic implementations in the optical, superconducting IFUs employ low-loss guided-wave structures, but also utilize the unique properties of superconductors to enable a variety of functions. It is a young and growing field of research, with multiple architectures being explored in parallel.

The overarching goal of enabling 3D volumetric surveys in the millimeter and submillimeter band. A range of astronomical and cosmological applications stand to benefit, from 3D tomographic line intensity mapping to study evolving galaxy populations [355], and cosmological 3D structure [370], to distortions and recombination imprints in the cosmic microwave background spectrum [371]. We encourage the participation of experts from the related fields, including astronomy, solid-state physics, electrical engineering, and data science to collaborate in bringing this technology to its full potential.

Acknowledgments

A portion of this research was carried out at the Jet Propulsion Laboratory, California Institute of Technology, under a contract with the National Aeronautics and Space Administration (80NM0018D0004). A E was supported by the European Union (ERC Consolidator Grant No. 101043486 TIFUUN). Views and opinions expressed are however those of the author(s) only and do not necessarily reflect those of the European Union or the European Research Council Executive Agency. Neither the European Union nor the granting authority can be held responsible for them.

11. Astrophotonic spectral filtering

Simon Ellis[1], *Sylvain Veilleux*[2] *and Joss Bland-Hawthorn*[3]
[1] Australian Astronomical Optics, Astrophysics and Space Technologies Research Centre, Macquarie University, North Ryde, NSW, Australia
[2] Department of Astronomy and Joint Space-Science Institute, University of Maryland, College Park, MD, United States of America
[3] Sydney Institute for Astronomy (SIfA), School of Physics, The University of Sydney, Sydney, Australia

Status

The frontiers of astrophysical knowledge inevitably lie at the limits of detection of the most advanced telescopes and instruments. To advance beyond these limits requires increasing the signal-to-noise of detections, via (i) larger telescopes, (ii) more efficient instruments, (iii) isolating the signal and reducing the sources of noise, or (iv) probing new properties of light, either different wavelengths or higher order moments (e.g. polarization). Astrophotonic filters are aimed at (iii), either by selectively filtering and measuring the signal of interest, or by removing the sources of noise.

Filters (absorptive, interference, holographic, etc) have long been a part of observational astronomy, but astrophotonic filters (i.e. filters embedded into waveguides) offer much more complex filtering with the ability to isolate multiple (>100) specific signals in a single waveguide. The first astrophotonic filters were FBGs, first developed in 2004 [22] to selectively filter the emission from atmospheric OH lines to reduce the background noise in NIR spectroscopy. FBGs have their origins in telecommunications, where typically one fiber can filter a single wavelength. A breakthrough in their application for astronomy was the ability to print *aperiodic* FBGs which can filter >100 wavelengths in a single fiber [9, 372]. Since FBGs require SM behavior, the PL (see sections 3 and 4) was developed in order to incorporate FBGs into the MM fibers necessary for efficient coupling with seeing-limited astronomical telescopes. Further development and refinement of FBGs led to on-sky experiments, GNOSIS [24, 25] and PRAXIS [23], which have demonstrated their efficacy, suppressing 103 OH doublets from 1.47 to 1.7 μm by factors of up to 40 dB (see figure 21), and resulting in a reduction of the integrated background by a factor 9. PRAXIS achieved an end-to-end throughput of ≈18% [23]. Figure 19 shows a sketch of the use of FBGs within an astronomical instrument; similar schemes can be used for other technologies and for multiplexed systems.

To date, SM FBGs in PLs are the only astrophotonic filters to have been incorporated into an astronomical instrument, but there has been considerable attention given to other platforms and other applications. Table 2 lists the different platforms (see figure 20) currently under development, as well as an estimate of their TRL (using NASA's TRL scale of 1–9) and comments on their advantages and challenges. These will be discussed more fully in the next section.

A different use for astrophotonic filters is to isolate the desired signal, for example using the reflected light in an FBG [373] or the drop port of an add-drop ring-resonator [374, 375] or cascaded MMIs [55]. Not only can a specific signal be selected this way, but multiple features can be selected and combined *photonically* in the same waveguide, with no associated electronic noise penalty. For example, exoplanets could be detected by selecting and combining multiple stellar spectral lines (see section 12), and monitoring the rise and fall in intensity (after photometric calibration using e.g. an 90/10 splitter to monitor the variable coupling due to changes of seeing etc) as the spectral features are Doppler shifted into and out of the filter bandpass. This technique could potentially dispense with the need for Doppler-spectroscopy, and the subsequent loss of signal-to-noise, as well as the requirement to observe parts of the spectrum not useful to the analysis, thereby reducing the need for expensive large 2D detector arrays.

Current and future challenges

The main challenges for astrophotonic filtering in general are (i) scaling the technologies to increase the number of modes, and thereby accessible field-of-view and multiplex, (ii) extending the wavelength range of the filters, (iii) integrating the technologies with other photonic components, and with astronomical instruments. Astrophotonic filtering with asymmetric waveguides has the added challenge (iv) of being polarization (TE/TM) dependent. Specific solutions also have their own particular challenges. We discuss these challenges in turn.

(i) *Multi-mode filtering.* Photonic filtering is fundamentally a SM process, since it requires precise control of the phase of the light propagating in the waveguide to produce interference effects, whereas the modes of a MM waveguide will necessarily propagate with different phase velocities making this control impossible. In the diffraction-limited case, e.g. when using AO with high performance correction, it is possible to feed SM waveguides directly [50]. However, the input beam in seeing-limited astronomy is multi-mode and therefore has to be split into SMs without incurring significant losses. Furthermore, this requires high numbers of

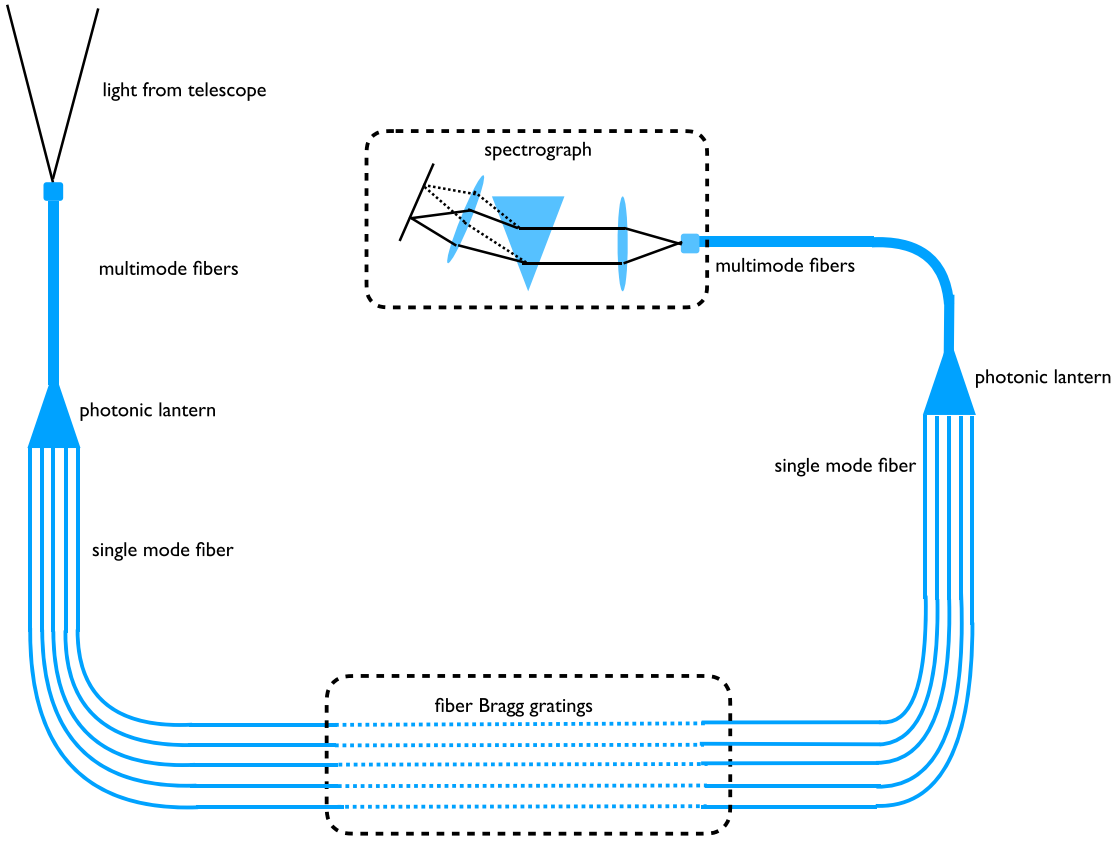

Figure 19. Sketch of a seeing-limited spectrograph employing FBGs embedded in photonic lanterns for spectral filtering of atmospheric emission lines. Light from a telescope is fed into a multimode fiber, which is then split into a number of single mode fibers via a photonic lantern (only five SMFs are shown for clarity, but photonic lanterns can be made with >100 modes). Each SMF then feeds an identical FBG, which performs the filtering, after which the SMFs undergo an inverse transition into a multimode fiber. The multimode fiber then feeds into a spectrograph. This scheme can be extended to multiple fiber inputs, either for multiplexed observations, or for spectral-imaging of a single object. Filters other than FBGs could be used in a similar manner.

replicated devices, all of which must achieve nearly identical performance (requiring high yield fabrication, or low cost). These must then be packaged into the astronomical instrument. For multiplexed observations typical of fiber optic spectroscopy this problem is likewise multiplied.

(ii) *Broad-band filtering.* To date, most astrophotonic filters have been centered on the telecom C band (1530–1565 nm), in order to exploit the R&D and fabrication processes already existing. A key challenge is to extend these processes to other wavelength ranges—ideally across the full UV-visible-NIR spectrum available for use with ground-based optical telescopes. The particular challenges in achieving this are very platform specific. However, some common difficulties are the SM cut-off limiting the bandwidth of a specific waveguide; the transmission of different types of waveguides (0.3 μm < SiO_2 < 1.8 μm; SOI > 1 μm) requiring the use of more exotic or doped glasses; the higher mode count at shorter wavelengths requiring narrower waveguides; the size of required structures scales with wavelength range (e.g. longer Bragg gratings, higher numbers of ring resonators); limitations in the FSR of periodic structures; precision of UV photolithography for UV/visible filtering; scattering errors from waveguide sidewall irregularities; stitching errors between e-beam fields. If accessing the reflected light, as for bandpass filters, then any optical circulators or coupling to drop-port waveguides also need to be broad-band and low-loss.

(iii) *Integration.* Integration has two equivalent challenges, coupling light from the telescope into the waveguides, and coupling light from the waveguides into the instrument. In the first place, there is the difficulty of coupling light into SMF already discussed in (i); see also section 2. This problem is exacerbated when using high-index contrast lithographic waveguides. For example, SOI may have a ~300 × 400 nm profile, leading to a mode-mismatch with SMF-28 causing ~13 dB of loss. For this reason, other lower contrast waveguides such as Si_3N_4 or SOS are often preferred. It is usually preferable to minimize the number of channels imaged onto the detector to avoid spreading the light over an unnecessarily large number of pixels increasing the electronic noise. If a MMF feed is used then it will be necessary to recombine the multiple SM waveguides back into an MM feed. If using an extreme-AO feed this problem can be avoided with direct coupling into SMF at reasonable (50%) efficiency.

Table 2. Techniques of astrophotonic filters, along with an estimate of their technology readiness level (TRL) and comments on their advantages (+) and challenges (−).

Technique Fibers	TRL	Comments
		Fibers
FBGs	8	+ on-sky demonstration [23–25] + complex phase masks for routine manufacture − single-mode usage only − backward cladding-mode coupling − inexpedient to scale to large numbers of modes
Direct write FBGs	4	+ does not require phase masks and photosensitized fibers like standard FBGs [376] − single-mode usage only − not yet demonstrated for complex filtering (e.g. 100 notches)
MCFBGs	3	+ multi-mode usage − uniformity across the multiple cores [377]
Ultra-deep ultra-narrow filters (UDUN)	3	+ very deep (>100 dB) notches + very narrow (<100 MHz) − currently single notch only
		Direct write waveguides
Direct write Bragg gratings	3	+ integrated structure reduces # of interfaces [377, 378] − depth and precision of notch profiles − not yet demonstrated for complex filtering (e.g. 100 notches)
		Integrated photonic circuits
Complex waveguide Bragg gratings (CWBGs)	4	+ compact design reduces stitching errors [90] + end-to-end throughput comparable to that of FBGs when used in combination with fiber-waveguide couplers with adiabatic tapers [90, 379] + ease of integration with other photonic components on a chip + thermo-mechanical stability for precision applications + lithographic printing enables replication + can be incorporated with MMIs to provide add-drop filtering [375] − single-mode usage only − backward cladding-mode coupling [90, 380] − polarization dependence
Ring resonators	3	+ optimized for single notch filtering [374, 375] + tunable using on-chip micro-heaters or stress-optic actuators + lithographic printing enables replication − scalability to complex filtering is not yet demonstrated − small FSR limits bandpass − single-mode usage only − polarization dependence

(iv) *Polarization dependence of asymmetric waveguides.* Waveguides on wafers are inherently polarization dependent, even when the cross-section of the waveguides is symmetric (square). Although there are some polarization independent waveguides these can only work over a relatively narrow wavelength range.

Advances in science and technology to meet challenges

We now discuss the possible solutions and necessary advances in technology needed to address the challenges described in the previous section.

(i) MM filtering. PLs were invented as a direct solution to this problem [7], allowing the conversion between MM and SMF and vice versa. Direct-write waveguide versions of this concept have also been proven [90, 378]. Scaling PLs to very high numbers of modes is difficult, and 'divide-and-conquer' methods [21] may need to be employed. Beyond this, multicore fibers offer an attractive solution, allowing the inscription of multiple Bragg gratings at the same time. Devices with Bragg gratings across 121 cores have been demonstrated, but so far all suffer from a variation in Bragg wavelength as a function of the distance from the

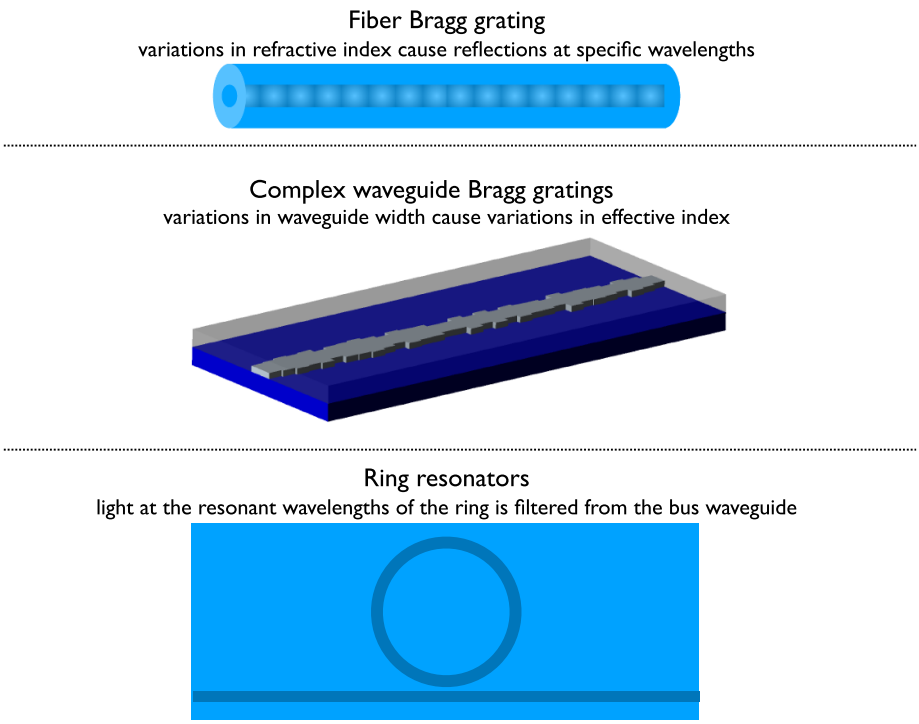

Figure 20. Sketch of the different methods of astrophotonic filtering. The top panel shows a fiber Bragg grating, in which there is a variation in the refractive index of the core, causing light of specific wavelengths to be rejected. The middle panel shows a complex waveguide Bragg grating, which works on the same principle, but the variations in effective index are achieved by varying the waveguide width. The bottom panel shows a ring resonator, in which light with a wavelength which is a unit fraction of the optical path length of the ring is filtered from the input bus waveguide. These same techniques can be applied to different platforms, e.g. fibers, planar waveguides, direct write ultrafast laser inscription etc, with different manufacturing techniques.

center of the core to the center of the fiber, which is not fully understood [381]. Direct-write PLs may offer a solution to this dilemma since then the Bragg gratings are written independently into each waveguide. A totally different approach is the use of extreme AO correction to feed SM waveguides at the diffraction limit [50, 74], with a theoretical coupling efficiency of ∼80%, with the best coupling-efficiency to date of >40% [50]. This technique will be even more apposite in the future era of ELTs with very high AO correction, and very small diffraction limited PSFs, see for example the MODHIS instrument [382].

(ii) *Broad-band filtering*. Part of the solution to this challenge rests in adapting current techniques to new materials, e.g. using fluoride fiber to access wavelengths >1.7 μm, or chalcogenide glasses to access wavelengths up to 20 μm, or UV-fused silica to extend to shorter wavelengths (>195 nm). New recipes for fabricating filters in these different glasses will need to be perfected. Even with the adoption of new materials, the wavelength range will be limited by mode-count, detector sensitivity and FSR, possibly requiring multiple divisions into different wavebands employing differently optimized filters. To extend lithographic filters to shorter wavelengths will require higher precision next-generation nanolithography (e.g. EUV, x-ray, e-beam, focused ion-beam, nanoimprint lithography) to create nm-scale structures and reduce scattering off sidewall irregularities. Losses at wavelengths >1 μm due to N–H and O–H absorption features in Si_3N_4 waveguides can be reduced by annealing *before* patterning to provide wider passbands (0.4–2.4 μm) [383].

(iii) *Integration*. There are several proposed solutions for matching fiber and waveguide modes. Lensed fibers can reduce the mode field diameter to <3 μm, while inverted taper waveguides can expand the waveguide modes to 3.5 μm. These solutions are now becoming mature, with commercial off-the-shelf (COTS) interposer chips available which provide an efficient interface between the chip and a fiber array (see section 23). Moreover, these can work over ultra-broad bands [190], unlike some other telecom devices. Other solutions such as grating couplers are wavelength dependent and therefore operate over limited passbands.

The coupling from the waveguide filters into instruments could be significantly improved with customized detectors. For example, directly bonding photonic devices to detectors with a small pixel pitch that properly samples the output of the photonic device would eliminate the free-space interfaces between the filters and detector and make devices more robust and stable; likewise custom formats of linear arrays or rectangular pixels would allow for more efficient integration in some case; energy resolving sensors (e.g. MKIDS; see sections 23 and 24) could help to alleviate the low FSR of certain types of filters such as ring-resonators.

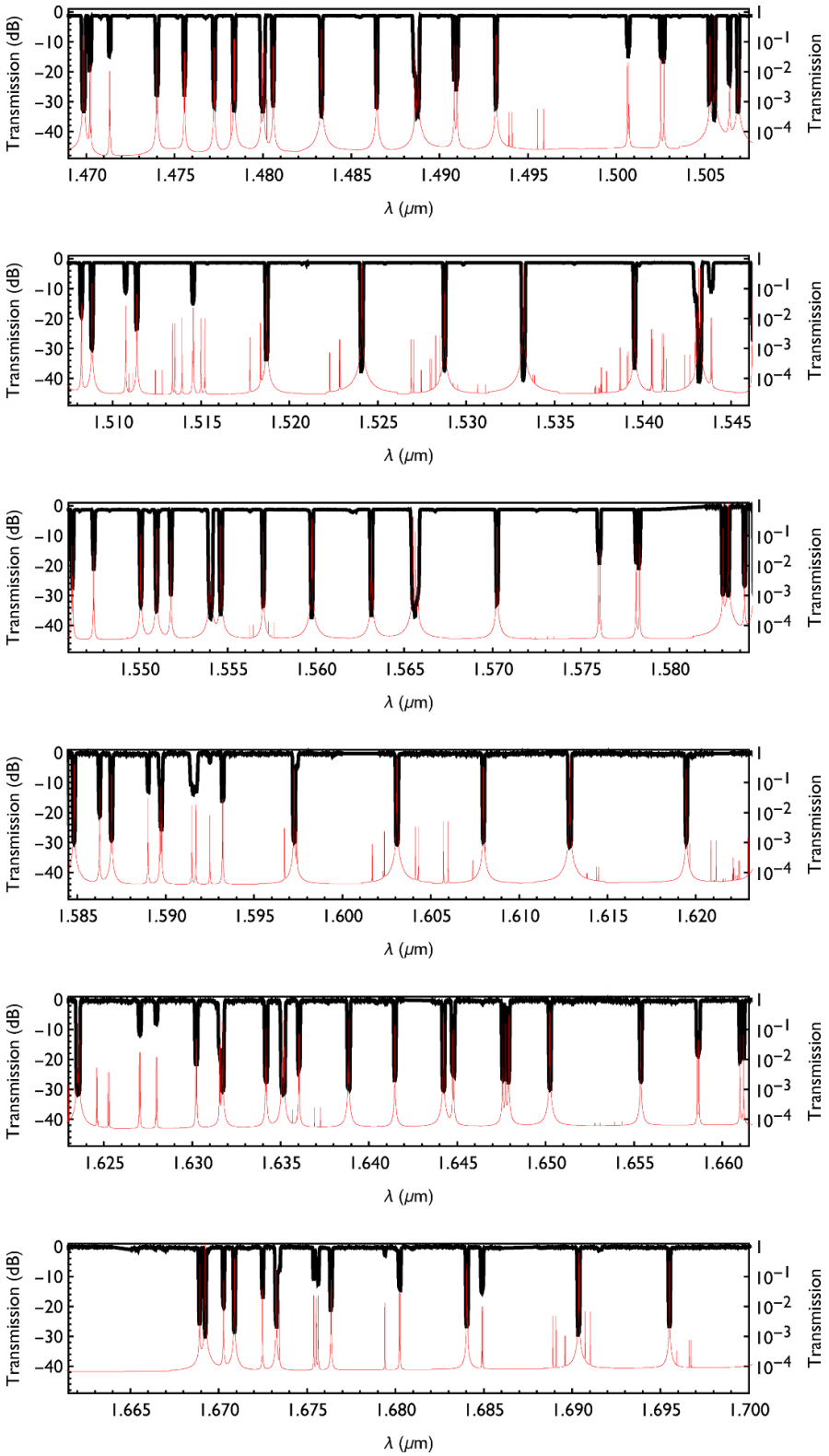

Figure 21. The measured transmission (black) of the FBGs used in the GNOSIS and PRAXIS experiments [24], which consists of two FBGs in series covering 1.47–1.58 μm and 1.58–1.7 μm respectively and filtering 103 OH doublets in total. Also shown is a model of the night sky OH spectrum (red). Note that the FBG response matches the wavelengths, line strength, and OH doublet separation perfectly. This remains the state-of-the-art in astrophotonic filtering, although significant progress is being made with other technologies, see table 2.

(iv) Polarization dependence of asymmetric waveguides. It is extremely challenging to make a polarization-independent waveguide that can work over a wide wavelength range. A more promising approach is to exploit the modular and replicable nature of lithographic photonics and use broad-band polarization splitters based on MMIs [384] or directional couplers [385], or to avoid the problem with fiber-based solutions or direct-write ULI of symmetric waveguides in fused silica.

In addition to the specific challenges described above there is a general need to streamline the fabrication of science-ready astrophotonic devices through dedicated access to facilities and expertise in fabrication, characterization, and packaging [38]. This access is becoming easier due to the availability of commercial foundries, especially those offering MPW fabrication services which significantly reduce the cost for making and testing prototypes.

Concluding remarks

Astrophotonic filters have already been shown to have significant promise for astronomy, most notably for NIR spectroscopy using FBGs to filter atmospheric emission lines. So far the science benefits of photonic filters have only been partially realized, and there are many science cases other than OH suppression which can profit from the complex filtering enabled by the devices discussed, including Doppler planet searches, emission line diagnostics, and wavelength calibration. Beyond this, there are several promising technology platforms being investigated, including novel ways to inscribe Bragg gratings in multicore fibers and direct-write waveguides which will help to enable a scaling-up of this technology for larger fields-of-view and higher multiplexing capability. A significant, but challenging, development is the integration of photonic filters on lithographic photonic circuits. This has the potential for extremely miniaturized devices, which are modular and easily integratable with other photonic devices such as arrayed-waveguide gratings (sections 6 and 7) and photonic beam combiners (sections 16, 17 and 20) with the ultimate aim of fully photonic instruments.

12. Measure what you need with optical correlation spectroscopy

Sebastiaan Y Haffert[1] *and Peter Tuthill*[2]
[1] Steward Observatory, University of Arizona, Tucson, AZ, United States of America
[2] Sydney Institute for Astronomy (SIfA), School of Physics, The University of Sydney, Sydney, Australia

Status

Technological advances driving ever larger telescope apertures have also increased the size of the instruments [386]. Competitive astrophysics demands ever higher spectral resolution, more simultaneous spatial points and larger bandwidths. In particular, high spectral resolving power is needed for identification of atomic and molecular gasses in astronomical objects as their spectral fingerprints may be distinguished at high resolution. Spectral differentiation between species is now used as a successful post-processing technique to search for exoplanets with direct imaging instruments [387, 388]. Applying such techniques to large fields would allow us to map the chemical compositions of many objects simultaneously, like stars in dense stellar clusters, or extended objects like the Orion Nebula. However, the competing requirements are difficult to fulfill for IFU s and MO spectrographs that require many simultaneously sampled spatial points. Conventional spectrographs—which must be built with real-world limitations on the size of the optics, number of pixels, and data rates—are therefore forced into compromises between spatial sampling, spectral resolving power and bandwidth. Optical cross-correlation offers a pathway to avoid this compromise based on the realization that acquiring the full spectrum may not be necessary for all science applications. We may require, say, only a measurement of the elemental composition, without details of all the lines present. Distinguishing information at high spectral resolution need not mandate the recovery of every single spectral channel.

Such measurements can be achieved through optical correlation spectroscopy (OCS) in which light passes through a spectral filter that partially mimics the spectrum of the element of interest [389] (see figure 22). The simplest example of a spectral filter might be a template tailored to match the response of one specific molecule, whose presence is then indicated by measuring the total intensity passing through. Most light passes through if the same lines are present in the analyzed spectrum and the filter. However, a lower intensity is measured if there are different lines present in the filter and the spectrum. This means that a single intensity measurement is sensitive to the presence or absence of specific species. Obtaining a high spectral specificity in a single sensor element breaks the trade-off above between resolution, spectral bandwidth, and density of spatial sampling. While a single intensity measurement is enough in theory, flux variations require two measurements (with and without the spectral filter) to normalize the incoming amount of light.

There are several different ways to implement an OCS. The earliest methods used gas-cells that contained the gas of interest [389]. These may be considered ideal spectral filters as they contain exactly all the lines of interest. A downside to the gas-cell correlators is that not all elements can be contained in a cell at astronomical temperatures and/or pressures. A tunable optical filter that replaces the gas-cell is preferred for OCS in astronomy where elements occur under conditions that cannot be reproduced on Earth, and also noting that astronomical objects are not observed in the same rest frame causing lines to undergo Doppler shifts [390].

Current and future challenges

OCS recovers a compressed data stream so generally requires simpler input optics, detectors and output signal train. The key challenge for implementation of OCS is realization of the spectral filter. To date this has been accomplished with several different implementations (see figure 23).

Interferometric filters

Interferometric filters use path length differences to create regularly spaced absorption peaks through constructive and destructive interference. This is often done with a Lyot Filter [391], Fabry–Perot [392, 393] or a Michelson [394] interferometer. More recently, photonic implementations use ring resonators [261] to create a regular pattern. While velocity shifts of the template can be achieved by adjusting the path length, this approach is unable to form a tailored match to spectra of arbitrary line spacing and complexity.

FBGs

While interferometric methods such as etalons can successfully exploit regularities in the spectral response of many gasses, the use of FBGs offers dramatically greater flexibility. In particular it is possible with modern aperiodic grating designs to obtain an excellent match even for complicated sets of irregularly spaced atomic or molecular lines. Such bespoke gratings may be tailored to target gas species with high specificity [395] and can be fabricated from the visible through the NIR. Such an optic may be integrated into a working sensor

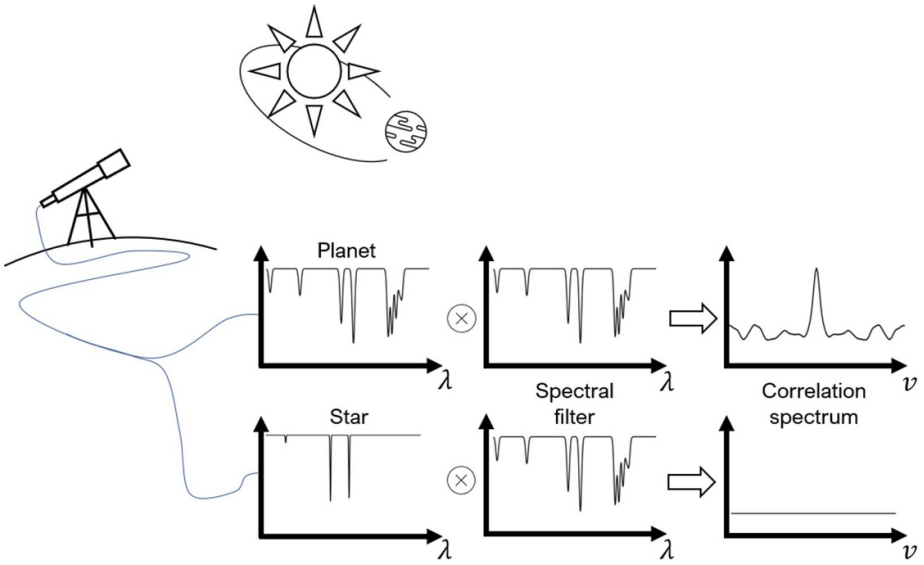

Figure 22. Light from two astrophysical sources (a star and a planet in this case) are fed to an optical cross-correlator spectrograph. The OSC passes the light of the objects through a spectral filter that is matched to a particular element in the planet's atmosphere. The planet has a strong correlation, while the star has no correlation signal at all. This allows the OCS to search for particular elements.

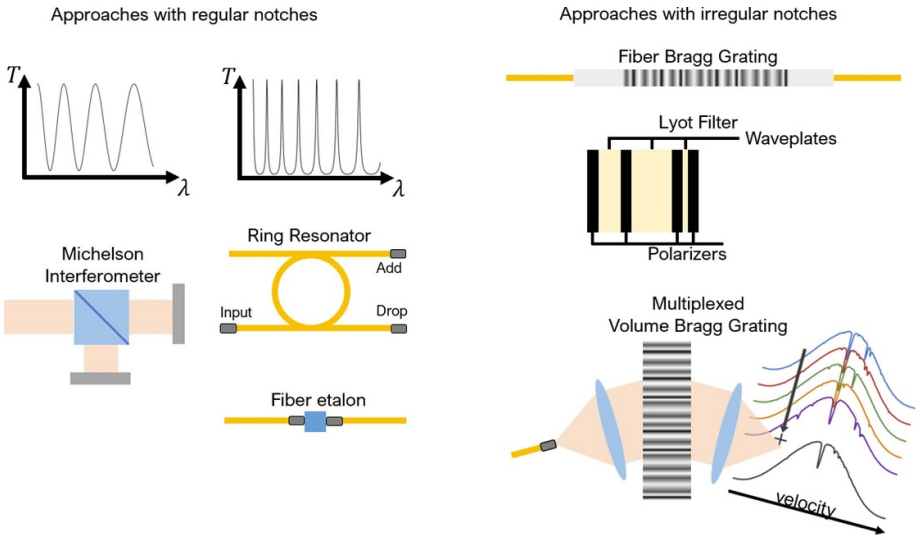

Figure 23. An overview of different ways to implement the optical correlation filter. The systems on the left create notches regularly spaced in frequency (diagrams at the top). The systems on the right create irregular notches by multi-step modulation. Figure 22 shows an example of irregular notches.

system [396] by imposing a variable filter velocity response (potentially by way of a fiber stretcher, or tuning the response with temperature), and ideally facilitates recovery of both the reflected and transmitted beams to optimize capability for accurate calibration. Current FBGs have reached a spectral resolution close to 100 000 which is more than sufficient for scientific observations. FBGs require that the light passes through a SMF. However, spatially coherent sources (such as stars) need high performing AO correction (see section 2) for efficient coupling into SMF [50], which is very challenging towards shorter wavelengths. Extreme AO systems deliver much higher performance at wavelengths upwards of 2.0 μm, but at those wavelengths the SMF needs different materials as silica is not transmissive anymore. FBGs have not yet been demonstrated at longer wavelengths.

Multiplexed Volume Bragg gratings

Volume Bragg gratings (VBGs) are thick transparent gratings that have a periodic modulation of the refractive index. The VBG diffracts only a narrow wavelength range around the Bragg wavelength. Multiple gratings can be created in a VBG at the same time if the refractive index profile is a superposition of the

individual grating profiles [397]. Such a grating is called a multiplexed VBG (MVBG). Each grating then diffracts its specific spectral line in the same direction (angle) where they incoherently combine on the same detector pixel. Effectively creating the OCS signal. An advantage of this method is that it creates a tiny spectrum around the diffracted wavelength. This tiny spectrum is the velocity correlation spectrum. The presence and velocity of the template gas species can be measured at the same time, which is an advantage over most other methods.

FBGs have recently been made for spectra with very complicated profiles, such as for OH-suppression filters [22]. The FBGs are inscribed inside the core of silica fibers by using holography and phase masks [398]. This fabrication approach fails for MVBGs due to their thickness: instead a method in which refractive index structures are laser engraved within a substrate (so-called 'direct write') [90] is used. However grating-based approaches have a strict tolerance on the written grating period: the relative precision is the inverse of the spectral resolving power. For MVBGs the precision has to be better than 1×10^{-5} to meet a design specification of $R = 100\,000$ and unfortunately current direct-write methods are not yet at the level where this is possible over sufficiently large areas (30×30 mm) due to aberrations in the writing systems [399].

Advances in science and technology to meet challenges

Most OCS instruments deployed to date have either been based on the gas-cell method or interferometric approaches due to simplicity of the technology and ease of implementation. They have demonstrated most success for molecules with rovibrational transitions that create lines with relatively regular spacing. However in reality lines are never exactly periodic, imposing a limitation on the interferometric approach to a small part of the spectrum (and consequently to bright objects). Many other species have complex line patterns that are not regular at all. Filters with regular spacings between the notches cannot create the required spectral templates. Complex filters with aperiodic notches are required for most cases. The multiplexed VBG and the aperiodic FBG are therefore the most promising methods for OCS as these provide the most flexibility in template spectra. However, as discussed before several challenges have to be solved.

Integral-field OCS with FBGs present challenges due to the SMF injection step. Single-mode IFUs, often exploiting a micro-lens array to inject into a matched array of fibers, have been successfully demonstrated in the past few years [78]. Nevertheless, the stringent spatial beam requirements for efficient SM injection drive challenges for IFU throughput and efficiency. Few-moded fibers in concert with lanterns may present one pathway for FBG based integral-field OCS to boost efficiency [21, 400]. However such arrays of low mode-count PLs have not been developed, with further innovations needed to couple them to banks of FBGs (see section 4).

A fundamental issue for the FBG is that at each moment in time only a single correlation match to the template is made, so that time modulation of the response is required to recover velocity information. At the cost of escalating optical complexity, a scheme might be envisaged whereby light from a first-stage FBG is passed to a second FBG tuned to a slightly different velocity. A cascade of such FBGs (where reflected light from one FBG is sent to the next FBG in the cascade and the transmitted light from all the FBGs is measured) can be used to create the velocity spectrum instantaneously with no need for a time sweep. The FBG alters the trade space from spectrograph real estate to telescope observing time and spectral templates. Measurements have to be taken sequentially if several species or Doppler shifts have to be measured. One possible scheme may implement a different FBG filter (tuned for various molecular species) that tiles some region of spatial extent in the image plane. Some scheme of dithering or field rotation would then bring different spatial elements into alignment with different FBG filters, over time sampling the whole scene with templates matched to all species.

The MVBG can provide access to multiple species and velocity channels in a single shot. However, the complexity of the grating increases with every additional information point. This requires very accurate control over the grating pattern which is not available with passive direct write methods. AO techniques are deployed to create stable and high precision direct-write setups and have shown promise in improving the write quality [401]. Acousto-optical gratings [397, 402], in which sound waves act to modulate the refractive index, are also being explored to provide an alternative. Multiplexed gratings can be realized by sending complex waveforms through the material. With active control of the acoustic synthesizer, the demanding requirements to implement an MVBG can be met. There are two technical challenges to overcome. The high-spectral resolution of $R = 100\,000$ requires a large piece of EO crystal with high homogeneity, which is difficult and expensive to source. Furthermore, the required acoustic power scales with λ^4. Large gratings require injection of significant acoustic power for lines at longer wavelengths which generates waste heat in the crystal that needs to be extracted.

Concluding remarks

Optical correlation spectroscopy is a promising technique to map gasses and elements, distilling information at high spectral resolution over significant fields-of-view. This technique allows us to think in a different way about observing. There are many advantages to compressing the information content of the data optically, before the light reaches the sensor, recovering the imprint of the chemical content in the spectrum, rather than the wealth of lines themselves. The method could accomplish our science with fewer targeted measurements, offering relief where constraints from instrumentation or data volume hamper progress. However, it is still a relatively new technique for astronomy and there remain hurdles to be overcome before working systems can be deployed to modern observatories.

Acknowledgments

Support for SYH was provided by NASA through the NASA Hubble Fellowship Grant #HST-HF2-51436.001-A awarded by the Space Telescope Science Institute, which is operated by the Association of Universities for Research in Astronomy, Incorporated, under NASA Contract NAS5-26555.

13. Laser frequency combs

Chad F. Bender[1], *Scott A Diddams*[2], *Tobias Herr*[3], *Stephanie Leifer*[5], *Ewelina Obrzud*[4] *and Kerry Vahala*[5]
[1] Steward Observatory, University of Arizona, Tucson, AZ, United States of America
[2] Electrical, Computer and Energy Engineering and Department of Physics, University of Colorado, Boulder, CO, United States of America
[3] Deutsches Elektronen-Synchrotron DESY, Germany and Universität Hamburg, Hamburg, Germany
[4] Centre Suisse d'Electronique et de Microtechnique, Neuchâtel, Switzerland
[5] Department of Applied Physics, California Institute of Technology, Pasadena, CA, United States of America

Status

LFC, the Nobel prize-winning technology recognized in 2005 [26, 27], have revolutionized time and frequency metrology. The LFC or, alternately, optical frequency comb (OFC) is an optical spectrum produced by a laser that consists of an array of delta-function-like frequency modes with perfectly uniform spacing determined by the laser's RF-domain pulse repetition rate, f_{rep}. All modes share a common frequency offset, f_0, that can be measured and controlled with the technique of $f-2f$ self-referencing [403]. In this way the frequency of each mode of the comb, f_n, is given by $f_n = nf_{\mathrm{rep}} + f_0$, where n is an integer and f_0 and f_{rep} can be referenced to an atomic clock with uncertainty given by the clock itself. For example, when referenced to the clocks in the global navigation satellite system, the LFC inherits a typical fractional uncertainty of 10^{-12} or 10^{-13}. It is accordingly a very precise 'spectral ruler' for measuring any frequency of light. In precision astronomical spectroscopy, LFCs are ideal calibration sources with performance that surpasses the systematic uncertainty introduced by existing spectrographs and astronomical processes such as stellar activity. On the other hand, the intrinsic noise in the LFC supports frequency synthesis at and below the 10^{-21} level [404]. As such, it also serves as the clockwork that links RF and optical domains to implement optical atomic clocks with present frequency uncertainty at the 10^{-18} level [405], which is two orders-of-magnitude more precise than current time standards. Thus, LFCs can be a critical tool for studying a wide range of challenging questions in physics and astronomy that involve precision frequency measurements.

There are a variety of methods of generating LFCs, and the resultant combs can be characterized by their mode spacing (f_{rep}), spectral bandwidth (visible through MIR), and optical power. The most mature comb technology, in terms of commercialization, is the fiber laser comb composed of all-optical-fiber components that form a passively mode-locked laser cavity in sequence with a fiber amplifier, supercontinuum generator, and f–$2f$ interferometer [406]. These low repetition rate combs ($f_{\mathrm{rep}} \sim 100$ MHz), operating in the NIR (center wavelength of 1550 nm), are used to form an essential component of a new generation of optical atomic clocks. A space-based network of optical atomic clocks that utilize LFCs as the clockwork with 10^{-18} accuracy has been proposed for gravitational wave detection [407, 408], relativistic geodesy, dark matter experiments [409], opportunities to search for violations of general relativity [410], the standard model, and the Einstein equivalence principle, and to provide the potential to discover new physics [411]. When used for femtosecond-level time transfer or synchronization, LFC technology could enable synchronization of distant sites such as those used for the Event Horizon Telescope [412], a global network of radio telescopes that can provide very high angular resolution imaging, thereby drastically reducing extensive, compute-intensive post processing needed to correctly align the constituent signals.

An LFC referenced to an atomic clock and the SI second has become an essential wavelength calibration tool. As the LO in a heterodyne radiometer [413], they could provide higher resolution Doppler maps of the sun than those produced by NASA's Solar Dynamics Observatory [414]. But in the astronomy community, LFCs have found their greatest application in ground-based Precision Radial Velocity (PRV) measurements, and when specialized for this role, are dubbed 'astrocombs' [28, 29, 415]. With absolute stability at the 10^{-12} level or better, corresponding to the Doppler shift of <1 cm s^{-1}, astrocombs provide sufficient precision in spectral calibrations for PRV spectrographs that aim to measure <10 cm s^{-1} Doppler shifts in absorption features of G-type stars, and in so doing, enable characterization of earth-like exoplanets. There are currently more than a dozen astrocombs demonstrated or in operation at major optical and NIR facilities that are pursuing this and related RV measurements [30, 31, 416]. They cover a range of wavelengths from $\sim$500 nm to greater than 2 μm, and have been customized to provide spectra with mode spacing appropriate for the unique spectrographs they calibrate (10–30 GHz). This flexibility makes astrocombs attractive calibration sources even for non-PRV spectrographs as a replacement for traditional hollow-cathode lamps that provide inferior calibration spectra due to a nonuniform line distribution over the spectral span, high dynamic range and line blending. Moreover, in some cases, such lamps are difficult to procure due to changing environmental and geopolitical restrictions. Figure 24 depicts comb generation by various methods, as well as various applications in astronomy as a function of RV precision and wavelength.

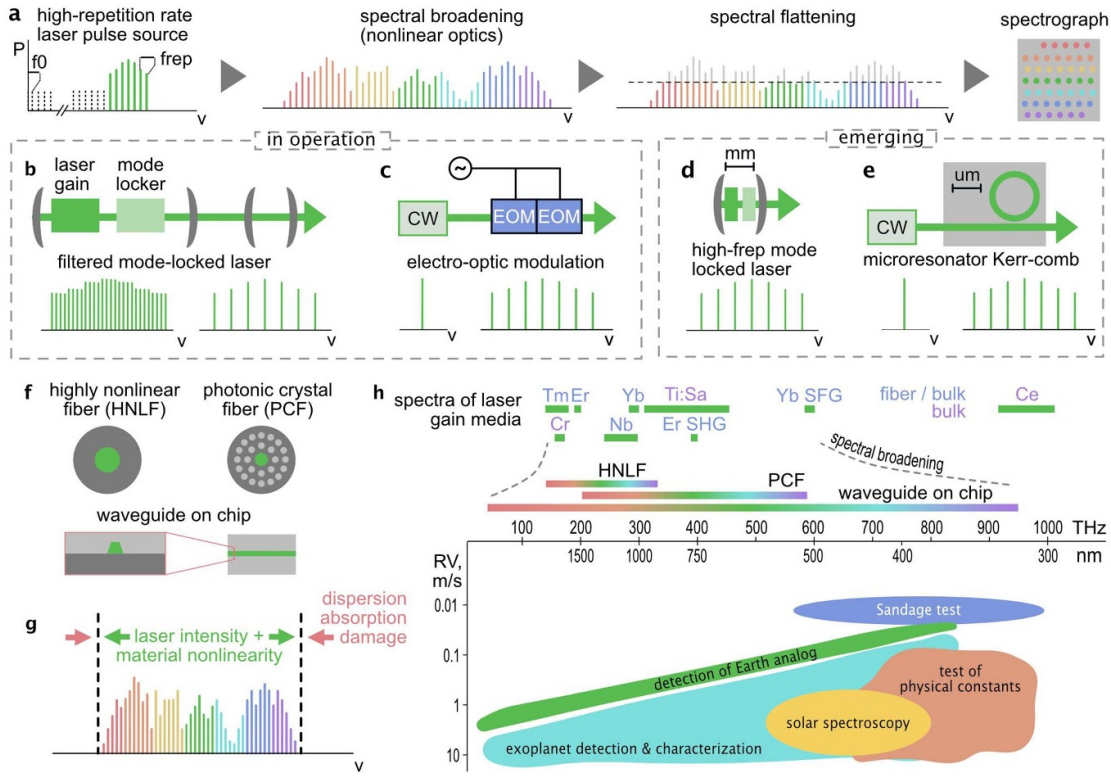

Figure 24. (a) Steps for astrocomb generation: generating a widely spaced, relatively narrow-band frequency comb from a high repetition rate pulsed laser, spectral broadening into a broadband spectrum with the same line spacing and spectral flattening for equal spectral flux across the detector. The comb spectrum is characterized by a frequency offset ($f0$) and the comb line spacing, equal to the pulse repetition rate (frep). The initial comb spectrum may be derived from a (b) filtered mode-locked laser or an (c) electro-optic modulation-based (EOM) comb generator; emerging sources include (d) high-repetition rate mode-locked lasers and (e) chip-integrated Kerr-nonlinear microresonators. (f) Highly-nonlinear fiber (HNLF) and photonic crystal fiber (PCF) are established silica-based fibers for nonlinear spectral broadening. More significant broadening may be observed in chip-integrated waveguides that permit even stronger light confinement and materials with higher optical nonlinearity. (g) Broadband spectral broadening relies on high laser intensity and optical material nonlinearity; the achieved bandwidth is usually limited due to chromatic dispersion, absorption or damage of the material. (h) Optical spectra of common laser gain media are sparse and narrowband. Spectral broadening by HNLF, PCF or chip-based waveguides can, in principle, generate broadband spectra from infrared to ultraviolet wavelength. Such broadband spectra are required to address important science cases of precision RV measurements; their spectral requirements along with their requirements for RV precision are highlighted.

Current and future challenges

The promise of astrocombs often belies coupled scientific and technical challenges that limit the widespread application of these highly complex systems. When one considers the details of frequency combs, there are many challenges that must be addressed including comb spectral flatness, low temporal variability, uniform coupling to MM spectrographs, and polarization effects in SM spectrographs. But the most critical issues at this point in time can be essentially described as: (1) overall complexity which is coupled to size, weight, need for maintenance, operation over many years, environmental stability, remote operability, and cost; and (2) full spectral coverage that matches that of stellar spectra, with particular shortcomings on the blue side of the frequency comb spectrum.

Frequency combs are significantly more complicated and costly than traditional calibration sources such as hollow-cathode discharge lamps or gas cells. This complication arises in part from the fact that they are built on active lasers, but it is compounded by the coupled requirements of large mode spacing ($f_{\mathrm{rep}} \sim$ 10–30 GHz) and broad spectral bandwidth (as large as $\Delta\lambda =$ 350–2500 nm). To achieve both of these at the same time requires combinations of average power and pulse duration that are not found in any common LFC. The canonical approach, shown in figure 24(a), involves creation of a high repetition rate pulse train (a comb with narrow spectral bandwidth), whose short pulses along with amplification permit spectral broadening through nonlinear optical processes. Finally, the spectral envelope of the broadened spectra is flattened to avoid over- and under-exposure of the detector, and detector effects such as the 'brighter-fatter' effect [32] that can induce erroneous RV signatures.

A first challenge is to identify a pulse source that permits operation at high pulse repetition rates. As shown in figure 24, comb technologies that are being explored include: (a) low repetition rate lasers that are subsequently filtered to provide large mode spacing [28, 29, 417, 418], (b) EO frequency combs that

intrinsically generate 10 GHz combs [419–421] (c) high-repetition rate active lasers [422, 423], and (d) microresonator frequency combs, also known as microcombs [57, 424]. There are tradeoffs that must be made in all of these technological approaches, e.g. wavelength of operation, permissible comb line spacing, size, complexity, cost and ease of operation.

Regardless of the pulse source, a fundamental challenge is that 10 GHz combs have low pulse energy which restricts the nonlinear optics required to generate broad spectral bandwidth, such that maximal RV information can be obtained. The most straightforward way to address this challenge is by increasing the average optical power to the multi-Watt level, but this comes with challenges of thermal management and damage in the LFC system and degradation of components. Such factors further drive the price and complexity, which restricts reliability. Presently, this is most challenging for frequency combs aimed at RV measurements on Sun-like G stars where the desired spectral coverage is ∼380 nm to beyond 800 nm, or more than 400 THz and 40 000 comb lines at 10 GHz comb spacing. Nonlinear spectral broadening in silica fibers has been developed to cover this spectral range. However, the reliability of such an approach is limited due to rapid damage of the fiber upon UV exposure [425]. Thus, reliable operation is only routinely achieved at wavelengths longer than approximately 500 nm, excluding nearly 200 THz of valuable spectral bandwidth. Continued research efforts are needed to provide reliable solutions for continuous nightly spectral LFC calibration down to the shortest blue wavelengths.

Advances in science and technology to meet challenges

Major technological advancement can be expected from new materials and their potential to be monolithically integrated on photonic chips for efficient nonlinear optics, compactness and cost reduction. The integration of comb systems requires a range of optical technologies to be co-located on a common silicon substrate. In recent years, the narrow bandwidth comb sources themselves have undergone rapid development based on two technologies: soliton microcombs and thin-film lithium niobate EO modulators [251, 426]. Moreover, integrated nonlinear waveguides have been fabricated showing dramatic spectral broadening and opportunity for spectral tailoring through optimized geometries potentially beyond what is possible in current nonlinear silica fibers [427–431]. Each of these platforms has created opportunities for the complete integration of future comb systems.

Soliton microcombs are miniature mode-locked parametric oscillators fabricated from high-Q optical microcavities [251]. They can be self-referenced and have been used to demonstrate all comb functions including optical clocks and optical synthesizers. While early microcombs were demonstrated as discrete devices, significant progress in optical loss reduction of CMOS-friendly materials such as silicon nitride has made possible microfabrication of more complex microcomb systems. These combine integrated waveguides as well as soliton repetition-rate tuning control. Also, these systems have been heterogeneously integrated with III–V semiconductor lasers for comb pumping. Surprisingly, the pumping of microcombs can be configured to simplify comb activation while also eliminating difficult-to-integrate functions like optical isolators. Compact, butterfly-packaged microcomb systems with optical pump and tuning controls have resulted [173, 252].

While microcombs are transitioning conventional table-top mode-locked combs to a semiconductor chip, there is also a renaissance in the world of EO combs. Here, the advent of the material system thin-film-$LiNO_3$ on silicon brings the key features of this photonic workhorse material (harmonic generation and EO modulation) into the realm of semiconductor microfabrication. The resulting capability to engineer dispersion and precisely control waveguide dimensions has enhanced the performance of devices like EO-modulators by lowering their V_pi values. It is also dramatically expanding the ways $LiNO_3$ can be fashioned into optical devices and complex systems on-a-chip. Miniature resonant modulators and even electro-optically controlled microcombs are two examples [426, 432].

With this rapid progress in microcomb and EO-comb technology, a pathway exists to compact, integrated astrocomb systems. However, before this can happen, efficient nanophotonic spectral broadening must also be integrated with the comb generator. Again, a challenge here is the low pulse energy that is available from the integrated micro and EO comb generators. Presently off-chip fiber amplifiers must be employed to boost peak power to a sufficient level (∼10–100 pJ in 100 fs) to achieve the required spectral broadening. Nonetheless, there is significant progress in the exploration of new materials that offer multi-order-of-magnitude enhancements to optical nonlinearity that are critical for broad spectrum generation. Material platforms of UV transparent media like MgO-doped $LiNO_3$ [428, 429, 433], AlN [430, 434] and diamond [435] show some promise based on efficient spectral broadening and harmonic generation including at the high-repetition rates of astrocombs [436]. Their nanophotonic integration offers new opportunities for tailored spectra, however, more research and development is required to achieve high-power handling capability and sufficient flux at short wavelengths.

Concluding remarks

Future LFC precision calibrators will need to balance mature and emerging technologies to address conflicting requirements of broadband calibration and high reliability at reduced cost. Integrated photonics will play an important part in this development and hold prospects not only for improved performance but also for low-complexity, robust monolithic systems at lower cost; in case of device failure, such systems could potentially be swapped like a light bulb. On a practical note, the development cost of these miniature systems will be shared with other application areas, including miniaturized precision timing and navigation systems, airborne radar systems, and field-deployable precision chemical sensors. To leverage the full potential of LFCs, dedicated data pipelines and instrumental interfaces (including spectral flatteners—see section 14) will need to be developed. Additional developments in AO and SMF-fed spectrographs may bring a significant advance when calibrated with LFCs. And finally, the reduction of size, weight and power consumption creates opportunities for space-based EPRV observations as well as unperturbed studies of planetary atmospheres.

Acknowledgments

S Diddams acknowledges support from NIST, JPL, and NSF Grants AST-1310875 and AST-2009982.

T Herr acknowledges support by the Helmholtz YIG VH-NG-1404 and the EU ERC StG 853564.

14. Spectral flattening of laser frequency combs on-a-chip

Nemanja Jovanovic[1], *Stephanie Leifer*[2] *and Charles Beichman*[3]
[1] Department of Astronomy, California Institute of Technology, Pasadena, CA, United States of America
[2] Department of Applied Physics, California Institute of Technology, Pasadena, CA, United States of America
[3] IPAC/NASA Exoplanet Science Institute, Jet Propulsion Laboratory, California Institute of Technology, Pasadena, CA, United States of America

Status

The PRV technique is critical to the detection and characterization of exoplanets and relies on the measurement of Doppler shifts of the host star's spectral features [437]. Key to the success of PRV observations is an ultrastable wavelength standard, ultimately requiring sub-cm s^{-1} long-term precision and accuracy to enable the detection of terrestrial planets in the habitable zones of solar-type stars, which induce shifts as small as ∼9 cm s^{-1} over a year [416]. LFCs offer exquisite long term stability making them ideal for this application (see section 13 in the roadmap). However, due to the nonlinear broadening processes that generate broad comb spectra, the amplitude of the comb lines can vary by many orders of magnitude (see figure 25). As Doppler precision scales with the square root of the number of lines used to derive the wavelength solution, it is critical to exploit the maximum number of lines when developing a wavelength solution. The limited dynamic range of astronomical detectors imposes limits on the amplitude variation that can be tolerated. In addition, the signal-to-noise per comb line scales with the square root of the number of photons per line. To achieve high precision with short integrations, it is clear that a flat, bright spectrum where each line is not saturating the detector would be ideal. In addition, the comb line amplitudes should be extremely stable, as changes to the comb profile of the spectrum can masquerade as erroneous Doppler shifts. To meet these requirements, a device called a 'flattener' is often used, downstream of the comb. Commonly, flatteners first collimate the LFC light from an optical fiber, disperse it with a grating, and then use a liquid crystal on silicon spatial light modulator (SLM) to control the amplitude of each spectral channel before recombining the spectrum and injecting it into another fiber [438]. These flatteners are large complex assemblies (see figure 25) requiring careful alignment, and the dynamic range afforded by the SLMs (20–30 dB) is often inadequate to flatten the spectrum produced by an LFC. Further, they are tailored for specific spectral bands and require developmental effort to move into new wavebands.

A photonic solution offers the possibility for a compact, portable, replicable, and inherently stable package that may even enable space-based applications. One such solution is an all-photonic spectral flattener based on SiN waveguides consisting of an AWG which disperses the light, MZIs to actively control the amplitude in each channel, thermo-optic phase modulators (TOPMs) to re-phase the channels, and a second AWG used in reverse to recombine the spectrum. Our group has recently demonstrated such a device with 20 channels providing ∼40 dB of dynamic amplitude modulation range for a linearly polarized input source [41, 42]. It was capable of flattening a temporally incoherent source to a residual amplitude variation of 3 dB, and an LFC spectrum to ∼5 dB where both sources started with >25 dB of variation over 250 nm (1400–1650 nm). The device has a millisecond response time (kHz) to make corrections and can handle optical power levels of hundreds of milliWatts. The current device operates in the near-IR, suitable for instruments designed to study planets orbiting cool, mid- to late M stars. Future devices could provide spectral flattening at optical wavelengths appropriate for instrumentation studying warmer, solar-type stars.

Another method for producing broad, relatively flat comb spectra is to accomplish it through engineering the appropriate combination of dispersion and geometry in the nonlinear photonic waveguides used for supercontinuum generation [439]. This would eliminate or reduce the need for an external flattener on-a-chip. Very broad spectra have been demonstrated in, for example, SiN [440], magnesium oxide doped lithium niobate thin films on silicon [428, 433], tantala [431, 441], and aluminum nitride structures [434].

Beyond LFC flattening, spectral shaping devices can find applications in other fields including add/drop multiplexing [442], gain flattening [43, 44], temporal pulse shaping [45, 46] as well as for targeted excitation of particular molecular species [47].

Current and future challenges

To advance all-photonic flattening technologies, requirements for specific science cases must be set with an understanding of how Doppler precision relates to the power stability of the comb spectrum. This has not been rigorously explored to date and requires simulations to understand how variations in the comb spectrum propagate to Doppler errors. Once the power stability requirement is determined for a specific science case, the device parameters (resolution, number of channels, overall bandwidth etc) can be established. Furthermore, other photonic devices, such as FBGs could be used to compensate for static, large

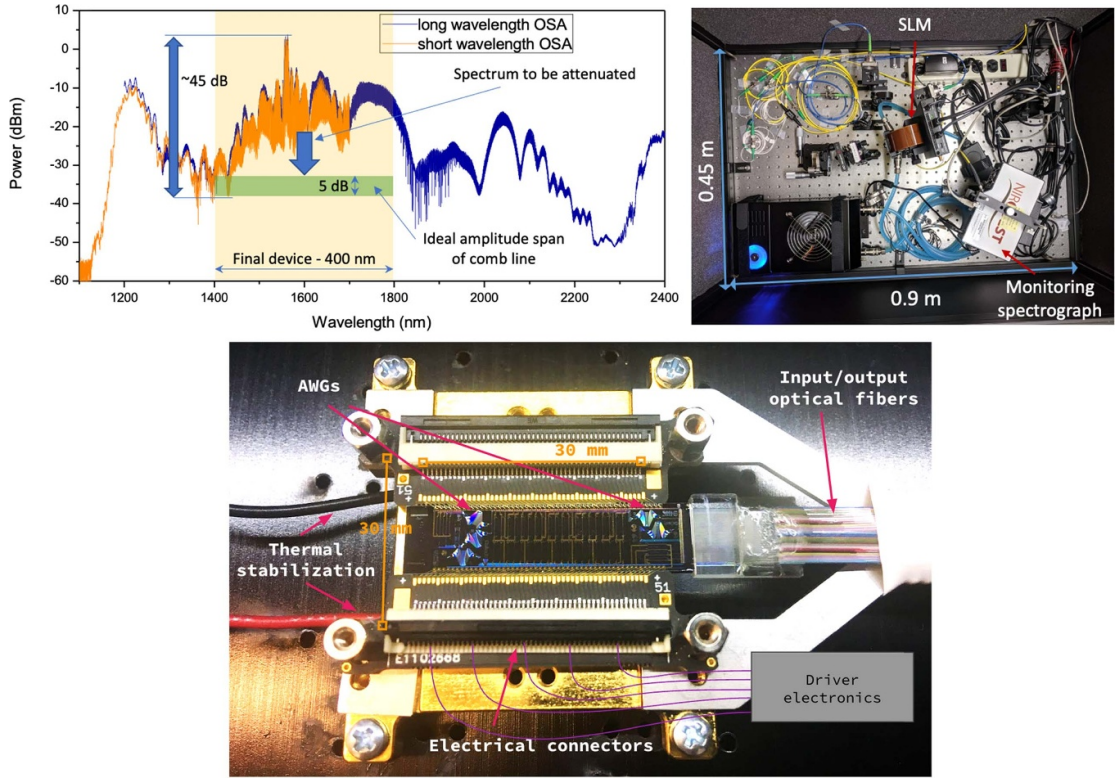

Figure 25. (Top) (Left) a spectrum of the Palomar Radial Velocity Instrument (PARVI) LFC showing the strong intensity modulations across the spectrum. (Right) PARVI's bulk optic flattener. The flattener occupies a volume of $1 \times 0.5 \times 0.5$ m^3. (Bottom) An image of the generation one all-photonic flattener device tested in the laboratory. Reprinted with permission from [42] © The Optical Society.

amplitude power variations such as those around the pump region of the comb. The division of flattening capability between these photonic solutions needs to be determined through careful characterization of the specific comb to be used.

Technical challenges include sufficient AWG channel spacing to correct for narrowband features around the pump region. Devices with higher channel counts will be necessary, requiring the addition of more MZIs and TOPMs, and their associated electrodes and driver electronics. These devices are non-negligible in size (2–3 $\times$ 1 mm using SiN) and will eventually push the circuit size beyond a single reticle. Devices can be made across multiple reticles, but there could be stitching errors, although these are improving over time with advances in manufacturing processes. In addition, narrower channels may be desirable in some regions of the spectrum and could be accomplished with a cascaded approach [180], where a low resolution device is used over a broad band and narrower devices are used as a secondary stage (see figure 26 for an example of this concept). Adding more AWGs to the chip or increasing the resolving power of an AWG with a fixed bandwidth both increase the chip size and is limited by either reticle size (limit for a single device) or total usable area on the wafer. In addition, making high resolution, large FSR AWGs is plagued with many issues in itself (see sections 6 and 7 in this roadmap). Although the number of channels can be increased from the first generation device demonstrated above, it is clear that with current technology and lithographic approaches it would be challenging to scale devices to 1000s of channels, which is the pixel count of commercially available SLMs.

Another challenge is the bandwidth of the device. LFCs are currently used across several astronomical bands ranging from 350 nm to 2.5 μm [418, 421]. Photonic devices have a limited range over which they operate with a single guided mode with acceptable bend losses. The prototype outlined above spans only a single astronomical band (H). The two primary options for broader spectral coverage are: (1) making a series of parallel devices optimized for different wavebands, or (2) making broadband devices in a single platform. This technology could have the greatest impact in the visible band where most PRV spectrographs currently operate. Developing efficient SM circuits with the necessary bandwidth could be challenging. LioniX International offers visible waveguides (400–700 nm) in SiN through their MPW offerings, with very low loss ($<$0.1 dB cm^{-1}) [443]. The lifetime of visible flattening devices would need to be assessed given the presence of UV photons generated by the combs.

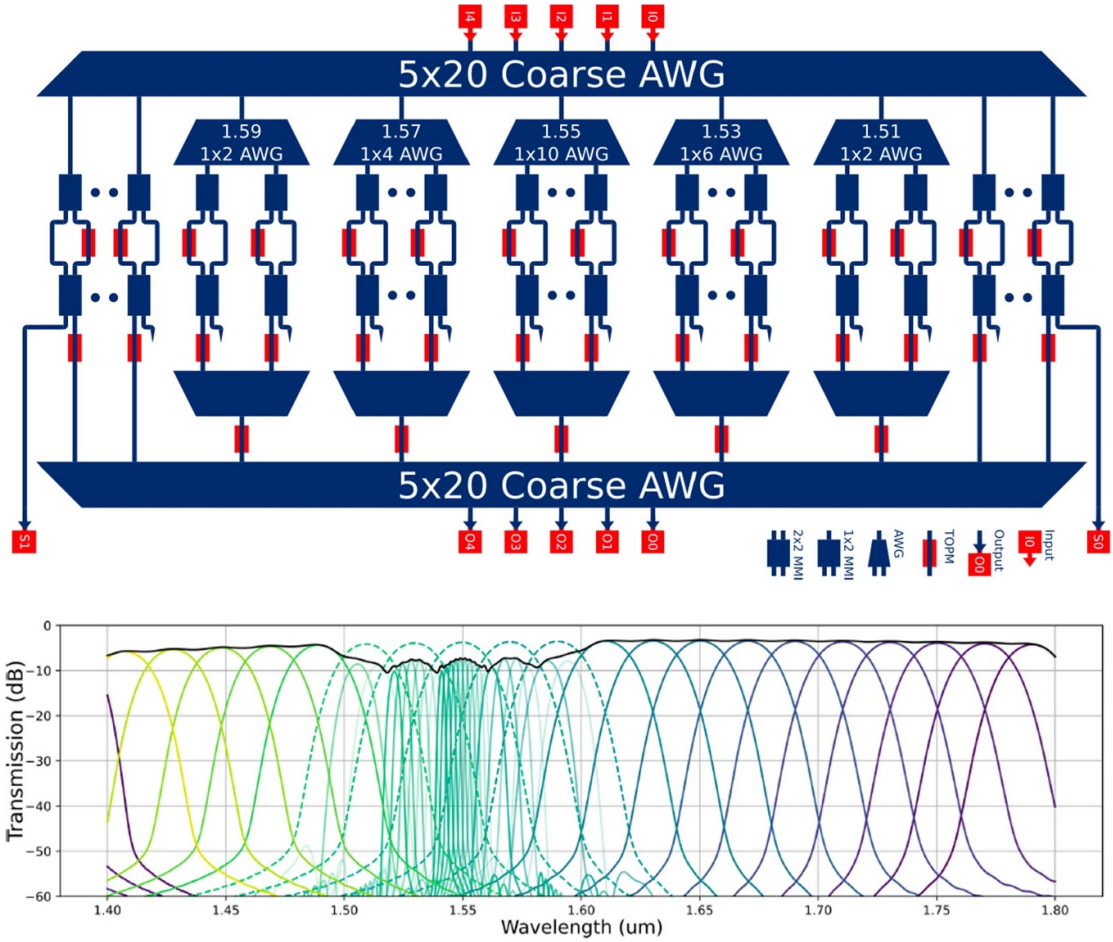

Figure 26. (Top) A schematic of an all-photonic flattener that uses cascaded AWGs to enable narrow linewidth channels in some regions of the spectrum. (Bottom) A simulated spectrum for such a device based on SiN waveguides (schematic and simulations carried out by BRIGHT Photonics Inc.).

Finally, the detection scheme used to drive the flattening algorithm could also be integrated onto the chip. Currently, an external, dedicated spectrograph is used to monitor and adjust the flatness of the spectrum. An alternative is to use the light rejected by the MZIs as probes to drive the flattener. This can be done by sensing the signal in the ports with a linear array detector or integrating individual photodiodes onto the chip (see section 24 for details). Routing the probe channels to the edge of the chip would incur a large number of waveguide crossings (see figure 26), which could compromise the performance of the device and/or use of the dropped ports as probes due to losses and crosstalk. Integrating photodiodes in place circumvents this issue. Alternatively, the beams could be ejected vertically upward out of the chip via vertical couplers and/or grating couplers onto a two-dimensional array above or a secondary chip with photodiodes flip-chipped bonded to the top. This option is also challenging as vertical and grating couplers are difficult to manufacture without imperfections and grating couplers are large. The concept may also require the use of 2×3 MM interference coupler at the output of the MZIs, so two rejected ports can be tracked to disambiguate amplitude changes in a given channel with other sources of drift. It would also require careful calibration of the non-common chromatic losses between the output of the MZIs and the final spectrograph.

Advances in science and technology to meet challenges

To advance the technology, all-photonic flattening devices should be designed, fabricated and characterized in various wavebands ranging from 350 to 2400 nm. Although SiN is transparent and applicable to nearly this entire region, other material platforms like SOS or ion-exchanged waveguides [444] could be considered. While the lower index contrast of these platforms would result in larger devices, they offer better mode matching to fibers and in the case of ion-exchanged waveguides offer better transparency beyond 2.2 μm, where SiN starts to become opaque.

Simulations and detailed design work will help to reveal the limitations on properties such as bandwidth, channel count, and losses across large bands, and channel-to-channel crosstalk as well as the potential of different material platforms. In addition, they will provide insight into how large and complex a device can be

realized within the limitations of the reticle and/or wafer size. Fabrication and testing will reveal limitations imposed by the manufacturing process including the impact of stitching errors at reticle boundaries.

With the maximum bandwidth of a single device established, several devices could be combined in parallel to span the full wavelength range of the comb. These solutions would require broadband beamsplitters, ideally based on photonics or highly miniaturized technologies. Such devices should be developed and tested in conjunction with photonic flatteners to demonstrate large spectral coverage.

Closed-loop control of these devices is a critical step to evaluating the technology and could soon be demonstrated in the field with the PARVI instrument [120], by utilizing a separate monitoring spectrometer. In a similar vein, the ability of the devices to create flat and reproducible spectra over the long term needs to be explored. Questions like do the high power levels impact the coupling losses from fiber to chip or lead to device degradation need to be understood. Ultimately, to make the flattener independent of system-specific architectures and portable, approaches that explore integrating the sensing with the chip should be tested as outlined in the section above.

Finally, other approaches or technologies should also be considered for all-photonic flattening as they may offer advantages in terms of channel count scaling. Section 7 of the roadmap presents several innovative approaches to dispersing the light that might be suitable for this application.

Concluding remarks

All-photonic spectral shapers provide an avenue to extreme miniaturization and simplification of flattening devices for intensity modulation across the output spectrum of an LFC. These could be useful at current ground based PRV facilities but will really be beneficial for future astrocomb applications in space (not necessarily for PRV science). To become useful across a broad range of applications, these devices will need to undergo further developments to understand bandwidth limitations, demonstrate operability in other wavebands, understand channel number and channel bandwidth scaling limitations, as well as closed loop demonstrations and studies into the optimum architectures for closed loop control as well as field testing.

Acknowledgments

The authors acknowledge the Keck Institute for Space Studies for funding and BRIGHT Photonics for their design and simulation efforts of the prototype devices presented herein. The research was carried out in part at the Jet Propulsion Laboratory, California Institute of Technology, under a contract with the National Aeronautics and Space Administration (80NM0018D0004). We would like to acknowledge technical contributions by Pradip Gatkine, Boquang Shen, Maodong Gao, Nick Cvetojevic, Jeffery Jewell and Gautam Vasisht during the development of the first generation all-photonic flattener described above.

15. Fabry–Perot Etalons as precision wavelength calibrators

Samuel Halverson[1], *Liang Tang*[2,3] *and Christian Schwab*[4]
[1] Jet Propulsion Laboratory, California Institute of Technology, Pasadena, CA, United States of America
[2] National Astronomical Observatories, Nanjing Institute of Astronomical Optics & Technology, Chinese Academy of Sciences, Nanjing, People's Republic of China
[3] Key Laboratory of Astronomical Optics & Technology, Nanjing Institute of Astronomical Optics & Technology, Chinese Academy of Sciences, Nanjing, People's Republic of China
[4] School of Mathematical and Physical Sciences, Macquarie University, Sydney, NSW, Australia

Status

Fabry–Perot Etalons (FPEs) have a rich history in the field of optical physics [445]. At its core, an etalon can be as simple as a pair of planar mirrors, which form an interferometric cavity that acts as a spectral filter. The cavity transmits a discrete set of modes, with wavelengths and line widths dictated by basic properties of the cavity such as mirror spacing, mirror reflectivity, and refractive index of the cavity medium. It is these transmitted modes that can serve as calibration features for a variety of spectroscopic applications, ranging from laser stabilization [446] to stellar spectroscopy [447–449]. In astronomy, FPEs have most recently been used as highly precise wavelength calibration references for high resolution, broadband Echelle spectrometers, as they are capable of producing sharp spectral features across wide wavelength ranges.

One of the most demanding spectroscopic applications in astronomy is exoplanet detection via high precision RV measurements, which inherently relies on exquisite calibration of high resolution spectrometers to measure the minute Doppler reflex motion in stellar spectra due to orbiting planets. The field of EPRV measurements is aiming for cm s^{-1} level spectroscopic measurements, equivalent to a $\sim 10^{-10}$ fractional wavelength measurement across wide wavelength ranges (hundreds of nanometers) [416]. This precision is orders of magnitudes smaller than the line widths in the stellar spectra; this goal is driven by the velocity signature of an Earth-like planet orbiting a Sun-like star, which imparts a $\sim$9 cm s^{-1} (3×10^{-10}) velocity signal. Achieving such precisions necessitates the use of novel calibration sources that provide a rich density of spectral features and are intrinsically very stable over many years.

These two requirements have driven the development of broadband 'astro-comb' LFC systems [28–30] (see section 13 in the roadmap), which combine unparalleled frequency accuracy with a high density of stable emission features. The primary drawbacks to these astro-comb systems are their intrinsic complexity (leading to limited reliability), limited wavelength coverage in particular in the blue part of the spectrum, and overall cost. These systems require significant upfront investment (>$1 M), and incur long-term costs due to maintenance and consumables [425].

Etalons, being intrinsically optically simple, are attractive for astronomical spectroscopy as they can produce a dense, comb-like spectrum similar to an LFC at a fraction of the cost and complexity. Additionally, the design flexibility of FPEs is high, with the FSR, i.e. spectral distance between adjacent peaks, finesse (ratio between the FSR and the full width at half maximum of the spectral peaks), and operating bandpass easily customizable for different spectrometers. These benefits have made etalons attractive calibration sources for the highest precision measurements, and most EPRV facilities now use etalons as part of their calibration strategy. Existing etalon systems include air-gap planar-planar cavities fed by SM or multi-mode optical fibers [450–455], entirely-fiber-based interferometer systems [11, 456], as well as microresonator-based systems [457]. Each system has distinct benefits and drawbacks, though all require technological improvements to reach the stability levels required for future EPRV instruments (see figure 27).

Current and future challenges

Etalon calibrators are typically intended as a simultaneous reference observed alongside with the stellar spectrum to track the instrumental drift during the exposure. To anchor the line positions of the etalon itself, an absolute reference like a thorium–argon (ThAr) hollow cathode lamp or an LFC can be used to calibrate the FPE periodically. Another solution is to concurrently monitor the wavelength of one or several peaks of the etalon to a very high precision by comparing it to an atomic frequency standard, e.g. a well-known optical transition; this technique tracks the drift of the etalon in real time [456]. In all cases, the etalon requires the relative peak position to be stable to a very high degree. As fundamentally passive optical elements (no innate frequency locking to an atomic standard), these 'astro-etalons' require excellent thermomechanical control to stabilize the output spectrum at the levels required for EPRV applications ($\sim 10 \times 10^{-10}$). While real-time monitoring of a single peak, as described above, can relax this requirement somewhat, this is unlikely to track any chromatic effects. This represents a technical challenge, especially for cavities designed around bulk materials such as SiO_2 (in the case of fiber-based etalons) or crystalline materials such as CaF_2 or MgF_2 (used in whispering-gallery-mode resonators) which have high coefficients

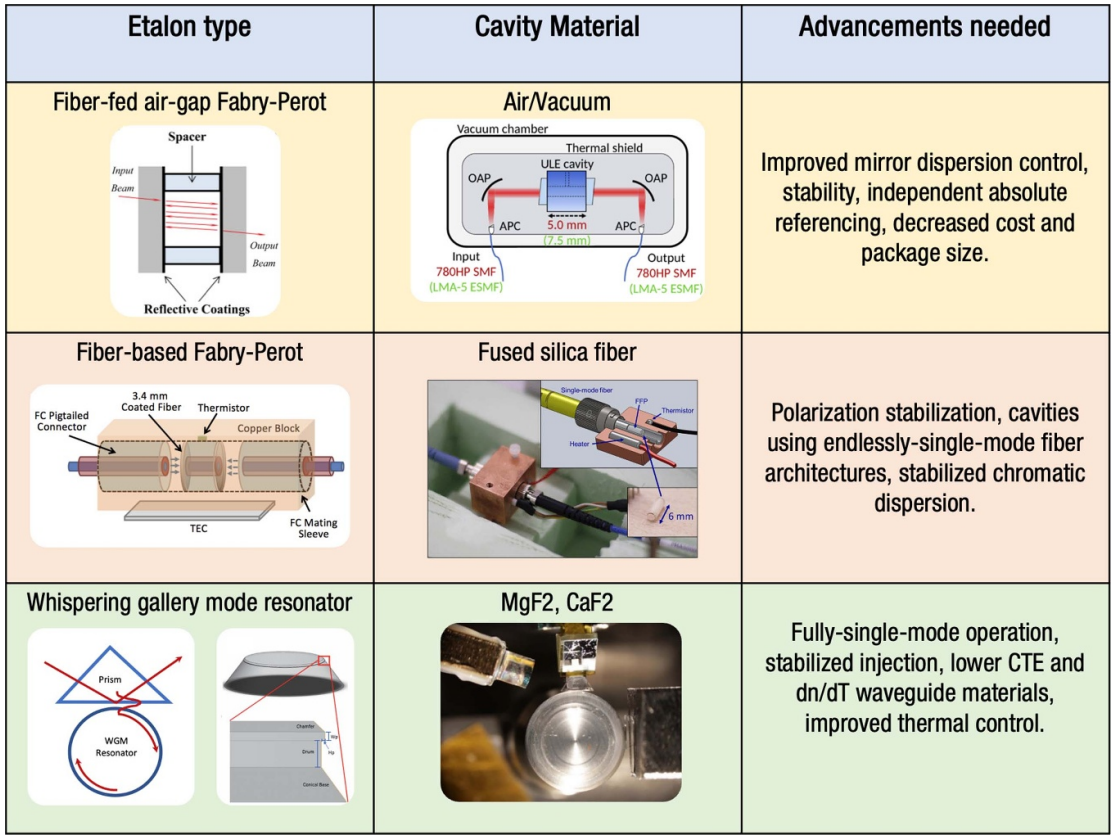

Figure 27. Examples of Fabry–Perot-Etalon (FPEs) used in astronomical spectroscopy. FPEs are valuable tools for precise wavelength calibration of high resolution spectrometers. In all cases, the interferometric cavities act as sharp filters of a continuum spectrum, providing a dense series of lines for high precision calibration. Reprinted with permission from [458] © The Optical Society. Reprinted with permission from [459] © The Optical Society.

of thermal expansion (CTE) and refractive index thermal coefficients (dn/dT). Even 'air-gap' etalon designs, which typically have spacers manufactured out of low-expansion materials such as Zerodur or ULE [460–462], still require thermal isolation and precise temperature control to maintain spectral stability (though not at the level of more standard glass materials). At the required level of control, even changes in the amount of injected light must be considered to avoid absorption-driven thermal variations.

Free-space or air-gap FPEs have been used extensively in RV applications [450–455] over the past ten years. These systems are optically simple, and revolve around a planar-planar cavity design fed by SM optical fibers. However, these systems require careful engineering to properly stabilize the cavity, including precise vacuum and temperature control, and to ensure stable illumination [463]. The structure of the etalon and the optical alignment require specialized techniques to maintain stability (optical contacting, athermal mount design, etc). Recently, it was shown that, in addition to an overall drift, bulk etalons show structured systematic drifts that vary as a function of wavelength (see figure 28) [454, 464]. The physical mechanism for this chromatic drift has yet to be identified, though it is likely associated with some variation in the FPE mirror stack properties. Careful investigations into the long term behavior of the optical dielectric coatings under realistic conditions (temperature stability, illumination, vacuum level) is needed to understand and mitigate these effects.

Fiber-based etalons have the benefit of being compact and easy to thermally stabilize, though birefringence issues can easily dominate the spectral stability noise floor. Unlike bulk etalons with a vacuum cavity, SM -fiber-based etalons exhibit birefringence due to inherent properties of the fiber that forms the cavity (see figure 28). Crucially, fiber cavities based on non-polarization-maintaining fiber [11, 456, 458] produce two distinct resonance modes, one for each polarization. The spectral displacement between these two modes is set by the cavity birefringence, and the relative amplitude between transmitted polarization modes is determined by the polarization conditions of the light source [459]. While careful polarization control can mitigate these problems to a high degree, this instability still limits the utility of fiber-based FPEs when aiming for the highest precision, as typical astronomical spectrometers will not be able to easily resolve the separated transmission modes. The superposition of the two modes may manifest as a single peak in the spectrometer, but the effective line centroid will drift should the polarization conditions change.

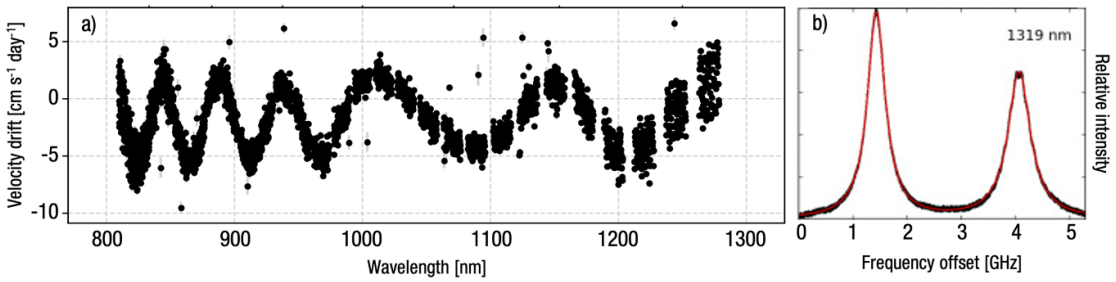

Figure 28. Left: Chromatic drift of an air-gapped 'astro-etalon' system, showing systematic structure as a function of wavelength [454]. This is a key area of research for future etalon systems that aim for the most precise (10×10^{-10} or lower) long term performance. Right: Observed birefringence in fiber-based etalon system, highlighting the two widely-separated polarization modes. These modes vary with incident polarization conditions, which are highly sensitive to input fiber geometry and thermomechanical drifts [463].

Whispering Gallery Modes (WGM)-based etalons [457] show great promise as compact spectral filters that produce a wide bandwidth of sharp features (see section 10 of the roadmap). WGM etalons are dielectric cavities with curved surfaces where light is trapped by total internal reflection from the dielectric boundary along which it travels; no optical coatings are required. Constructive interference occurs when the round-trip path length along the curved surface in the cavity is an integral of the wavelength. WGM resonators operate at any wavelength as long as the dielectric is transparent and the resonator surface is well-polished to reduce surface scattering losses.

Unlike ULE glass or Zerodur FP etalons, WGM etalons fabricated from optical crystals like MgF_2 and CaF_2 have significant thermal expansion that must be compensated to achieve a frequency stability suitable for PRV measurements. This has been attempted by engineering a composite WGM etalon that balances thermal expansion and thermo-refractive behavior [465].

Advances in science and technology to meet challenges

In the coming decade, the priority must be to develop stabilized systems that support broadband operation (100's of nm), with extreme stability ($<10 \times 10^{-10}$ fractional stability), and which are polarization insensitive. To meet these requirements, from the context of EPRV applications, multiple advancements must be made in a number of areas:

In the case of classical air-gap etalons, a more thorough understanding of interferometer mirror relaxation, dispersion, and coating stability are needed to better contextualize the observed behavior of current FPE systems (see figure 28 [454, 464]). A deeper exploration of manufacturing techniques and athermal materials, with a keen eye on maximizing long-term (months-years) stability is also needed to improve upon the current state-of-the-art, if FPEs are ever to become stand-alone EPRV calibrators. Advancements in these styles of FPEs will hinge on improved dispersion stability in mirror coatings, and advanced methods for optically contacting mirror substrates to etalon spacers. In both the air-gap and fiber-based FPE systems, further investigation of 'hard', low-dispersion mirror coatings is also crucial for improving stability at the cm s^{-1} level chromatically.

In fiber-based systems, migrating towards using polarization maintaining (PM), endlessly SM -fibers [466] as the cavity material may offer a solution to the current limitations of these systems (polarization modes, narrow bandwidth operation). However, to establish a fully PM system, the alignment of optical systems will have to be strictly controlled, especially during construction of the etalon cavity. Additional technical challenges are present if broadband performance is to be guaranteed. Air-gapped fiber etalons and MM-fiber-based versions are worth exploring in the future. Fiber-based systems have the benefit of very small thermal mass, which makes them quick to respond to thermal tuning. This facilitates driving a servo loop to lock an etalon line on external laser sources.

Advancements in WGM-based designs will require exploration of waveguide materials that support hundreds of nm of bandwidth with pure SM operation, as is required for broadband spectroscopic applications. WGM etalons have yet to be demonstrated in an observatory environment, and will likely require a significant amount of engineering and testing to be implemented in a complete system ready for on-sky operation.

Improvements in white-light sources to take full advantage of etalon bandwidth is foreseeable with technical advances in broadband-light sources. Current supercontinuum sources only go down to ~420 nm and the significantly lower output power towards shorter wavelength poses a challenge for broadband spectral flattening. Alternatively, laser driven light sources could offer broadband coverage down to the UV

band. Yet, high efficiency coupling into a SM device remains somewhat challenging. Spectral energy distribution and flux jitter of the feed source, as well as the illumination stability, which could introduce error when determining line centroids of the transmitted peaks [463], should be deliberated.

For any etalon architecture, a system that is referenced to an atomic standard (or standards) at one or even multiple wavelengths provides potentially much higher precision than a passive system. The number of wavelength 'anchors' required to fully characterize the etalon dispersion drift is unknown, though recent studies have shown that the chromatic drift can be highly structured [454, 464]. This indicates that the chromatic drift due to slow changes in the mirror coatings must be calibrated regularly against an absolute, broad-band reference (like a ThAr lamp or LFC), while faster drifts (within a night) can be corrected with the frequency reference. There is also room for a better understanding of the transient behavior, e.g. the approach to equilibrium after illumination of the system.

Concluding remarks

The simplicity and rigidity of the FPEs sets them apart as practical systems for generating evenly spaced spectral peaks for calibration purposes. Calibrators based on passively-stabilized, bulk-optics, vacuum-gap FPEs have already demonstrated <10 cm s^{-1} stability performance, when used in combination with an absolute reference. To operate independently from any other calibration source, the absolute wavelengths of the FPEs' transmitted peaks have to be anchored. One possible way is to laser-lock the etalon to spectroscopic references. The ultimate achievable broadband accuracy of such devices remains unknown; in particular, the chromatic behavior of the locked etalons has to be studied more extensively.

Photonic Etalons, such as fiber-based FPEs and chip-based microresonators have much smaller footprints compared with their bulk counterparts, and can be thermally tuned easily. The compactness of these photonic etalons enables new calibration applications, such as in space-borne missions, where traditional vacuum-enclosed solutions are not viable due to dimension or weight limitations.

The key technical challenges going forward include material limitations, thermal stability, polarization control, and dispersion behavior.

16. Future of photonic beam combining technologies for interferometers

Karine Perraut[1], *Guillermo Martin*[1], *Laurent Jocou*[1], *Elsa Huby*[2] *and Denis Mourard*[3]
[1] Université Grenoble Alpes, CNRS, IPAG, 38000 Grenoble, France
[2] LESIA, Observatoire de Paris, Université PSL, CNRS, Sorbonne Université, Université Paris Cité, Meudon, France
[3] Université Côte d'Azur, Observatoire de la Côte d'Azur, CNRS, Laboratoire Lagrange, Nice, France

Status

Optical long-baseline interferometry (OLBI) combines signals from separate telescopes and provides reconstructed images at the exquisite spatial resolution of the synthetic mirror whose aperture is sized by the separation between the telescopes. At visible and NIR wavelengths (e.g. in V, R, J, H, K bands; [0.5–2.5] μm), OLBI is routinely in operation at the Very Large Telescope Interferometer (VLTI, Chile), at the CHARA Array (California), and at the NPOI and LBTI arrays (Arizona), giving access to angular resolutions smaller than 1 millisecond of arc. Such an exquisite resolution opens the road for studying complex environments and determining accurate angular diameters of thousands of stars over the Hertzsprung-Russell diagram [467] which is invaluable in the era of *Gaia* and space missions like PLATO or ARIEL.

While this technique has been for a long time hampered by its limited sensitivity (light is not collected by the giant synthetic mirror), GRAVITY at the VLTI [75] has revolutionized NIR interferometry by providing milli-arcsecond resolution imaging up to K $\sim$ 19th magnitude and 20–50 μ arcsec astrometry, in addition to polarimetry and spectroscopy capabilities. GRAVITY has led to groundbreaking results covering the broad range of astrophysics which was targeted by OLBI long ago: the precision tests of Einstein's theory of general relativity and notably the strong experimental evidence that the compact mass in the Galactic Center is a Schwarzschild-Kerr hole [36, 37]; direct observations of the broad line regions surrounding quasars at sub-parsec scale [468]; high-resolution K-band spectra of several exoplanets [35]; the first resolved microlensed images [469]; and the resolution of several dozens of protoplanetary disks at a spatial scale where planets form [470]. For all these fields, zooming in with OLBI is of the utmost importance to reveal and constrain the physical phenomena at play in these complex and time-variable environments.

The GRAVITY breakthrough comes from a combination of fringe tracking, cooled optics, high-quality metrology, infrared AO, low-noise detectors, the upgrade of the VLTI infrastructure, and SM beam-combination. Focusing on the four-telescope (4 T) beam-combiners at the heart of the instrument, following the pioneering integrated optics (IO) components in the H band installed at IOTA [471] and in the PIONIER instrument at the VLTI [472], the design of a pairwise static ABCD combiner has been optimized for the K band. The main challenges of the GRAVITY developments are the throughput in this specific spectral range where silica is no longer highly transmissive, operation in vacuum at a temperature as low as 200 K, and a back-illumination with a 1.908 μm metrology laser. Huge efforts were undertaken to optimize the technological process: doping process to increase the refractive index difference, annealing at 1000 °C to remove the OH bonds present in the silica, manufacturing the 20 mm x 50 mm combiners in three stitched photolithographic reticles, as well as mastering the stress inside the component to limit the birefringence. All the challenges have been successfully tackled, leading to the most complex IO beam combiner (figure 29) in this very specific spectral range [33].

Current and future challenges

Increasing the number of beams. Snapshot imaging of variable and complex environments makes the recombination of more than four telescopes a key driver for the next photonic developments, with challenges about the length, the throughput, and the complexity of the combiners. As a prerequisite, the fringe coding, i.e. the design of the circuit and the achieved signal-to-noise ratio, should be optimized. As an example, the 6 T ABCD beam-combiner designed for the fringe-tracker of the visible SPICA instrument at the CHARA array optimizes the coding of the 15 fringe patterns. This 82-mm long chip exhibits a throughput higher than 50% for both polarizations over the whole H band [474]. Similar developments are ongoing for interferometers deployed on monolithic telescopes, such as pupil remapper instruments. Currently, a visible 9 T-combiner is being optimized for the FIRST instrument [475], and a complementary infrared multi-beam nuller interferometer is being developed for the GLINT instrument [12] (see section 19 for more details). Increasing the number of input beams to enhance the imaging capabilities of future instruments will come at the expense of complexity and a loss in signal-to-noise ratio. For more and more numerous input beams, within the context of limited wafer sizes, one future challenge would be to connect several chips together, which would make the interface, the optical path balancing, and the integration more complex.

Improving the beam-combiner transmission. Improving the OLBI sensitivity requires pushing the sensitivity of the beam-combiners by improving the intrinsic transmission of the materials, the coupling of

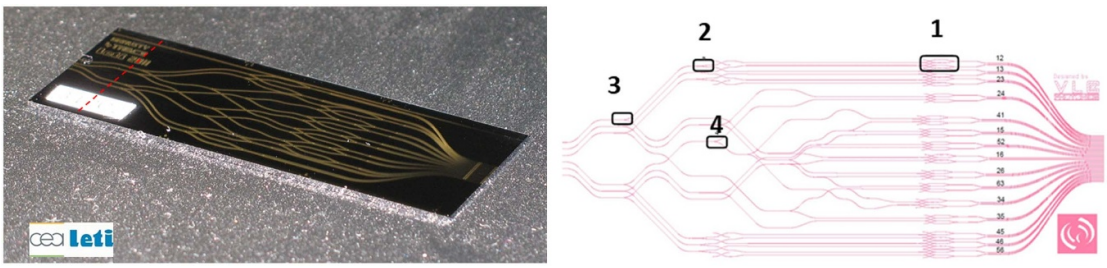

Figure 29. Left. Four-telescope beam-combiner of GRAVITY operating in K-band, designed and manufactured by photolithography of doped-silica on-silicon waveguides by CEA-LETI. Reproduced from [33]. CC BY 4.0. Right. Design (by VLC Photonics-OCA based on [473]) of the SPICA six-telescope fringe-sensor operating in H band. Reproduced with permission from [474]. Each beam is divided in five equal parts thanks to a smart succession of 60/40 (3), 50/50 (2), and 66/33 (4) couplers. Each of the 15 possible pairs is combined inside an ABCD circuit (1), sampling the fringes with fixed phase shifts of 0, $\pi/2$, π, and $3\pi/2$. This permits the instantaneous measurements of the phase-delay. Optical paths are equalized to avoid any bias in closure phase measurements.

the light into the waveguides, and the light collection at the output. Using larger refractive index contrast waveguides allows one to better confine the light, implement smaller radii bends and thus realize shorter optical functions, leading to more compact chips. This tackles the potential wafer size challenge. As a by-product, more compact chips could be more easily packaged and cooled down, notably for cryogenic and space applications. On top of that, more compact optical functions open up the possibility to integrate more capabilities on a single-chip (detector and/or metrology laser hybridation [476], phase control, see section 23 for more details) assuming manufacturing technologies are compatible.

Mastering spectral bandwidth and birefringence. As several astrophysical diagnoses are based on spectral analysis, operating in different bandwidths (V, R in visible; J, H, K in NIR; L, M, N in MIR (section 9)) is fundamental. As a consequence, efforts have to be made to optimize these technologies for a given band. Routine observations with precision astrometry and polarimetry requires mastering metrology propagation (not necessarily in the spectral range of the operation wavelength of the instrument), and birefringence as well as diattenuation inside the beam-combiner. As long as they are not time-variable at the observation timescale and calibratable through day-time procedures, none of these effects are insurmountable and it might even be possible to compensate for some at a system level (e.g. internal birefringence can be compensated with external $LiNbO_3$ waveplates).

Advances in science and technology to meet challenges

Towards more compact combiners. For greater than eight telescopes, planar lithographic chips require wafer sizes exceeding current technological limits when using low index difference waveguides (typ. 0.001). One option is to use high refractive index contrast waveguides (e.g. SiN/SiO_2 technologies with $\Delta n = 0.5$), where high confinement enables sharper bends (radii of tens of microns), and therefore compact devices with multiple optical functions (splitting, directional coupling, wavelength multiplexing) [477]. The issue that arises is that high numerical aperture (NA) waveguides require tapers to maximize the coupling with input/output fibers. These tapers have a highly polarization-dependent transmission, which requires specific efforts like the development of polarization independent mode converters [478] achieving high NA to low NA adiabatic transitions.

Enabling complex multi-channel and multi-band designs. Thanks to the ultrafast laser inscription (ULI [479]) technique, the refractive index of a substrate can be locally modified, in particular at different depths into the substrate. Interestingly, this technique can be applied to a large assortment of materials, thus allowing for optimized devices for different wavelength bands. The versatility of ULI allows for 3D waveguide architecture, expanding the variety of possible designs, with a large number of inputs and avoiding in-plane crossings, thus reducing crosstalk and propagation losses. Applications include combining light with waveguide lattices (see section 17 for more details), MM to singlemode conversion devices (like PLs (see section 3)), pupil remappers, converting a 2D input matrix into a 1D array (Dragonfly [480], GLINT [12]) and 3D directional couplers [481]. Challenges in ULI include the stabilization of the laser power during waveguide fabrication, and especially for writing waveguides deep inside the substrate, as power and focusing have to be finely tuned to ensure homogeneity of the refractive index modification.

On-chip integration of injection, modulation, and detection. The densification of the optical chip with new functions and many baselines is part of the efforts deployed to achieve fully integrated beam-combiners. Active functions based on EO [482], thermo-optic [483] or piezo-optic [99] materials are being developed to allow for modifications of the waveguide's effective refractive index, and thus phase control, at rates reaching

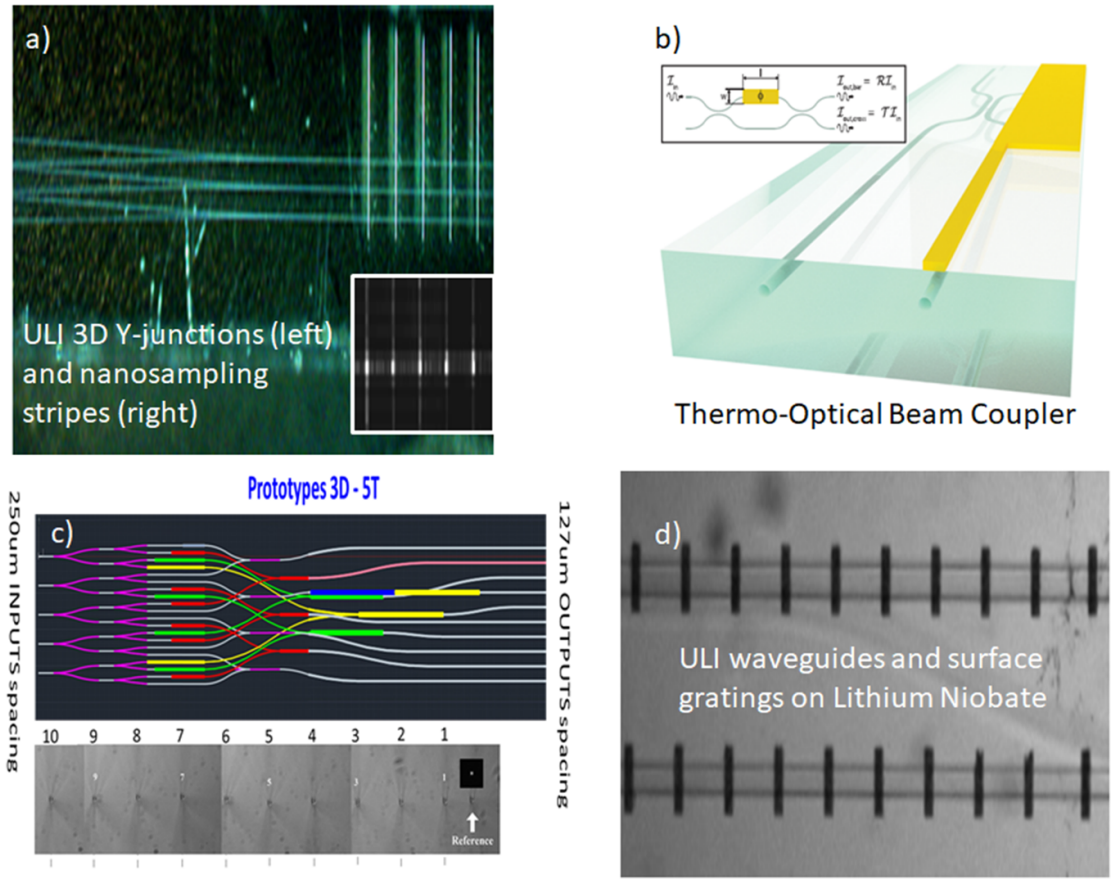

Figure 30. Examples of some ULI beam combiners; (a) image of a 3D 3 T beam combiner, with sampling grooves at the output waveguides. Reproduced with permission from [482]. (b) Scheme of a thermo-optic directional coupler. Reproduced from [483]. CC BY 4.0. Both examples (a) and (b) are singlemode in the near infrared. (c) Scheme of a visible 5 T 3D beam combiner for FIRST and white light image of the ten outputs. Reproduced with permission from [487]. And (d) mid-infrared waveguides and surface gratings written in $LiNbO_3$. Reproduced with permission from [488].

the MHz. This kind of hybrid device not only enables on-chip phase modulation but also fringe or null tracking [482, 484]. To increase the global throughput by optimal direct injection into the waveguide, microlenses can be directly integrated on the input/output facets of the chip thanks to 3D-printing [82]. In addition, novel approaches of detection consisting of growing single pixels directly over the waveguides increase readout time and output coupling efficiency [485]. This can be coupled to on-chip spectrometry using ULI (SWIFTS [486]) to obtain a fully integrated spectro-interferometer.

Different examples of the solutions discussed are shown in figure 30.

Concluding remarks

In recent years, astronomy has greatly benefited from the coming of age of photonic technologies for beam combination, opening new opportunities for optical long-baseline interferometry. The initiation and strengthening of collaborations between research teams and technology centers now allows for the routine development of components with mature technologies, and for a dynamic synergy to tackle the development and/or optimization of specific circuits (especially for non-standard telecom spectral bands), including new functions. Notably, the advent of high density pupil-remapping projects (full 30 inputs of FIRST at SUBARU, SPIDER project with 518 sub-apertures [489]) requiring input facets with tens of waveguides in a mm-size 2D distribution will be challenging, as refractive index modification must be homogeneous whatever the depth on the substrate. The requirements for the next generation of combiners will necessitate the exploration of new technologies as the substrate size and the yield of planar photonic circuits become limiting. The ULI process is probably one of the most promising alternatives as it allows for 3D-mapping, it optimizes the circuit length, produces 3D tapers and waveguides that are in principle independent of polarization, and it is well suited for waveguide fabrication in active materials and materials having transparency windows where classical waveguide fabrication techniques are not functional.

Acknowledgments

GRAVITY has been developed in a collaboration by the Max Planck Institute for Extraterrestrial Physics, LESIA of the Paris Observatory and IPAG of Université Grenoble Alpes/CNRS, the Max Planck Institute for Astronomy, the University of Cologne, the Centro Multidisciplinar de Astrofisica Lisbon and Porto, and the European Southern Observatory. We acknowledge the funding support of CNRS/INSU, Agence Nationale de la Recherche Contract #ANR-06-BLAN-0421, LabEx OSUG@2020 (Investissements d'avenir ANR10LABX56), LabEx FOCUS ANR-11-LABX-0013, Action Spécifique ASHRA of CNRS/INSU and CNES, and Observatoire des Sciences de l'Univers de Grenoble. SPICA-FT has been developed thanks to fundings from CNRS/INSU, OCA, UCA, Idex Jedi, and Région Sud. This work has been partially supported by the National Research Agency (ANR) through the French' Recherche Technologique de Base' Programme. The FIRST project has received support from Action Spécifique Haute Résolution Angulaire (ASHRA) of CNRS/INSU co-funded by CNES and from the French National Research Agency (ANR-21-CE31-0005).

17. Future prospects of discrete beam combination techniques

Abani Shankar Nayak[1], *Stefano Minardi*[2] *and Stefan Kraus*[3]
[1] Institut für Angewandte Physik, Friedrich-Schiller-Universität Jena, Jena, Germany
[2] Ams-OSRAM, Jena, Germany
[3] Department of Physics and Astronomy, University of Exeter, Exeter, United Kingdom

Status

OLBI is an important tool of modern astrophysics, enabling high angular resolution imaging of stellar surfaces, tight binaries and proto-planetary/accretion disks. OLBI facilities allow the interferometric combination of light collected by telescopes tens to hundreds of meters apart and are typically complex structures, where misalignment and vibration of the optical components can compromise the visibility of interference fringes. To counter the drawbacks of bulk optics at least in the beam combination instrument, Kern *et al* [490] proposed the use of IO components, which was successfully validated in the IONIC [491] and IONIC3 [492] instruments, and their successors, the PIONIER [472, 493] and GRAVITY [75] instruments at the VLTI facility that are currently delivering impressive high-angular observations of a multitude of objects [35, 494]. IO technologies (see section 16 for more details) are able to miniaturize complex optical setups on a few centimeter long chip that consists of several photonic functions such as waveguides, Y-splitters, X-couplers, and phase-shifter. Besides the reduction of footprint, IO devices offer much higher thermo-mechanical stability and a reduction of the maintenance costs as their bulk optics counterparts. More relevant to science is the opportunity to integrate on a small chip, an instrument for the simultaneous combination of many telescopes and deliver precise measurements of visibility amplitudes and closure phases (CP), two quantities required for the interferometric synthesis of images. IO devices are usually manufactured on a variety of silicon-based materials by means of photolithographic processes, which constrain the waveguide-network to a plane. Due to the planar topology, multi-telescope beam combiners feature waveguide crossovers, which are sources of crosstalk [495] between the interferometric baselines and reduce the precision of the measured visibilities.

A possible solution to this limitation of planar PICs is to exploit 3D manufacturing such as ultra-fast laser inscription (ULI—ultrashort laser pulses are used to locally modify the optical properties of a substrate material [90, 91, 479]) and avoid waveguide crossovers [496]. Therefore, a 3D-photonics approach to multi-telescope beam combination is the DBC (see figure 31), a ”photonic lattice” consisting of a periodic array of parallel SM waveguides (WGs) that interact through the evanescent field of individual waveguide modes. The name DBC derives from the term ”discrete optics”, indicating optical systems where light is mainly bound to a discrete set of evanescently coupled WGs [497]. Initially conceived by Minardi & Pertsch [498] for OLBI applications, the DBCs have been the focus of R&D studies aiming at measuring visibilities and CPs in multi-channel interferometers. These studies were not limited to numerical modeling [499], but included also the characterization of DBC prototypes operating at astronomical R- [500], J- [501], H- [502], L- [323]- bands and combining up to 3- [500], 4- [323, 503], and 6 [501]- telescopes. Recently, a 4-channel DBC was tested on-sky at the William Herschel Telescope during a pupil remapping experiment [502].

Compared to pairwise IO combiners [472], DBCs have a very simple design and employ only straight, relatively short SM waveguides, thus avoiding bending losses and have low propagation losses. Therefore, the main losses are derived from the coupling of starlight in the device, which could feature a pupil remapper [480] or a coherent reformatter [504] that has inherent bending or transition losses. Retaining high throughput or sensitivity is important for any interferometer, especially for facilities that combine many apertures for high-fidelity imaging, including proposed next-generation facilities such as the ‘Planet Formation Imager’ (PFI [505, 506]) or the Magdalena Ridge Optical Interferometer (MROI [507]). ULI inherently allows low cost manufacturing of the components in a variety of materials (see sections 8 and 9 for details) with the transparency windows extending from the visible to the MIR, the latter being crucial for the exploration of science cases related to dusty objects such as protoplanetary disks or active galactic nuclei. One important science objective, both for VLTI and CHARA, is to enable interferometry at very high resolving power $>20\,000$ to study molecular composition and kinematics from spectrally resolved lines (see figure 31). Other science cases, where DBCs could be potentially used are the characterization of exoplanet atmospheres [35], the study of the gas kinematics in the accretion/outflow launch region of young stars [508–510], and the measurement of spin-orbit alignment of exoplanet host stars [513]. Beyond OLBI applications, DBCs coupled to a PL may enable wavefront sensing for astronomical AO systems (see section 3 for details).

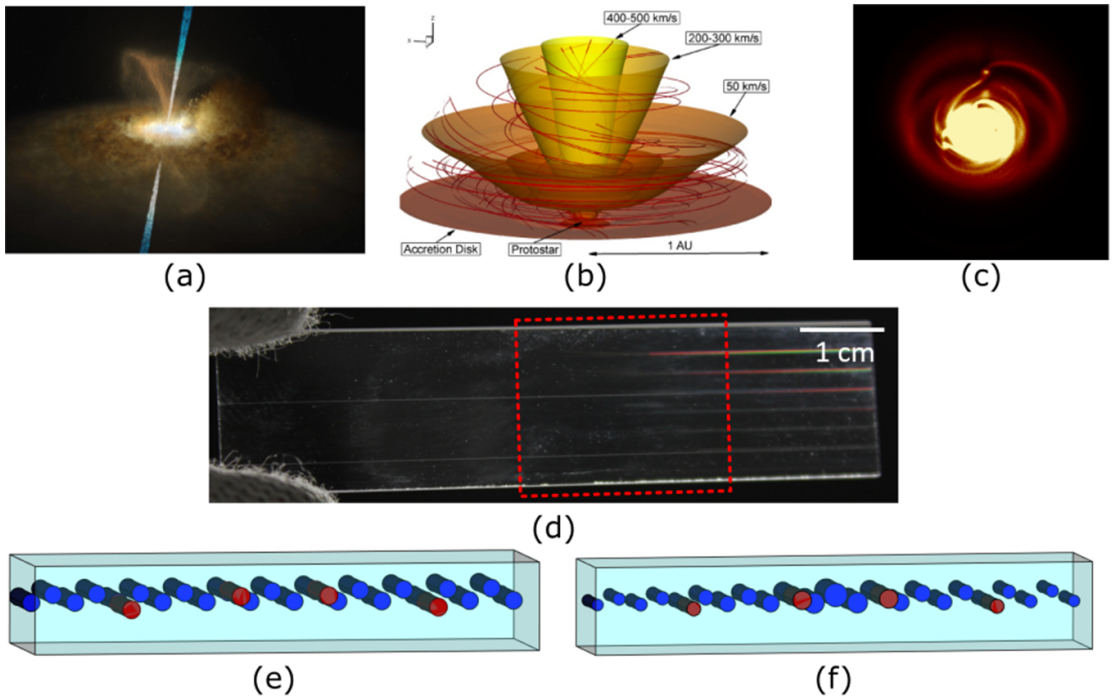

Figure 31. The science cases potentially addressable by a DBC-based interferometric combiner are shown in (a), (b) and (c). (a) Artist illustration of the environment around Active Galactic Nuclei (credit: ESO/M. Kornmesser and L. Calcada). (b) A model showing the magnetic field topology and velocity structure in the accretion region around a T Tauri star (credit: Romanova and Owocki). Reproduced with permission from [512]. (c) Radiative transfer simulations of a protoplanetary disk with embedded protoplanets, computed for wavelength of 10 μm (credit: Kraus *et al*). Reproduced with permission from [505]. (d) The IO chip used for on-sky tests at the William Herschel Telescope consists of pupil remappers, DBC (highlighted in red area) and coherent reformatters. Note that several DBC devices are contained in the red area (credit: AIP/A. Dinkelaker). (e) Design of current DBC with identical coupling coefficients across the width of the device. The red and blue cylinders are the input and output waveguides, respectively. (f) Design of a possible non-uniform DBC that has apodized coupling coefficients to enable broadband light measurements and precise estimation of visibilities.

Current and future challenges

Science cases requiring high-fidelity interferometric imaging need a dense sampling of the coherence function (uv-plane coverage) of the starlight. Usually this is achieved by collecting visibility data across many different baselines by changing the location of the combined telescopes and/or exploiting earth rotation. This approach is possible only assuming the stability over time of the target itself. Fast varying astronomical targets (e.g. novae, variable stars, dynamical inner-disk environments, orbital motion of companions/planets) but also the truthful imaging of extended structures like protoplanetary disks requires the simultaneous combination of larger arrays of telescopes and enable a better coverage of the uv-plane within a snapshot. For instance, for a hypothetical planet at 1 au around a solar-mass star in the Taurus star-forming region, the orbital motion is up to 0.12 mas per day, which is comparable to the beam size in a PFI-like facility with maximal baselines of $B = 1.2$ km at observing wavelengths of $\lambda = 1$ μm ($\lambda/2B = 0.09$ mas). Therefore, such an array needs to achieve sufficient uv-coverage for imaging in a single night. The DBC offers a straightforward approach for scaling the beam combiner to larger arrays of telescopes and the resulting PIC is far simpler and less prone to fabrication errors than pairwise IO combiners that have ABCD structures [472]. However scaling up DBCs to larger telescope arrays will face challenges such as: (1) the factorial scaling of the algorithm currently used to select the configuration of the input sites of the DBC, (2) the photometric loss due to the quadratic scaling of the number of output waveguides (a general problem for all-in-one combiners), and (3) the decreased throughput due to the requirement to have longer devices. To date, a 6-input DBC has already been fabricated and tested in the lab [501], but the design of e.g. an 8-input DBC would require a smarter approach to meet these challenges.

Another key requirement for any OLBI beam combiner is high instrumental fringe contrast, throughput, and broadband operation, which determines the device sensitivity. If we compare the performance metrics of a 4-input DBC (see figure 31) fabricated using ULI technology with its counterpart, the 4-input pairwise combiner [472] of the PIONIER instrument [493], we find that a DBC used with narrow-band light source (CW laser at 1600 nm) has an instrumental visibility (99%) and exhibit a closure phase accuracy (0.5°) comparable to that of the PIONIER combiner. However, astronomical applications need to combine light over a bandwidth comparable to an atmospheric transparency window (10% of carrier frequency). Because

of the strong chromatic dependence of the evanescent mode coupling, the challenge of current generation DBC is to achieve high instrumental visibility with a broadband light source. Laboratory measurements and simulations have shown that the chromatic nature of the DBC's transfer function reduces the accuracy of the retrieved visibilities with increasing bandwidth [500, 503]. A solution to this problem is to disperse the output light with a resolving power >50 and calibrate each individual color channel, as shown by Saviauk *et al* [500].

A further requirement from astronomy is to improve the precision of the visibility measurements and achieve a better dynamic range of the reconstructed image. This is crucial for the observation of exoplanets and protoplanetary disks, where the contrast between the colder object and the bright central star is huge. The SNR of visibility amplitude and phase would require ratios >1000:1. Besides coupling the DBC to low noise detectors, the control of depolarization effects in the waveguides [511] and the improvement of the transfer matrix calibration procedure are further challenges to be addressed.

Advances in science and technology to meet challenges

Broadband light extension: Achieving high accuracy in the measurement of visibilities across a broad spectrum is still an issue for DBCs. A compromise between chromatic dispersion control, bend losses and coupling strength may be achieved by building arrays of periodically bent and/or apodized waveguides [514], which could increase the broadband operation of the DBC (see figure 31 for a schematic of a nonuniform DBC). Alternatively, DBC can be used in spectro-interferometric settings, e.g. by employing a hybrid integration approach by bonding the DBC chip to an IO-based AWG (see section 6 for details) or an Echelle grating [515].

Polarization: Depolarization effects in waveguide interferometers decrease the interferometric contrast and reduce the accuracy of the retrieved visibilities and CPs. While low birefringence has already been achieved in Eagleglass ULI waveguides operating at J- and H-band, this is not the case for ULI on other substrates (e.g. Infrasil [516], GLS [323], IG2 [326]) suitable for other astronomical bands. In principle it may be possible to optimize processes also on these glasses, e.g. by introducing appropriate annealing processes [517].

Scalability: An analytical approach has to be developed to solve the issue of factorial scaling of the current algorithm used to select the input sites of the DBC. This may be facilitated by relying on a supermode model rather than on the coupled mode approximation. However, from sensitivity considerations, all-in-one combiners perform worse when the number of combined telescope increases, but a cluster approach to combine subsets (3- or 4-) of the telescope array may be an effective strategy for imaging interferometry methods.

Calibration: An accurate calibration procedure of the DBC transfer matrix is essential to obtain good results in the on-sky observations [502]. Thus future implementations of DBC components would require special care in the development of a suitable calibration test-bench with low noise detectors. For instance, an AO system [518] could be included in the optical characterization setup for a more robust determination of the DBC's transfer matrix.

Concluding remarks

The above works have demonstrated the viability of DBC techniques and in particular, as compared to concurring IO beam combiner design, its potential for the scalability of the beam combination to large arrays of telescopes. However, the development of a full instrument based on DBC requires further technological research to address issues like the chromatic dispersion, the algorithm for the input site choice and, on a second level, the tackling of depolarization effects in the device and the improvement of the transfer matrix calibration procedures and test-benches. Research on these issues is currently ongoing and the future years may bring a DBC component to sky, triggering new instrument development for instance for VLTI, CHARA, NPOI, MROI, or aperture masking interferometry. Such devices could also help enable the next generation of interferometric facilities and promise to solve some of the major challenges facing modern observational astrophysics.

Acknowledgments

A S N acknowledges the combined support from Deutsche Forschungsgemeinschaft (326946494) and Bundesministerium für Bildung und Forschung (03Z22AN11). S K acknowledges support from an European Research Council (ERC) Consolidator Grant (Grant Agreement ID 101003096). The authors would like to thank Dr Aline Dinkelaker for her valuable comments that improved the clarity of the paper.

18. Realizing extremely long-baseline interferometers by exploiting photonic technologies

Narsireddy Anugu[1], *Gautam Vasisht*[2] *and Ludovic Grossard*[3]
[1] The CHARA Array of Georgia State University, Mount Wilson Observatory, Mount Wilson, Altadena, CA 91203, United States of America
[2] Jet Propulsion Laboratory, California Institute of Technology, Pasadena, CA, United States of America
[3] Limoges, CNRS, XLIM, UMR 7252, F-87000 Limoges, France

Status

The next leap in understanding important astrophysical phenomena e.g. protoplanetary disks and planet formation, young and mature exoplanets, environments of supermassive black-holes, requires optical/IR measurements on 10–100 microarcsecond (μas) angular scales; this is equivalent to an array with multiple km baselines in the near-IR (0.8–5 μm) [37, 506]. For these reasons, km-scale fiber linked interferometers have been discussed since the 1980s for both ground- and space-based applications [519]. The OHANA project [520] in the 2000s was the first attempt to fiber-link the large telescopes on Mauna Kea, and succeeded in obtaining fringes between the two Kecks.

On km baselines fiber light transport becomes quite attractive relative to classical beam trains as one largely avoids: (i) higher infrastructural expense ($\propto$ baseline B; larger optics, vacuum pipes, pumping systems, etc) and large transport optics (diameter $\propto \sqrt{\lambda B}$) for minimizing diffraction losses (ii) site and environmental constraints due to the need for straight beam passage between telescopes and the laboratory (see figure 32). This constraint can block expansion of existing arrays, for example, both CHARA ($B < 330$ m) and VLTI ($B < 200$ m) are limited by site topography, and (iii) operational complexity, as it is harder to maintain the pupil and field from the telescope to the laboratory.

The alternative use of fibers was first discussed by Froehly in 1981 [519], when it became apparent that SMFs could offer significant advantages for both beam transport and combination. In a ground-based fiber interferometer, starlight collected by the telescope passes through a corrective AO system before injection into SMFs [85, 520–524]. Fibers from each telescope transport light to the combiner laboratory, where path lengths are equalized using internal delays. Ideally all delay equalization would be in-fiber, however gross km-scale delays are not easily implemented in traditional fiber because of strong material dispersion and so effective dispersion management needs to be realized [525–530]. Fine delay equalization, however, can be done in fiber by stretching fiber segments [525–528] prior to beam combination [520, 523]. Alternatively, as is done today, gross and fine delay equalization can be in free-space using mirror arrangements and moving delay line carts [520, 523, 526, 527], but this breaks the realization of an all fiber, all photonic interferometer.

Current and future challenges

The main challenges in km-baseline fiber interferometer can be summarized upfront:

1. Transmission losses in fiber transport across various astronomical bands in the infrared are high. Currently only silica fibers in H-band can compete with mirror transport over km distances.
2. In-fiber delay compensation remains a major current and future challenge due to dispersion
3. Polarization and OPD properties of the transport fibers could be actively monitored via laser or comb metrology. A challenge remains in demonstrating this over long distances.

Although fibers offer clear simplifications over distance, they add challenges due to their intrinsic properties (table 3)—material absorption, chromatic dispersion [525–530], polarization birefringence, and thermal and vibration induced OPD [531, 532]. Fibers are dispersive media, and dispersion due to fiber length mismatch, and fiber bending/stretching causes arbitrary phase delay as a function of the wavelength, which leads to a shift in the zero-order fringes and effectively loss of fringe visibility for broadband operation [525]. To minimize dispersion in the first order, all the static fiber lengths need to be equalized. Upstream air dispersion can be compensated with a double wedge glass system, translating one wedge with respect to the other to adjust thickness as implemented for CHARA [533]. Second-order differential chromatic dispersion can be compensated using a fiber stretcher or glass-based double wedge [525–530]. Unless dispersion can be minimized or controlled, in-fiber delay compensation is the major future challenge.

Due to their opto-elastic properties, the E-field vectors emergent from fibers are modified (unpredictably, chromatically) because of the bending and twisting, strongly reducing the fringe visibility. This can be remedied by splitting polarization states upstream, and using PM fiber transport, with any upstream differential birefringence corrected by adding controlled amounts using LiNbO3 plates [534, 535]. Fibers also induce total optical path change due to thermal-mechanical stresses. Differential OPD is introduced by

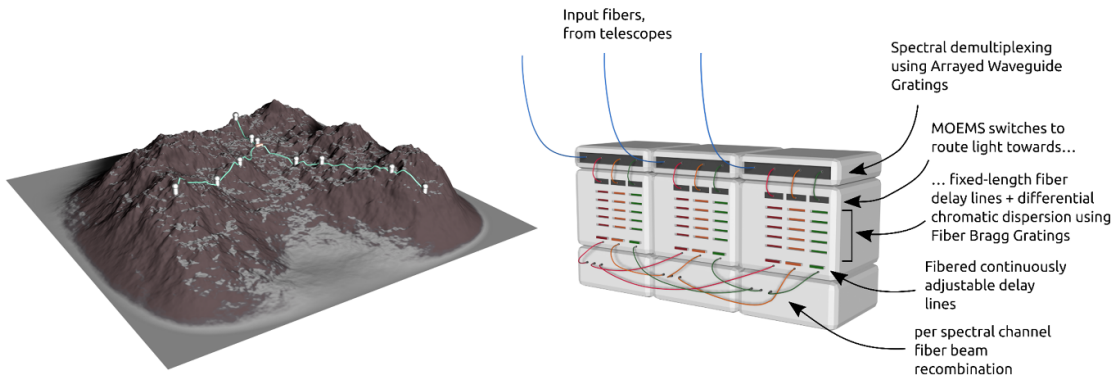

Figure 32. (Left) A conceptual future extremely long baseline interferometer (E-LBI) that can be implemented with fiber beam transport on uneven terrain. (Right) A compact proposed fiber stabilization and delay line system.

unequal longitudinal thermal gradients (OPD change of $\sim$1 mm km^{-1} K^{-1}), or fast differential vibrations [531, 532] which smear fringes on millisecond times or longer. While OPD errors can be reduced by careful passive insulation [523, 531, 532] and controlling the vibration environment, the OPD of fibers (and possibly the polarization state) can be monitored by using laser metrology and servo stabilized [531, 532].

As part of the CHARA Michelson Array/ALOHA project [147], this passive and active OPD stabilization of fibers was achieved with an accuracy better than 4 nm RMS [531, 532] for fiber lengths of 200 m. In this, a single metrology laser source operating at 1064 nm was split in two, injected into the same SMF used for the on-sky light transportation, and the signals from the two fibers were combined in the beam combiner laboratory and used to measured the differential OPDs by detecting fringe motion caused by the temperature fluctuations and vibrations. Next, these instrumental OPDs were corrected using fiber stretchers [531, 532]. In 2022, on-sky fringes [priv comm] at 810 nm were achieved at the CHARA Array between the South1 and South2 telescopes with fiber beam transport and with a first active fiber OPD stabilization system. However, we note that the fringes were obtained using the free space delay lines of CHARA, at a narrow bandwidth of 4 nm centered around 810 nm, and using a single polarization. Using a fiber for each polarization and making fringes separately in each polarization is interesting as it also brings science opportunities, e.g. for studying dust around AGNs. Perhaps in-band OFC metrology could be conceived to monitor the state of the fiber. These on-sky results are very encouraging. However, several challenges have to be overcome in obtaining fringes at broadband wavelengths and without splitting the polarizations.

Advances in science and technology to meet the challenges

An extremely long baseline (>1 km) interferometer with multiple telescopes (>12) is conceivably the next 'big project' after the completion of the extremely large telescopes. Realizing an all-fiber, all-photonic interferometer can make such an ambitious instrument quite cost-effective. We relist the challenges but herein offer potential solutions for development in the coming several years.

Transmission: A critical challenge is the efficiency and therefore sensitivity of the fiber interferometer, key to accessing faint primary targets ($K \geqslant 10$) which in turn impacts sky coverage. Although the transmission of silica fibers in the J-H bands is good at $\sim$0.3–0.5 dB km^{-1}, and that of ZBLAN fibers at K is tolerable, losses are much higher for other bands and are extreme in the mid-IR (5–13 μm) (table 3 and see section 5). Since mid-IR fibers have widespread uses, there is considerable research [536, 537] towards improving transmission with different materials and variations such as hollow-core fibers. Heterodyne interferometry and frequency mixing techniques offer alternatives by shifting the thermal wavelengths into the radio and NIR wavelengths respectively (see section 22). Currently, these techniques are limited to a narrow spectral bandwidth and lower sensitivity but they remain interesting for the future.

Wavelength coverage: Another challenge is maximizing broadband wavelength transportation while keeping the SMF properties and maximum fiber-coupling. For shorter wavelengths, the waveguide can become multimoded. For broadband wavelengths, the input beam size may not match the mode field diameter of the SMF leading to non-optimal fiber beam coupling. A promising alternative is the use of PM photonic crystal fiber, which are SM over the entire transparency range of silica (0.3–2 μm). The linear losses of this type of fiber are currently too high (>10 dB km^{-1}) to consider for the km scale baselines. Still this technology remains attractive in the future if losses and costs are reduced.

Fiber stabilization: Despite the availability of a state-of-the-art solution for the fiber stabilization for a two-fiber interferometer using a dedicated metrology laser [531, 532], we need a solution for multiple

Table 3. A compilation of Fiber optic materials that may be used in optical/IR interferometry. Hollow core fibers (HCF) and hollow core photonic bandgap fibers (HC-PBF) are not explicitly listed but have been demonstrated in silica and chalcogenide glasses. They are an active area of research [537, 539].

Fiber Type	Transmittance	Advantages	Disadvantages
Silica	High transmittance optical through H band 0.3 dB km^{-1} (1.2–2.0 μm) 5 dB km^{-1} (0.5–1.5 μm)	Non-toxic Non-hygroscopic Rugged, stable Photonic crystals and PMF available HC-PBF in rapid development	Brittle without proper coating
Fluoride: ZrF4 (ZBLAN) InF4	High transmittance in K-L bands 1 dB km^{-1} at 2.5 μm 3–4 dB km^{-1} at 3.5 μm	Non-toxic Stable with temperature Low dispersion Solid Core Photonic structures developed	Brittle without proper coating ZBLAN hygroscopic
Chalcogenide: As-S Ge-As-Se-Te (GAST) Ge-As-S-Se (GASS)	Transmittance in 0.7–10 μm 1 dB m^{-1} at 4.0–6.0 μm (As-S) 0.2 dB m^{-1} (8.0–11 μm GASS) Theoretical expectation for HC-PBF is 1 dB km^{-1}	Non hygroscopic HC-PBF in development SC Photonic structures developed	High refractive index (n) High dn/dT Toxic Fragile
Polycrystalline IR fiber (silver halide)	Transmittance in 3–17 μm 0.2 dB m^{-1} (9–13 μm)	Non-hygroscopic Non-toxic	Long term photodarkening SMF difficult to manufacture

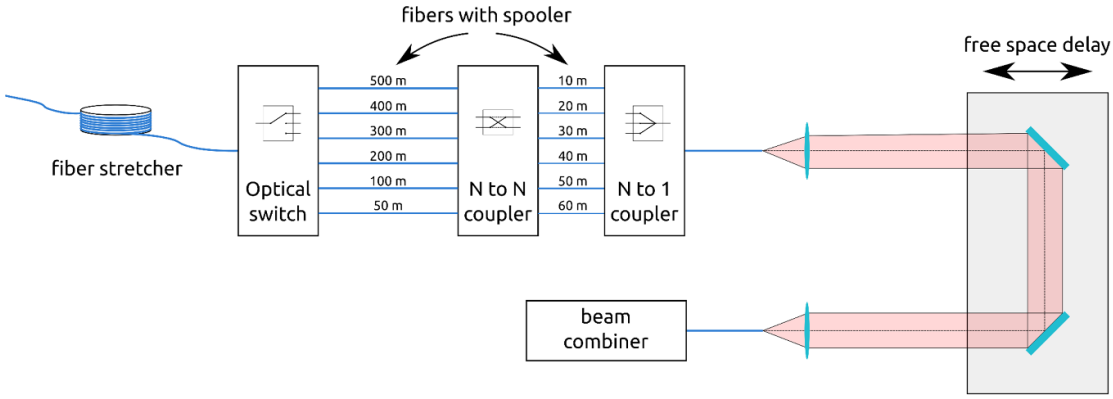

Figure 33. A schematic diagram of three stage delay lines: fiber stretcher, fiber delay lines with mechanical switches and free space delay. Since the additional delay is in glass, we would have to correct for dispersion differences to match the vacuum path in other telescope arms. This dispersion correction can potentially be realized with a custom dispersion compensating fiber Bragg grating (FBG) for each static fiber length. A combination of (i) longer static optical delays in fibers with fiber switches and small delays using (ii) fiber stretching or (iii) even free space delays of a few meters that address fast fringe tracking correction could be a solution to the current limitation of entirely free space delay lines.

telescopes, e.g. six telescopes of CHARA [85]. The main challenge would be after splitting the coherent metrology laser beam, how to send it to multiple telescopes separated on km scales and recombine the beams by building a multi-beam combiner to detect differential OPDs compared with a reference fiber.

Fiber delay lines: Existing interferometers use either free space air (VLTI/CHARA/NPOI) or vacuum-pipe delay lines (MROI) employing movable optomechanical trolleys. The delay lines are complex, and a low cost all-fiber solution would be attractive for a fiber interferometer. Only a few tens of cm of OPD [524–526] have been demonstrated by fiber stretching. However, fiber stretching can only come with side effects such as additional polarization, dispersion, and transmission issues, all of which depend on the stretch-state and wavelength [526–528]. Large fixed delays could be provided based on mechanical switches, e.g. micro-optoelectromechanical, that can allow the addition/removal of static fibers with a library of fixed lengths to the optical path similar to pipes of pan mirrors at CHARA [538] (see figure 33). Photonic

dispersion via an AWG spectrometer (see section 6), would allow for an input beam delivered by the fiber delay lines to be dispersed into discrete bands of interest, with each spectral channel coupled to a unique output fiber. In this way, the corresponding spectral channels from different telescopes could be combined with channel specific beam combiners, rather than broadband combiners, allowing for more optimal devices to be used. In addition, fringe tracking, via phase shifters on the beam combiner or fiber stretchers, could be more effectively used to compensate over the narrower bands of each channel. The approaches and technologies described here would require a comprehensive maturation program of technology development and demonstration before they can benefit long baseline interferometry.

Concluding remarks

For extreme long-baseline interferometry, beam transportation with SMF offers a unique advantage. Recent improvements in the transmission, wavelength coverage, and fiber control of the SMFs may already provide partial solutions to some existing challenges. However, active technology development in this area is required to maximize the transmission, wavelength coverage, and usage of fiber delays. These breakthrough technology developments could deliver transformative science results by expanding the baseline size beyond the current <1 km barrier.

Acknowledgments

We wish to thank Robert Ligon and François Reynaud for fruitful discussions. We would like to acknowledge suggestions about dispersion compensating FBGs and AWGs made by Nemanja Jovanovic.

19. Nulling interferometry with on-chip beam combination

Marc-Antoine Martinod[1], *Romain Laugier*[1], *Michael Ireland*[2] *and Jeffrey Jewell*[3]
[1] Institute of Astronomy, KU Leuven, Celestijnenlaan 200D, 3001 Leuven, Belgium
[2] The Australian National University, Canberra, Australia
[3] Jet Propulsion Laboratory, California Institute of Technology, Pasadena, CA, United States of America

Status

Exoplanetary science is amongst the most active fields in astronomy. While thousands of exoplanets have been discovered, few have been characterized, and even fewer have been detected from the habitable zone to the ice line. These regions are key to understanding planetary formation [540] and studying the exoplanets' features such as the surface [541], the atmosphere [542] or spectral biosignatures [543]. Such studies require careful measurement of the orbital parameters as well as the spectrum of the exoplanets, particularly in the infrared, ranging from 1.5 μm for close-in or young giant planets, up to 18.5 μm for characterizing temperate planets from space [339]. However, these observations are challenged by the small angular separation between the planet and its host star and the high contrast needed to discriminate the faint light of the planet from the overwhelming glare of the star. Although relevant planetary contrasts in the literature range from 10^3 to 10^{10}, the post-calibration contrast range for infrared nulling interferometry ranges from 10^4 for 50 Myr giant planets or typical hot Jupiters [544] to 10^9 for 4 μm thermal emission from an Earth-like planet around a solar-type star [339].

Nulling interferometry produces interference so that the on-axis light is nulled out (and redirected to a separate path), while the faint, off-axis source's light can be gathered and sent to a sensor or spectrograph [545]. This technique provides all the capabilities to address these scientific questions and tackle the challenges: resolving and revealing the star's surroundings at high contrast, measuring the relative position of companions, and spectrally analyzing their light. To maximize the impact of the nulling, we need stable suppression and a diversity of spatial information to improve observing efficiency. Doing so in the MIR enables compelling observations with less difficulty to meet the contrast requirement than at shorter wavelengths.

Nulling can equally be performed by combining the light from several telescopes as in long-baseline interferometry or by segmenting a single dish like aperture masking and using a photonic integrated-circuit (PIC). In all cases, the technical challenges for PIC developments remain similar. To date, the only attempt to observe on sky with an on-chip nulling beam combiner was by the GLINT instrument (figure 34), using integrated-optics to combine four sub-apertures from a monolithic telescope simultaneously with modal filtering [12], and spectroscopy [546]. The upcoming ASGARD/NOTT instrument (formerly Hi-5) operating in the L-band (3.5–4.0 μm) will use a PIC to implement the latest developments of nulling with the long baselines and large apertures of the VLTI [324]. Although they are currently lossy, photonic technologies offer several assets for nulling including: modal filtering, flexibility in the circuit design, stability, compactness and low mass. The last two are also attractive for the prospect of space missions [547]. These assets make the PIC an ideal platform to combine at least five apertures simultaneously and provide a minimum contrast of 10^5 (to get imaging capability). To achieve such a threshold, PICs will deliver most of the suppression but innovative data processing techniques can help enhance the contrast by an additional order of magnitude, such as numerical self-calibration [548] or ML techniques [89]. In the next sections, we will explore the challenges of using photonics for nulling and how we can address them over the next decade.

Current and future challenges

The most obvious challenge is the injection of the light into a SM waveguide. A high quality wavefront and stable PSF, either from a space telescope or from an AO system, is required to reach the best coupling (section 2). Any light failing to couple in the waveguide propagates through the bulk of the chip and can re-couple into the waveguides or contribute to a variable incoherent background. Using a sidestep on the input waveguides to get out of the stray light cone solves this issue [480] (figures 34(c) and 35(b)). Other solutions to investigate could be adding baffles inside the chip or modifying the surface of the chip to prevent total internal reflections.

Temporal fluctuations of the light that gets coupled into the waveguide leads to imbalance in the recombination, and additional light leakage. For this reason, input waveguides must feature photometric taps to sample the light of each beam [549] for real time monitoring and post-processing. However, they do not allow an active optimization of the injection against variable environmental conditions like vibrations or atmospheric turbulence (next section).

Once in the chip, the light of the on-axis source can be nulled. However, any instrumental deviation from the correct coherencing of the combined inputs leads to a leakage of the starlight in the nulled output that is

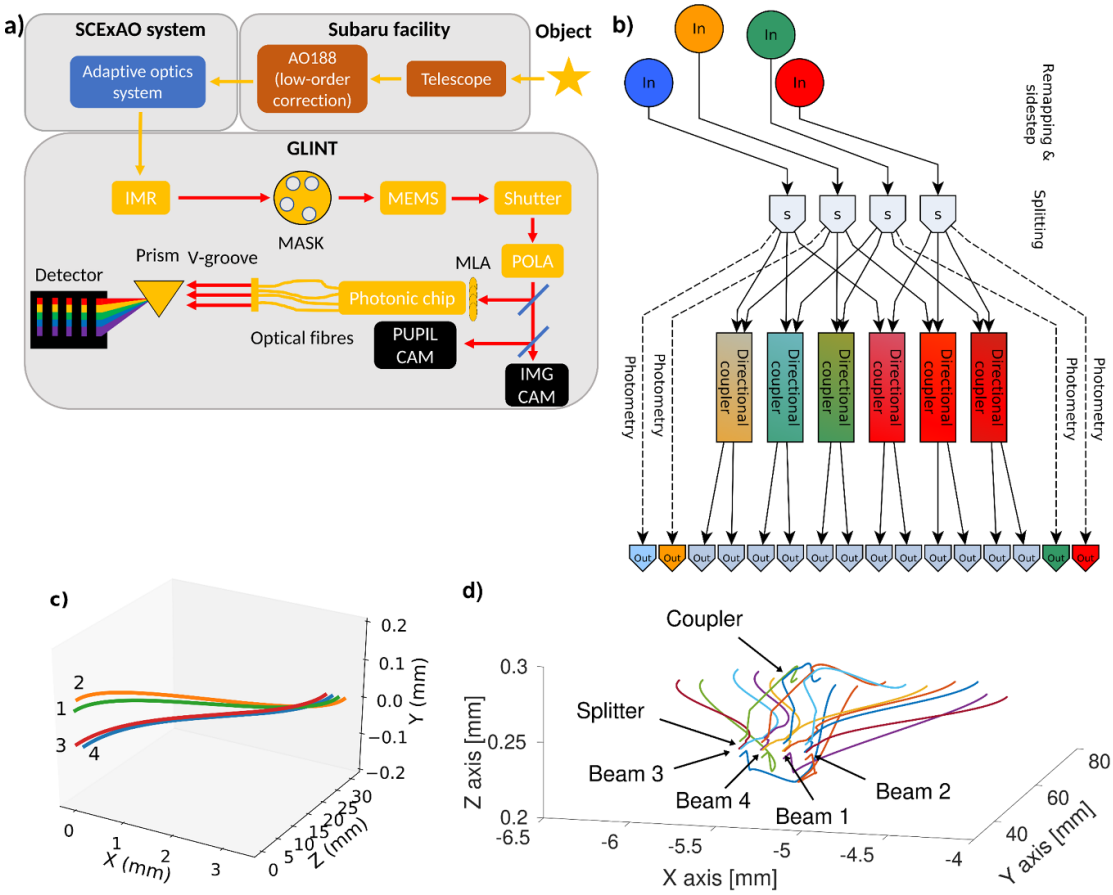

Figure 34. Schematics of GLINT and its integrated-optics chip. (a) Global schematic of GLINT and its integration within the Subaru Telescope and SCExAO. GLINT optics consist of the image rotator (IMR), a pupil mask, a segmented mirror (MEMS), a shutter and a linear polarizing beamsplitter (POLA). The science beam is then injected by a microlens array (MLA) into the photonic chip while the dichroic beamsplitter delivers light to cameras viewing both the image plane and pupil plane. The processed beams coming from the photonic chip are spectrally dispersed in the GLINT spectrograph then imaged on the science detector (C-Red 2). (b) Conceptual layout of GLINT showing the inputs (a pupil segmented into four sub-apertures), the sidestep, the remapping, the splitters, the directional couplers and the photometric paths, and the outputs. (c) Schematics of the pupil remapper of the chip, coherently transforming the 2D configuration of the inputs (on the left) matching the desired pupil sampling pattern into a 1D configuration (on the right). The waveguide paths have been optimized to match their optical path lengths despite taking different routes. (d) Perspective view of the beam combiner of the chip. Credit for (a), (c), (d). Reproduced from [546]. CC BY 4.0.

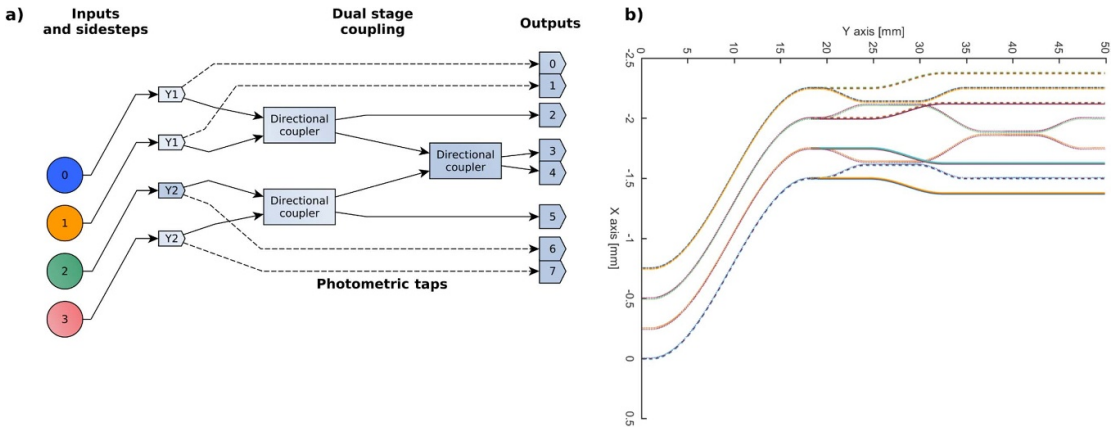

Figure 35. Diagram of the photonic chip of Nott. (a) Conceptual diagram showing the inputs, the sidesteps, the dual stage coupling (double-Bracewell) featuring tapered directional couplers to get achromatic coupling ratios, the photometric taps and the outputs. (b) Top-view of schematics of the chip.

difficult to disentangle from the planet's signal. Therefore, it is critical to control the amplitude and the phase of the light being combined. An AO system and a fringe tracker are necessary to handle these but they are insufficient. Simple combiners, like the Bracewell configuration, are sensitive to such light leakage. Combiners that are less sensitive to such effects and solutions providing a balanced and broadband coupling of light are needed (next section).

Additionally, the astrometry of the observed planet requires more diversity in the sampling of the UV plane; hence it is a driver for more complex nulling chips to simultaneously perform nulling on multiple baselines. GLINT pioneered it by using beamsplitters to attempt the simultaneous nulling of all six baselines [546]. However, differing optical paths inside the chip make nulling on more than two baselines simultaneously impossible. While such imperfections can be calibrated in an instrument like GRAVITY, they must be minimized for nulling devices to efficiently suppress the on-axis starlight.

However, front-end optics remain critical to correct biases such as alignment or beam layout to prepare for the injection. They are also useful to improve the nuller's capabilities (e.g. image rotator (figure 34(a)) or beam-switcher for a better sampling of the UV-plane).

Fabrication with the ULI technique in borosilicate and gallium lanthanum sulfide glass also face challenges. The low refractive index contrast delivered by this fabrication technique limits compactness (hence scalability and interest for space missions), especially to implement the aforementioned sidestep. Lithography provides higher index contrast but it does not offer the ability to realize circuits in three-dimensions like balanced 3D tricouplers (next section). In addition, nulling the maximum numbers of baselines simultaneously requires an accurate match of the optical paths between one input and the fed baselines. To date, there is no such criterion during the fabrication.

While the fabrication and the choice of the material are mature for chips used at 1.5 μm, there is little experience at longer wavelengths. Some possible materials have been identified (Si, Al2O3, Ge, GLS) but lithography and ULI are not routinely used for nulling chips working at wavelengths >3 μm. Efforts are required in the fabrication process to deliver cost-effective couplers and splitters that meet the requirements.

Advances in science and technology to meet challenges

All the challenges above can be overcome. The PL could be a promising solution to provide active control for injection (section 3). Such devices have been directly inscribed inside ULI-fabricated chips in the past [107] but their use for active injection has still to be demonstrated. In addition, photonic beam combiners are especially interesting for space-borne instruments but the injection of starlight in space-borne photonic devices is still to be demonstrated (e.g. the PICsat mission [550] that was lost). It would open the door to low-cost instrument concepts for space observatories.

In order to provide the possibility of building up to more complicated solutions utilizing photonics technologies, characterization should provide not just the coupling ratio but also the required wavelength-dependent relative input phase in order to achieve a deep null, and how polarized light propagates through the chip. Such characteristics are rarely available in the literature, except in the case of simulations.

Active control for on-chip tuning (e.g. photoelectric [551], thermo-optical [552], piezo-electric systems [99]) can relieve the requirement on the optical path match between the waveguides upstream of the couplers by allowing for tuning of the input phase. Careful configuration of the baselines and sophisticated combiners could help to reduce the leakage due to the spatial coherence of the source or the atmospheric turbulence. The main illustrations of these configurations and combiners include the double-Bracewell [553] and the kernel-nulling [554, section 20] variants. Another part of the difficulty in perfecting optical path control lies in the non-common path between the fringe tracker and the nuller. Three-dimensional tricouplers offer a combination of two bright outputs instead of one, allowing a measurement of the residual phase of the combination. Furthermore, symmetry in this 3D design is favorable to achieving a broadband null [481].

However, the integration of the tricoupler leads to the challenge of the dynamic range of the spectrograph's detector. Different sensors, providing short integration time and low latency for the bright channels and longer integration time and low dark current for the dark outputs could be used; such setups have yet to be tested, and are also required for the use of photonics lanterns for assisting with the active injection. A broadband nuller also requires an achromatic phase shift that simple air-delay lines cannot provide. A promising concept of an achromatic phase shifter of 180° made in ULI and placed upstream of a tricoupler has been explored [555]. Its association with a tricoupler enables the scalability of broadband nullers and is compatible with complex circuits. Last but not least, perfecting such phase shifters is crucial to enable nulling with new photonics platforms.

The push toward longer wavelengths demands operation at cryogenic temperatures. Temperatures below 100 K are required to make the background emission of the chip negligible compared to the telescope's thermal emission at 3.5 μm [554]. This constraint is a challenge for devices using glues or other bonding

techniques between multiple chips, V-grooves, or microlenses (sections 23 and 24) and may impact the refractive index contrast. The nulling instrument NOTT [324] will pioneer the development of photonics that can withstand these operating conditions. This nuller features a sidestep, an achromatic double-Bracewell combiner and photometric outputs embedded in a single chip with ULI technique (figure 35).

Concluding remarks

The prospect of nulling puts additional constraints on the requirement of interferometric beam combination. The need for precise matching of input phase and amplitude throughout the operation imposes a thorough characterization of the solutions in both phase and amplitude. While their host stars are bright, the planets are faint, leading to a need for throughput that encourages finding solutions to injection, achromatic coupling strategies and efficient on-axis light suppression.

Observations in the infrared region above 3.5 μm, require further development of circuitry with the mentioned requirements in a cryogenic environment for more ambitious ground and space projects, like the detection of different molecular signatures in the atmospheres of giant young planets. While the simple Bracewell combination is not expected to be sufficient for more ambitious goals, the challenges mentioned here pave the way towards efficient and sensitive nulling interferometers.

The single telescope nuller architectures described above are applicable to the HWO, which would address the main science focus. In addition, synergies between a long baseline space nulling interferometer and the HWO should also be considered and explored.

Acknowledgments

This work has received funding from the European Research Council (ERC) under the European Union's Horizon 2020 research and innovation program (Grant Agreement CoG—866070) and from the European Union's Horizon 2020 research and innovation programme under Grant Agreement No. 101004719.

20. Kernel nulling self-calibration

Nick Cvetojevic[1], *Frantz Martinache*[1] *and Sylvestre Lacour*[2]
[1] Université Côte d'Azur, Observatoire de la Côte d'Azur, CNRS, Laboratoire Lagrange, Nice, France
[2] LESIA, l'Observatoire de Paris, Université PSL, CNRS, Sorbonne Université, Université Paris Cité, Meudon, France

Status

The use of interferometric nulling for the direct characterization of extrasolar planets is an exciting prospect, but one that faces many practical challenges when deployed on telescopes. Despite the success of nulling interferometry [556], most photonic implementations thus far have been of the pairwise Bracewell type, and face considerable difficulties when implemented on-sky. With the key requirement of nulling interferometry being the stable destructive interference of two or more incoming interferometer arms, an exceptionally high level of up-stream wavefront control and pathlength matching is necessary to achieve this. This is needed to stabilize the injection into the SM waveguides, and provide high-speed correction of the differential piston between the arms which directly impacts the photometric leakage term in the null channel. With the key scientific driver of this kind of interferometry being high-contrast detections close to the stellar host, a large and time-varying photometric leakage is undesirable.

Various numerical self-calibration methods [12, 546, 548, 557] have been demonstrated to retrieve the astrophysical null in the presence of wavefront residuals, by exploiting the statistical distribution properties of the signal and various noise sources. However, these approaches have some limitations, with the model-fitting being fairly complex and scaling dramatically with more inputs, and the need for large datasets to obtain enough measurements to build accurate statistical models. Non-nulling interferometry typically makes extensive use of the production of self-calibrated observables, like CP [558, 559], and their generalized form, kernel phases [560], to sidestep the limitations brought about by wavefront residuals. Bringing together the benefits of self-calibration of interferometric observables and the photon-noise suppression of nulling is a powerful and exciting tool as it opens a previously unexploited parameter space.

The concept of creating a directly self-calibrated nulling observable capable of removing the effect of residual wavefront errors has been proposed in the past, by using a double-Bracewell architecture [553, 561, 562], and by exploiting the measurement of fringes in the leaked light of the nulled channel [563]. However, a more versatile solution exists where specially designed beam combiners can produce nulled outputs whose linear combinations produce self-calibrated observables [564]. These observables, called kernel-nulls, are robust to upstream differential pistons or phase errors. In general, kernel-nulls can be created by subtracting the measured intensities of two nulled outputs, provided the electric field in the two outputs are complex conjugates, with one possible 3-input configuration shown in figure 36. In practice, this is easily achieved in photonic interferometers by constructing a beam-combination architecture where input beams are recombined by mirroring phase offsets. It is also possible to create kennel nulling beam-combinations using bulk-optics [565]. Most of the techniques would use a number of cascaded beam-splitter cubes and delay lines to create the $\pm 2\pi/3$ phase delays in the different interferometer arms. However, because every output is a simultaneous combination of all the inputs, the number of optical elements scales, and the ultimate stability of the entire interferometer becomes more difficult to control. It is this ability to create complex beam combinations out of small integrated components that photonic technologies provide a distinct advantage.

Recent laboratory work has demonstrated the successful creation of kernel-nulls in 3-input [477] and 4-input [58] photonic beam combiners. These initial combiners avoided the use of classic pairwise combination using directional (evanescent field) couplers, and instead integrated the beam splitting and recombination into a single photonic component. This component is the MMI, a planar MM waveguide section (often rectangular) where multiple incoming waveguides are allowed to interfere spatially to form the required intensity profile at the MMI end face. By varying specific parameters (such as the length and width of the MM waveguide section), the exact beam-combination required to achieve kernel-nulling can be directly designed into the MMI.

Current and future challenges

In addition to the challenges shared with most astrophotonic interferometers, the unique beam-combination techniques required for kernel nulling raise additional technological challenges. The key requirement faced by any implementation of kernel nulling is the stable, accurate, and broadband pathlength control of the incoming beams prior to a beam combiner. While traditional pairwise Bracewell nulling also faces this challenge, kernel nulling often necessitates second, or third stage beam combiners, all of which must be accurately path-matched to an accuracy of a few degrees in phase. While bulk-optic discrete designs are being explored for kernel nulling, particularly in the context of space interferometers [339], the required stability

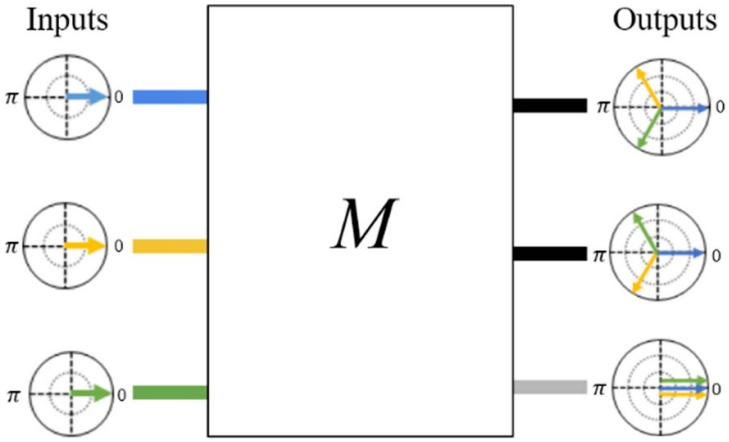

Figure 36. The electric field is represented by colored phasors on a complex polar plot, with the length of the vector being the amplitude and the angle showing the phase. For three in phase inputs, the Kernel Nuller creates three outputs. One bright channel where the input E-fields are in phase creating constructive interference, and two nulled channels where the input beams are given a $\pm 2\pi/3$ phase offset before being combined. In these channels the E-fields interfere destructively creating a null. Figure is adapted from figure 1. Reproduced from [477]. CC BY 4.0.

and accuracy are challenging to achieve. Integrated photonic solutions are far more accommodating in this respect, but add complexity beyond what is seen in standard nullers. Because kernel nullers cannot function in a pairwise fashion (nulling one interferometric baseline at a time), and must interfere all incoming beams together in the null channels, any design using two-by-two beam combiners must be cascaded into multiple subsequent recombinations.

An alternative method to cascading 2-beam couplers is to instead collapse all the combinations into a single MMI. While utilizing MMIs as the primary beam combination component has distinct advantages (such as simplicity, robustness to manufacturing errors, and scalability), it does come with its own set of drawbacks. The primary challenge arises from the MM nature of the interference inside the MMI, which is inherently wavelength-dependent. While more tolerant than its directional-coupler counterparts, this unwanted chromatic behavior can further be exacerbated by manufacturing errors, particularly in high refractive index contrast materials. While traditional directional couplers are also chromatic, the methods of creating broadband MMIs are different and need to be developed further in an astronomical context. Additionally, kernel-nulling imposes further constraints on the level of phase offset accuracy, and photometric balance in the splitting, as the self-calibration degrades the further they deviate from the ideal. Unlike traditional architectures, where each splitter and coupler are individual components on a chip and can be developed independently, utilizing an MMI for both tasks requires a more thorough design procedure to ensure it maintains performance across a wide wavelength band.

While a 4-input kernel nuller has been demonstrated in the laboratory using a single 4×4 MMI, this method does not produce all the possible kernel null observables. To make a complete kernel nuller for four input beams requires a second stage of beam-recombination after the initial nulling stage, shown in figure 37. The practical impact of this is that any processes used upstream to phase up the interferometer arms (delay lines, DMs) can no longer be used without dephasing the first stage. Thus, either the pathlength-matching of the waveguides in the second stage must be made to very high tolerance, or the use of on-chip phase control is paramount. Thermo-optic phase actuators (TOPAs) integrated into the photonic chip are capable of correcting pathlength errors due to manufacturing or environmental drift, in a reproducible and stable manner. However, because the phase delay is created by a change in the effective refractive index of the waveguide, it is wavelength dependent. While the chromaticity is negligible for small TOPA strokes (less than ten degrees of phase), correcting larger path lengths of a few π becomes difficult to do achromatically. As these devices will be required to work over large wavelength bands the underlying waveguide structure inside the TOPAs need to also be made as achromatic as possible. This is especially true if correcting for OPD errors that arise before injection into the photonic chip, when attempting to stabilize an atmospherically perturbed wavefront for example.

Advances in science and technology to meet challenges

To do efficient astrophysical nulling one should sample as many baselines as the telescope arrangement allows, and create the complete set of kernel nulls for that number of inputs. With state of the art optical long baseline interferometers having four (VLTI) or six (CHARA) telescopes, one can create efficient Kernel

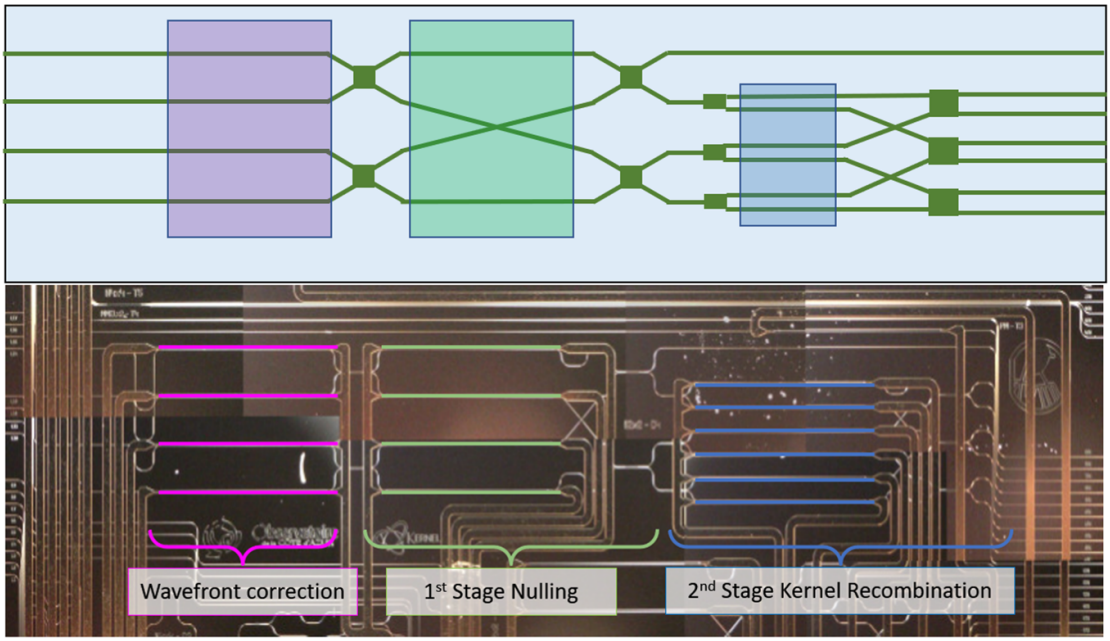

Figure 37. A schematic of a 4-input Kernel nuller device (top) achieved by the use of traditional waveguides, 2 × 2 directional couplers, and 1 × 2 splitters (green). TOPAs (colored) are used to control the internal path length matching of the interferometer arms inside the chip and correct for any error coming from either outside the chip (pink), inside the first stage nulling (green), and the beam-recombination that creates the kernel nulls. Microscope image (bottom) of the fabricated device, on a silicon nitride platform. Here the TOPAs are colored to their corresponding function.

nulling devices with a small number of inputs. This is similar for long baseline concepts in space, which would likely have four or five inputs. However, in the case of the ELTs a pupil segmentation regime would likely require many more inputs (30 or 40) to make full use of the aperture area. While the exact trade-offs regarding the ideal number of apertures to get the best sensitivity are being studied, it is likely that future on-sky devices will require efficient broadband operation over at least one wavelength band, and potentially handle many more inputs simultaneously.

To date, only 3-input [477] and 4-input [58] kernel nullers have been realized. However, it is possible to create a kernel nuller with an arbitrary number of inputs [566], which can probe a much greater UV coverage on-sky. The drawback is the waveguide routing becomes very complex so new design work needs to be undertaken to realize this in a low-loss manner. Ultra low-loss waveguide crossings, routing, and pathlength matching are critical to achieving this.

To make broadband MMIs, a more complex design is required than those typically used as standard for telecommunication applications. The internal wavelength-dependency can be compensated for by creating a non-uniform effective refractive index inside the MM waveguide [567], either by changing the width of the MMI along the propagation direction, or by inserting more complex structures inside the cavity. The use of sub-wavelength grating structures inside the MMI has been shown to greatly increase the operating bandpass [568], and recent development in inverse design using deep neural networks makes the design of these complex structures far easier to derive [569]. To enable this, either high accuracy fabrication methods capable of achieving the required feature sizes need to be available for commercial foundries, or post processing using E-beam/Ion-beam lithography. Furthermore, robust modeling and design tools need to be developed to reliably and rapidly design prototypes for astronomical use. Similarly, the process of making broadband TOPAs requires modification of the waveguide core and thus has similar requirements. However, a more powerful technique to create true integrated dispersion compensation is the integration of low resolution wavelength dispersion, such as by AWGs (see section 7 for more details), in combination with traditional TOPAs. In this concept an AWG would disperse each input into a number of wavelength channels (few 10's of nanometers wide), with each one having a TOPA phase actuator to correct the phase individually, or a Mach-Zehnder configuration for amplitude control, before being recombined into a single waveguide by another AWG. This would enable direct control of the amplitude and phase at various wavelength channels over a broad wavelength band (see section 14 for details). To enable this, ultra low-loss waveguide crossings must be developed because of the extra routing required after the AWGs, along with active control systems for a much larger number of TOPAs.

Concluding remarks

The self-calibration of nulling observables enabled by kernel nulling can greatly reduce the impact of upstream wavefront residuals on the performance of nulling interferometers. This relaxes the requirements for upstream optics such as delay-lines, fringe-trackers, and DMs, and enables the use of nulling interferometry in non-ideal conditions. While the fundamentals have been demonstrated at NIR wavelengths, to truly exploit this technology for future astronomical instrumentation the photonic components that underpin a kernel-nuller should be developed to work over a wide wavelength band and at different wavelength regimes. Furthermore, the use of active-photonics in the form of on-chip phase control, enables the practical use of more complex designs that have thus far been beyond the reach of astrophotonic interferometry.

Acknowledgments

The authors acknowledge the funding from the European Research Council (ERC) under the European Union's Horizon 2020 research and innovation program (Grant Agreement CoG—683029).

21. Nulling interferometry with optical fibers and photonic lanterns

Yinzi Xin[1], *Sergio Leon-Saval*[2] *and Eugene Serabyn*[3]
[1] Department of Astronomy, California Institute of Technology, Pasadena, CA, United States of America
[2] Sydney Astrophotonics Instrumentation Laboratory (SAIL), School of Physics, The University of Sydney, Sydney, Australia
[3] Jet Propulsion Laboratory, California Institute of Technology, Pasadena, CA, United States of America

Status

The combination of diffraction due to a telescope's finite pupil diameter and scattering due to imperfect wavefronts leads to bright halos of light surrounding typical stellar images. This severely limits a telescope's ability to detect faint sources near bright stars, such as that from exoplanets and circumstellar dust. As a result, optical techniques that enable high contrast observations at the smallest possible angular separations are of great interest, with compelling applications on the ground as well as on future space telescopes such as the HWO [40]. Interfering the light arriving at different parts of a telescope aperture (sub-apertures) can potentially yield improved resolution, and appropriately phasing the sub-apertures can interferometrically suppress (null) starlight. This technique of nulling interferometry [570] across a telescope's aperture can enable observations closer to a star than classical full-aperture coronagraphic imaging, providing access to separations where exoplanets are expected to be brighter and more numerous. Nulling interferometry is increasingly turning to photonic devices to reach deep stellar rejection. In this work, we focus on approaches that inject an interferometrically-combined beam into a photonic device (e.g. a SMF or PL [7]), exploiting the interplay of the beam's phase with the spatial mode structure of the device, as well as leveraging the spatial filtering the device provides. These systems rely on appropriately phasing the different parts of the telescope pupil prior to beam combination, which results in a class of nulling interferometry instruments architecturally distinct from those employing pairwise beam-combination.

The first photonic nuller was the Palomar Fiber Nuller (PFN) [557], which combined the light from a pair of sub-apertures on the Hale Telescope by focusing them in anti-phase (π radians out of phase) onto the tip of an SMF. Anti-phasing provides an asymmetric stellar point-spread-function (PSF) that cannot propagate within a symmetric spatial mode, thus excluding the on-axis starlight [571, 572]. At the same time, SM operation also serves to greatly reduce the sensitivity of the null to telescope aberrations [573]. While the PFN was based on multi-axial focal-plane beam-combination at an SMF, co-axial pupil-plane beam combination could also be used prior to SMF injection, either with a standard beam splitter, or by focusing a pair of sub-aperture beams from opposite sides of the pupil onto a focal-plane grating to superpose their $+1$ and -1 orders [574]. However, combining light only from small pupil sub-apertures implies an efficiency loss. This can be obviated (figure 38) by applying a relevant phase pattern to the entire pupil, such as a vortex-phase or simple π radian phase-step (i.e. 'phase-knife') pattern [575–577], which yield respectively, circular and linear fringes. Such a Vortex Fiber Nuller (VFN), has recently been deployed at the Keck Observatory [74, 578]. A Photonic Lantern Nuller (PLN) [579] leverages the same principles, but replaces the SMF with a MSPL [19], which maps specific LP modes into individual SM outputs [580], resulting in multiple ports that null on-axis starlight but have different spatial sensitivities to off-axis light sources. The operating principles of the PLN are summarized in figure 39. While such techniques largely eliminate the need for free-space beam-combiner optics, one can go a step further, and carry out both beam combination and phase shifting within a photonic chip (see sections 15, 16 and 18). Additional layers of beam combination may also be useful for reducing residual stellar leakage in the null that result from device imperfections. Here we discuss the current and future challenges of fiber and PL-based approaches and the technology advances needed to meet the challenge of deep stellar nulling.

Current and future challenges

Deep nulling requires an exquisite balancing of beam parameters, with any imbalance in amplitude or phase resulting in increased stellar leakage [570, 581]. With commercial SMFs, multi-axial fiber-nullers have reached differing null depths as a function of wavelength and bandpass, with raw laboratory null depths $\sim 10^{-6}$ with a 633 nm laser [572] and $\sim 7 \times 10^{-5}$ for broadband NIR ($\sim 1.65\ \mu$m) light [582]. Meanwhile, laboratory tests of the VFN have achieved null depths of $\sim 6 \times 10^{-5}$ with a 635 nm laser [576]. This null depth is consistent with known static aberrations in the optical testbed, but the VFN will also eventually be limited by fiber-related performance limitations in systems with better wavefront quality.

These limitations can be attributed to a number of fiber imperfections that do not usually receive much attention, but will need to be understood for further progress, such as the deviation of the fiber beam profile from the theoretically symmetric SM shape (which can lead to a small coupling to asymmetric input modes), or light leaking into the fiber core from the bright starlight originally entering the fiber cladding (which can

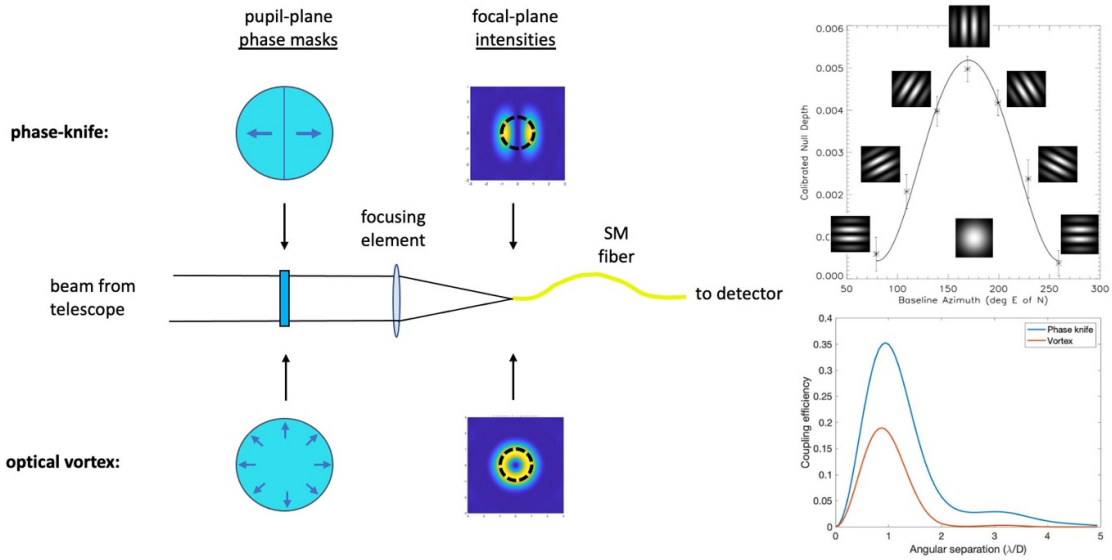

Figure 38. Left: Schematic fiber nuller layout. A phase mask is first applied in the pupil plane. Here, a phase knife is depicted on top, and a vortex on the bottom. After the mask, the beam is focused and injected into a single-mode fiber that routes the light to a detector or spectrograph. The PSFs for the two cases are also shown with approximate single-mode acceptance angles indicated by the dashed circles. Top right: The null-depth rotation curve measured on the spectroscopic binary star eta Peg using the PFN, showing both the binary response and the few $\times 10^{-4}$ leakage due to the primary star's finite size. Reproduced from [557]. The inserts show the fringe orientations for each measurement (the binary orientation was roughly horizontal) and the PSF of the full telescope aperture near the bottom of that panel. Bottom right: Comparison of fiber-nuller coupling efficiencies as a function of off-axis angle, in units of λ/D, where λ is the wavelength and D the telescope diameter. On-axis starlight is nulled, but throughput for off-axis sources peaks near λ/D. Reproduced from [577].

limit stellar rejection). At longer MIR wavelengths ($\sim$10 μm), there are fewer materials available to make fibers, and fiber lengths are limited [583, 584], both potentially limiting the approach to true SM rejection. SMFs are also sensitive to environmental (i.e. thermal) changes, but they are not sensitive when used in the common-mode configuration used for fiber nulling, where the SM fiber is essentially used in the combined beam.

Nulling with PLs will also be limited by practical limitations in PL design and manufacturing. The PLN relies on the symmetry properties of LP modes, as nulls are generated by the orthogonality of the stellar (on-axis) electric field with specific LP modes. Imperfections in mode shape caused by cross-talk amongst modes may break these symmetries, which will cause on-axis light to leak into the nulled channels. The limit of cross-talk currently achievable in MSPLs is around $\sim$1%, limiting achievable contrast ratios to the 10^{-2} level. Moreover, the modal structure of a PL varies with wavelength, deviating from perfect LP modes as the wavelength diverges from the design wavelength. Significant theoretical and experimental work is necessary to understand the fundamental limits of PLs, effectively characterize them in the lab, and implement them in a nulling configuration.

Advances in science and technology to meet challenges

In the past, optical fiber-based nulling beam combiners have used a standard SM step-index fiber. However, the active optical fiber community has developed a myriad of new and improved optical fiber types, e.g. extremely low-loss (low scattering) graded index fibers [585], photonic crystal fibers (a.k.a. microstructured fibers), hollow-core fibers [586], and low-loss mid-IR (1–18 μm) optical fibers [587]. We envision that exploring these new SMF technologies for fiber nulling could provide extended wavelength ranges (e.g. SM hollow core fibers in the infrared), improved null depths by increasing cladding mode suppression and reducing mismatch with the fundamental mode (e.g. cladding mode suppressed photosensitive fibers), and improved fundamental mode input selectivity (e.g. using SM graded index fibers with a larger effective index separation between the fundamental mode and the second mode, which leads to a large acceptance angle separation).

Some limitations of PLs have already been studied and improved in devices for other applications. For example, new telecom MSPL devices provide a broadband operation (more than 600 nm of bandwidth in the near-IR) and highly circularly symmetric mode structure outputs (resembling quasi-perfect LP modes) [155]. However, the need to push input modal cross-talk to its limit is unique to high contrast astronomy, since a cross-talk of 10–20 dB is considered sufficient in telecommunications applications [156]. Significant work via both simulations and fabrication and testing is needed to understand the intrinsic limitations of

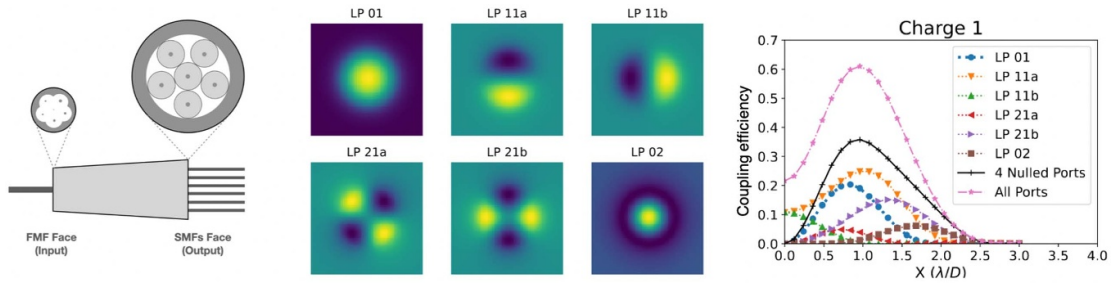

Figure 39. Left: Schematics of a 6-port mode-selective photonic lantern spatial-multiplexer fiber system. Each LP mode at the few mode fiber (FMF) face is mapped to one of the six single-mode ports of the SMF face, such that light with an LP mode shape at the FMF side will result in flux in the corresponding SMF core. The device is bi-directional, so light injected into one of the SMF ports will propagate into the LP mode corresponding to that port at the FMF face. Middle: The field amplitudes of the first six LP modes, corresponding to the ideal modes of six-port MSPL. Right: Coupling efficiency for each port as a function of off-axis separation when used with a charge 1 vortex phase mask. Note that the coupling efficiency is not circularly symmetric for all ports, and that *x*-axis cross-sections are shown here subfigures reprinted from [579].

broadband mode selectivity and cross-talk in MSPLs, as well as the steps needed to push designs towards those limits. Additionally, robust methods for experimentally measuring cross-talk have yet to be fully established. Current characterization techniques include measuring modal purity through near and far field mode profiles [48], or leveraging refractive index differences to disperse the modes [585]. However, these approaches do not comprehensively measure the PL's structure. Other techniques, such as interferometry, phase diversity, or neural network methods need to be explored in order to fully characterize a PL's complex modal structure.

New geometric structures and waveguide properties may further improve the multi-mode-to-SMF mapping, hence increasing on-axis starlight rejection and exoplanet spatial information. In the meantime, the VFN and the PLN are relatively new instrument designs, and new instrument structures may also open different approaches. For instance, the use of hybrid MSPL [112] behind a vortex could potentially bring the best of both worlds: SMF nulling, wavefront sensing, and coupling optimization on a single device without introducing non-common paths. Techniques to remove residual stellar leakage, such as wavefront control or back-end beam-combination, will need to be explored. Criteria that future PLs must meet for viable broadband PLN usage still need to be established, and the performance of PLN designs with currently manufacturable PLs still need to be experimentally characterized. In parallel, however, many of the known and predicted limitations can be addressed by advances in photonics technology.

Concluding remarks

The injection of an interferometrically-combined beam into an optical fiber or a PL is a promising approach to nulling interferometry, encompassing instrument configurations such as the PFN, VFN, the PLN, and the recently proposed Phase-knife Nuller. Besides the fiber itself, several of these approaches also rely on specialized pupil-plane phase masks, which can generally be manufactured with existing technologies such as spatially variant liquid crystal polymers or microstructures. Real-time configurable phase masks would be a further step forward. However, the stellar null can be degraded by fiber and PL imperfections, such as modal shape impurity, cross-talk, and cladding leakage, which will need to be mitigated in the future. Recent advances in the design and fabrication of fibers and lanterns may already provide solutions to some of these limitations, but further research will be necessary to understand them and push the limits of these techniques for higher contrast astronomy applications.

Acknowledgments

This work was supported by the National Science Foundation under Grant No. 2109232, and by the National Science Foundation Graduate Research Fellowship under Grant No. 1122374. Part of this work was carried out at the Jet Propulsion Laboratory, California Institute of Technology, under contract with NASA (80NM0018D0004).

22. Heterodyne interferometry and frequency mixing techniques

Jean-Philippe Berger[1], *Azzurra Bigioli*[2], *Guillaume Bourdarot*[3], *Ludovic Grossard*[4], *John Monnier*[5] *and François Reynaud*[4]
[1] Univ. Grenoble Alpes, CNRS, IPAG, 38000 Grenoble, France
[2] Katholieke Universiteit Leuven, Belgium
[3] Max Planck Institute for Extraterrestrial Physics, Garching, Germany
[4] Limoges, CNRS, XLIM, UMR 7252, F-87000 Limoges, France
[5] Department of Astronomy, University of Michigan, Ann Arbor, MI, United States of America

Status

Several important fields of astronomy such as planet formation or black-hole environments studies request observations at angular resolutions that lie far beyond the performances of current facilities. Optical interferometers offer the potential of reaching resolutions of a few tens of micro-arcseconds. Yet, the technologies at the heart of existing interferometers cannot be simply extrapolated to future arrays with kilometric baselines and tens of telescopes since they are costly, complex and require high maintenance (see e.g. [506]). One of the major simplifications of such infrastructures consists in replacing the free-space optical trains by photonic links. In the visible and near infrared, fiber links can be envisioned (see section 18). Unfortunately, such technologies are much less mature in the mid infrared domain (e.g. from 3 to 20 μm) where several key astrophysical processes such as planet formation, or dust formation and evolution, leave an important radiative imprint (see section 5 for early but interesting developments of specialty fibers and sections 8 and 9 for new photonics technologies). Newly developed heterodyne and frequency mixing techniques have the potential to expand to thermal wavelengths the concept of optical links, i.e. systems that avoid most of the free-space propagation from the telescopes to the central interferometric correlation unit,. Moreover, the advent of quantum optics coupled with heterodyne technologies allows potentially revolutionary concepts to be explored.

Heterodyne interferometry uses the interference beat between the celestial signal and a local oscillator (LO) synchronized in phase between all telescopes to generate radio-frequency signals whose correlation will allow image of the brightness distribution of the object to be reconstructed (see figure 40). This approach allows the multiple splitting of the signal requested to correlate the electromagnetic field of one telescope with all the others to be compensated by amplification without loss of signal. The Berkeley Infrared Spatial Interferometer was a complete MIR (10 μm) infrastructure that demonstrated, through valuable astronomical observations, the feasibility of astronomical heterodyne interferometry albeit with some sensitivity limitations [588]. It used two CO_2 lasers synchronized in phase as LOs that were propagated to the telescopes and interfered with the celestial signal on ~3 GHz HgCdTe detectors.

Frequency mixing techniques use the non-linear sum frequency generation effect to shift the spectrum of the collected light from the thermal infrared to the near infrared or visible as close as possible to the telescope focus where the signal is extracted from the surrounding thermal noise. It thus allows the coherent propagation of the converted MIR light with silica optical fibers or guided optics (figure 41). The nonlinear interaction between the astronomical signal and a highly coherent laser beam occurs in a second order nonlinear waveguide. In 2015, first interference fringes on the sky were obtained using periodically poled lithium niobate (PPLN) nonlinear ridge waveguides with a 1550 nm to 630 nm frequency up-conversion interferometer installed on the CHARA telescope array [589]. On-sky tests were also performed at 3.5 μm on a single interferometric arm. Starlight up to magnitude $L_{\mathrm{mag}} = 2.8$ at 3.5 μm was successfully detected after conversion to 820 nm in a PPLN ridge waveguide [590].

Heterodyne interferometry with entangled photons has been proposed to mitigate the LO photon shot noise that adds in quadrature at each output. This background acts as a substantial noise floor for wavelengths shorter than ~50 μm. The use of $N = 1$ quantum states or heralded single photons via entanglement (e.g. from spontaneous parametric down-conversion) promises to suppress shot noise and was explored for the case of heterodyne interferometry by Gottesman *et al* [591]. When such a quantum local oscillator (QLO) is split, sent to two telescopes, then mixed with starlight, the photon counts can be scrutinized for coincidence at the combiners. Two detected photons at the same time in different telescopes means the QLO and a stellar photon mixed and non-local interference can be recovered. A preliminary laboratory proof of principle was presented in [592]. There is still a 50% theoretical loss in efficiency compared to 'direct detection' as sometimes the two photons show up at the same telescope, but the improvement over shot-noise limited operation can be dramatic.

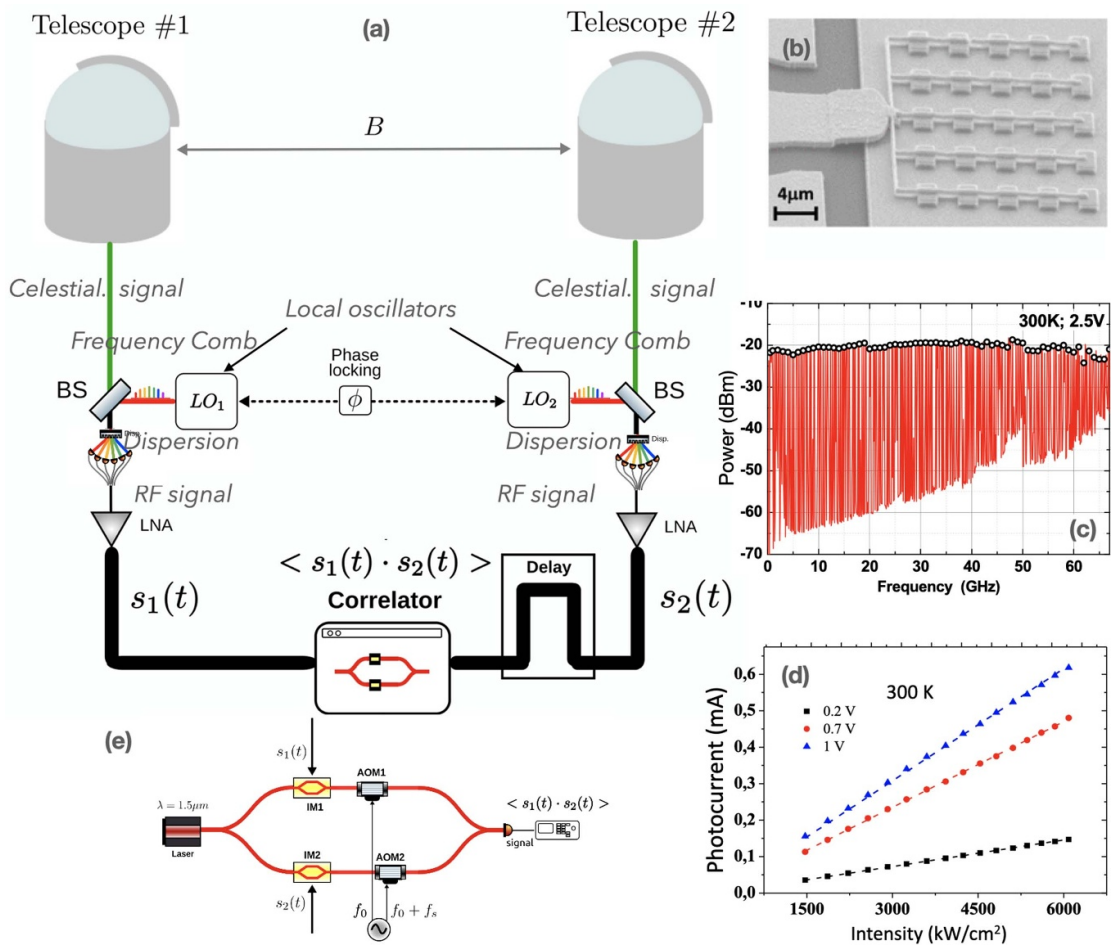

Figure 40. (a) Schematic principle of an optical heterodyne two telescope interferometer. Incoming light celestial light from telescopes is mixed with a synchronized frequency comb that acts as a local oscillator. The resulting RF beating signal is correlated to extract information on the emitting source. The (b) SEM photograph of a multiple quantum well infrared photodetector quantum well infrared photodetector (QWIP) patchy hetero-structure. Reprinted with permission from [594]. Copyright (2010) American Chemical Society. (c) Heterodyne beat spectrum on a QWIP at 10 μm showing high bandwidth behavior. Reprinted with permission from [594]. Copyright (2010) American Chemical Society. (b) and (c) adapted with permission from Hakl *et al.* ACS Photonics 2021, 8, 2, 464–471 (d) QWIP photocurrent curves as a function of incident intensity showing the linearity and high dynamic range. Reproduced from [595]. CC BY 4.0. © 2019 The Authors. Published by WILEY-VCH Verlag GmbH & Co. KGaA, Weinheim. (e) Detail of the simplest photonic two-way analogical correlator. Two incoming RF signals modulate intensity modulators in a linear regime. Their mutual interference provides the correlation signal (see [596, 597] for discussions).

Current and future challenges

Both heterodyne and frequency mixing techniques suffer from significant sensitivity limitations with respect to 'classical', direct interferometry. Both have intrinsic narrow spectral bandpasses caused respectively by the detector bandpass and the non-linear up-conversion process with a narrow-band laser.

In **heterodyne interferometry** the beating of a highly coherent LO with celestial thermal radiation adds a corresponding shot noise penalty that severely limits its practical use in astronomy in the MIR. Improving the sensitivity of the measurement chain requires increasing the overall spectral bandpass. This is achieved by two means: augmenting the detector temporal bandwidth (and thus, spectral bandpass) and using several spectral channels. First, detector bandwidths of the order of 30 GHz would be highly desirable (from current ~3 GHz commercial devices). This characteristic, at 30 THz (~10 μm), corresponds to a 10 nm spectral bandwidth. Secondly, in order to span a significant fraction of the astronomical *N* [8–13 μm] and *Q* [15–27 μm] bands, one should aim at developing focal planes combining a high number of such detectors. This would allow adjacent spectral bins to be sampled by dispersing the celestial light onto the detectors and having it interfere with a MIR LFC in which each line is tuned on the desired pixel central wavelength (see figure 40(a)). This would require MIR frequency combs with repetition rates of the order of several tens of GHz capable of producing of the order of 100 lines in order to provide several hundred nanometers of spectral coverage (see section 4 for details). Moreover, LOs at each telescope have to be synchronized in phase to allow the correlation. Therefore, a dedicated synchronization scheme between each oscillator is required. Finally, since classical digital radio correlation techniques with such high bandwidth signals request

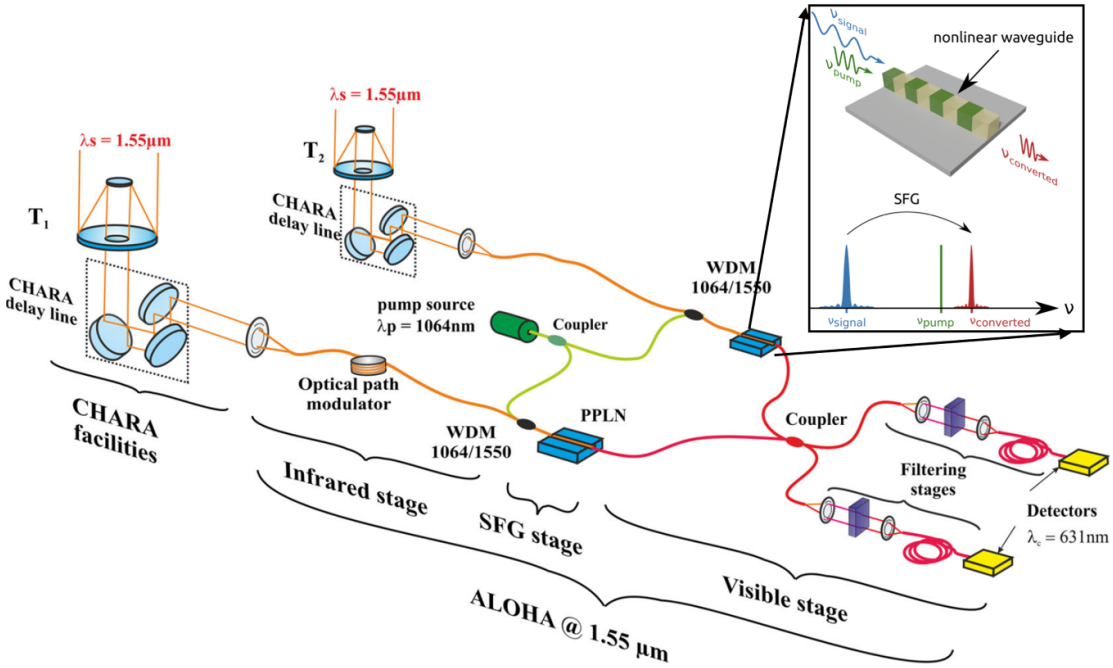

Figure 41. Schematic of a two telescope interferometer with coherent upconversion of the celestial signal through a nonlinear crystal (ALOHA project). Reproduced from [589].

prohibitive digitization and computing power [593], technologies capable of correlating high bandwidth signals have to be demonstrated.

Frequency conversion's limited bandpass has to be tackled as well. For example, the current bandwidth with a single line pump laser at 3.5 μm is only 37 nm for a 2 cm long piece of PPLN. Two possible strategies can be envisioned: (1) injecting several pumps, for example using a comb, in the same crystal and demultiplexing through a multichannel spectral mode [598] or (2) multiplexing different signals on different crystals (with different periodicity to ensure wavelength sampling) which presents the advantage of allowing the conversion of large bandwidth signals with only one monochromatic pump laser. A second important challenge related to sensitivity is to improve the overall efficiency of the conversion chain which requires better mode overlap between the astronomical and pump fields in the nonlinear ridge waveguide, coupling efficiency at the input and output of the waveguide, conversion efficiency and possibly noise-free detection in order to compensate for the losses.

The **heterodyne interferometry with entangled photons** technique offers the unique promise of operating at all wavelengths. Yet, it is difficult to implement as the entangled photons still need to be coherently distributed in real time with near unity transmission, though future advances in quantum communications may make this practical [599]. Similarly, as for heterodyne and frequency up-conversion schemes, there is a similar limitation in bandwidth. Therefore, a dense spectral-multiplexing should be envisioned to cover a broad astronomical bandpass.

Advances in science and technology to meet challenges

High bandwidth detectors

N-band heterodyne interferometry requires high dynamic range, fast and sensitive single-pixel detectors. To overcome the limited speed (<3 GHz) of the HgCdTe detector, the most advanced alternative for the 10 μm spectral range is provided by quantum well infrared photodetectors (QWIPs), and quantum cascade detectors (QCDs) in unbiased mode. Thanks to their unipolar electronic transport (no hole mobility is involved), they can achieve flat responses up to more than 70 GHz [594] and saturation intensity up to kW cm^{-2} [595] (see figures 40(b)–(d)). A 20 GHz–3 dB QCD for 4.6 μm radiation has entered the market as of 2021. Following the integration of a QWIP into a metamaterial acting as a micro-antenna and a cavity [600], the research on photonic-enhanced QWIPs and QCDs is increasingly promising [601]. An optimized photonic architecture could combine speed with a Quantum Efficiency of at least 40%, allowing the electromagnetic field confinement in the material to be maximized without increasing the doping density and thus the dark current [602]. Other fast technologies have been proposed, namely using graphene [603].

However, their short dynamic range, with a response saturation for power $<10\ \mu$W, prohibits the regime where the laser shot noise dominates over the detector noise contributions.

(Synchronized) Mid-infrared LFCs
Although LFCs have already been used for astronomical precision spectroscopy at short wavelengths [417] such technologies in the MIR are still in their infancy and have never been used in an actual instrument. In order to cover a sufficiently large spectral bandpass of the astronomical MIR filters, LFC are needed to act as LOs. They should span several 100 GHz with repetition rates or comb line spacings corresponding to the spectral bandwidth of each detector (e.g. several 10's of GHz). This can be achieved by difference frequency generation in quadratic nonlinear media [604]. Quantum Cascade Lasers are another promising technology since they were demonstrated to operate as frequency combs [605]. Further research could consider quantum cascade laser chips that include several emitting heads tuned to study specific lines and continuum. Ultrafast optical parametric oscillators with several GHz repetition rates have been demonstrated in the near infrared and [606], this could be one way forward in the MIR. Beyond that, LOs need to be synchronized in-phase across the array. One could find inspiration for this in the demonstration of the stabilization of a MIR (10.6 μm) laser to an atomic clock through a 43 km fiber link. A near infrared comb is locked onto a primary frequency reference and propagated on a phase-stabilized link to each telescope station. At the telescope level it is upconverted to the MIR to provide the LO locking signal [604].

High bandwidth correlation
The correlation of high bandwidth signals requested by heterodyning could be done numerically at the price of huge computing power [593]. However, analog photonic correlation schemes using amplitude modulators have proven to be a robust way of propagating and correlating very large bandwidth (up to 100 GHz) heterodyne signals over telecom fibers (see e.g. [596, 597]). They should be investigated further.

Reliable nonlinear crystals
The deployment of parametric conversion schemes requires the manufacturing of reliable nonlinear crystals. This in turns begs for robust industrial processes that allow a proper control of the spectral acceptance, waveguide structure and the management and reduction of the noise due to spontaneous parametric down conversion.

Miscellaneous developments
Both heterodyne and frequency upconversion techniques would dramatically benefit from compact high transmission discrete or continuous kilometric delay lines. The first one because it needs an external co-phasing instrument capable of measuring atmospheric phase fluctuations, the later because it is intrinsically a direct interferometry technique that requires optical path compensation. Finally single-photon LOs are required as well as fast time-stamped photon-counting detectors in the search for the optimal quantum protocol to achieve the best possible visible and NIR telescope resolution of faint astronomical objects. More generally, the availability of true quantum networks, developed in other industrial contexts, would represent a major advance for this application.

Concluding remarks
The expansion of optical astronomical interferometric arrays requires an increase in their imaging capabilities, angular resolution and sensitivity. This cannot be simply extrapolated from current technologies. Technological breakthroughs in the field of photonics and quantum technologies present new opportunities to envision radically different array architectures. Heterodyne interferometry, both classical and with single-photon LOs, as well as frequency up-conversion offer the perspective of arrays with infrastructure free links thus dramatically reducing their complexity.

23. Efficient hybrid photonic and electronic integration to realize multi-functional instruments

Sherif Soliman[1], *Katarzyna Ławniczuk*[2], *Nemanja Jovanovic*[3], *Jeroen Duis*[1] *and Ronald Broeke*[2]
[1] PHIX Photonics Assembly, Enschede, Netherlands
[2] Bright Photonics BV, Eindhoven, The Netherlands
[3] Department of Astronomy, California Institute of Technology, Pasadena, CA, United States of America

Status

The ultimate goal for astrophotonics is to be able to realize multi-functional and efficient integrated photonic instruments. Given that various functions, such as dispersion, spectral filtering, switching, etc, have been developed and optimized over a range of material platforms (SiN, SOI, InP, etc), it will be necessary to exploit hybrid integration—the integration of disparate technologies, materials and chiplets—to be able to assemble these and realize multi-functional instruments.

Four of the most critical aspects which are currently preventing the mainstream adoption of astrophotonic technologies are (1) low throughputs (fiber to chip, propagation and bend losses, device losses, grating/vertical couplers, etc), (2) difficulties with scaling to large channel count devices needed for large bandwidths and high resolutions, (3) efficient integration with detectors and 4) issues with feeding large-port-count fiber arrays to planar photonic chips. Astrophotonic technologies can also be used to more generally support observations by enabling high bandwidth data links driven by the extremely high data rates of the square-kilometer array (SKA) (0.1–1 TB s^{-1}), for example [607], or for free space laser communications systems, critical to future astrophysics space missions. In addition, numerous astronomy applications require wide optical bandwidths, which imposes selection criteria on transparency and absorption in different photonic material platforms. For these reasons, developing efficient hybrid integration processes is key to the success of astrophotonic technologies.

To address issues related to coupling to high index contrast PICs from low index contrast fiber arrays, interposer devices can be used. These consist of tapered waveguides that provide better mode matching between technologies which can also augment the pitch between the waveguides simultaneously. For example, the Teem photonics interposer solution, referred to as the waveguide array to fiber transposers (WAFTs), allows for efficient coupling (<0.7 dB) between Si based PICs and silica-based optical fiber arrays [608, 609]. However, they are now also being used with SiN and InP PICs as well. These WAFTs consist of ion exchange waveguides imprinted into glass-based PICs. The company provides three versions of the WAFT, including (1) an edge coupling version which combines fiber spacing concentrators (FSC) with spot size converters/tapers (SSCs) (2) a top coupling variant which adds a mirror at the tip of the structure and combines it with FSCs that provides wafer level and grating coupler compatibility (see in figure 42(a)) and (3) an evanescent coupling version [608].

In a similar vein, being able to couple the light efficiently from 2D fiber arrays, (e.g. an MCF) and a PIC is also crucial. Two possible solutions exist for this currently including using a 2D array of grating couplers on the chip to inject the light from above [610] (see figure 42(c)) and/or utilizing fan-out structures that remap a 2D array of waveguides to a linear array [611]. However, neither option is efficient currently, with the former suffering from losses associated with the grating couplers due to manufacturing imperfections, their narrow bands of operation and the stringent requirement of the angle of incidence of the input beam for efficient coupling and the latter limited by realizing mode-matched waveguides and tapers with the ULI process. These technologies both require further development.

Integrating detectors, be it 2D or 1D arrays or single pixel devices with PICs is also critical to eliminating losses, minimizing cross-talk and realizing integrated instruments. We refer the reader to a full discussion in section 24.

Hybrid lasers based on III–V materials like GaAs or InP can also be integrated onto a Si or SOI chip [612] and could be used for either calibration or metrology via say soliton microcombs [613].

To drive active components, including lasers, detectors, phase shifters, etc, electronic integration is necessary. Typical electronic integration involves mounting PICs onto PCBs and using micro-wire bonding. But this does not scale when hundreds or thousands of active components are needed. Innovative solutions are being explored where the electronic integrated circuits (EIC) are etched into the PIC for transceiver applications. Different technologies are being proposed to meet the PIC and EIC integration requirements like advanced packaging substrates and new fiber-to-chip connectivity solutions [614]. Regardless of how the electronics are integrated, astronomical applications will demand low noise characteristics.

Photonic instruments may also require micro-optics, either micro-transfer printed [615, 616], 3D printed [80, 617] or metasurfaces etched into the PIC [618, 619] to feed flip-chipped PICs (PICs mounted above the primary chip) and/or detectors [620].

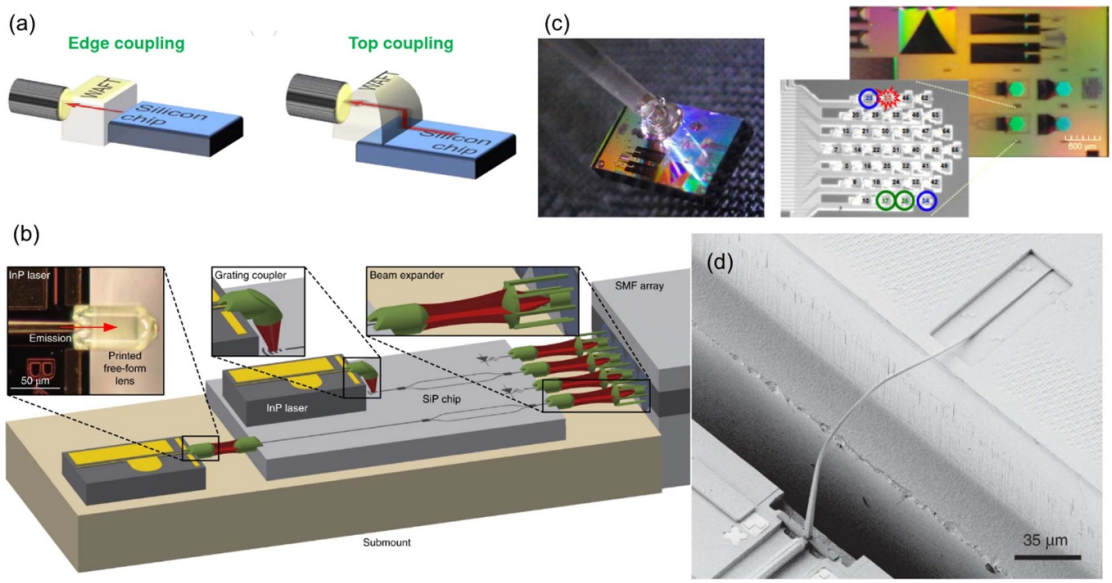

Figure 42. (a) Shows two different WAFT interposer variants. Reproduced with permission from [WAFT Teem Photonics]. (b) Conceptual as well as microscope images of 3D printed micro-lenses and micro-mirrors connecting PICs and fiber arrays with 88% efficiency. Reproduced with permission from [80]. © [2015] IEEE. (c) An example of integrating a MCF with a PIC. Reprinted, with permission, from [624]. (d) An SEM of a photonic wire bond. Reprinted with permission from [625] © The Optical Society.

While hybrid integration refers to integrating two or more PICs/devices into a single package, heterogeneous integration involves combining two or more material technologies into a single PIC chip, for instance, III–V materials for lasers or detectors onto Si/SiN PICs [621–623]. Some of the key approaches to achieving heterogeneous integration include flip-chip assembly, heterogenous bonding, micro-transfer printing, and epitaxial growth. Each technology is at a different level of maturity and has different alignment accuracy requirements (summarized in table 1 in [616]). These technologies offer a more compact alternative to 'hybrid integration', but have their own limitations in integrating material platforms such as high alignment accuracy (for all), complex back-end process flow (for heterogeneous bonding), and lattice matching (for epitaxial growth) [616].

Current and future challenges

Optical mode matching is critical to efficiently couple the light between different photonic components realized in different material platforms. As light may be delivered to the PIC instrument via an optical fiber or may need to pass to other optical components located on another chip, mode matching is key to ensure maximum throughput. This is achieved with SSCs that relax the tolerances on in- and out- coupling requirements. SSCs are often realized as a taper, including lateral and inverted tapers, segmented and 3D tapers. Inverted tapers are prevalent but are typically highly polarizing (birefringence and diattenuation) and when large exit beams are needed (i.e. 10 μm for example), require a very small and precise exit taper width, making precise mode size selection challenging. Segmented tapers are more tolerant, but require extremely small feature sizes, i.e. sub-wavelength to prevent diffractive effects. This requires special processing (e.g. e-beam lithography), which can be very challenging for mass production. Finally, 3D tapers can mitigate the polarization sensitivities and deliver a circular output beam, but are harder to implement and are only offered by a handful of foundries (e.g. LioniX [443], Fraunhofer [626]) as part of their MPW or custom runs.

Due to the limitations in SSC performance, SSCs can be combined with interposer devices, like WAFTs. The WAFTs outlined above can generate circularly symmetric modes that can be tapered from 3 to 10 μm, with high efficiency, and insertion losses of $<$1.5 dB [608]. This reduces the requirement on the more complex and limited on-chip SSCs, and by combining the two, efficient transitions could be realized. Despite the existence of these technologies, optimizing each to maximize overall performance, especially over broadbands still remains a challenge.

Another loss that comes about from hybrid integration is that of Fresnel reflection brought about by the different indices of the materials used. In some applications, index matching glues are used between devices. To minimize the residual Fresnel reflections between the chips and the glue, anti-reflection coatings are placed on the end faces of the two chips. AR coatings range from single wavelength operation (e.g. for narrowband lasers) to coatings functioning over very broad spectral bands of $>$100 nm wide. Challenges

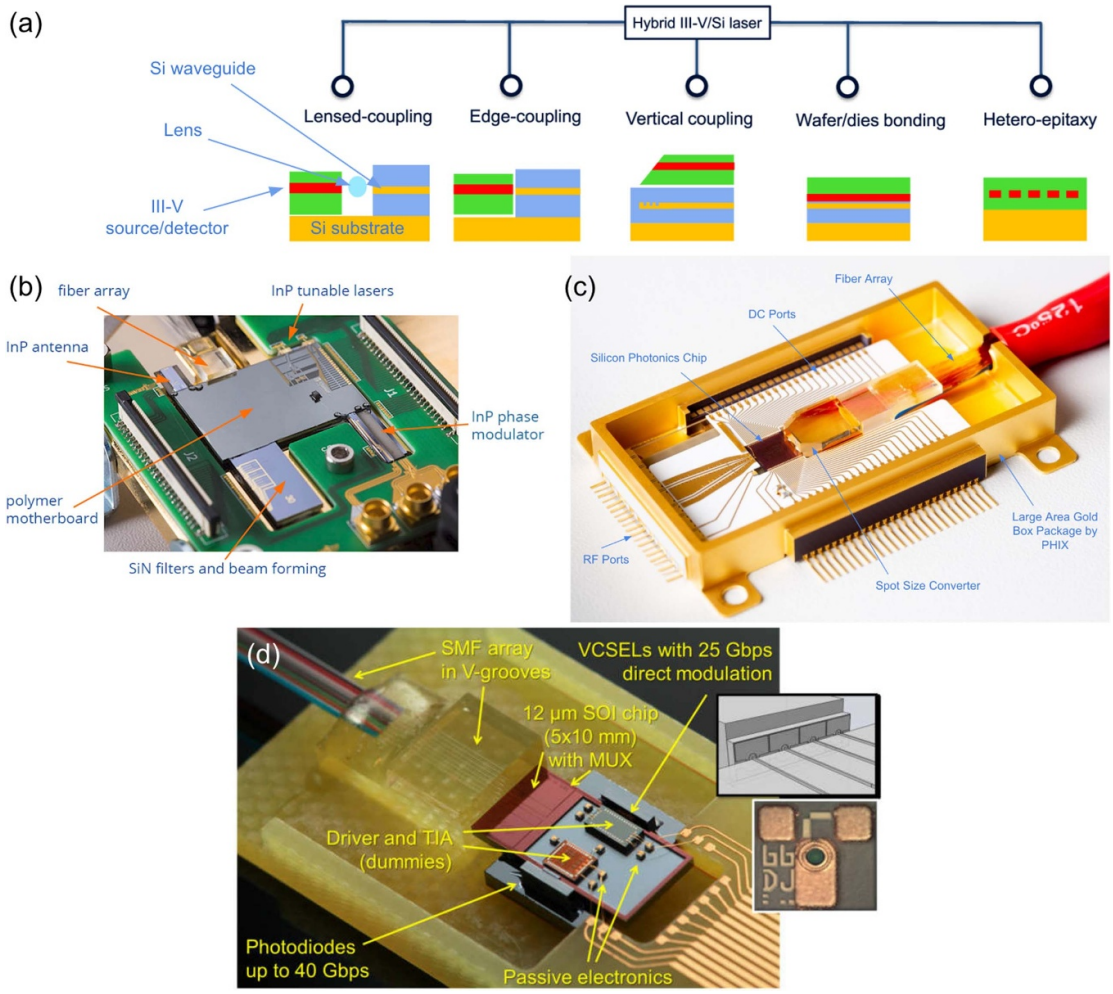

Figure 43. (a) A schematic diagram of several different processes by which lasers or detectors can be integrated with PICs. Reprinted, with permission, from [631]. © [2018] IEEE. (b)–(d) show examples of hybrid packages. (b) A photo of a millimeter wave transceiver for the Teraway project [632, image courtesy of Phix Photonics Assembly]. (c) A silicon PIC with a fiber array and a WAFT assembled in a box using Phix's standard packaging [633], image courtesy of Phix Photonics Assembly. (d) Mechanical test assembly that illustrates a transceiver concept based on 12 μm SOI waveguides and directly modulated VCSELs. The VCSEL-SOI integration concept is also illustrated schematically. A microscope image of a VCSEL is shown on the right. Reproduced with permission from [634].

remain with respect to finding suitable bonding adhesives with high transmission across all spectral regions of interest to astronomy applications (<380 nm up to >5 μm), as well as implementing low loss coatings across various material platforms and broader bandwidths.

There are multiple challenges and approaches towards integrating laser sources onto PICs [616]. Among the existing methods are: monolithic integration of lasers using InP-based material platforms, hetero-epitaxial growth of lasers on Si substrates, as well as hybrid integration approaches via micro-transfer-printing, flip-chip, vertical coupling, and lensed coupling, as well as die-to-wafer and wafer-to-wafer bonding, with some approaches schematically shown in figure 43(a) [627]. The challenges for hybrid integration are high alignment accuracy required in case of e.g. flip-chip, vertical coupling, and lensed coupling; as well as throughput, reliability, scalability, yield, and process and test complexity in case of e.g. die-to-wafer and wafer-to-wafer bonding. The main challenge in case of monolithic integration, in the context of astrophotonics instruments, is limited material transparency and optical gain bandwidth, typically covering telecommunication and data-communication C- and O-bands, as well as insufficient throughput (high losses).

When many active devices are needed on the chip, be it PDs, lasers, amplitude or phase shifters, it is necessary to also miniaturize the electronics. Etching the EIC into the PIC is a solution that allows scaling to hundreds or thousands of active devices and is been demonstrated [628] and is being offered commercially [629], but is challenging due to the mismatch between EIC and PIC lithographic technologies and not offered on a large range of material platforms. Further, even if this was solved, the number of devices that can

be placed on a chip will eventually be limited by the finite size of the photonic components, rather than the electronics.

Hybrid integration of different photonic components is challenging since the components are typically more fragile than electrical components and have extremely tight optical alignment tolerances, often <1 μm to minimize losses between devices/chips [630]. This is exacerbated by CTE mismatches as low noise detection in astronomy is typically conducted at 70 K for near infrared observations. In the same vein, more general space qualification (e.g. radiation hardening and vibration/shock) testing for hybrid integrated devices needs to be undertaken to prepare them for any future missions.

Advances in science and technology to meet challenges

The goal is to reach fiber-to-waveguide and chip-to-chip coupling efficiencies of >95% per facet (<0.4 dB). This has been demonstrated in fiber-to-SiN waveguides over a broad band (1450–1650 nm) using inverted tapers [190]. However, this required lithographic processing with very small feature sizes, which is not offered as part of standard contact/stepper lithography fabrication and hence is not currently scalable. To enable this, more foundries need to offer new and improved processing techniques which allow for smaller feature sizes (necessary for inverted and segmented tapers) as well as 3D tapers as part of their standard services. Design tools also need to be advanced to optimize the SSCs given these new limitations for broadband applications.

The ion exchange technology for WAFTs could potentially be used to realize 3D circuits in future. Fanout devices that not only route the output of a MCF to a PIC, but also provide optimal mode matching between the disparate technologies could be realized in this way for the first time.

Alternative technologies such as SU8 polymer interposers or tapered waveguides (eg: bilayered inverse taper in lithium niobate [635]) could also be used in place of WAFTs. In addition, there are a host of other fiber tapers including capped adiabatic tapered fibers, lensed fibers [636], or cascaded tapers and cantilever tapers [637]. Interconnects are also critical to connect different photonic devices. One example is shown in figure 42(d), where a photonic wire bond is used to transmit light from a laser to a waveguide [625]. Polymer interconnects such as those using ZPU12 polymer additionally provide the required flexibility for interconnects [638]. The optical losses of PolyBoard PICs were reported to be $\sim$0.7 db cm^{-1} at 1550 nm. The fabrication process of the PolyBoard platform provides the added advantage of achieving multilayer waveguide structures by using alternating waveguide and cladding layers and a semi-automated assembly process has been demonstrated using commercially available equipment which eases the scaling from prototypes to production. A completely different approach utilizes 3D printed micro-optics to achieve mode-matching between PICs (figure 42(b)), beam shaping, and PIC-to-fiber-array efficiencies as high as 88% [80], albeit without the flexibility of interconnect approaches.

Finally, advances in heterogeneous integration are critical to minimize the losses, attain high stability and scalability, and thereby, maximize the integration advantage in astrophotonics. The key challenges of heterogeneous integration approaches are the necessity of high alignment accuracy (<0.5 μm) and the high pressures (200 mg/bump) that may be needed for bonding [630, 639]. However, new approaches such as mass-reflow of copper bumps have demonstrated a final self-alignment with $\sim$0.5 μm accuracy in flip-chip assembly of SOI grating couplers and a microlens die, with an initial misalignment tolerance of 10 μm with only 5.5 mg/bump of applied pressure [630]. To achieve the highest possible coupling efficiencies with small waveguide modes ($\sim$3 μm) in high-contrast materials, alignment accuracies of $\sim$0.1 μm will be needed. Further advances are also required in making such precision assembly processes scalable for various other material platform combinations.

Concluding remarks

Processes such as heterogeneous integration and hybrid integration are critical to realizing compact all-photonic instruments for astronomy. Developments in regards to advancing SSCs, developing 3D interposers, scaling processes to integrate many detectors with chips, enabling efficient and cross-talk free waveguide crossings, improving processes to integrate micro-optics, and advancing the design and performance of vertical and grating couplers are all critical to realizing efficient astrophotonic instruments.

Acknowledgments

We would like to acknowledge informative technical discussions with Pradip Gatkine.

24. Semiconductor detectors and integrated photonics

Donald F Figer
Center for Detectors, Rochester Institute of Technology, Rochester, NY, United States of America

Status

Semiconductor detectors are central to astronomical discovery and have been the principal tool used in the vast majority of high impact discoveries in the field over the past 40 years, such as the discovery of dark energy, dark matter, exoplanets, and the identifications of black holes in the centers of galaxies, including our own. These detectors convert photons of sufficient energy into charge carriers that they then integrate in a storage well that is often formed as a pn junction. They are the detector of choice for a large range of wavelengths spanning x-rays through MIR wavebands (∼0.1–30 000 nm). Their application includes imaging and spectroscopy, and they are the primary detectors in the HST, James Webb Space Telescope, and the vast majority of telescopes on the ground. In general, they are integrated at the focal planes of bulk optical systems. They are almost always implemented as two-dimensional arrays of PDs.

The most commonly-used arrays are in charge-coupled devices (CCDs) and CMOS active pixel sensors. CCDs move integrated charge to a readout circuit. CMOS devices convert charge to voltage within a pixel and use a readout integrated circuit (ROIC) to transfer the voltage to the output. Simple ROICs consist of a source-follower per pixel, row/clock-select circuits, and a buffer that connects to external electronics. Complex ROICs perform operations such as multiple sample correlated reads. Very low noise semiconductor detectors can now count single photons and resolve photon numbers at optical [640] and infrared [641] wavelengths. Some other single photon detectors use Geiger-mode avalanche gain, such as SPADs (single-photon avalanche diodes) [642], but those generally have significantly lower fill factor and cannot count photon number. Single-element detectors (PDs) are rarely used in astronomy applications, but they are useful in photonic circuits [234]. A number of groups have implemented PDs using a variety of fabrication processes and material systems]. For example [643], present a recent PD architecture using InP waveguides with monolithic p-i-n PDs integrated in a two-step organometallic vapor phase epitaxy process. Also [644], present a Ge PD integrated on an SIO based waveguide platform.

A new class of CMOS detectors enable applications where it is important to detect, and sometimes count, individual photons. These devices have very low read noise, typically less than 0.5 e^-. Examples include devices from Gigajot Technology [640], Hamamatsu [645], and BAE Systems [646]. In all cases, the small capacitance of the sense node produces a very large conversion gain, on the order of hundreds of microvolts per electron. This technique will work for individual detector elements integrated in a PIC, but it requires a PIC process that provides a small design node and integration of complex electronics, two things that are not common at the present time. A short-term solution could be to use these imaging arrays with ad hoc coupling of photonic elements, such as fibers, or to use micro-lenses. Other types of low noise detectors, such as EMCCDs, MKIDs, SNSPDs, etc could have some utility, and are discussed elsewhere in this volume.

The ultra-low read noise of emerging CMOS array detectors presents enormous opportunities for photonic circuit applications. As an example, one can implement a circuit which splits light in a multi-mode fiber into SMFs and detect that light without degrading the signal-to-noise ratio as would be the case with a detector that cannot detect single photons. Similarly, noiseless rebinning provides flexibility when pixel sizes do not perfectly match waveguides and the beam is oversampled.

Current and future challenges

While semiconductor detectors for astronomy have evolved primarily into 2D formats, such as for imaging applications, integrated photonic implementations may benefit from other formats because the detection no longer needs to be made at a focal plane. In fact, it is challenging to integrate 2D detector formats into planar photonic circuits, making it difficult to take advantage of their near-gigapixel array formats.
One-dimensional arrays are more easily integrated into planar architectures through edge-coupling, but they also present challenges when attempting to connect many optical channels from the chip to the array because of routing complexities to avoid waveguide crossings, which introduce loss and cross-talk. Finally, the most flexible format is single PDs that can have arbitrary physical relationships to each other.

Regardless of dimensional format, there are several challenges to realize the potential of integrated photonics when used with semiconductor detectors, i.e.: (1) materials, (2) routing and coupling, (3) form factor, (4) fabrication and (5) temperature control. In several important ways, dimensional format dictates the nature of the challenges in the aforementioned categories. For instance, coupling for 2D arrays requires some way for the PIC to emit light orthogonal to its surface, whereas the light can be in-plane for 1D and PD formats.

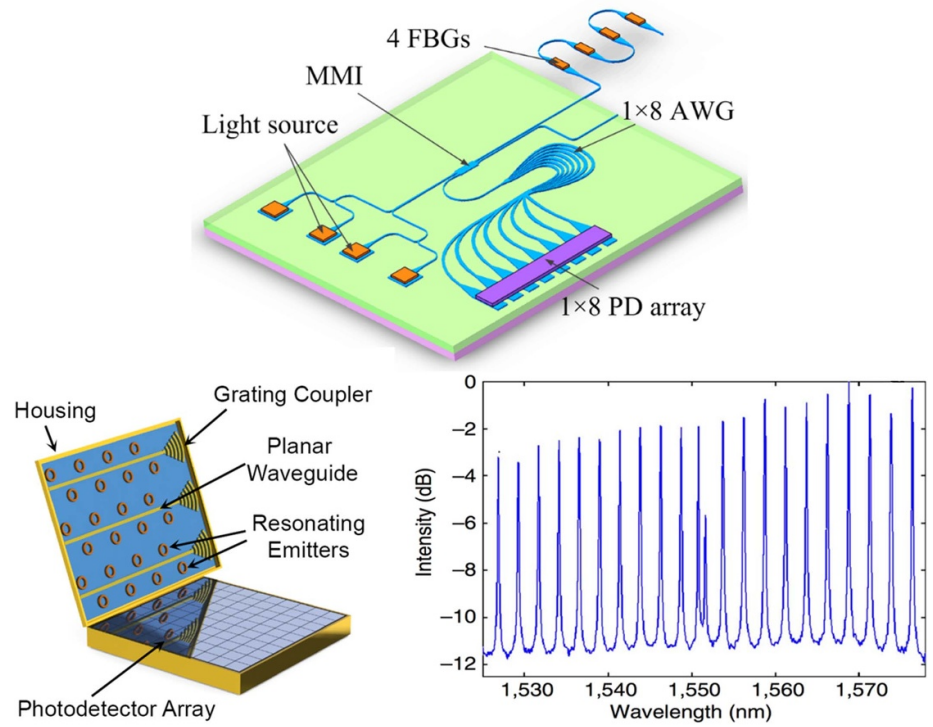

Figure 44. The panels show a linear array of 1D detectors in an interrogator circuit (top, Reproduced from [59] CC BY 4.0) and a photonic spectrograph coupled to a 2D array of detectors on the bottom left. Once the housing is closed on to the photodetector array, light enters through the grating coupler and travels through the planar waveguides, after which it is evanescently-coupled to the resonating emitters that vertically eject the light into the 2D array of detectors. The resulting transmission spectrum is on the bottom right. Reproduced from [648].

Detector materials are chosen for their wavelengths of detection, and their compatibility with PIC materials, so they can be either deposited or pick-and-placed on the PIC (Si, SOI, SiN, InP). The detector materials detect light with wavelengths shorter than their bandgap wavelengths, which for silicon is $\sim$1.1 μm, allowing visible applications. Ge, InP, InGaAs, HgCdTe, and InSb have suitable band gaps to detect infrared light, and they have generally been developed to deliver high performance. Wide bandgap semiconductor materials, such as AlGaN and AlN, are promising for UV wavelengths; although they are not as well developed as delta-doped silicon and some non-semiconductor designs that mate scintillating material or micro-channel plates with silicon. Silicon is again the material of choice for even shorter wavelengths in the x-ray regime up to energies of 10 keV, above which materials with higher atomic mass, such as CdTe, have better quantum efficiency. For wavelengths shorter than visible, Lattice mismatch presents serious challenges, limiting the combinations of detector and PIC materials that can be used. Coupling and fabrication techniques vary widely for each combination of materials.

Routing light inside a PIC to a detector pixel needs to be carefully considered to prevent excess loss and cross-talk. This becomes extremely challenging to achieve when thousands of pixels are needed. In this case, ejecting the light orthogonal to the plane of the chip as soon as it is ready, reduces the complexity of maintaining many low loss, cross-talk free channels inside the chip. It also provides a natural way to use a 2D array or a second PIC with PDs with a planar PIC device. This vertical ejection could be achieved with grating or vertical couplers [647]. Both of these devices are extremely challenging to realize efficiently currently and are not offered as part of the cost-effective multi-project-wafer (MPW) fabrication runs offered by foundries. Other challenges of this approach include mode-matching, which may require micro-optics and anti-reflection coatings to minimize losses. To exploit 1D edge-coupled arrays, low loss, cross-talk free routings become the primary challenge. Directly integrated PDs on the PIC can help circumvent the routing issue but are still susceptible to Fresnel reflection losses if not carefully engineered. Figure 44 shows examples of an integrated 1D array of PDs and vertical ejection into a 2D array of detectors.

The form factor of PDs is one limitation when considering direct integration onto the PIC. For example, PDs can be integrated via direct growth or bonding after picking-and-placing the PD and can be coupled to in a number of ways, including via evanescent coupling (see figure 45 for details and also [649]) and butt-coupling. The architecture in the figure for example needs relatively long pathlengths for the evanescent coupling to be efficient. It is also labor intensive to produce, and thus relatively expensive. On the other hand,

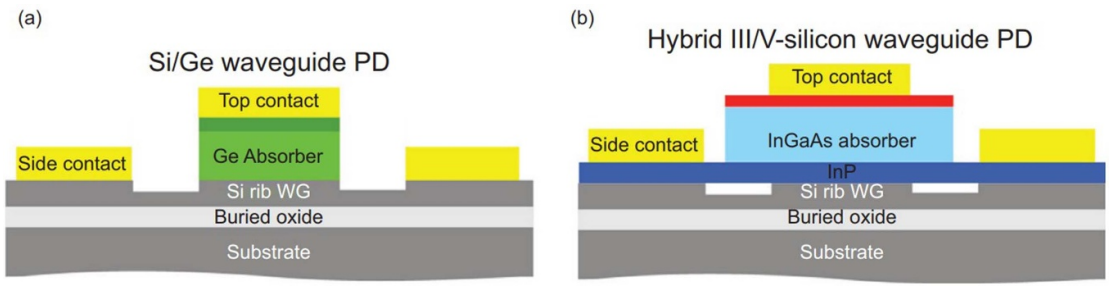

Figure 45. The figure shows an evanescently-coupled waveguide (WG) below absorbers containing two different materials, Ge (a) and InGaAs (b). Reprinted from [234], Copyright (2016), with permission from Elsevier.

coupling efficiencies can approach ∼100%. The PDs footprint will depend on the type of optical coupling and the materials used. Fitting a large number of PDs directly on the chip while avoiding excessive crosstalk from waveguides is challenging.

Fabrication might be the principal future challenge in realizing the promise of PICs with detectors. Ideally, the fabrication process would provide a menu of elements and materials that are manufacturable and integrable in a foundry setting, such as described in a process design kit. A central challenge is the cost required for all the specialized tooling that is needed for growth and integration. Typically, the tools cannot be used for multiple material systems due to risk of contamination.

Temperature can be a relevant environmental challenge in several different ways. One, some semiconductor detectors require low temperatures, e.g. $T \sim 70$ K, in order to function with low dark current. This requirement implies an architecture that is very bulky and resource-intensive, requiring cryogenic dewars and complex readout electronics. Another way in which temperature is important is in architectures where elements need very stable temperatures. One example is the fine tuning of frequency that is commonly implemented for ring resonators (whispering gallery modes). If these elements are near a detector, and the detector generates transient heating, particularly through clocking lines, then there will be a coupling between the two elements that will require careful thermal management.

Advances in science and technology to meet challenges

Although 2D detector arrays offer a large number of pixels, they can cost 5–20× the cost of a custom PIC in the IR. Despite the fact that PICs can be replicated to reduce cost, highly replicable astrophotonic instruments could be limited by the cost of IR detectors. There is a strong demand for low-cost, high sensitivity IR arrays to address this limitation and enable massively replicated instrument designs.

The materials mismatch challenge can be reduced by developing custom anti-reflection coatings and choosing materials with better index-matching to minimize losses due to coupling. On-die integration is a common solution to reduce these loses and also minimize path-length loses in waveguides/fiber, but that then makes fabrication and integration more complicated for non-silicon-based devices that require significant processing outside the standard CMOS foundry flow and more complex heterogeneous integration, such as flip-chip processing [620, 650]. See also [649] for monolithic heterogeneous integration. Another method to reduce the effects of materials mismatch is to use intermediate buffer layers. This reduces defect growth and dark current [651]. Foundries would ideally offer some of these newer processes and the photonic design kit (PDK) must accommodate mismatched materials in the design; very few combinations are now supported.

Several advances are needed to eject light vertically out of the PIC to PDs or detector arrays efficiently [620]. Firstly, vertical and grating coupler design and performance needs to be improved to realize the efficient ejection of a high quality beam over a broad wavelength range. Secondly, foundries need to offer these specialized components as part of MPW fabrication runs and provide them in standard PDKs. Cross-talk free waveguide crossings are needed to exploit butt-coupling of the edge of a PIC with a 1D or 2D detector array with low loss. Multilayer integration schemes that rely on evanescent coupling between layers have been demonstrated [652, 653], but they need further development to extend the bandwidth. Gratings are also used to eject light out of the circuit plane [654]. An example uses ring resonators to inject resonant photons [653] into a two-dimensional detector array. Another example is the use of a dielectric antenna [655]. One could use these kinds of devices to obtain a spectrum at approximately a thousand spatial locations for a megapixel array. This might be considered to be an 'intermediate' solution while fully integrated architectures mature. In addition to losses in couples, it is often the case that the optical elements are larger than the pixel spacing, which in turn introduces another inefficiency in the system. New foundry capabilities are addressing the fabrication challenge through technology transfer from academic and

government labs, such as in AIM Photonics which can accommodate simple PDs within PICs in both Si and Ge. Integrating other materials is more of a challenge and outside of the current process. Europe has foundry capability for integrating InP and Si [650].

Another geometry that is difficult to accommodate with a flat array of detectors is a curved focal plane, for example as would be produced by the Rowland circle of a photonic Echelle grating or an AWG. In these cases, it may be more convenient to use PDs arranged along an arc.

Finally, progress is needed in the arena of single photon counting and photon number resolving detectors in PIC format. Some photonic techniques use small beams, $\sim$1 μm, which implies small pixel size for the optimum coupling. This is fortuitous because the majority of semiconductor foundry capacity is optimized for the small pixels in smart phone cameras. Indeed, the Gigajot devices have pixels of roughly the same size and single photon sensitivity.

Concluding remarks

Semiconductor detectors are the workhorse for astrophysics applications over a broad range of wavelengths, and they are likely to become key elements in PIC implementations for those applications in the future. They have already achieved single photon sensing and photon number resolving capability at room temperature, making them an attractive option for integration into PICs. While there are challenges to using them, several research groups have made progress in implementing them, especially in single-detector (PD) formats. To realize much higher detector numbers, one must decide whether it is more cost-effective to implement currently-available high pixel count 2D and 1D arrays, such as in formats having many pixels in arrays, or to use lower dimensional form factors.

25. Integrated superconducting detectors for optical and IR astrophotonics

Benjamin A Mazin[1], *Alexander B Walter*[2] *and Chang-Ling Zou*[3]
[1] Department of Physics, University of California, Santa Barbara, CA, United States of America
[2] Jet Propulsion Laboratory, California Institute of Technology, Pasadena, CA, United States of America
[3] CAS Key Laboratory of Quantum Information, University of Science and Technology of China, Hefei, Anhui, People's Republic of China

Status

Astrophotonics harnesses the power of PICs and other guided light technologies to create components or even entire instruments for astronomy. For all astrophotonic applications a detector is needed for the final conversion of photons into electrical signals. For example, detectors can be designed by placing the photoelectric materials on top of waveguides, such that the propagating photons can be efficiently absorbed through the evanescent field of the waveguide [656, 657]. Below we discuss two different superconducting detector technologies that are currently being pursued for integration with astrophotonics: SNSPDs [658–660] and MKIDs [661–663]. There is also ongoing work using optical transition edge sensors [664, 665] and quantum capacitance detectors (QCDs) [666] are emerging as a promising detector technology for the near future. Superconducting detectors are naturally compatible with SM waveguide spectrometers due to the sub-micron dimensions of an SNSPD hairpin or an MKID inductor (see figures 46(b) and (d)). While superconducting detectors can add complexity, the sensitivity of these technologies can enable new capabilities, reduce the size, weight, and power (SWaP) and cost of instruments, and improve performance.

Superconducting detectors like SNSPDs or MKIDs detect individual photons that are absorbed in a superconducting film. They are known for high speed and low noise. The critical advantage of superconducting detectors over conventional technologies is the lack of read noise of a true photon counting detector without after-pulsing and their negligible dark counts ($<10^{-5}$ cps for SNSPDs and $<10^{-3}$ cps for MKIDs). This makes them ideal detectors for low-flux applications involving a SM spectrometer, such as characterization of exoplanet atmospheres or observation of faint extragalactic sources.

SNSPDs were first fabricated on a GaAs waveguide over a decade ago [656]. Soon after [657], directly coupled SNSPDs to a Si waveguide on-chip photonic network and demonstrated 91% detection efficiency. Since then, SNSPDs have been integrated on many waveguide platforms including Si, SiN, AlN, GaAs, LiNbO3, and diamond, as well as coupled to AWGs, on-chip echelle gratings, Rowland circle spectrometer, quantum dots, on-chip photonic crystal cavities, MEMs switches, and other photonic components. See [667] for a review. The relatively simple structure of SNSPDs and their exquisite timing performance with UV to Mid-IR demonstrations of <5 ps jitter and up to 10^7 Hz maximum count rate make them favored detectors for many science and commercial applications of integrated quantum photonics systems [668]. While MKIDs lack this history in photonics, their similarly high performance and their natural multiplexability into large arrays make them interesting for astronomical applications.

The complex, high speed, power-hungry, and often custom readout electronics required for superconducting detectors, as well as their cryogenic cooling requirements, can make them undesirable if their high performance is not required. SNSPDs are notoriously difficult to multiplex into the large arrays required for astronomical imaging or spectroscopy [268, 669, 670]. MKIDs on the other hand, are naturally frequency multiplexable and the 20 440 pixel MEC instrument at the Subaru Telescope combined with the SCExAO instrument is the largest superconducting camera in the world [663]. Both technologies require expensive cryogenic cooling with NbN, NbTiN, WSi, or MoSi SNSPDs operating at $\sim<4$ K while TiN or PtSi MKIDs operate even colder at $\sim$0.10 K. Recently, efficient SNSPDs working at 7 K have been reported [671], opening up several applications with a low-cost cryostat for ground- and space-based telescopes.

Current and future challenges

The first kilo-pixel SNSPD array, a 32×32 array of WSi nanowires, was demonstrated by [268] using a row-column multiplexing technique. Conventionally, SNSPDs are DC biased near their critical current such that when a photon is absorbed a local hotspot forms. The highly resistive hotspot temporarily redirects the bias current into the readout circuit thus generating an AC pulse signal. In the row-column multiplexing scheme this signal is split with a resistive-inductive network such that half is propagated along the row and column feedlines respectively. Since photon events are recorded by searching for coincidence events in the rows and columns this readout scheme is susceptible to confusion during multi-photon events. Furthermore, the splitting of the signal as well as parasitics in the resistive network reduce the signal-to-noise ratio presenting a major challenge for scaling to megapixel arrays. More recently [670], have demonstrated a kilo-pixel SNSPD array using an orthogonal time-amplitude multiplexing method. Other multiplexing schemes exist including thermal row-column [673], frequency multiplexing [674], and SFQ readouts [675]

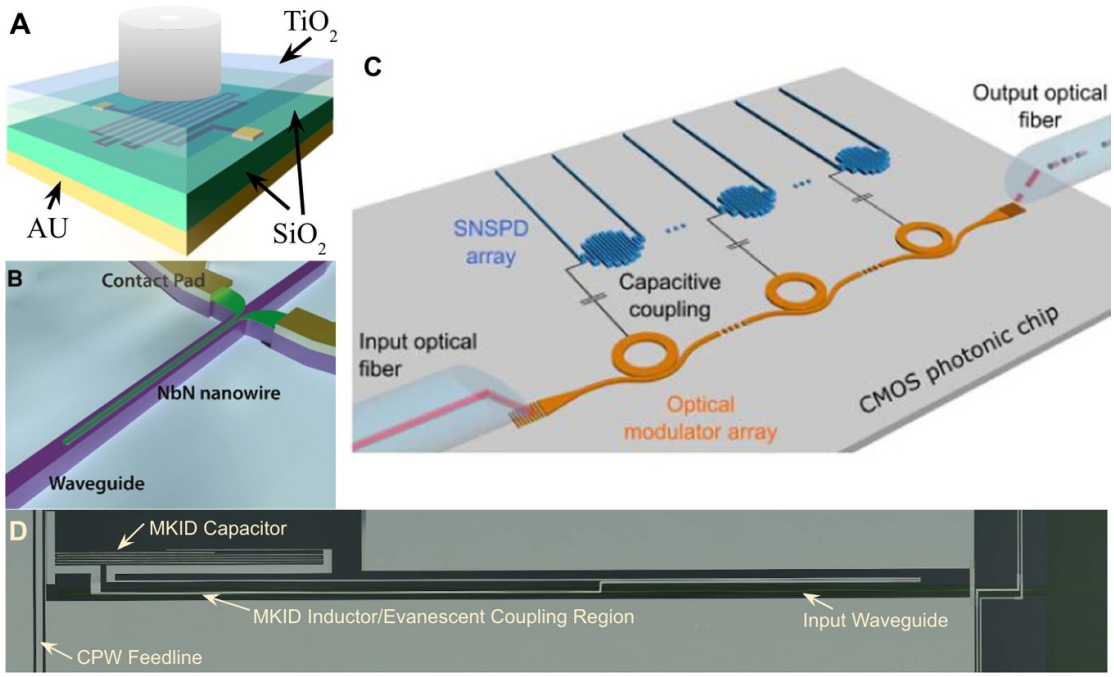

Figure 46. (A) and (B) A fiber coupled SNSPD and waveguide integrated SNSPD respectively are depicted. The fiber coupled SNSPD will typically employ anti-reflection coatings and be embedded into an optical cavity to raise the coupling efficiency, whereas, the waveguide integrated SNSPD can take advantage of evanescent coupling to reach near unity efficiencies. Reproduced from [667]. CC BY 4.0. (C) A photonic readout scheme transforms the electrical signal from an SNSPD into an optical signal on a fiber using micro-ring resonators. By tuning the resonators to different wavelengths the pixels can be wavelength division multiplexed. D) A microscope image of a waveguide integrated MKID. The waveguide is the dark green strip running horizontally across the center of the image. The MKID inductor, made of Niobium and Hafnium, partially overlaps the waveguide for evanescent coupling. Reproduced from [672]. CC BY 4.0.

but these are less mature and have increasingly complex fabrication steps that generally include multiple lithographic layers with complicated electrical wiring. Coupling light directly on-chip with integrated photonics adds to this complexity due to the experimentally challenging growth or transfer of high-quality functional material, including semiconductors, two-dimensional material layers, and also superconducting nanofilms, to dielectric photonic materials. These functional materials also introduce complexities in the nanofabrication processes.

MKIDs consist of lithographed microwave resonators whose resonant frequency temporarily changes when a photon interacts with the superconducting metal of the detector. The magnitude of this frequency change, usually measured as the phase shift of a microwave probe tone, encodes both the energy ($R = 35$ at 400 nm) [676] and arrival time (1 μs) of the photon. Since an MKID resonator has high quality factor Q and unity transmission off-resonance, many resonators can be read out over a single microwave feedline allowing for easy fabrication into large arrays. MKIDs require a very clean and uniform substrate to deposit their superconducting film on in order to attain the very high internal Q's (>2e5) and low two level system (TLS noise, see [677]) required for optimal performance. One challenge with realizing waveguide-integrated MKIDs is to use dielectric materials which simultaneously have low optical loss and low TLS density, and to mitigate the effects of TLS noise from amorphous dielectrics such as SiO_2. Maintaining high cleanliness and inter-material compatibility at interfaces represent the primary challenges when simultaneously fabricating photonic components.

A cryogenic operating temperature creates additional complications. First, the optical properties of PICs can change slightly from room temperature, adding another variable to fabrication. This is not well explored in literature. Second, efficient self-aligned coupling from a SM optical fiber to a PIC at sub-Kelvin temperatures has remained a challenge for the community, as the maintenance of sub-micron alignment of the optical fiber is necessary to maintain efficient coupling. A space-based astrophotonics instrument must have an alignment that survives the vibrations of the launch, and then the autonomous cooling en-route to the final orbit. Thirdly, increased cost, complexity, and SWaP is needed to cool these superconducting detectors. This may be prohibitive for optical astronomy but useful for mid-IR astronomy where cryogenic cooling is always required for reduced thermal backgrounds.

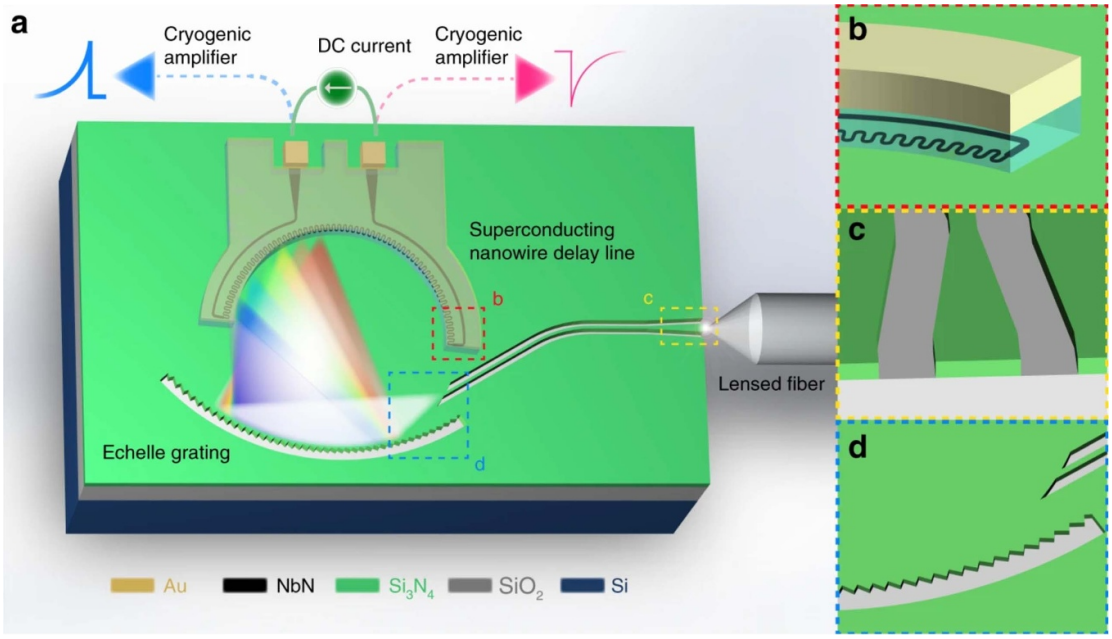

Figure 47. Light from a waveguide is dispersed with a photonic Echelle grating onto a superconducting nanowire implementing an on-chip spectrometer. Reproduced from [678]. CC BY 4.0.

Advances in science and technology to meet challenges

A novel application of integrated photonics could implement on-chip waveguides into the readout circuit of an imaging array of SNSPDs. In [672] they demonstrate a UV sensitive MoSi SNSPD pixel electrically coupled to a photonic MRR as depicted in figure 46(c). The voltage pulse from a photon event in the detector is used to forward bias the resonator influencing its refractive index and imprinting the signal on an optical carrier propagated along a Si waveguide. The signal is then coupled to a SMF through a vertical grating coupler and readout at room temperature. This approach allows for wavelength division multiplexing of SNSPDs which avoids the system tradeoffs of other multiplexing techniques by preserving high sensitivity, high efficiency, high maximum count rates/dynamic range, and a robustness to crosstalk or pickup noise. Future developments will need to demonstrate many pixels multiplexed to a single optical fiber and mitigate the thermal power dissipation of the MRRs. Ultimately, an imaging array of SNSPDs suitable for astronomy may utilize several different multiplexing techniques which could be tailor fit to the application. Megapixel arrays of SNSPDs could emerge by the end of the decade, but a more dedicated research effort would produce them considerably sooner. Apart from light intensity measurements, the single-photon detections by SNSPDs might also benefit the 'intensity correlation measurement' for astronomy applications [679]. For example, the second-order correlation and even high-order correlations of photons have been demonstrated within a single photonic chip recently [680, 681].

A highly desired photonic technology for astronomy is the monolithic integration of spectrographs with detectors that offer a compact solution and high efficiency by avoiding losses when imaging the guided light to on-chip detectors. They would consume significantly less SWaP, enjoy higher stability, be cheaper to produce, and be easier to use. For the faint sources targeted by astronomers, photon counting, low dark rates, low read noise, broadband sensitive detectors like SNSPDs or MKIDs are ideal. A moderate resolution (2.2 nm) but very small bandwidth (24 nm at 1550 nm wavelengths) has already been demonstrated with SNSPDs coupled to narrowband nanophotonic circuits [267]. Kong *et al* [682] demonstrated a single-pixel SNSPD with broadband responsivity ranging from 660–1900 nm, which was able to achieve a spectral resolution of $<$10 nm at telecom wavelengths by varying the quantum efficiency over time. Cheng *et al* [678] demonstrated the first broadband on-chip spectrometer with 200 effective spectral channels between 600 and 2000 nm wavelengths. Light manipulated by a waveguide is dispersed by a lithographically defined Si3N4 Echelle grating onto a NbN SNSPD which is read out with time-of-flight multiplexing (figure 47). The design allows for easy scalability to higher spectral resolution. For this proof of concept the system detection efficiency was $\sim<$0.1% at 1550 nm although future implementations could reach 50% with some significant optimizations of the 8–9 dB nanowire absorption loss and 7–8 dB diffraction efficiency loss in the grating. Dedicated efforts are also needed in scaling the number of on-chip detectors integrated with the PICs (e.g. several thousands for spectrographs).

Work is on-going at UCSB to build waveguide integrated MKIDs with the goal of integrating these detectors with an AWG spectrograph, as shown in figure 46(d). This PIC spectrometer uses the intrinsic spectral resolution ($R \sim 35$ at 400 nm now, up to $R \sim 100$ in the future) of the MKIDs to determine what order a photon came from [683], allowing an octave or greater bandwidth spectrometer with significantly higher spectral resolution than the MKIDs alone can deliver ($R = 1-100k$). This on-chip spectrometer could be extremely compact, allowing tens to hundreds of them to reside in a single dewar.

Concluding remarks

Combining photonics with on-chip superconducting detectors allows instrument designers to bring extremely powerful light processing tools together with the most powerful photon counting detectors available. We are at the very start of this field, but the promise is considerable. Potential instruments include high-resolution fiber-fed integral field spectrographs for exoplanets direct imaging using high dispersion coronagraphy, inexpensive time-resolved high-resolution spectrometers, mid-IR space-based exoplanet transit spectrometers, WFSs [53], on-chip interferometric instruments [546], and significantly less expensive and more stable EPRV instruments.

Acknowledgments

Thanks to Matthew Shaw, Miguel Daal, and Majid Mohammed for comments and advice. A portion of this research was carried out at the Jet Propulsion Laboratory, California Institute of Technology, under a contract with the National Aeronautics and Space Administration (NASA) (80NM0018D0004).

Data availability statement

The data that support the findings of this study are available upon reasonable request from the authors.

ORCID iDs

Nemanja Jovanovic https://orcid.org/0000-0001-5213-6207
Pradip Gatkine https://orcid.org/0000-0002-1955-2230
Narsireddy Anugu https://orcid.org/0000-0002-2208-6541
Ritoban Basu Thakur https://orcid.org/0000-0002-3351-3078
Chad F. Bender https://orcid.org/0000-0003-4384-7220
Jean-Philippe Berger https://orcid.org/0000-0001-5025-0428
Azzurra Bigioli https://orcid.org/0000-0003-1008-3682
Joss Bland-Hawthorn https://orcid.org/0000-0001-7516-4016
Guillaume Bourdarot https://orcid.org/0000-0002-6777-6386
Charles M Bradford https://orcid.org/0000-0001-5261-7094
Julia Bryant https://orcid.org/0000-0003-1627-9301
Kevin Bundy https://orcid.org/0000-0001-9742-3138
Ross Cheriton https://orcid.org/0000-0003-0522-0187
Nick Cvetojevic https://orcid.org/0000-0002-7465-4176
Momen Diab https://orcid.org/0000-0001-6556-9378
Scott A Diddams https://orcid.org/0000-0002-2144-0764
Aline N Dinkelaker https://orcid.org/0000-0002-4111-4763
Jeroen Duis https://orcid.org/0009-0003-3230-3209
Stephen Eikenberry https://orcid.org/0000-0002-1332-5061
Simon Ellis https://orcid.org/0000-0002-0742-379X
Akira Endo https://orcid.org/0000-0003-0379-2341
Donald F Figer https://orcid.org/0000-0002-4206-733X
Michael P. Fitzgerald https://orcid.org/0000-0002-0176-8973
Itandehui Gris-Sanchez https://orcid.org/0000-0001-5756-5107
Simon Gross https://orcid.org/0000-0001-5130-183X
Ludovic Grossard https://orcid.org/0000-0002-4022-5736
Olivier Guyon https://orcid.org/0000-0002-1097-9908
Sebastiaan Y Haffert https://orcid.org/0000-0001-5130-9153
Samuel Halverson https://orcid.org/0000-0003-1312-9391
Jinping He https://orcid.org/0000-0002-1899-3384
Tobias Herr https://orcid.org/0000-0002-5966-6697

Philipp Hottinger https://orcid.org/0000-0002-9489-1160
Michael Ireland https://orcid.org/0000-0002-6194-043X
Laurent Jocou https://orcid.org/0000-0001-9376-1818
Stefan Kraus https://orcid.org/0000-0001-6017-8773
Lucas Labadie https://orcid.org/0000-0001-5342-5713
Sylvestre Lacour https://orcid.org/0000-0002-6948-0263
Romain Laugier https://orcid.org/0000-0002-2215-9413
Jonathan Lin https://orcid.org/0000-0001-8542-3317
Stephanie Leifer https://orcid.org/0000-0002-8980-7825
Sergio Leon-Saval https://orcid.org/0000-0002-5606-3874
Guillermo Martin https://orcid.org/0000-0002-6531-5615
Marc-Antoine Martinod https://orcid.org/0000-0002-0989-9302
Benjamin A Mazin https://orcid.org/0000-0003-0526-1114
John D Monnier https://orcid.org/0000-0002-3380-3307
Denis Mourard https://orcid.org/0000-0001-7425-5055
Abani Shankar Nayak https://orcid.org/0000-0002-4666-9282
Ewelina Obrzud https://orcid.org/0000-0001-9856-0484
Karine Perraut https://orcid.org/0000-0003-3099-757X
François Reynaud https://orcid.org/0000-0002-6402-9748
Steph Sallum https://orcid.org/0000-0001-6871-6775
David Schiminovich https://orcid.org/0000-0003-2666-4430
Christian Schwab https://orcid.org/0000-0002-4046-987X
Sherif Soliman https://orcid.org/0009-0008-8938-2880
Andreas Stoll https://orcid.org/0000-0001-7105-2930
Peter Tuthill https://orcid.org/0000-0001-7026-6291
Gautam Vasisht https://orcid.org/0000-0002-1871-6264
Sylvain Veilleux https://orcid.org/0000-0002-3158-6820
Alexander B Walter https://orcid.org/0000-0002-4427-4551
Edward J Wollack https://orcid.org/0000-0002-7567-4451
Yinzi Xin https://orcid.org/0000-0002-6171-9081
Zongyin Yang https://orcid.org/0000-0003-2869-406X
Stephanos Yerolatsitis https://orcid.org/0000-0002-6268-3674
Yang Zhang https://orcid.org/0000-0003-1754-8796
Chang-Ling Zou https://orcid.org/0000-0003-2484-7292

References

[1] Allington-Smith J and Bland-Hawthorn J 2010 Astrophotonic spectroscopy: defining the potential advantage *Mon. Not. R. Astron. Soc.* **404** 232–8
[2] Jovanovic N, Schwab C, Cvetojevic N, Guyon O and Martinache F 2016 Enhancing stellar spectroscopy with extreme adaptive optics and photonics *Publ. Astron. Soc. Pac.* **128** 121001
[3] Kern P and Malbet F 1997 Astrofib'96: integrated optics for astronomical interferometry *Integrated Optics for Astronomical Interferometry* (available at: https://ui.adsabs.harvard.edu/abs/1997ioai.book.....K/abstract)
[4] Bland-Hawthorn J and Kern P 2009 Astrophotonics: a new era for astronomical instruments *Opt. Express* **17** 1880
[5] Bryant J J, Thomson R R and Withford M J 2017 Focus issue introduction: recent advances in astrophotonics *Opt. Express* **25** 19966
[6] Dinkelaker A N, Rahman A, Bland-Hawthorn J, Cantalloube F, Ellis S, Feautrier P, Ireland M, Labadie L and Thomson R R 2021 Astrophotonics: introduction to the feature issue *J. Opt. Soc. Am.* B **38** AP1
[7] Leon-Saval S G, Birks T A, Bland-Hawthorn J and Englund M 2005 Multimode fiber devices with single-mode performance *Opt. Lett.* **30** 2545
[8] Gillessen S *et al* 2010 GRAVITY: a four-telescope beam combiner instrument for the VLTI *Proc. SPIE* **7734** 77340Y
[9] Bland-Hawthorn J *et al* 2011 A complex multi-notch astronomical filter to suppress the bright infrared sky *Nat. Commun.* **2** 581
[10] Cvetojevic N, Jovanovic N, Lawrence J, Withford M and Bland-Hawthorn J 2012 Developing arrayed waveguide grating spectrographs for multi-object astronomical spectroscopy *Opt. Express* **20** 2062
[11] Halverson S *et al* 2014 Development of fiber Fabry-Perot interferometers as stable near-infrared calibration sources for high resolution spectrographs *Publ. Astron. Soc. Pac.* **126** 445–58
[12] Norris B R M *et al* 2020 First on-sky demonstration of an integrated-photonic nulling interferometer: the GLINT instrument *Mon. Not. R. Astron. Soc.* **491** 4180–93
[13] Noordegraaf D, Skovgaard P M, Nielsen M D and Bland-Hawthorn J 2009 Efficient multi-mode to single-mode coupling in a photonic lantern *Opt. Express* **17** 1988
[14] Noordegraaf D, Skovgaard P M W, Maack M D, Bland-Hawthorn J, Haynes R and Lægsgaard J 2010 Multi-mode to single-mode conversion in a 61 port Photonic Lantern *Opt. Express* **18** 4673
[15] Noordegraaf D, Skovgaard P M W, Sandberg R H, Maack M D, Bland-Hawthorn J, Lawrence J S and Lægsgaard J 2012 Nineteen-port photonic lantern with multimode delivery fiber *Opt. Lett.* **37** 452

[16] Fontaine N K, Ryf R, Bland-Hawthorn J and Leon-Saval S G 2012 Geometric requirements for photonic lanterns in space division multiplexing *Opt. Express* **20** 27123
[17] Birks T A, Mangan B J, Díez A, Cruz J L and Murphy D F 2012 "Photonic lantern" spectral filters in multi-core fibre *Opt. Express* **20** 13996
[18] Leon-Saval S G, Argyros A and Bland-Hawthorn J 2013 Photonic lanterns *Nanophotonics* **2** 429–40
[19] Leon-Saval S G, Fontaine N K, Salazar-Gil J R, Ercan B, Ryf R and Bland-Hawthorn J 2014 Mode-selective photonic lanterns for space-division multiplexing *Opt. Express* **22** 1036
[20] Birks T A, Gris-Sánchez I, Yerolatsitis S, Leon-Saval S G and Thomson R R 2015 The photonic lantern *Adv. Opt. Photonics* **7** 107
[21] Leon-Saval S G *et al* 2017 Divide and conquer: an efficient solution to highly multimoded photonic lanterns from multicore fibres *Opt. Express* **25** 17530
[22] Bland-Hawthorn J, Englund M and Edvell G 2004 New approach to atmospheric OH suppression using an aperiodic fibre Bragg grating *Opt. Express* **12** 5902
[23] Ellis S C *et al* 2020 First demonstration of OH suppression in a high-efficiency near-infrared spectrograph *Mon. Not. R. Astron. Soc.* **492** 2796–806
[24] Trinh C Q *et al* 2013 GNOSIS: the first instrument to use fiber Bragg gratings for OH suppression *Astron. J.* **145** 51
[25] Ellis S C *et al* 2012 Suppression of the near-infrared OH night-sky lines with fibre Bragg gratings—first results: OH suppression with FBGs *Mon. Not. R. Astron. Soc.* **425** 1682–95
[26] Hänsch T W 2006 Nobel lecture: passion for precision *Rev. Mod. Phys.* **78** 1297–309
[27] Hall J L 2006 Nobel lecture: defining and measuring optical frequencies *Rev. Mod. Phys.* **78** 1279–95
[28] Braje D A, Kirchner M S, Osterman S, Fortier T and Diddams S A 2008 Astronomical spectrograph calibration with broad-spectrum frequency combs *Eur. Phys. J.* D **48** 57–66
[29] Li C-H *et al* 2008 A laser frequency comb that enables radial velocity measurements with a precision of 1 cm s^{-1} *Nature* **452** 610–2
[30] McCracken R A, Charsley J M and Reid D T 2017 A decade of astrocombs: recent advances in frequency combs for astronomy [Invited] *Opt. Express* **25** 15058
[31] Herr T and McCracken R A 2019 Astrocombs: recent advances *IEEE Photonics Technol. Lett.* **31** 1890–3
[32] Blackman R T *et al* 2020 Performance verification of the extreme precision spectrograph *Astron. J.* **159** 238
[33] Perraut K *et al* 2018 Single-mode waveguides for GRAVITY: I. The cryogenic 4-telescope integrated optics beam combiner *Astron. Astrophys.* **614** A70
[34] Abuter R *et al* 2020 Detection of the Schwarzschild precession in the orbit of the star S2 near the Galactic centre massive black hole *Astron. Astrophys.* **636** L5
[35] Lacour S *et al* 2019 First direct detection of an exoplanet by optical interferometry: astrometry and *K* -band spectroscopy of HR 8799 e *Astron. Astrophys.* **623** L11
[36] Abuter R *et al* 2018 Detection of orbital motions near the last stable circular orbit of the massive black hole SgrA *Astron. Astrophys.* **618** L10
[37] Abuter R *et al* 2018 Detection of the gravitational redshift in the orbit of the star S2 near the Galactic centre massive black hole *Astron. Astrophys.* **615** L15
[38] Gatkine P *et al* 2019 State of the profession: astrophotonics *Bull. Am. Astron. Soc.* **51** 285
[39] Jovanovic N *et al* 2019 Enabling the next generation of scientific discoveries by embracing photonic technologies *Bull. Am. Astron. Soc.* (arXiv:1907.07742)
[40] National Academies of Sciences, Engineering, and Medicine; Division on Engineering and Physical Sciences; Space Studies Board; Board on Physics and Astronomy; Decadal Survey on Astronomy and Astrophysics 2020 (Astro2020) 2021 *Pathways to Discovery in Astronomy and Astrophysics for the 2020s* (National Academies Press) (https://doi.org/10.17226/26141)
[41] Jovanovic N *et al* 2022 An all-photonic, dynamic device for flattening the spectrum of a laser frequency comb for precise calibration of radial velocity measurements *Proc. SPIE* **12188** 121885D
[42] Jovanovic N *et al* 2022 Flattening laser frequency comb spectra with a high dynamic range, broadband spectral shaper on-a-chip *Opt. Express* **30** 36745
[43] Lewis S A E *et al* 2000 Rayleigh noise suppression using a gain flattening filter in a broadband Raman amplifier *Optical Fiber Communication Conf., Technical Digest PostConf. Edition. Trends in Optics and Photonics Vol. 37 (IEEE Cat. No. 00CH37079)* (*Baltimore, MD, USA*) vol 4 pp 109–11
[44] Harumoto M, Shigehara M and Suganurna H 2002 Gain-flattening filter using long-period fiber gratings *J. Lightwave Technol.* **20** 1027–33
[45] Roelens M A, Bolger J A, Williams D and Eggleton B J 2008 Multi-wavelength synchronous pulse burst generation with a wavelength selective switch *Opt. Express* **16** 10152
[46] Weiner A M 2011 Ultrafast optical pulse shaping: a tutorial review *Opt. Commun.* **284** 3669–92
[47] Moroz P, Klein W P, Akers K, Vore A, Kholmicheva N, Razgoniaeva N, Khon D, Díaz S A, Medintz I L and Zamkov M 2017 Lifting the spectral crosstalk in multifluorophore assemblies *J. Phys. Chem.* C **121** 26226–32
[48] Velázquez-Benítez A M *et al* 2018 Scaling photonic lanterns for space-division multiplexing *Sci. Rep.* **8** 8897
[49] Zhang B, Yuan R, Sun J, Cheng J and Alouini M-S 2021 Free-space optical communication using non-mode-selective photonic lantern-based coherent receiver *IEEE Trans. Commun.* **69** 5367–80
[50] Jovanovic N *et al* 2017 Efficient injection from large telescopes into single-mode fibres: enabling the era of ultra-precision astronomy *Astron. Astrophys.* **604** A122
[51] Fried D L 1966 Optical resolution through a randomly inhomogeneous medium for very long and very short exposures *J. Opt. Soc. Am.* **56** 1372
[52] Rigaut F and Neichel B 2018 Multiconjugate adaptive optics for astronomy *Annu. Rev. Astron. Astrophys.* **56** 277–314
[53] Norris B R M, Wei J, Betters C H, Wong A and Leon-Saval S G 2020 An all-photonic focal-plane wavefront sensor *Nat. Commun.* **11** 5335
[54] Anagnos T *et al* 2021 3D-M3: high-spatial-resolution spectroscopy with extreme AO and 3D-printed micro-lenslets *Appl. Opt.* **60** D108
[55] Xie S, Zhan J, Hu Y, Zhang Y, Veilleux S, Bland-Hawthorn J and Dagenais M 2018 Add–drop filter with complex waveguide Bragg grating and multimode interferometer operating on arbitrarily spaced channels *Opt. Lett.* **43** 6045
[56] Gatkine P, Veilleux S and Dagenais M 2019 Astrophotonic spectrographs *Appl. Sci.* **9** 290
[57] Obrzud E *et al* 2019 A microphotonic astrocomb *Nat. Photon.* **13** 31–35
[58] Chingaipe P M, Martinache F and Cvetojevic N 2022 4-input photonic kernel-nulling for the VLTI *Proc. SPIE* **12183** 1218319

[59] Li H, Zhang S, Zhang Z, Zuo S, Zhang S, Sun Y, Zhao D and Zhang Z 2020 Silicon waveguide integrated with germanium photodetector for a photonic-integrated FBG interrogator *Nanomaterials* **10** 1683
[60] Norris B and Bland-Hawthorn J 2019 Astrophotonics: the rise of integrated photonics in astronomy *Opt. Photon. News* **30** 26
[61] Ghez A M 2008 Measuring distance and properties of the Milky Way's central supermassive black hole with stellar orbits *Astrophys. J.* **689** 1044–62
[62] Gillessen S 2009 Monitoring stellar orbits around the massive black hole in the galactic center *Astrophys. J.* **692** 1075–109
[63] Rigaut F *et al* 2020 MAVIS conceptual design *Proc. SPIE* **11447** 114471R
[64] Minowa Y *et al* 2020 ULTIMATE-Subaru: system performance modeling of GLAO and wide-field NIR instruments *Proc. SPIE* **11450** 114500O
[65] Macintosh B 2014 First light of the Gemini planet imager *Proc. Natl Acad. Sci.* **111** 12661–6
[66] Beuzit J-L 2019 SPHERE: the exoplanet imager for the very large telescope *Astron. Astrophys.* **631** A155
[67] Lozi J 2018 SCExAO, an instrument with a dual purpose: perform cutting-edge science and develop new technologies *Proc. SPIE* **10703** 1070359
[68] Males J R 2020 MagAO-X first light *Proc. SPIE* **11448** 114484M
[69] Milli J *et al* 2018 Low wind effect on VLT/SPHERE: impact, mitigation strategy, and results *Proc. SPIE* **10703** 107032A
[70] Skaf N *et al* 2022 On-sky validation of image-based adaptive optics wavefront sensor referencing *Astron. Astrophys.* **659** A170
[71] Bos S P, Bottom M, Ragland S, Delorme J-R, Cetre S and Pueyo L 2021 Fast and furious focal-plane wavefront sensing at W.M Keck Observatory *Proc. SPIE* **11823** 118231E
[72] Vievard S *et al* 2019 Overview of focal plane wavefront sensors to correct for the low wind effect on SUBARU/SCExAO *Proc. AO4ELT6* (available at: http://arxiv.org/abs/1912.10179)
[73] Crass J *et al* 2020 Final design and on-sky testing of the iLocater SX acquisition camera: broadband single-mode fiber coupling *Mon. Not. R. Astron. Soc.* **18** 2250–67
[74] Delorme J-R *et al* 2021 Keck planet imager and characterizer: a dedicated single-mode fiber injection unit for high-resolution exoplanet spectroscopy *J. Astron. Telesc. Instrum. Syst.* **7** 035006
[75] Abuter R *et al* 2017 First light for GRAVITY: phase referencing optical interferometry for the very large telescope interferometer *Astron. Astrophys.* **602** A94
[76] Bland-Hawthorn J *et al* 2011 Hexabundles: imaging fiber arrays for low-light astronomical applications *Opt. Express* **19** 2649
[77] Por E H and Haffert S Y 2020 The Single-mode Complex Amplitude Refinement (SCAR) coronagraph: I. Concept, theory, and design *Astron. Astrophys.* **635** A55
[78] Haffert S Y *et al* 2020 Diffraction-limited integral-field spectroscopy for extreme adaptive optics systems with the multicore fiber-fed integral-field unit *J. Astron. Telesc. Instrum. Syst.* **6** 045007
[79] Cabral A *et al* 2022 NIRPS—The Near Infra-Red Planet Searcher: design, integration and tests of the atmospheric dispersion corrector *Proc. SPIE* **12184** 121844M
[80] Dietrich P-I-I *et al* 2018 *In situ* 3D nanoprinting of free-form coupling elements for hybrid photonic integration *Nat. Photon.* **12** 241–7
[81] Goodwin M, Richards S, Zheng J, Lawrence J, Leon-Saval S, Argyros A and Alcalde B 2014 Miniaturized Shack-Hartmann wavefront sensors for starbugs *Proc. SPIE* **9151** 91514T
[82] Dietrich P-I, Harris R J, Blaicher M, Corrigan M K, Morris T J, Freude W, Quirrenbach A and Koos C 2017 Printed freeform lens arrays on multi-core fibers for highly efficient coupling in astrophotonic systems *Opt. Express* **25** 18288
[83] Hottinger P *et al* 2021 On-sky results for the novel integrated micro-lens ring tip-tilt sensor *J. Opt. Soc. Am.* B **38** 1–12
[84] Gendron E *et al* 2011 MOAO first on-sky demonstration with CANARY *Astron. Astrophys.* **529** L2
[85] Shaklan S and Roddier F 1988 Coupling starlight into single-mode fiber optics *Appl. Opt.* **27** 2334–8
[86] Lin J, Jovanovic N and Fitzgerald M P 2021 Design considerations of photonic lanterns for diffraction-limited spectrometry *J. Opt. Soc. Am.* B **38** A51–A63
[87] Norris B R M *et al* 2022 Demonstration of a photonic-lantern focal-plane wavefront sensor using fiber mode conversion and deep learning *Proc. SPIE* **12185** 1218530
[88] Guyon O *et al* 2022 High contrast imaging at the photon noise limit with WFS-based PSF calibration *Proc. SPIE* **12185** 121850E
[89] Norris B *et al* 2022 Optimal self-calibration and fringe tracking in photonic nulling interferometers using machine learning *Proc. SPIE* **12183** 121831J
[90] Thomson R R, Kar A K and Allington-Smith J 2009 Ultrafast laser inscription: an enabling technology for astrophotonics *Opt. Express* **17** 1963
[91] Gross S and Withford M J 2015 Ultrafast-laser-inscribed 3D integrated photonics: challenges and emerging applications *Nanophotonics* **4** 332–52
[92] Harris N C, Ma Y, Mower J, Baehr-Jones T, Englund D, Hochberg M and Galland C 2014 Efficient, compact and low loss thermo-optic phase shifter in silicon *Opt. Express* **22** 10487
[93] Deo V *et al* 2022 Controlling petals using fringes: discontinuous wavefront sensing through sparse aperture interferometry at Subaru/SCExAO *Proc. SPIE* **12185** 121850Z
[94] Pike F A, Benoît A, MacLachlan D G, Harris R J, Gris-Sánchez I, Lee D, Birks T A and Thomson R R 2020 Modal noise mitigation for high-precision spectroscopy using a photonic reformatter *Mon. Not. R. Astron. Soc.* **497** 3713–25
[95] Huby E *et al* 2012 FIRST, a fibered aperture masking instrument. I. First on-sky test results *Astron. Astrophys.* **541** A55
[96] Lin J, Fitzgerald M P, Xin Y, Guyon O, Leon-Saval S, Norris B and Jovanovic N 2022 Focal-plane wavefront sensing with photonic lanterns: theoretical framework *J. Opt. Soc. Am.* B **39** 2643–56
[97] Lewoczko-Adamczyk W, Schiemangk M, Müller H and Peters A 2009 Thermoacoustic optical path length stabilization in a single-mode optical fiber *Appl. Opt.* **48** 704
[98] Errando-Herranz C, Takabayashi A Y, Edinger P, Sattari H, Gylfason K B and Quack N 2020 MEMS for photonic integrated circuits *IEEE J. Sel. Top. Quantum Electron.* **26** 8200916
[99] Dong M, Clark G, Leenheer A J, Zimmermann M, Dominguez D, Menssen A J, Heim D, Gilbert G, Englund D and Eichenfield M 2022 High-speed programmable photonic circuits in a cryogenically compatible, visible–near-infrared 200 mm CMOS architecture *Nat. Photon.* **16** 59–65
[100] Miller D A B 2013 Self-aligning universal beam coupler *Opt. Express* **21** 6360
[101] Guyon O 2018 Extreme adaptive optics *Annu. Rev. Astron. Astrophys.* **56** 315–55
[102] Rigaut F 2015 Astronomical adaptive optics *Publ. Astron. Soc. Pac.* **127** 1197
[103] Sauvage J-F *et al* 2016 Tackling down the low wind effect on SPHERE instrument *Proc. SPIE* **9909** 408–16

[104] Bland-Hawthorn J et al 2010 PIMMS: photonic integrated multimode microspectrograph Proc. SPIE 7735 77350N
[105] Corrigan M, Morris T J, Harris R J and Anagnos T 2018 Demonstration of a photonic lantern low order wavefront sensor using an adaptive optics testbed Proc. SPIE 10703 107035H
[106] Wright T A, Yerolatsitis S, Harrington K, Harris R J and Birks T A 2022 All-fibre wavefront sensor Mon. Not. R. Astron. Soc. 514 5422–8
[107] Thomson R R, Birks T A, Leon-Saval S G, Kar A K and Bland-Hawthorn J 2011 Ultrafast laser inscription of an integrated photonic lantern Opt. Express 19 5698–705
[108] Xin Y et al 2022 Efficient detection and characterization of exoplanets within the diffraction limit: nulling with a mode-selective photonic lantern Astrophys. J. 938 140
[109] Benoît A, Yerolatsitis S, Harrington K, Birks T A and Thomson R R 2021 Focal-ratio degradation (FRD) mitigation in a multimode fibre link using mode-selective photonic lanterns Mon. Not. R. Astron. Soc. 502 2381–8
[110] Diab M, Tripathi A, Davenport J, Dinkelaker A N, Madhav K and Roth M M 2021 Simulations of mode-selective photonic lanterns for efficient coupling of starlight into the single-mode regime Appl. Opt. 60 D9–D14
[111] Yerolatsitis S, Gris-Sánchez I and Birks T A 2014 Adiabatically-tapered fiber mode multiplexers Opt. Express 22 608
[112] Norris B, Betters C, Wei J, Yerolatsitis S, Amezcua-Correa R and Leon-Saval S 2022 Optimal broadband starlight injection into a single-mode fibre with integrated photonic wavefront sensing Opt. Express 30 34908
[113] Diab M and Minardi S 2019 Modal analysis using photonic lanterns coupled to arrays of waveguides Opt. Lett. 44 1718–21
[114] Marois C, Christian D L, Macintosh B and Doyon R 2008 Confidence level and sensitivity limits in high-contrast imaging Astrophys. J. 673 647–56
[115] Minardi S et al 2019 Discrete beam combiners from astronomy to lasers Proc. SPIE 10921 117–24
[116] Davenport J, Diab M, Deka P, Tripathi A, Madhav K and Roth M 2021 Photonic lanterns: a practical guide to filament tapering Opt. Mater. Express 11 2639–49
[117] Mennesson B et al 2021 The Roman space telescope coronagraph technology demonstration: current status and relevance to future missions Proc. SPIE 11823 335–46
[118] Ellis S C, Bland-Hawthorn J and Leon-Saval S G 2021 General coupling efficiency for fiber-fed astronomical instruments J. Opt. Soc. Am. B 38 A64
[119] Crepp J R et al 2016 iLocater: a diffraction-limited Doppler spectrometer for the Large Binocular Telescope Proc. SPIE 9908 990819
[120] Gibson R K, Oppenheimer R, Matthews C T and Vasisht G 2019 Characterization of the C-RED 2: a high-frame rate near-infrared camera J. Astron. Telesc. Instrum. Syst. 6 1
[121] Mawet D et al 2022 Fiber-fed high-resolution infrared spectroscopy at the diffraction limit with Keck-HISPEC and TMT-MODHIS: status update Proc. SPIE 12184 121841R
[122] Bechter A J, Crass J, Tesch J, Crepp J R and Bechter E B 2020 Characterization of single-mode fiber coupling at the large binocular telescope Publ. Astron. Soc. Pac. 132 015001
[123] Leon-Saval S G, Betters C H and Bland-Hawthorn J 2012 The photonic TIGER: a multicore fiber-fed spectrograph Proc. SPIE 8450 84501K
[124] Betters C H et al 2016 Precision radial velocities with inexpensive compact spectrographs Proc. SPIE 9908 99081B
[125] Schwab C, Leon-Saval S G, Betters C H, Bland-Hawthorn J and Mahadevan S 2012 Single mode, extreme precision doppler spectrographs Proc. IAU 8 403–6
[126] Bailey J 1998 Detection of pre-main-sequence binaries using spectro-astrometry Mon. Not. R. Astron. Soc. 301 161–7
[127] Whelan E and Garcia P 2008 Spectro-astrometry: the method, its limitations, and applications Jets from Young Stars II: Clues from High Angular Resolution Observations (Lecture Notes in Physics) ed F Bacciotti, L Testi and E Whelan (Springer) pp 123–49
[128] Pontoppidan K M, Blake G A and Smette A 2011 The structure and dynamics of molecular gas in planet-forming zones: a CRIRES spectro-astrometric survey Astrophys. J. 733 84
[129] Brannigan E, Takami M, Chrysostomou A and Bailey J 2006 On the detection of artefacts in spectro-astrometry Mon. Not. R. Astron. Soc. 367 315–22
[130] Kim Y J et al 2022 Spectroastrometry with photonic lanterns Proc. SPIE 12184 1218449
[131] Swift J J et al 2015 Miniature exoplanet radial velocity array I: design, commissioning, and early photometric results J. Astron. Telesc. Instrum. Syst. 1 027002
[132] Eikenberry S S, Bentz M, Gonzalez A, Harrington J, Jeram S, Law N, Maccarone T, Quimby R and Townsend A 2019 Astro2020 project white paper: PolyOculus—low-cost spectroscopy for the community (arXiv:1907.08273)
[133] Roth M M et al 2022 MARCOT Pathfinder at Calar Alto progress report Proc. SPIE 12182 121820M
[134] Bender C F et al 2022 The large fiber array spectroscopic telescope: fiber feed and spectrometer conceptual design Proc. SPIE 12184 121844J
[135] Moraitis C D et al 2022 Demonstration of high-efficiency photonic lantern couplers for PolyOculus Proc. SPIE 12188 198
[136] Croom S M et al 2012 The Sydney-AAO multi-object integral field spectrograph: the Sydney-AAO multi-object IFS Mon. Not. R. Astron. Soc. 421 872–93
[137] Bundy K et al 2015 Overview of the sdss-iv manga survey: mapping nearby galaxies at apache point observatory Astrophys. J. 798 7
[138] Aghamousa A et al 2016 The DESI experiment part II: instrument design (arXiv:1611.00037)
[139] Chandrasekharan H K et al 2017 Multiplexed single-mode wavelength-to-time mapping of multimode light Nat. Commun. 8 14080
[140] Chun M R, Abdurrahman F, Service M, Toomey D, Baranec C, Hayano Y, Oya S, Fohring D, Lu J R and Lai O 2018 On-sky results from the wide-field ground-layer adaptive optics demonstrator'imaka Proc. SPIE 10703 107030J
[141] Sheinis A I, Nigra L and Kuhlen M Q 2006 MEMs-based speckle spectrometer Proc. SPIE 6272 62724U
[142] Angel J R P, Adams M T, Boroson T A and Moore R L 1977 A very large optical telescope array linked with fused silica fibers Astrophys. J. 218 776
[143] Hill J M, Angel J R P, Scott J S, Lindley D and Hintzen P 1980 Multiple object spectroscopy—The Medusa spectrograph Astrophys. J. 242 L69
[144] Gray P M 1984 Fibre optic coupled aperture plate (FOCAP) system at the AAO Proc. SPIE 0445 57–64
[145] Vanderriest C, Courtès G and Donas J 1984 Field spectrography with optical fibers in astronomy: development of a ground-based instrument; proposals for the space telescope J. Opt. 15 237–41
[146] Hubbard E N, Angel J R P and Gresham M S 1979 Operation of a long fused silica fiber as a link between telescope and spectrograph Astrophys. J. 229 1074

[147] Gies D, ten Brummelaar T, Schaefer G, Baron F and White R 2019 The CHARA Michelson Array *Bull. Am. Astron. Soc.* **51** 226
[148] Colless M *et al* (the 2dFGRS Team) 2001 The 2dF galaxy redshift survey: spectra and redshifts *Mon. Not. R. Astron. Soc.* **328** 1039–63
[149] York D G *et al* 2000 The sloan digital sky survey: technical summary *Astron. J.* **120** 1579–87
[150] Coudé du Foresto V and Ridgway S T 1992 Fluor—a stellar interferometer using single-mode fibers *European Southern Observatory Conf. and Workshop Proc., European Southern Observatory Conf. and Workshop Proc.* p 731
[151] Mawet D *et al* 2017 A fiber injection unit for the keck planet imager and characterizer (KPIC) *Proc. SPIE* **10400** 82
[152] Cvetojevic N, Jovanovic N, Betters C, Lawrence J S, Ellis S C, Robertson G and Bland-Hawthorn J 2012 First starlight spectrum captured using an integrated photonic micro-spectrograph *Astron. Astrophys.* **544** L1
[153] Pfuhl O *et al* 2014 The fiber coupler and beam stabilization system of the GRAVITY interferometer *Proc. SPIE* **9146** 914623
[154] Leon-Saval S G, Argyros A and Bland-Hawthorn J 2010 Photonic lanterns: a study of light propagation in multimode to single-mode converters *Opt. Express* **18** 8430
[155] Leon-Saval S G, Fontaine N K and Amezcua-Correa R 2017 Photonic lantern as mode multiplexer for multimode optical communications *Opt. Fiber Technol.* **35** 46–55
[156] Richardson D J, Fini J M and Nelson L E 2013 Space-division multiplexing in optical fibres *Nat. Photon.* **7** 354–62
[157] Alvarado-Zacarias J C *et al* 2019 Low-loss 19 core fan-in/fan-out device using reduced-cladding graded index fibers *Optical Fiber Communication Conf. (OFC) 2019* (Optica Publishing Group) p Th3D.2
[158] Gris-Sánchez I, Haynes D M, Ehrlich K, Haynes R and Birks T A 2017 Multicore fibre photonic lanterns for precision radial velocity science *Mon. Not. R. Astron. Soc.* **475** 3065–75
[159] Haffert S Y *et al* 2020 Multi-core fibre-fed integral-field unit (MCIFU): overview and first-light *Proc. SPIE* **11448** 114484M
[160] Jovanovic N, Harris R J and Cvetojevic N 2020 Astronomical applications of multi-core fiber technology *IEEE J. Sel. Top. Quantum Electron.* **26** 1–9
[161] Gris-Sánchez I, Van Ras D and Birks T A 2016 The Airy fiber: an optical fiber that guides light diffracted by a circular aperture *Optica* **3** 270
[162] Harrington K, Yerolatsitis S, Van Ras D, Haynes D M and Birks T A 2017 Endlessly adiabatic fiber with a logarithmic refractive index distribution *Optica* **4** 1526
[163] Jasion G T *et al* 2022 0.174 dB/km hollow core double nested antiresonant nodeless fiber (DNANF) *Optical Fiber Communication Conf. (OFC) 2022* (Optica Publishing Group) p Th4C.7
[164] Ding W, Wang Y-Y, Gao S-F, Wang M-L and Wang P 2020 Recent progress in low-loss hollow-core anti-resonant fibers and their applications *IEEE J. Sel. Top. Quantum Electron.* **26** 1–12
[165] Dekany R G *et al* 2022 SIGHT: the Palomar 5m telescope LGS AO system maximizing visible-light spectroscopic sensitivity *Proc. SPIE* **12185** 121850P
[166] Baranec C *et al* 2012 Robo-AO: autonomous and replicable laser-adaptive-optics and science system *Proc. SPIE* **8447** 844704
[167] Wang J J *et al* 2021 Detection and bulk properties of the HR 8799 planets with high-resolution spectroscopy *Astron. J.* **162** 148
[168] Winter B, Birks T A and Wadsworth W J 2019 Multimode hollow-core anti-resonant optical fibres *Frontiers in Optics* (Optica Publishing Group) p JTu4A.18
[169] Shere W, Jasion G T, Fokoua E N and Poletti F 2021 Design rules for multi-mode anti-resonant hollow-core fibres *Optical Fiber Communication Conf. (OFC) 2021* (Optica Publishing Group) p F4C.4
[170] Petry M, Markos C, Correa R A and Habib M S 2022 Multi-mode guidance in enhanced inhibited coupling hollow-core anti-resonant fibers *Conf. on Lasers and Electro-Optics. Presented at the CLEO: Applications and Technology* (Optica Publishing Group) p JTh3B.42
[171] Suslov D, Komanec M, Numkam Fokoua E R, Dousek D, Zhong A, Zvánovec S, Bradley T D, Poletti F, Richardson D J and Slavík R 2021 Low loss and high performance interconnection between standard single-mode fiber and antiresonant hollow-core fiber *Sci. Rep.* **11** 8799
[172] Ren H, Shen L, Runge A F J, Hawkins T W, Ballato J, Gibson U and Peacock A C 2019 Low-loss silicon core fibre platform for mid-infrared nonlinear photonics *Light Sci. Appl.* **8** 105
[173] Thomson R R, Bookey H T, Psaila N D, Fender A, Campbell S, MacPherson W N, Barton J S, Reid D T and Kar A K 2007 Ultrafast-laser inscription of a three dimensional fan-out device for multicore fiber coupling applications *Opt. Express* **15** 11691
[174] Li A, Yao C, Xia J, Wang H, Cheng Q, Penty R, Fainman Y and Pan S 2022 Advances in cost-effective integrated spectrometers *Light Sci. Appl.* **11** 174
[175] Leijtens X J M, Kuhlow B and Smit M K 2006 Arrayed waveguide gratings *Wavelength Filters in Fibre Optics* (*Springer Series in Optical Sciences*) ed H Venghaus (Springer) pp 125–87
[176] Blind N, Le Coarer E, Kern P and Gousset S 2017 Spectrographs for astrophotonics *Opt. Express* **25** 27341
[177] Okamoto K 2014 Wavelength-division-multiplexing devices in thin SOI: advances and prospects *IEEE J. Sel. Top. Quantum Electron.* **20** 248–57
[178] Zheng S, Cai H, Song J, Zou J, Liu P Y, Lin Z, Kwong D-L and Liu A-Q 2019 A single-chip integrated spectrometer via tunable microring resonator array *IEEE Photon. J.* **11** 1–9
[179] Zhang Z, Wang Y and Tsang H K 2021 Tandem configuration of microrings and arrayed waveguide gratings for a high-resolution and broadband stationary optical spectrometer at 860 nm *ACS Photonics* **8** 1251–7
[180] Takada K, Abe M, Shibata T and Okamoto K 2002 A.2.5 GHz-spaced 1080-channel tandem multi/demultiplexer covering the. S-, C-, and L-bands using an arrayed-waveguide grating with Gaussian passbands as a primary filter *IEEE Photonics Technol. Lett.* **14** 648–50
[181] Van Wijk A, Doerr C R, Ali Z, Karabiyik M and Akca B I 2020 Compact ultrabroad-bandwidth cascaded arrayed waveguide gratings *Opt. Express* **28** 14618
[182] Stoll A, Madhav K and Roth M 2021 Design, simulation and characterization of integrated photonic spectrographs for astronomy II: low-aberration generation-II AWG devices with three stigmatic points *Opt. Express* **29** 36226
[183] Liu J, Huang G, Wang R N, He J, Raja A S, Liu T, Engelsen N J and Kippenberg T J 2021 High-yield, wafer-scale fabrication of ultralow-loss, dispersion-engineered silicon nitride photonic circuits *Nat. Commun.* **12** 2236
[184] Chavez Boggio J M, Bodenmüller D, Fremberg T, Haynes R, Roth M M, Eisermann R, Lisker M, Zimmermann L and Böhm M 2014 Dispersion engineered silicon nitride waveguides by geometrical and refractive-index optimization *J. Opt. Soc. Am.* B **31** 2846
[185] Blumenthal D J, Heideman R, Geuzebroek D, Leinse A and Roeloffzen C 2018 Silicon nitride in silicon photonics *Proc. IEEE* **106** 2209–31

[186] Bauters J F, Heck M J R, John D, Dai D, Tien M-C, Barton J S, Leinse A, Heideman R G, Blumenthal D J and Bowers J E 2011 Ultra-low-loss high-aspect-ratio Si_3N_4 waveguides *Opt. Express* **19** 3163
[187] Gatkine P, Veilleux S, Hu Y, Bland-Hawthorn J and Dagenais M 2017 Arrayed waveguide grating spectrometers for astronomical applications: new results *Opt. Express* **25** 17918
[188] Shang K, Pathak S, Qin C and Yoo S J B 2017 Low-loss compact silicon nitride arrayed waveguide gratings for photonic integrated circuits *IEEE Photon. J.* **9** 1–5
[189] Crass J *et al* 2021 Final design and on-sky testing of the iLocater SX acquisition camera: broad-band single-mode fibre coupling *Mon. Not. R. Astron. Soc.* **501** 2250–67 (available at: https://academic.oup.com/mnras/article/501/2/2250/5944143)
[190] Zhu T, Hu Y, Gatkine P, Veilleux S, Bland-Hawthorn J and Dagenais M 2016 Ultrabroadband high coupling efficiency fiber-to-waveguide coupler using Si_3N_4/SiO_2 waveguides on silicon *IEEE Photon. J.* **8** 7102112
[191] Desmet A, Radosavljevic A, Missinne J, Van Thourhout D and Van Steenberge G 2021 Laser written glass interposer for fiber coupling to silicon photonic integrated circuits *IEEE Photon. J.* **13** 1–12
[192] Goh T, Suzuki S and Sugita A 1997 Estimation of waveguide phase error in silica-based waveguides *J. Lightwave Technol.* **15** 2107–13
[193] Kamalakis T, Sphicopoulos T and Syvridis D 2002 An estimation of performance degradation due to fabrication errors in AWGs *J. Lightwave Technol.* **20** 1779–87
[194] Stoll A, Zhang Z, Haynes R and Roth M 2017 High-resolution arrayed-waveguide-gratings in astronomy: design and fabrication challenges *Photonics* **4** 30
[195] Gatkine P, Jovanovic N, Hopgood C, Ellis S, Broeke R, Ławniczuk K, Jewell J, Wallace J K and Mawet D 2021 Potential of commercial SiN MPW platforms for developing mid/high-resolution integrated photonic spectrographs for astronomy *Appl. Opt.* **60** D15
[196] Gehl M, Trotter D, Starbuck A, Pomerene A, Lentine A L and DeRose C 2017 Active phase correction of high resolution silicon photonic arrayed waveguide gratings *Opt. Express* **25** 6320
[197] Jovanovic N *et al* 2017 Demonstration of an efficient, photonic-based astronomical spectrograph on an 8-m telescope *Opt. Express* **25** 17753
[198] Nishi H, Tsuchizawa T, Kou R, Shinojima H, Yamada T, Kimura H, Ishikawa Y, Wada K and Yamada K 2012 Monolithic integration of a silica AWG and Ge photodiodes on Si photonic platform for one-chip WDM receiver *Opt. Express* **20** 9312
[199] D'Agostino D, Desbordes T, Broeke R, Boerkamp M, Mink J, Ambrosius H P M M and Smit M K 2014 A monolithically integrated AWG based wavelength interrogator with 180 nm working range and pm resolution *Advanced Photonics for Communications. Presented at the Integrated Photonics Research, Silicon and Nanophotonics* (Optica Publishing Group) p IM2A.4.
[200] Gatkine P R, Jovanovic N, Wallace J K, Jewell J B and Mawet D P 2022 A continuously-sampled high-resolution astrophotonic spectrograph using silicon nitride *Proc. SPIE* **12188** 121882D
[201] Wang D, Jin G, Yan Y and Minxian W 2001 Aberration theory of arrayed waveguide grating *J. Lightwave Technol.* **19** 279–84
[202] Hu Y 2020 Ultra-low-loss silicon nitride waveguide gratings and their applications in astrophotonics *Doctoral Dissertation* University of Maryland
[203] Zhan J, Zhang Y, Hsu W-L, Veilleux S and Dagenais M 2023 Design and implementation of a Si_3N_4 three-stigmatic-point arrayed waveguide grating with a resolving power over 17,000 *Opt. Express* **31** 6389
[204] Sun X, Alam M Z, Aitchison J S and Mojahedi M 2016 Compact and broadband polarization beam splitter based on a silicon nitride augmented low-index guiding structure *Opt. Lett.* **41** 163
[205] Sacher W D, Huang Y, Ding L, Barwicz T, Mikkelsen J C, Taylor B J F, Lo G-Q and Poon J K S 2014 Polarization rotator-splitters and controllers in a Si_3N_4-on-SOI integrated photonics platform *Opt. Express* **22** 11167
[206] Bustamante Y R R, De Paula R A and Aldaya I 2021 Inverse design of a broadband silicon nitride polarization rotor *Frontiers in Optics* (Optica Publishing Group) p JW7A.91
[207] Goi K, Ogawa K, Guan N, Sakuma K, Tan Y T, Yu M B, Teo H G and Lo G Q 2010 Design method of Bragg grating waveguides on substrate for optical filters *OECC 2010 Technical Digest* pp 228–9 (available at: https://ieeexplore.ieee.org/document/5587941)
[208] Inoue Y, Itoh M, Hashizume Y, Hibino Y, Sugita A and Himeno A 2001 Novel birefringence compensating AWG design *Optical Fiber Communication Conf. and Int. Conf. on Quantum Information* (*Anaheim, CA*) p WB4
[209] Lang T, He J-J, Kuang J-G and He S 2007 Birefringence compensated AWG demultiplexer with angled star couplers *Opt. Express* **15** 15022
[210] Meng Y *et al* 2021 Optical meta-waveguides for integrated photonics and beyond *Light Sci. Appl.* **10** 235
[211] Luque-González J M, Sánchez-Postigo A, Hadij-elhouati A, Ortega-Moñux A, Wangüemert-Pérez J G, Schmid J H, Cheben P, Molina-Fernández Í and Halir R 2021 A review of silicon subwavelength gratings: building break-through devices with anisotropic metamaterials *Nanophotonics* **10** 2765–97
[212] Cheben P, Halir R, Schmid J H, Atwater H A and Smith D R 2018 Subwavelength integrated photonics *Nature* **560** 565–72
[213] Stanton E J, Spott A, Davenport M L, Volet N and Bowers J E 2016 Low-loss arrayed waveguide grating at 760 nm *Opt. Lett.* **41** 1785
[214] Zhang Z, Wang Y and Tsang H K 2020 Ultracompact 40-channel arrayed waveguide grating on silicon nitride platform at 860 nm *IEEE J. Quantum Electron.* **56** 1–8
[215] Liu J *et al* 2020 Monolithic piezoelectric control of soliton microcombs *Nature* **583** 385–90
[216] Yamada H 1998 Crosstalk reduction in a 10-GHz spacing arrayed-waveguide grating by phase-error compensation *J. Lightwave Technol.* **16** 364
[217] Ismail N, Sun F, Sengo G, Wörhoff K, Driessen A, De Ridder R M and Pollnau M 2011 Improved arrayed-waveguide-grating layout avoiding systematic phase errors *Opt. Express* **19** 8781
[218] Takada K and Abe M 2003 UV trimming of AWG devices *Bragg Gratings, Photosensitivity, and Poling in Glass Waveguides* (*Monterey, CA*) ed B Gratings p TuA1
[219] Bogaerts W, Pérez D, Capmany J, Miller D A B, Poon J, Englund D, Morichetti F and Melloni A 2020 Programmable photonic circuits *Nature* **586** 207–16
[220] Zhang Y, Zhan J, Veilleux S and Dagenais M 2022 Arrayed waveguide grating with reusable delay lines (RDL-AWG) for high resolving power, highly compact, photonic spectrographs *2022 IEEE Photonics Conf. (IPC)* (IEEE) pp 1–2
[221] Liu Y, Sun W, Xie H, Zhang N, Xu K, Yao Y, Xiao S and Song Q 2019 Adiabatic and ultracompact waveguide tapers based on digital metamaterials *IEEE J. Sel. Top. Quantum Electron.* **25** 1–6
[222] Kuang W, Ma L and He Z 2020 Low loss polymer wavelength (De)multiplexer interposing Si waveguide and single-mode fiber using topology optimization *2020 Opto-Electronics and Communications Conf. (OECC)* (IEEE) pp 1–3

[223] Vallée J-M, Jean P and Shi W 2019 Hybrid silicon-fiber tunable multiwavelength laser with switchable frequency spacing *IEEE J. Sel. Top. Quantum Electron.* **26** 1–8
[224] Wu D, Wu S-Z, Niu L-G, Chen Q-D, Wang R, Song J-F, Fang H-H and Sun H-B 2010 High numerical aperture microlens arrays of close packing *Appl. Phys. Lett.* **97** 031109
[225] Jung H and Jeong K-H 2015 Monolithic polymer microlens arrays with high numerical aperture and high packing density *ACS Appl. Mater. Interfaces* **7** 2160–5
[226] Ahmed R, Yetisen A K and Butt H 2017 High numerical aperture hexagonal stacked ring-based bidirectional flexible polymer microlens array *ACS Nano* **11** 3155–65
[227] Yu S, Zuo H, Sun X, Liu J, Gu T and Hu J 2020 Optical free-form couplers for high-density integrated photonics (OFFCHIP): a universal optical interface *J. Lightwave Technol.* **38** 3358–65
[228] Ahn D, Hong C, Liu J, Giziewicz W, Beals M, Kimerling L C, Michel J, Chen J and Kärtner F X 2007 High performance, waveguide integrated Ge photodetectors *Opt. Express* **15** 3916
[229] Smit M *et al* 2014 An introduction to InP-based generic integration technology *Semicond. Sci. Technol.* **29** 083001
[230] Marchetti R, Lacava C, Carroll L, Gradkowski K and Minzioni P 2019 Coupling strategies for silicon photonics integrated chips [Invited] *Photon. Res.* **7** 201
[231] Song Y, Panas R M and Hopkins J B 2018 A review of micromirror arrays *Precis. Eng.* **51** 729–61
[232] Lu T-J *et al* 2018 Aluminum nitride integrated photonics platform for the ultraviolet to visible spectrum *Opt. Express* **26** 11147
[233] Stoll A, Madhav K and Roth M 2020 Performance limits of astronomical arrayed waveguide gratings on a silica platform *Opt. Express* **28** 39354
[234] Piels M and Bowers J E 2016 *Photodetectors for Silicon Photonic Integrated Circuits* ed B Nabet (Woodhead Publishing) pp 3–20
[235] Hu T, Zhang X, Zhang M and Yan X 2021 A high-resolution miniaturized ultraviolet spectrometer based on arrayed waveguide grating and microring cascade structures *Opt. Commun.* **482** 126591
[236] Zhu H H *et al* 2020 A high-resolution integrated spectrometer based on cascaded a ring resonator and an AWG *Conf. on Lasers and Electro-Optics (CLEO): Applications and Technology* (Optica Publishing Group) p JTu2G.32
[237] Ridgway S T and Brault J W 1984 Astronomical Fourier transform spectroscopy revisited *Annu. Rev. Astron. Astrophys.* **22** 291–317
[238] Souza M C M M, Grieco A, Frateschi N C and Fainman Y 2018 Fourier transform spectrometer on silicon with thermo-optic non-linearity and dispersion correction *Nat. Commun.* **9** 665
[239] Le Coarer E, Blaize S, Benech P, Stefanon I, Morand A, Lérondel G, Leblond G, Kern P, Fedeli J M and Royer P 2007 Wavelength-scale stationary-wave integrated Fourier-transform spectrometry *Nat. Photon.* **1** 473–8
[240] Bonneville C *et al* 2013 SWIFTS: a groundbreaking integrated technology for high-performance spectroscopy and optical sensors *Proc. SPIE* **8616** 86160M
[241] Hajian A R *et al* 2007 Initial results from the USNO dispersed Fourier transform spectrograph *Astrophys. J.* **661** 616–33
[242] Kita D M, Miranda B, Favela D, Bono D, Michon J, Lin H, Gu T and Hu J 2018 High-performance and scalable on-chip digital Fourier transform spectroscopy *Nat. Commun.* **9** 4405
[243] Dostart N, Zhang B, Khilo A, Brand M, Al Qubaisi K, Onural D, Feldkhun D, Wagner K H and Popović M A 2020 Serpentine optical phased arrays for scalable integrated photonic lidar beam steering *Optica* **7** 726
[244] Brand M, Zhang B, Onural D, Al Qubaisi K, Popović M, Dostart N and Wagner K 2021 High-resolution and compact serpentine integrated grating spectrometer *J. Opt. Soc. Am.* B **38** A75
[245] Shen H, Fan L, Wang J, Wirth J C and Qi M 2010 A taper to reduce the straight-to-bend transition loss in compact silicon waveguides *IEEE Photonics Technol. Lett.* **22** 1174–6
[246] Cheben P, Schmid J H, Wang S, Xu D-X, Vachon M, Janz S, Lapointe J, Painchaud Y and Picard M-J 2015 Broadband polarization independent nanophotonic coupler for silicon waveguides with ultra-high efficiency *Opt. Express* **23** 22553
[247] Papes M *et al* 2016 Fiber-chip edge coupler with large mode size for silicon photonic wire waveguides *Opt. Express* **24** 5026
[248] Marchetti R, Lacava C, Khokhar A, Chen X, Cristiani I, Richardson D J, Reed G T, Petropoulos P and Minzioni P 2017 High-efficiency grating-couplers: demonstration of a new design strategy *Sci. Rep.* **7** 16670
[249] Melati D, Grinberg Y, Kamandar Dezfouli M, Janz S, Cheben P, Schmid J H, Sánchez-Postigo A and Xu D-X 2019 Mapping the global design space of nanophotonic components using machine learning pattern recognition *Nat. Commun.* **10** 4775
[250] Shang K, Pathak S, Guan B, Liu G and Yoo S J B 2015 Low-loss compact multilayer silicon nitride platform for 3D photonic integrated circuits *Opt. Express* **23** 21334
[251] Kippenberg T J, Gaeta A L, Lipson M and Gorodetsky M L 2018 Dissipative Kerr solitons in optical microresonators *Science* **361** eaan8083
[252] Stern B, Ji X, Okawachi Y, Gaeta A L and Lipson M 2018 Battery-operated integrated frequency comb generator *Nature* **562** 401–5
[253] Rao A, Moille G, Lu X, Westly D A, Sacchetto D, Geiselmann M, Zervas M, Papp S B, Bowers J and Srinivasan K 2021 Towards integrated photonic interposers for processing octave-spanning microresonator frequency combs *Light Sci. Appl.* **10** 109
[254] Del'Haye P, Arcizet O, Schliesser A, Holzwarth R and Kippenberg T J 2008 Full stabilization of a microresonator-based optical frequency comb *Phys. Rev. Lett.* **101** 053903
[255] Yang Q-F *et al* 2019 Vernier spectrometer using counterpropagating soliton microcombs *Science* **363** 965–8
[256] Niu R, Wan S, Li J, Zhao R-C, Zou C-L, Guo G-C and Dong C-H 2021 Fast spectroscopy based on a modulated soliton microcomb *IEEE Photon. J.* **13** 1–4
[257] Hadibrata W, Noh H, Wei H, Krishnaswamy S and Aydin K 2021 Compact, high-resolution inverse-designed on-chip spectrometer based on tailored disorder modes *Laser Photonics Rev.* **15** 2000556
[258] Redding B, Liew S F, Sarma R and Cao H 2013 Compact spectrometer based on a disordered photonic chip *Nat. Photon.* **7** 746–51
[259] Yang Z *et al* 2019 Single-nanowire spectrometers *Science* **365** 1017–20
[260] Bao J and Bawendi M G 2015 A colloidal quantum dot spectrometer *Nature* **523** 67–70
[261] Cheriton R *et al* 2020 Spectrum-free integrated photonic remote molecular identification and sensing *Opt. Express* **28** 27951–65
[262] Hong J, Spring A M, Qiu F and Yokoyama S 2019 A high efficiency silicon nitride waveguide grating coupler with a multilayer bottom reflector *Sci. Rep.* **9** 12988
[263] Molesky S, Lin Z, Piggott A Y, Jin W, Vucković J and Rodriguez A W 2018 Inverse design in nanophotonics *Nat. Photon.* **12** 659–70
[264] So S, Badloe T, Noh J, Bravo-Abad J and Rho J 2020 Deep learning enabled inverse design in nanophotonics *Nanophotonics* **9** 1041–57
[265] Pestourie R, Pérez-Arancibia C, Lin Z, Shin W, Capasso F and Johnson S G 2018 Inverse design of large-area metasurfaces *Opt. Express* **26** 33732

[266] Piels M, Bauters J F, Davenport M L, Heck M J R and Bowers J E 2014 Low-loss silicon nitride AWG demultiplexer heterogeneously integrated with hybrid III–V/silicon photodetectors *J. Lightwave Technol.* **32** 817–23
[267] Kahl O, Ferrari S, Kovalyuk V, Vetter A, Lewes-Malandrakis G, Nebel C, Korneev A, Goltsman G and Pernice W 2017 Spectrally multiplexed single-photon detection with hybrid superconducting nanophotonic circuits *Optica* **4** 557–62
[268] Wollman E E, Verma V B, Lita A E, Farr W H, Shaw M D, Mirin R P and Woo Nam S 2019 Kilopixel array of superconducting nanowire single-photon detectors *Opt. Express* **27** 35279–89
[269] Chen B-U, Tang C L and Telle J M 1974 cw harmonic generation in the uv using a thin-film waveguide on a nonlinear substrate *Appl. Phys. Lett.* **25** 495–8
[270] Spitzer L 1946 Astronomical advantages of an extra-terrestrial observatory reprinted Astr *Quart* **7** 1990
[271] Blumenthal D J 2020 Photonic integration for UV to IR applications *APL Photonics* **5** 020903
[272] Tian K, Yu J, Lei F, Ward J, Li A, Wang P and Nic Chormaic S 2022 Blue band nonlinear optics and photodarkening in silica microdevices *Photon. Res.* **10** 2073
[273] Olson S L, Schwieterman E W, Reinhard C T, Ridgwell A, Kane S R, Meadows V S and Lyons T W 2018 Atmospheric seasonality as an exoplanet biosignature *Astrophys. J. Lett.* **858** L14
[274] Zhao D, Lin Z, Zhu W, Lezec H J, Xu T, Agrawal A, Zhang C and Huang K 2021 Recent advances in ultraviolet nanophotonics: from plasmonics and metamaterials to metasurfaces *Nanophotonics* **10** 2283–308
[275] Alfaraj N, Min J-W, Kang C H, Alatawi A A, Priante D, Subedi R C, Tangi M, Ng T K and Ooi B S 2019 Deep-ultraviolet integrated photonic and optoelectronic devices: a prospect of the hybridization of group III–nitrides, III–oxides, and two-dimensional materials *J. Semicond.* **40** 121801
[276] Barwicz T and Haus H A 2005 Three-dimensional analysis of scattering losses due to sidewall roughness in microphotonic waveguides *J. Lightwave Technol.* **23** 2719–32
[277] Hanada Y, Sugioka K and Midorikawa K 2010 UV waveguides light fabricated in fluoropolymer CYTOP by femtosecond laser direct writing *Opt. Express* **18** 446
[278] Bérubé J-P and Vallée R 2016 Femtosecond laser direct inscription of surface skimming waveguides in bulk glass *Opt. Lett.* **41** 3074
[279] Day M L, Choonee K, Chaboyer Z, Gross S, Withford M J, Sinclair A G and Marshall G D 2021 A micro-optical module for multi-wavelength addressing of trapped ions *Quantum Sci. Technol.* **6** 024007
[280] Osellame R, Cerullo G and Ramponi R (eds) 2012 *Femtosecond Laser Micromachining: Photonic and Microfluidic Devices in Transparent Materials* (*Topics in Applied Physics*) (Springer) pp 443–65
[281] Nikzad S *et al* 2016 Single photon counting UV solar-blind detectors using silicon and III-nitride materials *Sensors* **16** 927
[282] Tseng M L *et al* 2022 Vacuum ultraviolet nonlinear metalens *Sci. Adv.* **8** eabn5644
[283] Ossiander M, Meretska M L, Hampel H K, Lim S W D, Knefz N, Jauk T, Capasso F and Schultze M 2023 Extreme ultraviolet metalens by vacuum guiding *Science* **380** 59–63
[284] Liu X, Bruch A W and Tang H X 2023 Aluminum nitride photonic integrated circuits: from piezo-optomechanics to nonlinear optics *Adv. Opt. Photonics* **15** 236
[285] Taniyasu Y, Kasu M and Makimoto T 2006 An aluminium nitride light-emitting diode with a wavelength of 210 nanometres *Nature* **441** 325–8
[286] Hollington D, Baird J T, Sumner T J and Wass P J 2015 Characterising and testing deep UV LEDs for use in space applications *Class. Quantum Grav.* **32** 235020
[287] Letson B C, Barke S, Wass P, Mueller G, Ren F, Pearton S J and Conklin J W 2023 Deep UV AlGaN LED reliability for long duration space missions *J. Opt. Soc. Am.* A **41** 013202
[288] Oto M, Kikugawa S, Sarukura N, Hirano M and Hosono H 2001 Optical fiber for deep ultraviolet light *IEEE Photonics Technol. Lett.* **13** 978–80
[289] Klein K-F, Gonschior C P, Beer D, Eckhardt H-S, Belz M, Shannon J, Khalilov V, Klein M and Jakob C 2013 Silica-based UV-fibers for DUV applications: current status *Proc. SPIE* **8775** 87750B
[290] Galleani G, Ledemi Y, De Lima Filho E S, Morency S, Delaizir G, Chenu S, Duclere J R and Messaddeq Y 2017 UV-transmitting step-index fluorophosphate glass fiber fabricated by the crucible technique *Opt. Mater.* **64** 524–32
[291] Gao S-F, Wang Y-Y, Ding W and Wang P 2018 Hollow-core negative-curvature fiber for UV guidance *Opt. Lett.* **43** 1347
[292] Li J, Gholipour B, Piccinotti D, MacDonald K F and Zheludev N I 2020 Ultraviolet hollow-core waveguides with sub-unitary index chalcogenide cladding *Opt. Mater. Express* **10** 2254
[293] Hoang V T, Stępniewski G, Kasztelanic R, Pysz D, Long V C, Dinh K X, Klimczak M and Buczyński R 2021 Enhancement of UV-visible transmission characteristics in wet-etched hollow core anti-resonant fibers *Opt. Express* **29** 18243
[294] Mridha M K, Novoa D, Bauerschmidt S T, Abdolvand A and Russell P S J 2016 Generation of a vacuum ultraviolet to visible Raman frequency comb in H_2-filled kagomé photonic crystal fiber *Opt. Lett.* **41** 2811
[295] Belli F, Abdolvand A, Chang W, Travers J C and Russell P S J 2015 Vacuum-ultraviolet to infrared supercontinuum in hydrogen-filled photonic crystal fiber *Optica* **2** 292
[296] Tuttle S E, Schiminovich D, Grange R, Rahman S, Matuszewski M, Milliard B, Deharveng J-M and Martin D C 2010 FIREBALL: the first ultraviolet fiber fed spectrograph *Proc. SPIE* **7732** 773227
[297] Gilliam W, Fleming B T, Vorobiev D, Winter B, Wadsworth W and Birks T 2021 Far-ultraviolet optical fibers for instrumentation in the sub-200 nm regime *Proc. SPIE* **11819** 118190L
[298] Colombe Y, Slichter D H, Wilson A C, Leibfried D and Wineland D J 2014 Single-mode optical fiber for high-power, low-loss UV transmission *Opt. Express* **22** 19783
[299] Gebert F, Frosz M H, Weiss T, Wan Y, Ermolov A, Joly N Y, Schmidt P O and Russell P S J 2014 Damage-free single-mode transmission of deep-UV light in hollow-core PCF *Opt. Express* **22** 15388
[300] West G N, Loh W, Kharas D, Sorace-Agaskar C, Mehta K K, Sage J, Chiaverini J and Ram R J 2019 Low-loss integrated photonics for the blue and ultraviolet regime *APL Photonics* **4** 026101
[301] Hennessy J, Jewell A D and Nikzad S 2021 Advances in detector-integrated filter coatings for the far ultraviolet *Proc. SPIE 11821, UV, X-Ray, and Gamma-Ray Space Instrumentation for Astronomy XXII* vol 118211A (available at: www.spiedigitallibrary.org/conference-proceedings-of-spie/11821/2595524/Advances-in-detector-integrated-filter-coatings-for-the-far-ultraviolet/10.1117/12.2595524.full?SSO=1)
[302] Sorace-Agaskar C, Kharas D, Yegnanarayanan S, Maxson R T, West G N, Loh W, Bramhavar S, Ram R J, Chiaverini J, Sage J and Juodawlkis P 2019 Versatile Silicon Nitride and Alumina Integrated Photonic Platforms for the Ultraviolet to Short-Wave Infrared *IEEE J. Sel. Top. Quantum Electron* **25** 1–15

[303] Huang C, Zhang H and Sun H 2020 Ultraviolet optoelectronic devices based on AlGaN-SiC platform: towards monolithic photonics integration system *Nano Energy* **77** 105149
[304] Morin T J, Chang L, Jin W, Li C, Guo J, Park H, Tran M A, Komljenovic T and Bowers J E 2021 CMOS-foundry-based blue and violet photonics *Optica* **8** 755
[305] Shin W, Sun Y, Soltani M and Mi Z 2021 Demonstration of green and UV wavelength high Q aluminum nitride on sapphire microring resonators integrated with microheaters *Appl. Phys. Lett.* **118** 211103
[306] Piacentini S, Vogl T, Corrielli G, Lam P K and Osellame R 2021 Space qualification of ultrafast laser-written integrated waveguide optics *Laser Photonics Rev.* **15** 2000167
[307] Takahashi H 2003 Planar lightwave circuit devices for optical communication: present and future *Proc. SPIE* **5246** 520
[308] Siew S Y *et al* 2021 Review of silicon photonics technology and platform development *J. Lightwave Technol.* **39** 4374–89
[309] Xiang C, Jin W and Bowers J E 2022 Silicon nitride passive and active photonic integrated circuits: trends and prospects *Photon. Res.* **10** A82
[310] Boes A, Corcoran B, Chang L, Bowers J and Mitchell A 2018 Status and potential of lithium niobate on insulator (LNOI) for photonic integrated circuits *Laser Photonics Rev.* **12** 1700256
[311] Qi Y and Li Y 2020 Integrated lithium niobate photonics *Nanophotonics* **9** 1287–320
[312] Gross S, Jovanovic N, Sharp A, Ireland M, Lawrence J and Withford M J 2015 Low loss mid-infrared ZBLAN waveguides for future astronomical applications *Opt. Express* **23** 7946
[313] Labadie L and Wallner O 2009 Mid-infrared guided optics: a perspective for astronomical instruments *Opt. Express* **17** 1947
[314] Mennesson B, Mariotti J M, Coudé du Foresto V, Perrin G, Ridgway S, Ruilier C, Traub W A, Carleton N P, Lacasse M G and Mazé G 1999 Thermal infrared stellar interferometry using single-mode guided optics: first results with the TISIS experiment on IOTA *Astron. Astrophys.* **346** 181–9
[315] Hô N, Phillips M C, Qiao H, Allen P J, Krishnaswami K, Riley B J, Myers T L and Anheier N C 2006 Single-mode low-loss chalcogenide glass waveguides for the mid-infrared *Opt. Lett.* **31** 1860
[316] Vigreux-Bercovici C, Bonhomme E, Pradel A, Broquin J-E, Labadie L and Kern P 2007 Transmission measurement at 10.6μm of $Te_2As_3Se_5$ rib waveguides on As_2S_3 substrate *Appl. Phys. Lett.* **90** 011110
[317] Ksendzov A, Lay O, Martin S, Sanghera J S, Busse L E, Kim W H, Pureza P C, Nguyen V Q and Aggarwal I D 2007 Characterization of mid-infrared single mode fibers as modal filters *Appl. Opt.* **46** 7957
[318] Ksendzov A, Lewi T, Lay O P, Martin S R, Gappinger R O, Lawson P R, Peters R D, Shalem S, Tsun A and Katzir A 2008 Modal filtering for midinfrared nulling interferometry using single mode silver halide fibers *Appl. Opt.* **47** 5728
[319] Labadie L, Martín G, Anheier N C, Arezki B, Qiao H A, Bernacki B and Kern P 2011 First fringes with an integrated-optics beam combiner at 10 μ m: a new step towards instrument miniaturization for mid-infrared interferometry *Astron. Astrophys.* **531** A48
[320] Ródenas A, Martin G, Arezki B, Psaila N, Jose G, Jha A, Labadie L, Kern P, Kar A and Thomson R 2012 Three-dimensional mid-infrared photonic circuits in chalcogenide glass *Opt. Lett.* **37** 392
[321] Arriola A, Mukherjee S, Choudhury D, Labadie L and Thomson R R 2014 Ultrafast laser inscription of mid-IR directional couplers for stellar interferometry *Opt. Lett.* **39** 4820
[322] Tepper J, Labadie L, Diener R, Minardi S, Pott J-U, Thomson R and Nolte S 2017 Integrated optics prototype beam combiner for long baseline interferometry in the *L* and *M* bands *Astron. Astrophys.* **602** A66
[323] Diener R, Tepper J, Labadie L, Pertsch T, Nolte S and Minardi S 2017 Towards 3D-photonic, multi-telescope beam combiners for mid-infrared astrointerferometry *Opt. Express* **25** 19262–74
[324] Defrère D *et al* 2018 The path towards high-contrast imaging with the VLTI: the Hi-5 project *Exp. Astron.* **46** 475–95
[325] Gross S, Arriola A, Withford M, Labadie L, Minardi S, Diener R, Tepper J, Muthusubramanian B, Pott J-U and Nolte S 2018 Photonics-based mid-infrared interferometry: 4-year results of the ALSI project and future prospects *Proc. SPIE* **10701** 107011R
[326] Butcher H L, MacLachlan D G, Lee D, Thomson R R and Weidmann D 2018 Demonstration and characterization of ultrafast laser-inscribed mid-infrared waveguides in chalcogenide glass IG2 *Opt. Express* **26** 10930–43
[327] Montesinos-Ballester M *et al* 2019 On-chip Fourier-transform spectrometer based on spatial heterodyning tuned by thermo-optic effect *Sci. Rep.* **9** 14633
[328] Vigreux C, Escalier R, Pradel A, Bastard L, Broquin J-E, Zhang X, Billeton T, Parent G, Barillot M and Kirschner V 2015 Telluride buried channel waveguides operating from 6 to 20μm for photonic applications *Opt. Mater.* **49** 218–23
[329] Tepper J, Labadie L, Gross S, Arriola A, Minardi S, Diener R and Withford M J 2017 Ultrafast laser inscription in ZBLAN integrated optics chips for mid-IR beam combination in astronomical interferometry *Opt. Express* **25** 20642
[330] Kenchington Goldsmith H-D, Ireland M, Ma P, Cvetojevic N and Madden S 2017 Improving the extinction bandwidth of MMI chalcogenide photonic chip based MIR nulling interferometers *Opt. Express* **25** 16813
[331] Roelkens G *et al* 2014 Silicon-based photonic integration beyond the telecommunication wavelength range *IEEE J. Sel. Top. Quantum Electron.* **20** 394–404
[332] Lin H, Luo Z, Gu T, Kimerling L C, Wada K, Agarwal A and Hu J 2017 Mid-infrared integrated photonics on silicon: a perspective *Nanophotonics* **7** 393–420
[333] Marris-Morini D *et al* 2018 Germanium-based integrated photonics from near- to mid-infrared applications *Nanophotonics* **7** 1781–93
[334] Haas J, Artmann P and Mizaikoff B 2019 Mid-infrared GaAs/AlGaAs micro-ring resonators characterized *via* thermal tuning *RSC Adv.* **9** 8594–9
[335] Gretzinger T, Gross S, Arriola A and Withford M J 2019 Towards a photonic mid-infrared nulling interferometer in chalcogenide glass *Opt. Express* **27** 8626
[336] Madden G E, Choudhury D, MacPherson W N and Thomson R R 2017 Development of low-loss mid-infrared ultrafast laser inscribed waveguides *Opt. Eng.* **56** 075102
[337] Butcher H L, MacLachlan D G, Lee D, Thomson R R and Weidmann D 2018b Ultrafast laser-inscribed mid-infrared evanescent field directional couplers in GeAsSe chalcogenide glass *OSA Contin.* **1** 221
[338] Vigreux C, Barthélémy E, Bastard L, Broquin J E, Barillot M, Ménard S, Parent G and Pradel A 2011 Realization of single-mode telluride rib waveguides for mid-IR applications between 10 and 20 μm *Opt. Lett.* **36** 2922–4
[339] Quanz S P *et al* (the LIFE Collaboration) 2022 Large interferometer for exoplanets (LIFE): I. Improved exoplanet detection yield estimates for a large mid-infrared space-interferometer mission *Astron. Astrophys.* **664** A21
[340] Abel-Tiberini L, Labadie L, Arezki B, Kern P, Grille R, Labeye P and Broquin J-E 2007 Transmission behaviors of single mode hollow metallic waveguides dedicated to mid-infrared nulling interferometry *Opt. Express* **15** 18005

[341] Jung S, Palaferri D, Zhang K, Xie F, Okuno Y, Pinzone C, Lascola K and Belkin M A 2019 Homogeneous photonic integration of mid-infrared quantum cascade lasers with low-loss passive waveguides on an InP platform *Optica* **6** 1023
[342] Soref R A, Emelett S J and Buchwald W R 2006 Silicon waveguided components for the long-wave infrared region *J. Opt. A: Pure Appl. Opt.* **8** 840–8
[343] Chluba J *et al* 2021 New horizons in cosmology with spectral distortions of the cosmic microwave background *Exp. Astron.* **51** 1515–54
[344] Chluba J and Ali-Haïmoud Y 2016 COSMOSPEC: fast and detailed computation of the cosmological recombination radiation from hydrogen and helium *Mon. Not. R. Astron. Soc.* **456** 3494–508
[345] Stacey G J 2011 THz low resolution spectroscopy for astronomy *IEEE Trans. Terahertz Sci. Technol.* **1** 241–55
[346] Mirzaei M *et al* 2020 μ-spec spectrometers for the EXCLAIM instrument *Proc. SPIE* **11453** 114530M
[347] Day P, LeDuc H, Mazin B, Vayonakis A and Zmuidzinas J 2003 A broadband superconducting detector suitable for use in large arrays *Nature* **3** 817–21
[348] Zmuidzinas J 2012 Superconducting microresonators: physics and applications *Annu. Rev. Condens. Matter Phys.* **3** 169–214
[349] Baselmans J J *et al* 2017 A kilo-pixel imaging system for future space based far-infrared observatories using microwave kinetic inductance detectors *Astron. Astrophys.* **601** A89
[350] Endo A *et al* 2019 First light demonstration of the integrated superconducting spectrometer *Nat. Astron.* **3** 989–96
[351] Cataldo G, Hsieh W-T, Huang W-C, Moseley S H, Stevenson T R and Wollack E J 2014 Micro-Spec: an ultracompact, high-sensitivity spectrometer for far-infrared and submillimeter astronomy *Appl. Opt.* **53** 1094–102
[352] Bigiel F, Leroy A, Walter F, Brinks E, de Blok W J, Madore B and Thornley M D 2008 The star formation law in nearby galaxies on sub-kpc scales *Astron. J.* **136** 2846–71
[353] Redford J *et al* 2018 The design and characterization of a 300 channel, optimized full-band millimeter filterbank for science with SuperSpec *Proc. SPIE* **10708** 107081O
[354] Karkare K S *et al* 2020 Full-array noise performance of deployment-grade superspec mm-wave on-chip spectrometers *J. Low Temp. Phys.* **199** 849–57
[355] Switzer E R *et al* 2021 Experiment for cryogenic large-aperture intensity mapping: instrument design *J. Astron. Telesc. Instrum. Syst.* **7** 044004
[356] Basu Thakur R, Klimovich N, Day P K, Shirokoff E, Mauskopf P D, Faramarzi F and Barry P S 2020 Superconducting on-chip Fourier transform spectrometer *J. Low Temp. Phys.* **200** 342–52
[357] Basu Thakur R, Steiger A, Shu S, Faramarzi F, Klimovich N, Day P K, Shirokoff E, Mauskopf P D and Barry P S 2022 Development of superconducting on-chip Fourier transform spectrometers *J. Low Temp. Phys.* **211** 227–36
[358] Thomas C N, Withington R. S, Maiolino D J G, Acedo E, Wagg J, Blundell R, Paine S and Zeng L 2014 The CAMbridge emission line surveyor (CAMELS) (arXiv:1401.4395)
[359] Vial J *et al* 2020 The Leighton Chajnantor Telescope: project update and mechanical structural analysis in preparations for new deployment in Chajnantor, Chile *Proc. SPIE* **11445** 114453C
[360] Thoen D J, Murugesan V, Pascual Laguna A, Karatsu K, Endo A and Baselmans J J A 2022 Combined ultraviolet- and electron-beam lithography with micro-resist-technology GmbH ma-N1400 resist *J. Opt. Soc. Am.* B **40** 052603
[361] Hailey-Dunsheath S *et al* 2016 Low noise titanium nitride KIDs for SuperSpec: a millimeter-wave on-chip spectrometer *J. Low Temp. Phys.* **184** 180–7
[362] Hähnle S, Kouwenhoven K, Buijtendorp B, Endo A, Karatsu K, Thoen D J, Murugesan V and Baselmans J J 2021 Superconducting microstrip losses at microwave and submillimeter wavelengths *Phys. Rev. Appl.* **16** 014019
[363] Buijtendorp B T, Vollebregt S, Karatsu K, Thoen D J, Murugesan V, Kouwenhoven K, Hähnle S, Baselmans J J A and Endo A 2022 Hydrogenated amorphous silicon carbide: a low-loss deposited dielectric for microwave to submillimeter wave superconducting circuits *Phys. Rev. Appl.* **18** 064003
[364] McRae C R H, Wang H, Gao J, Vissers M R, Brecht T, Dunsworth A, Pappas D P and Mutus J 2020 Materials loss measurements using superconducting microwave resonators *Rev. Sci. Instrum.* **91** 091101
[365] Cataldo G and Wollack E J 2016 Submillimeter and far-infrared dielectric properties of thin films *Proc. SPIE* **9914** 99142W
[366] Noroozian O, Day P K, Eom B H, Leduc H G and Zmuidzinas J 2012 Crosstalk reduction for superconducting microwave resonator arrays *IEEE Trans. Microw. Theory Tech.* **60** 1235–43
[367] Yates S J C *et al* 2017 Surface wave control for large arrays of microwave kinetic inductance detectors *IEEE Trans. Terahertz Sci. Technol.* **7** 789–99
[368] Baselmans J J A, Facchin F, Pascual Laguna A, Bueno J, Thoen D J, Murugesan V, Llombart N and de Visser P 2022 Ultra-sensitive THz microwave kinetic inductance detectors for future space telescopes *Astron. Astrophys.* **665** A17
[369] Karatsu K, Endo A, Bueno J, de Visser P J, Barends R, Thoen D J, Murugesan V, Tomita N and Baselmans J J A 2019 Mitigation of cosmic ray effect on microwave kinetic inductance detector arrays *Appl. Phys. Lett.* **114** 032601
[370] Karkare K S *et al* 2022 SPT-SLIM: a line intensity mapping pathfinder for the south pole telescope *J. Low Temp. Phys.* **209** 758–65
[371] Sunyaev R A and Chluba J 2009 Signals from the epoch of cosmological recombination—Karl Schwarzschild Award Lecture 2008 *Astron. Nachr.* **330** 657–74
[372] Bland-Hawthorn J, Buryak A and Kolossovski K 2008 Optimization algorithm for ultrabroadband multichannel aperiodic fiber Bragg grating filters *J. Opt. Soc. Am.* A **25** 153–8
[373] Mariën G *et al* 2012 Fibre Bragg gratings for high spectral and temporal resolution astronomical observations *Mon. Not. R. Astron. Soc.* **421** 3641–8
[374] Ellis S C *et al* 2017 Photonic ring resonator filters for astronomical OH suppression *Opt. Express* **25** 15868–89
[375] Liu P, Czaplewski D A, Ellis S, Kehoe R, Kuehn K, Spinka H M, Stern N P, Underwood D G and Kuhlmann S 2021 Optimizing photonic ring-resonator filters for OH-suppressed near-infrared astronomy *Appl. Opt.* **60** 3865–73
[376] Goebel T A, Bharathan G, Ams M, Richter D, Krämer R G, Heck M, Siems M P, Fuerbach A and Nolte S 2018 Ultrashort pulse point-by-point written aperiodic fiber Bragg gratings for suppression of OH-emission lines *Proc. SPIE* **10706** 107066N
[377] Lindley E, Min S-S, Leon-Saval S, Cvetojevic N, Lawrence J, Ellis S and Bland-Hawthorn J 2014 Demonstration of uniform multicore fiber Bragg gratings *Opt. Express* **22** 31575–81
[378] Spaleniak I, Gross S, Jovanovic N, Williams R J, Lawrence J S, Ireland M J and Withford M J 2014 Multiband processing of multimode light: combining 3D photonic lanterns with waveguide Bragg gratings *Laser Photonics Rev.* **8** L1–L5
[379] Zhu T, Hu Y, Gatkine P, Veilleux S, Bland-Hawthorn J and Dagenais M 2016a Arbitrary on-chip optical filter using complex waveguide Bragg gratings *Appl. Phys. Lett.* **108** 101104

[380] Zhan J, Jafari Z, Veilleux S, Dagenais M and De Leon I 2020 High-Q nanobeam cavities on a silicon nitride platform enabled by slow light *APL Photonics* **5** 066101
[381] Ellis S C, Min S S, Leon-Saval S G and Bland-Hawthorn J 2018 On the origin of core-to-core variations in multi-core fibre Bragg gratings *Proc. SPIE* **10706** 1377–88
[382] Mawet D *et al* 2022 Fiber-fed high-resolution infrared spectroscopy at the diffraction limit with Keck-HISPEC and TMT-MODHIS: status update *Proc. SPIE* **12184** 599–621
[383] Hu Y-W, Xie S, Zhan J, Zhang Y, Veilleux S and Dagenais M 2020 Integrated arbitrary filter with spiral gratings: design and characterization *J. Lightwave Technol.* **38** 4454–61
[384] Zhan J, Brock J, Veilleux S and Dagenais M 2021a Silicon nitride polarization beam splitter based on polarization-independent MMIs and apodized Bragg gratings *Opt. Express* **29** 14476–85
[385] Zhan J, Dagenais M, Yang G and Veilleux S 2021b A broadband Si_3N_4 polarization beam splitter based on asymmetric directional couplers *2021 Photonics North (PN)* (*Toronto, ON, Canada*) pp 1–1
[386] Ramsay S *et al* 2020 The ESO extremely large telescope instrumentation programme *Proc. SPIE* **11203** 1120303
[387] Snellen I, de Kok R, Birkby J L, Brandl B, Brogi M, Keller C, Kenworthy M, Schwarz H and Stuik R 2015 Combining high-dispersion spectroscopy with high contrast imaging: probing rocky planets around our nearest neighbors *Astron. Astrophys.* **576** A59
[388] Hoeijmakers H J, Schwarz H, Snellen I A G, de Kok R J, Bonnefoy M, Chauvin G, Lagrange A M and Girard J H 2018 Medium-resolution integral-field spectroscopy for high-contrast exoplanet imaging-Molecule maps of the β Pictoris system with SINFONI *Astron. Astrophys.* **617** A144
[389] Sandsten J, Edner H and Svanberg S 1996 Gas imaging by infrared gas-correlation spectrometry *Opt. Lett.* **21** 1945–7
[390] Baranne A, Mayor M and Poncet J L 1979 Coravel—a new tool for radial velocity measurements *Vistas Astron.* **23** 279–316
[391] Snik F and Keller C U 2019 Apparatus for determining presence of a gas Netherlands NL2020863B1, 11. 12 (available at: https://patents.google.com/patent/NL2020863B1/en)
[392] Fuchs C, Kuhn J, Bobrowski N and Platt U 2021 Quantitative imaging of volcanic SO_2 plumes using Fabry–Pérot interferometer correlation spectroscopy *Atmos. Meas. Tech.* **14** 295–307
[393] Cheriton R, Densmore A, Sivanandam S, de Mooij E, Cheben P, Xu D-X, Schmid J H and Janz S 2021 Fiber Fabry–Perot astrophotonic correlation spectroscopy for remote gas identification and radial velocity measurements *Appl. Opt.* **60** 1252–10263
[394] Verlaan A L *et al* 2017 Higs-instrument: design and demonstration of a high performance gas concentration imager *Proc. SPIE* **10562** 105625Z
[395] Gbadebo A A, Turitsyna E G and Williams J A R 2018 Fabrication of precise aperiodic multichannel fibre Bragg grating filters for spectral line suppression in hydrogenated standard telecommunications fibre *Opt. Express* **26** 1315–23
[396] Tuthill P 2022 Optical sensor and system *Australian Provisional Patent #* 2022901208
[397] Haffert S Y, Por E H and Keller C U 2019 Highly multiplexed Bragg gratings for large field of view gas sensing in planetary atmospheres *Opt. Express* **27** 33925–41
[398] Min S-S *et al* 2012 Multicore fibre Bragg grating developments for OH suppression *Proc. SPIE* **8450** 84503L
[399] MacLachlan D G *et al* 2014 Developing ultrafast laser inscribed volume gratings *Proc. SPIE* **9151** 91511H
[400] Haffert S Y 2021 Fundamental limit of single-mode integral-field spectroscopy *J. Opt. Soc. Am.* B **38** A27–A35
[401] McArthur S R, Siliprandi J, MacLachlan D G, Benoît A, Thomson R R and Ross C A 2022 Ultrafast laser inscription of efficient volume Bragg gratings deep in fused silica using active wavefront shaping *Opt. Mater. Express* **12** 3589–99
[402] Auer F F, Haffert S, Keller C, Snik F and Por E 2020 Exoplanet detection and characterization with highly multiplexed Bragg gratings *Proc. SPIE* **11447** 114474J
[403] Jones D J, Diddams S A, Ranka J K, Stentz A, Windeler R S and Hall J L 2000 Carrier-envelope phase control of femtosecond mode-locked lasers and direct optical frequency synthesis *Science* **288** 635–9
[404] Yao Y, Jiang Y, Yu H, Bi Z and Ma L 2017 Optical frequency divider with division uncertainty at the 10–21 level *Natl Sci. Rev.* **3** 463–9
[405] Boulder Atomic Clock Optical Network (BACON) Collaboration 2021 Frequency ratio measurements at 18-digit accuracy using an optical clock network *Nature* **591** 564–9
[406] Sinclair L C, Deschênes J-D, Sonderhouse L, Swann W C, Khader I H, Baumann E, Newbury N R and Coddington I 2015 Invited Article: a compact optically coherent fiber frequency comb *Rev. Sci. Instrum.* **86** 81301
[407] Yu N, Grudinin I and Tinto M 2017 Optical frequency comb application in time-delay interferometer *2017 Joint Conf. of the European Frequency and Time Forum and IEEE Int. Frequency Control Symp. (EFTF/IFCS)* pp 126–7
[408] Loeb D M 2015 Using atomic clocks to detect gravitational waves (arXiv:1501.00996)
[409] Derevianko A and Pospelov M 2014 Hunting for topological dark matter with atomic clocks *Nat. Phys.* **10** 933–6
[410] Ashby N *et al* 2009 Measurement of gravitational time delay using drag-free spacecraft and an optical clock *Proc. Int. Astron. Union* **5** 414–9
[411] Derevianko A, Gibble K, Hollberg L, Newbury N, Oates C, Safronova M, Sinclair L and Yu N 2021 Fundamental physics with a state-of-the-art optical clock in space (arXiv:2112.10817)
[412] Akiyama K *et al* 2019 First M87 event horizon telescope results. I. The shadow of the supermassive black hole *Astrophys. J. Lett.* **875** L4
[413] Frederick C, Olsen F, Terrien R, Mahadevan S, Quinlan F and Diddams S 2022 Thermal-light heterodyne spectroscopy with frequency comb calibration *Optica* **9** 221–30
[414] Scherrer P H 2012 The helioseismic and magnetic imager (HMI) investigation for the solar dynamics observatory (SDO) *Sol. Phys.* **275** 207–27
[415] Murphy M T, Th. Udem R H, Sizmann A, Pasquini L, Araujo-Hauck C, Dekker H, D'Odorico S, Fischer M, Hänsch T W and Manescau A 2007 High-precision wavelength calibration of astronomical spectrographs with laser frequency combs *Mon. Not. R. Astron. Soc.* **380** 839–47
[416] Fischer D A *et al* 2016 State of the field: extreme precision radial velocities *Publ. Astron. Soc. Pac.* **128** 066001
[417] Steinmetz T *et al* 2008 Laser frequency combs for astronomical observations *Science* **321** 1335–7
[418] Ycas G G *et al* 2012 Demonstration of on-sky calibration of astronomical spectra using a 25 GHz near-IR laser frequency comb *Opt. Express* **20** 6631
[419] Yi X *et al* 2016 Demonstration of a near-IR line-referenced electro-optical laser frequency comb for precision radial velocity measurements in astronomy *Nat. Commun.* **7** 1–9
[420] Metcalf A J *et al* 2019 Stellar spectroscopy in the near-infrared with a laser frequency comb *Optica* **6** 233

[421] Obrzud E et al 2018 Broadband near-infrared astronomical spectrometer calibration and on-sky validation with an electro-optic laser frequency comb Opt. Express 26 34830–41
[422] Bartels A, Heinecke D and Diddam S A 2009 10-GHz self-referenced optical frequency comb Science 326 681
[423] Endo M, Ito I and Kobayashi Y 2015 Direct 15-GHz mode-spacing optical frequency comb with a Kerr-lens mode-locked Yb: Y_2O_3 ceramic laser Opt. Express 23 1276–82
[424] Suh M G et al 2019 Searching for exoplanets using a microresonator astrocomb Nat. Photon. 13 25–30
[425] Girard S et al 2019 Overview of radiation induced point defects in silica-based optical fibers Rev. Phys. 4 100032
[426] Zhang M, Buscaino B, Wang C, Shams-Ansari A, Reimer C, Zhu R, Kahn J M and Lončar M 2019 Broadband electro-optic frequency comb generation in a lithium niobate microring resonator Nature 568 373–7
[427] Hickstein D D et al 2017 Ultrabroadband supercontinuum generation and frequency-comb stabilization using on-chip waveguides with both cubic and quadratic nonlinearities Phys. Rev. Appl. 8 014025
[428] Yu M, Desiatov B, Okawachi Y, Gaeta A L and Lončar M 2019 Coherent two-octave-spanning supercontinuum generation in lithium-niobate waveguides Opt. Lett. 44 1222–5
[429] Wu T, Ledezma L, Fredrick C, Sekhar P, Sekine R, Guo Q, Briggs R, Marandi A and Diddams S A 2022 Ultraviolet to near-infrared frequency comb generation in lithium niobate nanophotonic waveguides with chirped poling Conf. on Lasers and Electro-Optics, Technical Digest Series (Optica Publishing Group) pp FW4J.2
[430] Liu X, Bruch A W, Lu J, Gong Z, Surya J B, Zhang L, Wang J, Yan J and Tang H X 2019 Beyond 100 THz-spanning ultraviolet frequency combs in a non-centrosymmetric crystalline waveguide Nat. Commun. 10 2971
[431] Lamee K F, Carlson D R, Newman Z L, Su-Peng Y and Papp S B 2020 Nanophotonic tantala waveguides for supercontinuum generation pumped at 1560 nm Opt. Lett. 45 4192–5
[432] Li M et al 2022 Integrated pockels laser Nat. Commun. 13 5344
[433] Juanjuan L, Surya J B, Liu X, Yuntao X and Tang H X 2019 Octave-spanning supercontinuum generation in nanoscale lithium niobate waveguides Opt. Lett. 44 1492–5
[434] Chen H et al 2021 Supercontinuum generation in high order waveguide mode with near-visible pumping using aluminum nitride waveguides ACS Photonics 8 1344–52
[435] Amirhassan S-A et al 2019 Supercontinuum generation in angle-etched diamond waveguides Opt. Lett. 44 4056–9
[436] Nakamura K, Kashiwagi K, Okubo S and Inaba H 2021 Erbium-doped-fiber-based broad visible range frequency comb with a 30 GHz mode spacin g for astronomical applications (arXiv:2110.03823)
[437] Lovis C and Fischer D 2010 Exoplanets ed S Seager (University of Arizona Press) pp 27–53 (available at: https://ui.adsabs.harvard.edu/abs/2010exop.book...27L/abstract)
[438] Probst R A, Steinmetz T, Wilken T, Wong G K L, Hundertmark H, Stark S P, Russell P S J, Hänsch T W, Holzwarth R and Udem T 2013 Spectral flattening of supercontinua with a spatial light modulator Proc. SPIE 8864 706–13
[439] Carlson D R, Hutchison P, Hickstein D D and Papp S B 2019 Generating few-cycle pulses with integrated nonlinear photonics Opt. Express 27 37374
[440] Porcel M A G et al 2017 Two-octave spanning supercontinuum generation in stoichiometric silicon nitride waveguides pumped at telecom wavelengths Opt. Express 25 1542–54
[441] Woods J R C, Daykin J, Tong A S K, Lacava C, Petropoulos P, Tropper A C, Horak P, Wilkinson J S and Apostolopoulos V 2020 Supercontinuum generation in tantalum pentoxide waveguides for pump wavelengths in the 900 nm to 1500 nm spectral region Opt. Express 28 32173–84
[442] Baxter G et al 2006 Highly programmable wavelength selective switch based on liquid crystal on silicon switching elements 2006 Optical Fiber Communication Conf. and the National Fiber Optic Engineers Conf. (Anaheim, CA) p 3
[443] Lionix International Multi Project Wafer Services (available at: www.lionix-international.com/photonics/mpw-services/)
[444] Tervonen A, West B R and Honkanen S 2011 Ion-exchanged glass waveguide technology: a review Opt. Eng. 50 071107
[445] Perot A and Fabry C 1899 On the application of interference phenomena to the solution of various problems of spectroscopy and metrology Astrophys. J. 9 87
[446] Park N, Dawson J W and Vahala K J 1993 Frequency locking of an erbium-doped fiber ring laser to an external fiber Fabry–Perot resonator Opt. Lett. 18 879–81
[447] Ben-Ami S, López-Morales M, Garcia-Mejia J, Abad G G and Szentgyorgyi A 2018 High-resolution spectroscopy using Fabry–Perot interferometer arrays: an application to searches for O_2 in exoplanetary atmospheres Astrophys. J. 861 79
[448] Prabhakar M, Raju K P and Chandrasekhar T 2019 Characteristics of the solar coronal line profiles from Fabry–Perot interferometric observations Sol. Phys. 294 26
[449] Bailén F J, Orozco Suárez D and Del Toro Iniesta J C 2020 On Fabry–Pérot Etalon-based instruments. III. Instrument applications Astrophys. J. Suppl. Ser. 246 17
[450] Wildi F, Pepe F, Chazelas B, Curto G L and Lovis C 2010 A Fabry-Perot calibrator of the HARPS radial velocity spectrograph: performance report Proc. SPIE 7735 11
[451] Mégevand D et al 2014 ESPRESSO: the radial velocity machine for the VLT Proc. SPIE 9147 91471H
[452] Cersullo F, Wildi F, Chazelas B and Pepe F 2017 A new infrared Fabry-Pérot-based radial-velocity-reference module for the SPIRou radial-velocity spectrograph Astron. Astrophys. 601 A102
[453] Schäfer S, Guenther E W, Reiners A, Winkler J, Pluto M and Schiller J 2018 Two Fabry-Pérots and two calibration units for CARMENES Proc. SPIE 10702 1070276
[454] Terrien R C et al Broadband stability of the habitable zone planet finder Fabry–Pérot Etalon calibration system: evidence for chromatic variation Astron. J. 161 252
[455] Stuermer J et al 2016 A rubidium traced white-light etalon calibrator for MAROON-X Proc. SPIE 9912 991229
[456] Schwab C, Stürmer J, Gurevich Y V, Führer T, Lamoreaux S K, Walther T and Quirrenbach A 2015 Stabilizing a Fabry–Perot Etalon Peak to 3 cm s^{-1} for spectrograph calibration Publ. Astron. Soc. Pac. 127 880
[457] Leifer S et al 2020 A microresonator-based etalon for visible light precision radial velocity measurements Proc. SPIE 11447 114471L
[458] Tang L, Ye H, Hao J, Wei R and Xiao D 2021 Design and characterization of a thermally stabilized fiber Fabry–Perot etalon as a wavelength calibrator for high-precision spectroscopy Appl. Opt. 60 D1–D8
[459] Jennings J, Halverson S, Terrien R, Mahadevan S, Ycas G and Diddams S A 2017 Frequency stability characterization of a broadband fiber Fabry-Perot interferometer Opt. Express 25 15599–613
[460] Hartmann P, Jedamzik R, Carré A, Krieg J and Westerhoff T 2021 Glass ceramic ZERODUR®: even closer to zero thermal expansion: a review, part 1 J. Astron. Telesc. Instrum. Syst. 7 020901

[461] Hartmann P, Jedamzik R, Carré A, Krieg J and Westerhoff T 2021 Glass ceramic ZERODUR®: even closer to zero thermal expansion: a review, part 2 *J. Astron. Telesc. Instrum. Syst.* **7** 020902
[462] Gulati S T and Edwards M J 1997 ULE—Zero expansion, low density, and dimensionally stable material for lightweight optical systems *Proc. SPIE* **10289** 1028909
[463] Hao J, Tang L, Ye H, Hao Z, Han J, Zhai Y, Zhang K, Wei R and Xiao D 2021 Effect of near-field distribution on transmission characteristics of fiber-fed Fabry–Perot Etalons *Astron. J.* **161** 258
[464] Schmidt T M, Chazelas B, Lovis C, Dumusque X, Bouchy F, Pepe F, Figueira P and Sosnowska D 2022 Chromatic drift of the espresso Fabry-Pérot Etalon *Astron. Astrophys.* **664** A191
[465] Savchenkov M 2018 Calcium fluoride whispering gallery mode optical resonator with reduced thermal sensitivity *J. Opt.* **20** 035801
[466] Birks T A, Knight J C and Russell P S J 1997 Endlessly single-mode photonic crystal fiber *Opt. Lett.* **22** 961–3
[467] Mourard D, Bério P, Perraut K, Clausse J-M, Creevey O, Martinod M-A, Meilland A, Millour F and Nardetto N 2017 SPICA, stellar parameters and images with a cophased array: a 6T visible combiner for the CHARA array *J. Opt. Soc. Am.* A **34** A37–A46
[468] GRAVITY Collaboration 2018 Spatially resolved rotation of the broad-line region of a quasar at sub-parsec scale *Nature* **563** 657–60
[469] Dong S *et al* 2019 First resolution of microlensed images *Astrophys. J.* **871** 70
[470] Perraut K *et al* (The GRAVITY Collaboration) 2019 The GRAVITY Young Stellar object survey: I. Probing the disks of Herbig Ae/Be stars in terrestrial orbits *Astron. Astrophys.* **632** A53
[471] Berger J P, Haguenauer P, Kern P, Perraut K, Malbet F, Schanen I, Severi M, Millan-Gabet R and Traub W 2001 Integrated optics for astronomical interferometry: IV. First measurements of stars *Astron. Astrophys.* **376** L31–L34
[472] Benisty M, Berger J-P, Jocou L, Labeye P, Malbet F, Perraut K and Kern P 2009 An integrated optics beam combiner for the second generation VLTI instruments *Astron. Astrophys.* **498** 601–13
[473] Labeye P 2008 Composants optiques intégrés pour l'Interférométrie astronomique *Theses* Institut National Polytechnique de Grenoble—INPG
[474] Pannetier C *et al* 2022 SPICA-FT: the new fringe-tracker of the CHARA array *Proc. SPIE* **11446** 1218309
[475] Martin G *et al* 2022a Hybrid electro-optic visible multi-telescope beam combiner for next generation FIRST/SUBARU instruments *Proc. SPIE* **12188** 121885Y
[476] Miarabbas Kiani K, Frankis H C, Naraine C M, Bonneville D B, Knights A P and Bradley J D B 2022 Lasing in a hybrid rare-earth silicon microdisk *Laser Photonics Rev.* **16** 2100348
[477] Cvetojevic N, Martinache F, Chingaipe P, Laugier R, Ławniczuk K, Broeke R G, Ligi R, N'Diaye M and Mary D 2022 3-beam self-calibrated Kernel nulling photonic interferometer (arXiv:2206.04977)
[478] Jia L, Song J, Liow T-Y, Luo X, Tu X, Fang Q, Koh S-C, Yu M and Lo G 2014 Mode size converter between high-index-contrast waveguide and cleaved single mode fiber using SiON as intermediate material *Opt. Express* **22** 23652
[479] Davis K M, Miura K, Sugimoto N and Hirao K 1996 Writing waveguides in glass with a femtosecond laser *Opt. Lett.* **21** 1729–31
[480] Jovanovic N *et al* 2012 Starlight demonstration of the Dragonfly instrument: an integrated photonic pupil-remapping interferometer for high-contrast imaging: starlight demonstration of Dragonfly *Mon. Not. R. Astron. Soc.* **427** 806–15
[481] Martinod M-A, Tuthill P, Gross S, Norris B, Sweeney D and Withford M J 2021 Achromatic photonic tricouplers for application in nulling interferometry *Appl. Opt.* **60** D100
[482] Martin G, Vázquez De Aldana J R, Rodenas A, d'Amico C and Stoian R 2016 Recent results on photonic devices made by laser writing: 3D 3T near IR waveguides, mid-IR spectrometers and electro-optic beam combiners *Proc. SPIE* **9907** 990739
[483] Ceccarelli F, Atzeni S, Prencipe A, Farinaro R and Osellame R 2019 Thermal phase shifters for femtosecond laser written photonic integrated circuits *J. Lightwave Technol.* **37** 4275–81
[484] Martin G, Heidmann S, Rauch J-Y, Jocou L and Courjal N 2014 Electro-optic fringe locking and photometric tuning using a two-stage Mach–Zehnder lithium niobate waveguide for high-contrast mid-infrared interferometry *Opt. Eng.* **53** 034101
[485] Vergara G, Linares Herrero R, Gutíerrez Álvarez R, Fernández-Montojo C, Gómez L J, Villamayor V, Baldasano Ramírez A and Montojo M T 2013 80×80 VPD PbSe: the first uncooled MWIR FPA monolithically integrated with a Si-CMOS ROIC *Proc. SPIE* **8704** 87041M
[486] Callejo M, Bonduelle M, Morand A, Zhang G, Lv J, Cheng G, D'Amico C, Stoian R and Martin G 2022 Waveguide scattering antennas made by direct laser writing in bulk glass for spectrometry applications in the short-wave IR *Appl. Opt.* **61** 7173
[487] Martin G *et al* 2022b FIRST 5T 3D: a laser written device for FIRST/SUBARU reducing crosstalk and propagation losses *Proc. SPIE* **12188** 121882T
[488] Bonduelle M, Martin G, Morand A, Vazquez De Aldana R, Romero Vázquez J, Courjal C and Coste N A 2022 Development of mid-IR waveguides to implement high resolution spectrometers in integrated optics *Proc. SPIE* **12188** 121885R
[489] Kendrick R, Duncan A, Wilm J, Thurman S T, Stubbs D M and Ogden C 2013 Flat panel space based space surveillance sensor *Advanced Maui Optical and Space Surveillance Technologies Conf.*
[490] Kern P, Malbet F, Schanen-Duport I and Benech P 1997 Integrated optics single-mode interferometric beam combiner for near infrared astronomy *Integrated Optics for Astronomical Interferometry* p 115
[491] LeBouquin J B *et al* 2004 First observations with an H-band integrated optics beam combiner at the VLTI *Astron. Astrophys.* **424** 719–26
[492] Berger J P *et al* 4838 Integrated-optics 3-way beam combiner for IOTA *Proc. SPIE* **4838** 1099–106
[493] Le Bouquin J B, Berger J P, Lazareff B, Zins G, Haguenauer P, Jocou L and Ventura N 2011 PIONIER: a 4-telescope visitor instrument at VLTI *Astron. Astrophys.* **535** A67
[494] Montargès M, Norris R, Chiavassa A, Tessore B, Lèbre A and Baron F 2018 The convective photosphere of the red supergiant CE Tauri-I. VLTI/PIONIER H-band interferometric imaging *Astron. Astrophys.* **614** A12
[495] Sanchis P, Galan J V, Griol A, Marti J, Piqueras M A and Perdigues J M 2007 Low-crosstalk in silicon-on-insulator waveguide crossings with optimized-angle *IEEE Photonics Technol. Lett.* **19** 1583–5
[496] Ródenas A, McCarthy J, Psaila N D, Brown G, Bookey H T, Thomson R R and Kar A K 2012 Mid-infrared photonics enabled by 3D laser writing chalcogenide glass *Proc. SPIE* **8542** 854217
[497] Christodoulides D, Lederer F and Silberberg Y 2003 Discretizing light behaviour in linear and nonlinear waveguide lattices *Nature* **424** 817–23
[498] Minardi S and Pertsch T 2010 Interferometric beam combination with discrete optics *Opt. Lett.* **35** 3009–11
[499] Minardi S 2012 Photonic lattices for astronomical interferometry *Mon. Not. R. Astron. Soc.* **422** 2656–60

[500] Saviauk A, Minardi S, Dreisow F, Nolte S and Pertsch T 2013 3D-integrated optics component for astronomical spectro-interferometry *Appl. Opt.* **52** 4556–65
[501] Pedretti E, Piacentini S, Corrielli G, Osellame R and Minardi S 2018 A six-apertures discrete beam combiners for J-band interferometry *Proc. SPIE* **10701** 316–25
[502] Nayak A S *et al* 2021 First stellar photons for an integrated optics discrete beam combiner at the William Herschel Telescope *Appl. Opt.* **60** D129–42
[503] Shankar Nayak A, Poletti T, Kumar Sharma T, Madhav K, Pedretti E, Labadie L and Roth M M 2020 Chromatic response of a four-telescope integrated-optics discrete beam combiner at the astronomical L band *Opt. Express* **28** 34346–61
[504] Harris R J, Tepper J, Davenport J J, Pedretti E, Haynes D M, Hottinger P and Haynes R 2018 NAIR: novel astronomical instrumentation through photonic reformatting *Proc. SPIE* **10706** 157–71
[505] Kraus S, Monnier J, Harries T, Dong R, Bate M, Whitney B, and van Belle G 2014 The science case for the Planet Formation Imager (PFI) *Proc. SPIE* **9146** 326–38
[506] Monnier J D *et al* 2018 The planet formation imager *Exp. Astron.* **46** 517–29
[507] Creech-Eakman M J, Buscher D F, Haniff C A and Romero V D 2004 The Magdalena Ridge Observatory Interferometer: a fully optimized aperture synthesis array for imaging *Proc. SPIE* **5491** 405–14
[508] Malbet F, Benisty M, De Wit W J, Kraus S, Meilland A, Millour F and Ventura N 2007 Disk and wind interaction in the young stellar object MWC 297 spatially resolved with AMBER/VLTI *Astron. Astrophys.* **464** 43–53
[509] Kraus S, Hofmann K H, Benisty M, Berger J P, Chesneau O, Isella A and Weigelt G 2008 The origin of hydrogen line emission for five Herbig Ae/Be stars spatially resolved by VLTI/AMBER spectro-interferometry *Astron. Astrophys.* **489** 1157–73
[510] Bouvier J, Perraut K, Le Bouquin J B, Duvert G, Dougados C, Brandner W and Alécian E 2020 Probing the magnetospheric accretion region of the young pre-transitional disk system DoAr 44 using VLTI/GRAVITY *Astron. Astrophys.* **636** A108
[511] Diener R, Nolte S, Pertsch T and Minardi S 2018 Effects of stress on neighboring laser written waveguides in gallium lanthanum sulfide *Appl. Phys. Lett.* **112** 111908
[512] Romanova M M and Owocki S P 2015 Accretion, outflows, and winds of magnetized stars *Space Sci. Rev.* **191** 339–89
[513] Kraus S, Le Bouquin J B, Kreplin A, Davies C L, Hone E, Monnier J D and Hinkley S 2020 Spin–orbit alignment of the β Pictoris planetary system *Astrophys. J. Lett.* **897** L8
[514] Garanovich I L, Longhi S, Sukhorukov A A and Kivshar Y S 2012 Light propagation and localization in modulated photonic lattices and waveguides *Phys. Rep.* **518** 1–79
[515] Wang Y, Luo J, Sun K, Roth B and Zhang Z 2019 Integrated echelle gratings as compact spectrometer for VIS and NIR astronomy *2019 Conf. on Lasers and Electro-Optics Europe & European Quantum Electronics Conf. (CLEO/Europe-EQEC)* (*Munich, Germany*) p 1
[516] Benoît A *et al* 2021 Ultrafast laser inscription of asymmetric integrated waveguide 3 dB couplers for astronomical K-band interferometry at the CHARA array *J. Opt. Soc. Am.* B **38** 2455–64
[517] Corrielli G, Atzeni S, Piacentini S, Pitsios I, Crespi A and Osellame R 2018 Symmetric polarization-insensitive directional couplers fabricated by femtosecond laser writing *Opt. Express* **26** 15101–9
[518] Diab M, Dinkelaker A N, Davenport J, Madhav K and Roth M M 2021 Starlight coupling through atmospheric turbulence into few-mode fibres and photonic lanterns in the presence of partial adaptive optics correction *Mon. Not. R. Astron. Soc.* **501** 1557–67
[519] Froehly C 1981 Coherence and interferometry through optical fibers *Scientific Importance of High Angular Resolution at Infrared and Optical Wavelengths* pp 285–93
[520] Perrin G 2006 Interferometric coupling of the Keck telescopes with single-mode fibers *Science* **311** 194
[521] Shaklan S B and Roddier F 1987 Single-mode fiber optics in a long-baseline interferometer *Appl. Opt.* **26** 2159–63
[522] du Foresto V C, Perrin G S, Ruilier C, Mennesson B P, Traub W A and Lacasse M G 1998 FLUOR fibered instrument at the IOTA interferometer *Proc. SPIE* **3350** 856–63
[523] Woillez J, Lai O, Perrin G, Reynaud F, Baril M, Dong Y and F´edou P 2017 AGILIS: agile guided interferometer for longbaseline imaging synthesis. Demonstration and concepts of reconfigurable optical imaging interferometers *Astron. Astrophys.* **602** A116
[524] Peiqian Z, Mariotti J-M, du Foresto V C, Lena P J and Perrin G S 1995 Multistage fiber optic delay line for astronomical interferometry *Proc. SPIE* **2476** 108–19
[525] Reynaud F, Alleman J J and Connes P 1992 Interferometric control of fiber lengths for a coherent telescope array *Appl. Opt.* **31** 3736–43
[526] Simohamed L M, Auguste J L, Rioublanc J, Blondy M and Reynaud F 1999 Analysis of chromatic dispersion variation in optical fiber under large stretching *Opt. Fiber Technol.* **5** 403–11
[527] Allured A and Ashcom J B 2021 Broadband chromatic dispersion in fiber-coupled optical interferometry *Appl. Opt.* **60** 6371–84
[528] Sato K, Nishikawa J, Yoshizawa M, Fukushima T, Torii Y, Matsuda K K, Iwashita H, Suzuki S and Saint-Jacques D 2000 Experiments with the fiber-connected interferometer for the MIRA project *Proc. SPIE* **4006** 1102–6
[529] Huss G, Delage L, Longueteau E and Reynaud F 2003 Characterization of the differential dispersion in a kilometric silica fiber stellar interferometer *Proc. SPIE* **4838** 321–8
[530] Vergnole S, Kotani T, Perrin G, Delage L and Reynaud F 2005 Calibration of silica fibers for the Optical Hawaiian Array for Nanoradian Astronomy ('OHANA): temperature dependence of differential chromatic dispersion *Opt. Commun.* **251** 115–23
[531] Lehmann L 2019 Environmental characterisation and stabilisation of a 2×200-meter outdoor fibre interferometer at the CHARA array *Exp. Astron.* **47** 303–12
[532] Magri J, Grossard L, Reynaud F, Fabert M, Delage L, Krawczyk R and Le Duigou J M 2022 Outdoor fibre link between two telescopes and the lab of the CHARA array at 810 nm. Demonstration of the optical path servo control *Research Square Preprint* (Version 1) (https://doi.org/10.21203/rs.3.rs-2014442/v1)
[533] Pannetier C, Mourard D, Cassaing F, Lagarde S, Le Bouquin J B, Monnier J, Sturmann J and Ten Brummelaar T 2021 Compensation of differential dispersion: application to multiband stellar interferometry *Mon. Not. R. Astron. Soc.* **507** 1369–80
[534] Lazareff B, Le Bouquin J-B and Berger J-P 2012 A novel technique to control differential birefringence in optical interferometers-demonstration on the PIONIER-VLTI instrument *Astron. Astrophys.* **543** A31
[535] Anugu N *et al* 2020 MIRC-X: a highly sensitive six-telescope interferometric imager at the CHARA array *Astron. J.* **160** 158
[536] Caillaud C, Renversez G, Brilland L, Mechin D, Calvez L, Adam J-L and Troles J 2014 Photonic bandgap propagation in all-solid chalcogenide microstructured optical fibers *Materials* **7** 6120–9
[537] Jiang X, Joly N Y, Finger M A, Babic F, Wong G K L, Travers J C and Russell P S J 2015 Deep-ultraviolet to mid-infrared supercontinuum generated in solid-core ZBLAN photonic crystal fibre *Nat. Photon.* **9** 133–9
[538] Sturmann J The pipes of pan mirrors

[539] Vergnole S, Delage L, Reynaud F, Labonté L, Roy P, Mélin G and Gasca L 2005 Test of photonic crystal fiber in broadband interferometry *Appl. Opt.* **44** 2496–500
[540] Fulton B J *et al* 2021 California legacy survey. II. Occurrence of giant planets beyond the ice line *Astrophys. J. Suppl. Ser.* **255** 14
[541] Fujii Y, Kawahara H, Suto Y, Taruya A, Fukuda S, Nakajima T and Turner E 2010 Colors of a second earth: estimating the fractional areas of ocean, land, and vegetation of earth-like exoplanets *Astrophys. J.* **715** 866–80
[542] Seager S and Deming D 2010 Exoplanet atmospheres *Annu. Rev. Astron. Astrophys.* **48** 631–72
[543] Seager S, Bains W and Petkowski J J 2016 Toward a list of molecules as potential biosignature gases for the search for life on exoplanets and applications to terrestrial biochemistry *Astrobiology* **16** 465–85
[544] Wallace A L, Ireland M J and Federrath C 2021 Constraints on planets in nearby young moving groups detectable by high-contrast imaging and Gaia astrometry *Mon. Not. R. Astron. Soc.* **508** 2515–23
[545] Bracewell R N 1978 Detecting nonsolar planets by spinning infrared interferometer *Nature* **274** 780–1
[546] Martinod M-A *et al* 2021 Scalable photonic-based nulling interferometry with the dispersed multi-baseline GLINT instrument *Nat. Commun.* **12** 2465
[547] Quanz S P, Kammerer J, Defrère D, Absil O, Glauser A M and Kitzmann D 2018 Exoplanet science with a space-based mid-infrared nulling interferometer *Proc. SPIE* **10701** 107011I
[548] Hanot C, Mennesson B, Martin S, Liewer K, Loya F, Mawet D, Riaud P, Absil O and Serabyn E 2011 Improving interferometric null depth measurements using statistical distributions: theory and first results with the palomar fiber nuller *Astrophys. J.* **729** 110
[549] Lagadec T, Norris. B, Gross S, Arriola A, Gretzinger T, Cvetojevic N, Martinod M-A, Jovanovic N, Withford M and Tuthill P 2021 The GLINT south testbed for nulling interferometry with photonics: design and on-sky results at the Anglo-Australian telescope *Publ. Astron. Soc. Aust.* **38** 2021
[550] Nowak M, Lacour S, Lapeyrère V, David L, Crouzier A, Dufoing C, Faiz H, Lemoult T and Trébuchet P 2016 Reaching sub-milimag photometric precision on Beta Pictoris with a nanosat: the PicSat mission *Proc. SPIE* **9904** 99044L
[551] Martin G *et al* 2020 Recent results on electro-optic visible multi-telescope beam combiner for next generation FIRST/SUBARU instruments: hybrid and passive devices *Proc. SPIE* **11446** 1144626
[552] Cvetojevic N, Martinache F, Chingaipe P, Laugier R, N'Diaye M, Ligi R and Mary D 2022 Closed-loop on-chip phase control and fringe tracking in photonic interferometers *Proc. SPIE* **12183** 1218318
[553] Angel J R P and Woolf N J 1997 An imaging nulling interferometer to study extrasolar planets *Astrophys. J.* **475** 373–9
[554] Laugier R *et al* 2023 Asgard/NOTT: L-band nulling interferometry at the VLTI. I. Simulating the expected high-contrast performance *Astron. Astrophys.* **671**
[555] Klinner-Teo T, Martinod M-A, Tuthill P, Gross S, Norris B and Leon-Saval S 2022 Achromatic design of a photonic tricoupler and phase shifter for broadband nulling interferometry *J. Astron. Telesc. Instrum. Syst.* **8** 2022
[556] Spalding E, Defrère D and Ertel S 2022 Unveiling exozodiacal light *Phys. Today* **75** 46–52
[557] Serabyn E, Mennesson B, Martin S, Liewer K and Kühn J 2019 Nulling at short wavelengths: theoretical performance constraints and a demonstration of faint companion detection inside the diffraction limit with a rotating-baseline interferometer *Mon. Not. R. Astron. Soc.* **489** 1291–303
[558] Jennison R C 1958 A phase sensitive interferometer technique for the measurement of the Fourier transforms of spatial brightness distributions of small angular extent *Mon. Not. R. Astron. Soc.* **118** 276–84
[559] Baldwin J E, Haniff C A, Mackay C D and Warner P J 1986 Closure phase in high-resolution optical imaging *Nature* **320** 595–7
[560] Martinache F 2010 Kernel phase in Fizeau interferometry *Astrophys. J.* **724** 464
[561] Velusamy T, Angel R P, Eatchel A, Tenerelli D and Woolf N J 2003 Single and double Bracewell nulling interferometer in space *ESASP* vol 539 pp 631–6
[562] Serabyn E, Mennesson B, Martin C, M. M, Koresko C and Kuchner M J 2012 The keck interferometer nuller *Astrophys. J.* **748** 55
[563] Lacour S, Tuthill P, Monnier J D, Kotani T, Gauchet L and Labeye P 2014 A new interferometer architecture combining nulling with phase closure measurements *Mon. Not. R. Astron. Soc.* **439** 4018–29
[564] Martinache F and Ireland M J 2018 Kernel-nulling for a robust direct interferometric detection of extrasolar planets *Astron. Astrophys.* **619** 1–10
[565] Guyon O, Mennesson B, Sarabyn E and Martin S 2013 Optimal beam combiner design for nulling interferometers *Publ. Astron. Soc. Pac.* **125** 951
[566] Laugier R, Cvetojevic N and Martinache F 2020 Kernel nullers for an arbitrary number of apertures *Astron. Astrophys.* **642** A202
[567] Stirling C J *et al* 2021 Broadband 2 × 2 multimode interference coupler for mid-infrared wavelengths *Opt. Lett.* **46** 5300–3
[568] Halir R, Cheben P, Luque-González J M, Sarmiento-Merenguel J D, Schmid J H, Wangüemert-Pérez G, Xu D-X, Wang S, Ortega-Moñux A and Molina-Fernández Í 2016 Ultra-broadband nanophotonic beamsplitter using an anisotropic sub-wavelength metamaterial *Laser Photonics Rev.* **10** 1039–46
[569] Kojima K, Tahersima M H, Koike-Akino T, Jha D K, Tang Y, Wang Y and Parsons K 2021 Deep neural networks for inverse design of nanophotonic devices *J. Lightwave Technol.* **39** 1010–9
[570] Serabyn E 2021 The WSPC handbook of astronomical instrumentation *Nulling Interferometry* vol 3 ed A M Moore UV, Optical & IR Instrumentation: Part 2 (World Scientific) pp 71–89
[571] Wallner O, Perdigues Armengol J M and Karlsson A L 2004 Multiaxial single-mode beam combiner1 *Proc. SPIE* **5491** 798
[572] Haguenauer P and Serabyn E 2006 Deep nulling of laser light with a single-mode-fiber beam combiner *Appl. Opt.* **45** 2749
[573] Mennesson B, Ollivier M and Ruilier C 2002 Use of single-mode waveguides to correct the optical defects of a nulling interferometer *J. Opt. Soc. Am.* A **19** 596
[574] Martin S, Serabyn G, Liewer K and Mennesson B 2017 Achromatic broadband nulling using a phase grating *Optica* **4** 110
[575] Ruane G, Wang J, Mawet D, Jovanovic N, Delorme J-R, Mennesson B and Wallace J K 2018 Efficient spectroscopy of exoplanets at small angular separations with vortex fiber nulling *Astrophys. J.* **867** 143
[576] Echeverri D, Ruane G, Jovanovic N, Mawet D and Levraud N 2019 Vortex fiber nulling for exoplanet observations I Experimental demonstration in monochromatic light *Opt. Lett.* **44** 2204
[577] Serabyn E, Ruane G J and Echeverri D 2022 Observing inside the coronagraphic regime with optimized single-mode nulling interferometry *Proc. SPIE* **12180** 199–210
[578] Echeverri D *et al* 2022 Phase II of the Keck Planet Imager and characterizer: system-level laboratory characterization and preliminary on-sky commissioning *Proc. SPIE* **12184** 658–70
[579] Xin Y *et al* 2022 Efficient detection and characterization of exoplanets within the diffraction limit: nulling with a mode-selective photonic lantern *Astrophys. J.* **938** 140
[580] Paschotta R 2022 LP modes *RP Photonics* (available at: www.rp-photonics.com/lp_modes.html)

[581] Serabyn E 2000 Nulling interferometry: symmetry requirements and experimental results *Proc. SPIE* **4006** 328
[582] Martin S, Serabyn E, Liewer K, Loya F, Mennesson B, Hanot C and Mawet D 2008 The development and applications of a ground-based fiber nulling coronagraph *Proc. SPIE* **7013** 70131Y
[583] Gappinger R O, Diaz R T, Ksendzov A, Lawson P R, Lay O P, Liewer K M, Loya F M, Martin S R, Serabyn E and Wallace J K 2009 Experimental evaluation of achromatic phase shifters for mid-infrared starlight suppression *Appl. Opt.* **48** 868
[584] Ksendzov A *et al* 2006 Measurement of spatial filtering capabilities of single mode infrared fibers *Proc. SPIE* **6268** 626838
[585] Sillard P 2020 Advances in few-mode fiber design and manufacturing *Optical Fiber Communication Conf. (OFC) 2020* (Optica Publishing Group) p W1B.4
[586] Poletti F 2022 Recent updates on hollow core fibre technology *Proc. SPIE* **PC12142** PC1214210
[587] Artyushenko V, Bocharnikov A, Sakharova T and Usenov I 2014 Mid-infrared fiber optics for 1–18 μm range: IR-fibers and waveguides for laser power delivery and spectral sensing *Opt. Photon.* **9** 35–39
[588] Hale D D S, Bester M, Danchi W C, Fitelson W, Hoss S, Lipman E A, Monnier J D, Tuthill P G and Townes C H 2000 The berkeley infrared spatial interferometer: a heterodyne stellar interferometer for the mid-infrared *Astrophys. J.* **537** 998
[589] Darré P, Baudoin R, Gomes J-T, Scott N J, Delage L, Grossard L, Sturmann J, Farrington C, Reynaud F and Ten Brummelaar T A 2016 First on-sky fringes with an up-conversion interferometer tested on a telescope array *Phys. Rev. Lett.* **117** 233902
[590] Lehmann L *et al* 2019 Towards a mid-infrared *L* band up-conversion interferometer: first on-sky sensitivity test on a single arm *Mon. Not. R. Astron. Soc.* **485** 3595–9
[591] Gottesman D, Jennewein T and Croke S 2012 Longer-baseline telescopes using quantum repeaters *Phys. Rev. Lett.* **109** 070503
[592] Brown M, Valerian T, Markus A, Michael R, Brian S, Paul K and John M 2022 Long-baseline interferometry using single photon states as a non-local oscillator *Proc. SPIE* **12015** 120150E
[593] Ireland M J and Monnier J D 2014 A dispersed heterodyne design for the planet formation imager *Proc. SPIE* **9146** 914612
[594] Hakl M *et al* 2021 Ultra-fast quantum-well infared photodetectors operating at 10 μm with flat response up to 70GHz at room temperature *ACS Photonics* **8** 464–71
[595] Bigioli A *et al* 2020 Mixing properties of room temperature patch-antenna receivers in a mid-infrared ($\lambda \approx 9$ μm) heterodyne system *Laser Photonics Rev.* **14** 1900207
[596] Bourdarot G, Berger J-P and de Chatellus H G 2022 Multi-delay photonic correlator for wideband RF signal processing *Optica* **9** 325
[597] Bourdarot G, Berger J-P and de Chatellus H G 2021 Architecture of photonics correlation for infrared heterodyne interferometry: demonstration of amplitude-modulation based correlation *J. Opt. Soc. Am.* B **38** 3105
[598] Lehmann L, Darré P, Boulogne H, Delage L, Grossard L and Reynaud F 2018 Multichannel spectral mode of the ALOHA up-conversion interferometer *Mon. Not. R. Astron. Soc.* **477** 190–4
[599] Bland-Hawthorn J, Sellars M and Bartholomew J 2021 Quantum memories and the double-slit experiment: implications for astronomical interferometry *J. Opt. Soc. Am. B* **38** A86–A98
[600] Palaferri D *et al* 2018 Room-temperature nine-μm-wavelength photodetectors and GHz-frequency heterodyne receivers *Nature* **556** 85–88
[601] Quinchard G *et al* 2022 High speed, antenna-enhanced 10.3 μm quantum cascade detector *Appl. Phys. Lett.* **120** 091108
[602] Rodriguez E, Bonazzi T, Dely H, Mastrangelo M, Pantzas K, Beaudoin G, Sagnes I, Vasanelli A, Todorov Y and Sirtori C 2022 Metamaterial engineering for optimized photon absorption in unipolar quantum devices *Opt. Express* **30** 20515
[603] Cakmakyapan S, Lu P K, Navabi A and Jarrahi M 2018 Gold-patched graphene nano-stripes for high-responsivity and ultrafast photodetection from the visible to infrared regime *Light Sci. Appl.* **7** 20
[604] Ye H, Leroi F, Pontagnier L, Santarelli G, Boullet J and Cormier E 2022 High-power nonlinear amplification of an ultrafast electro-optic frequency comb with flexible GHz repetition rate *Opt. Express* **30** 10605–13
[605] Kowligy A S, Carlson D R, Hickstein D D, Timmers H, Lind A J, Schunemann P G, Papp S B and Diddams S A 2020 Mid-infrared frequency combs at 10 GHz *Opt. Lett.* **45** 3677–80
[606] Faist J, Villares G, Scalari G, Rösch M, Bonzon C, Hugi A and Beck M 2016 Quantum cascade laser frequency combs *Nanophotonics* **5** 272–91
[607] Cordes J The square kilometre array (available at: www.nrao.edu/A2010/rfi/SKA.pdf)
[608] WAFT interposers—waveguide array to fiber transposers SSC—spot size converters (available at: www.teemphotonics.com/integrated-photonics/waft-ssc-pic-packaging/)
[609] WAFT Series The silicon chip-to-fiber interface solution (available at: www.teemphotonics.com/wp-content/uploads/2018/08/Datasheet-edge-coupling-WAFT-201802-ev.pdf)
[610] De Heyn P *et al* 2017 Ultra-dense 16x56Gb/s NRZ GeSi EAM-PD arrays coupled to multicore fiber for short-reach 896Gb/s optical links *Optical Fiber Communication Conf., OSA Technical Digest (online)* (Optica Publishing Group) p Th1B.7
[611] Thomson R R, Harris R J, Birks T A, Brown G, Allington-Smith J and Bland-Hawthorn J 2012 Ultrafast laser inscription of a 121-waveguide fan-out for astrophotonics *Opt. Lett.* **37** 2331–3
[612] Sun X, Liu J, Kimerling L C and Michel J 2009 Toward a germanium laser for integrated silicon photonics *IEEE J. Sel. Top. Quantum Electron.* **16** 124–31
[613] Shen B *et al* 2020 Integrated turnkey soliton microcombs *Nature* **582** 365–9
[614] Brusberg L *et al* 2018 On-board optical fiber and embedded waveguide interconnects *2018 7th Electronic System-Integration Technology Conf. (ESTC)* (*Dresden, Germany*) pp 1–9
[615] Meitl M A, Zhu Z T, Kumar V, Lee K J, Feng X, Huang Y Y, Adesida I, Nuzzo R G and Rogers J A 2006 Transfer printing by kinetic control of adhesion to an elastomeric stamp *Nat. Mater.* **5** 33–38
[616] Zhang J *et al* 2019 III-V-on-Si photonic integrated circuits realized using micro-transfer-printing *APL Photonics* **4** 110803
[617] Quantum X align 2023 (available at: www.nanoscribe.com/en/products/quantum-x-align?utm_source=&utm_medium=referral&utm_campaign=quantum-x-align-phix)
[618] Kim S, Westly D A, Roxworthy B J, Li Q, Yulaev A, Srinivasan K and Aksyuk V A 2018 Photonic waveguide to free-space Gaussian beam extreme mode converter *Light Sci. Appl.* **7** 72
[619] Yulaev A, Zhu W, Zhang C, Westly D A, Lezec H J, Agrawal A and Aksyuk V 2019 Metasurface-integrated photonic platform for versatile free-space beam projection with polarization control *ACS Photonics* **6** 2902–9
[620] Theurer M *et al* 2020 Flip-chip integration of InP to SiN photonic integrated circuits *J. Lightwave Technol.* **38** 2630–6
[621] Park H, Fang A W, Jones R, Cohen O, Raday O, Sysak M N, Paniccia M J and Bowers J E 2007 A hybrid AlGaInAs-silicon evanescent waveguide photodetector *Opt. Express* **15** 6044–52

[622] Komljenovic T, Huang D, Pintus P, Tran M A, Davenport M L and Bowers J E 2018 Photonic integrated circuits using heterogeneous integration on silicon *Proc. IEEE* **106** 2246–57
[623] Roelkens G *et al* 2015 III-V-on-silicon photonic devices for optical communication and sensing photonics *Photonics* **2** 969–1004
[624] Two-dimensional, 37-channel, high-bandwidth, ultra-dense silicon photonics optical interface *IEEE J. Mag.*
[625] Won R 2018 Wire-bonding assembly *Nat. Photon.* **12** 500
[626] 2023 (available at: www.hhi.fraunhofer.de/en/departments/pc/research-groups/photonic-inp-foundry/our-offer.html)
[627] de Valicourt G *et al* 2018 Photonic integrated circuit based on hybrid III–V/silicon integration *J. Lightwave Technol.* **36** 265–73
[628] Zhang Y, Samanta A, Shang K and Yoo S J B 2020 Scalable 3D silicon photonic electronic integrated circuits and their applications *IEEE J. Sel. Top. Quantum Electron.* **26** 8201510
[629] 2023 Silicon photonics grasp the future of electro-optical design (available at: https://gf.com/technology-platforms/technology-platforms/silicon-photonics/)
[630] Mourier T *et al* 2021 Self-assembly and mass reflow of copper bumps for flip-chip hybridization in photonic applications *2021 IEEE 71st Electronic Components and Technology Conf. (ECTC)* (*San Diego, CA, USA*) pp 225–30
[631] Photonic integrated circuit based on hybrid III–V/silicon integration *IEEE J. Mag.*
[632] 2021 Terahertz technology for ultra-broadband and ultra-wideband operation of backhaul and fronthaul links in systems with SDN management of network and radio resources (available at: https://ict-teraway.eu/)
[633] STANDARD PACKAGE TYPES 2023 (available at: www.phix.com/our-offering/standard-package-types/)
[634] Aalto T, Harjanne M, Offrein B-J, Caër C, Neumeyr C, Malacarne A, Guina M, Noel Sheehan R, Hudson Peters F and Melanen P 2016 Integrating III–V, Si, and polymer waveguides for optical interconnects: RAPIDO *Proc. SPIE* **9753** 97530D
[635] Lingyan H, Zhang M, Shams-Ansari A, Zhu R, Wang C and Marko L 2019 Low-loss fiber-to-chip interface for lithium niobate photonic integrated circuits *Opt. Lett.* **44** 2314–7
[636] Xiao Y, Xu Y, Dong Y, Zhang B and Ni Y 2022 A 60 μm-long fiber-to-chip edge coupler assisted by subwavelength grating structure with ultralow loss and large bandwidth *Photonics* **9** 413
[637] Wood M, Sun P and Reano R M 2012 Compact cantilever couplers for low-loss fiber coupling to silicon photonic integrated circuits *Opt. Express* **20** 164–72
[638] Kleinert M *et al* 2019 A platform approach towards hybrid photonic integration and assembly for communications, sensing, and quantum technologies based on a polymer waveguide technology *2019 IEEE CPMT Symp. Japan (ICSJ)* (*Kyoto, Japan*) pp 25–30
[639] Bernabé S, Kopp C, Volpert M, Harduin J, Fédéli J-M and Ribot H 2012 Chip-to-chip optical interconnections between stacked self-aligned SOI photonic chips *Opt. Express* **20** 7886–94
[640] Ma J, Zhang D, Robledo D, Anzagira L and Masoodian S 2022 Ultra-high-resolution quanta image sensor with reliable photon-number-resolving and high dynamic range capabilities *Sci. Rep.* **12** 13869
[641] Finger G, Baker I, Alvarez D, Eisenhauer F, Hechenblaikner G, Ives D, Mehrgan L, Meyer M, Stegmeier J and Weller H J 2019 On-sky performance verification of near infrared eAPD technology for wavefront sensing at ground based telescopes, demonstration of e-APD pixel performance to improve the sensitivity of large science focal planes and possibility to use this technology in space *Int. Conf. on Space Optics; ICSO 2018* vol 11180 p 111806L (available at: www.spiedigitallibrary.org/conference-proceedings-of-spie/11180/2536156/On-sky-performance-verification-of-near-infrared-eAPD-technology-for/10.1117/12.2536156.full?SSO=1)
[642] Tudisco S *et al* 2007 A new generation of SPAD: single photon avalanche diodes *3rd European Workshop on Optical Fibre Sensors* vol 6619 p 66193N (available at: www.spiedigitallibrary.org/conference-proceedings-of-spie/6619/1/A-new-generation-of-SPAD-single-photon-avalanche-diodes/10.1117/12.738659.full)
[643] Okimoto T, Yagi H, Ebihara K, Yamazaki K, Okamoto S, Ohkura Y, Horino K, Ashizawa K, Ekawa M and Yoneda Y 2021 InP-based PIC integrated with butt-joint coupled waveguide p-i-n PDs for 100GBaud coherent networks *Optical Fiber Communication Conf. (OFC) 2021* ed P Dong, J Kani, C Xie, R Casellas, C Cole and M Li (Optica Publishing Group) p F2C.6 (available at: https://opg.optica.org/abstract.cfm?uri=ofc-2021-F2C.6)
[644] Lischke S *et al* 2020 Ge photodiode with −3 dB OE bandwidth of 110 GHz for PIC and ePIC platforms *2020 IEEE Int. Electron Devices Meeting (IEDM)* pp 2020–3
[645] Wolley O, Gregory T, Beer S, Higuchi T and Padgett M 2022 Quantum imaging with a photon counting camera *Sci. Rep.* **12** 8286
[646] 2021 HWK1411 ultra low-light image sensor enables night vision in overcast starlight conditions (available at: www.baesystems.com/en-us/article/hwk1411-ultra-low-light-image-sensor-enables-night-vision-in-overcast-starlight-conditions)
[647] Dutta H S, Goyal A K, Srivastava V and Pal S 2016 Coupling light in photonic crystal waveguides: a review *Photon. Nanostruct: Fundam. Appl.* **20** 58
[648] Zemcov M 2023 private communication
[649] Wen P *et al* 2022 Waveguide coupled III–V photodiodes monolithically integrated on Si *Nat. Commun.* **13** 909
[650] Smit M, Williams K and van der Tol J 2019 Past, present, and future of InP-based photonic integration *APL Photonics* **4** 050901
[651] Hanold B, Figer D, Lee J, Kolb K, Marcuson I, Corrales E, Getty J and Mears L 2015 Large format MBE HgCdTe on silicon detector development for astronomy *SPIE Proc.* **9609** 96090Y
[652] Sacher W D *et al* 2017 Tri-layer silicon nitride-on-silicon photonic platform for ultra-low-loss crossings and interlayer transitions *Opt. Express* **25** 30862–75
[653] Cai X, Wang J, Strain M J, Johnson-Morris B, Zhu J, Sorel M, O'Brien J L, Thompson M G and Yu S 2012 Integrated compact optical vortex beam emitters *Science* **338** 363
[654] Tian Z-T, Zhuang Z-P, Fan Z-B, Chen X-D and Dong J-W 2022 High-efficiency grating couplers for pixel-level flat-top beam generation *Photonics* **9** 207
[655] Qiu C, Chen J, Xia Y and Xu Q 2012 Active dielectric antenna on chip for spatial light modulation *Sci. Rep.* **2** 855
[656] Sprengers J P *et al* 2011 Waveguide superconducting single-photon detectors for integrated quantum photonic circuits *Appl. Phys. Lett.* **99** 1–3
[657] Pernice W, Schuck C, Minaeva O, Li M, Goltsman G N, Sergienko A V and Tang H X 2012 High-speed and high-efficiency traveling wave single-photon detectors embedded in nanophotonic circuits *Nat. Commun.* **3** 1325
[658] Natarajan C M, Tanner M G and Hadfield R H 2012 Superconducting nanowire single-photon detectors: physics and applications *Supercond. Sci. Technol.* **25** 063001
[659] Wollman E E *et al* 2021 Recent advances in superconducting nanowire single-photon detector technology for exoplanet transit spectroscopy in the mid-infrared *J. Astron. Telesc. Instrum. Syst.* **7** 011004

[660] Esmaeil Zadeh I, Chang J, Los J W N, Gyger S, Elshaari A W, Steinhauer S, Dorenbos S N and Zwiller V 2021 Superconducting nanowire single-photon detectors: a perspective on evolution, state-of-the-art, future developments, and applications *Appl. Phys. Lett.* **118** 190502
[661] Day P K, Leduc H G, Mazin B A, Vayonakis A and Zmuidzinas J 2003 *Nature* **425** 817
[662] Szypryt P *et al* 2017 *Opt. Express* **25** 25894
[663] Walter A B *et al* 2020 *Publ. Astron. Soc. Pac.* **132** 125005
[664] Nagler P C, Sadleir J E and Wollack E J 2021 Transition-edge sensor detectors for the origins space telescope *J. Astron. Telesc. Instrum. Syst.* **7** 011005
[665] Lita A E *et al* 2022 Development of superconducting single-photon and photon-number resolving detectors for quantum applications *J. Lightwave Technol.* **40** 7578–97
[666] Echternach P M, Pepper B J, Reck T and Bradford C M 2018 Single photon detection of 1.5 THz radiation with the quantum capacitance detector *Nat. Astron.* **2** 90–97
[667] Ferrari S, Schuck C and Pernice W 2018 Waveguide-integrated superconducting nanowire single-photon detectors *Nanophotonics* **7** 1725–58
[668] Moody G *et al* 2022 2022 Roadmap on integrated quantum photonics *J. Phys. Photon.* **4** 012501
[669] Zhao Q Y, Zhu D, Calandri N, Dane A E, McCaughan A N, Bellei F, Wang H-Z, Santavicca D F and Berggren K K 2017 Single-photon imager based on a superconducting nanowire delay line *Nat. Photon.* **11** 247–51
[670] Kong L D *et al* 2023 Readout-efficient superconducting nanowire single-photon imager with orthogonal time–amplitude multiplexing by hotspot quantization *Nat. Photon.* **17** 65–72
[671] Gourgues R, Los J W N, Zichi J, Chang J, Kalhor N, Bulgarini G, Dorenbos S N, Zwiller V and Esmaeil Zadeh I 2019 Superconducting nanowire single photon detectors operating at temperature from 4 to 7 K *Opt. Express* **27** 24601–9
[672] de Cea M, Wollman E E, Atabaki A H, Gray D J, Shaw M D and Ram R J 2020 Photonic readout of superconducting nanowire single photon counting detectors *Sci. Rep.* **10** 9470
[673] Allmaras J P, Wollman E E, Beyer A D, Briggs R M, Korzh B A, Bumble B and Shaw M D 2020 Demonstration of a thermally coupled row-column SNSPD imaging array *Nano Lett.* **20** 2163–8
[674] Doerner S, Kuzmin A, Wuensch S, Charaev I, Boes F, Zwick T and Siegel M 2017 Frequency-multiplexed bias and readout of a 16-pixel superconducting nanowire single-photon detector array *Appl. Phys. Lett.* **111** 032603
[675] Yabuno M, Miyajima S, Miki S and Terai H 2020 Scalable implementation of a superconducting nanowire single-photon detector array with a superconducting digital signal processor *Opt. Express* **28** 12047–57
[676] Nicholas Zobrist W H C, Coiffard G, Daal M, Swimmer N, Day P and Mazin B A 2022 Demonstration of a thermally coupled row-column SNSPD imaging array *Phys. Rev. Lett.* **129** 017701
[677] Gao J, Daal M, Martinis J M, Vayonakis A, Zmuidzinas J, Sadoulet B, Mazin B A, Day P K and Leduc H G 2008 A semiempirical model for two-level system noise in superconducting microresonators *Appl. Phys. Lett.* **92** 212504
[678] Cheng R, Zou C L, Guo X, Wang S, Han X and Tang H X 2019 Broadband on-chip single-photon spectrometer *Nat. Commun.* **10** 4104
[679] Barbieri C *et al* 2007 Astronomical applications of quantum optics for extremely large telescopes *J. Mod. Opt.* **54** 191–197
[680] Najafi F *et al* 2015 On-chip detection of non-classical light by scalable integration of single-photon detectors *Nat. Commun.* **6** 5873
[681] Cheng R, Zhou Y, Wang S, Shen M, Taher T and Tang H X 2023 A 100-pixel photon-number-resolving detector unveiling photon statistics *Nat. Photon.* **17** 112–9
[682] Kong L *et al* 2021 Single-detector spectrometer using a superconducting nanowire *Nano Lett.* **21** 9625–32
[683] Obrien K 2020 KIDSpec: an MKID-based medium-resolution, integral field spectrograph (available at: https://link.springer.com/content/pdf/10.1007/s10909-020-02347-z.pdf)